Exhumation of the Caledonian Orogenic Infrastructure in West Norway

Concepts – Structures – Ages – Reactivation

Johannes Daniel Wiest

Thesis for the degree of Philosophiae Doctor (PhD)
University of Bergen, Norway
2020

UNIVERSITY OF BERGEN

Exhumation of the Caledonian Orogenic Infrastructure in West Norway

Concepts – Structures – Ages – Reactivation

Johannes Daniel Wiest

Thesis for the degree of Philosophiae Doctor (PhD)
at the University of Bergen

Date of defense: 19.05.2020

Year: 2020

Title: Exhumation of the Caledonian Orogenic Infrastructure in West Norway

Name: Johannes Daniel Wiest

Print: Skipnes Kommunikasjon / University of Bergen

panta rhei

Scientific environment

This dissertation was carried out at the Department of Earth Science, University of Bergen (UiB), Norway, between January 2017 and February 2020. The research project was funded by VISTA – a basic research program in collaboration between The Norwegian Academy of Science and Letters, and Equinor [grant number 6271]. Additional funding was provided by a student grant from the Meltzer fond at UiB. Geochronological analyses were carried out at the Nordsim laboratory (Stockholm, Sweden) and by Morgan Ganerød at the Norwegian Geological Survey (Trondheim). The DEEP research school provided a travel grant for an intensive course at UNIS and allowed course participation at the University of Tromsø. The Fourth EGU Summer School 2017 in structural analysis of crystalline rocks strongly enhanced the course component of this PhD. The work was supervised by Prof. Joachim Jacobs (UiB), Prof. Haakon Fossen (UiB) and Prof. Per Terje Osmundsen (Norwegian University of Science and Technology, Trondheim and University of Oslo).

UNIVERSITY OF BERGEN

NORGES GEOLOGISKE UNDERSØKELSE

- NGU -

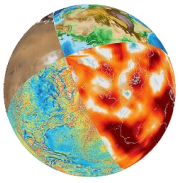

DEEP

Norwegian Research School for Dynamics and Evolution of Earth and Planets

Acknowledgements

If it were not for the contribution of many people, you would not read this thesis.

First and foremost, I thank my supervisors Joachim Jacobs, Haakon Fossen and Per Terje Osmundsen for making this project possible. I especially thank Joachim for welcoming me to Bergen and for giving me the chance and the freedom to follow my own curiosity. Your constant trust and positive attitude were as important for the success of this project as your ability to step in when needed! I thank Haakon for contributing his large expertise of Norwegian and structural geology. Your thorough feedback improved not only my writing, but largely helped to develop my ideas. For finalizing the thesis, it was invaluable. I thank Per Terje for his complementary perspectives from Mid Norway and from above the brittle-ductile transition, which provided valuable input.

I thank former VISTA coordinator Håkon Sandbakken and Grégoire Messager (& colleagues at Equinor) for creating a pleasant project environment. I thank the staff at the department of Earth Science (UiB), in particular Irina Dumitru for preparing countless samples and Irene Heggstad for helping with the SEM. Big thanks go to Morgan Ganerød (NGU, Trondheim) for timely Ar-Ar analyses and Martin Whitehouse and his team (Nordsim, Stockholm) for great help with U-Pb zircon geochronology. I am very grateful for the cooperation with Thilo Wrona, Rob Gawthorpe, Marit Stokke Bauck and Jan Inge Faleide and for the access to seismic data from CGG, which allowed onshore-offshore correlations.

I want to thank all the great (PhD) colleagues and friends at UiB, but in particular Sebastian (the long way we have gone together, your modeler's insights and hospitality (takk Birte!)), Thilo (your thoughts are as inspiring as your pragmatic way of trying new things and of course your spaghetti), Eric (always great company), Edos (lending his beautiful voice to Le Potet), Åse (rock chocolates), Cheng-Cheng (taking over the Precambrian), Anna (getting started in Bergen), Thomas (good modelling discussions), Fabian (whisky & cigarettes), Vilde (sharing Tingviken), Felix (my plants owe you) and Stéphane (your really positive attitude).

I warmly thank Deta Gasser and Thomas Scheiber for their warm hospitality, great field trips and valuable input; Espen Torgersen and Hans-Jørgen Kjøll for a great weekend on Hardangervidda; Renee Tamblyn for reducing my petrological ignorance; Trond Slagstad, Bernard Bingen, Christian Teyssier and Donna Whitney for motivating discussions. Field work would not have been possible without the company of my friends from Bergen as well as Arne, Theo, Anne, Daniel and Saad. I thank Per Sjöberg for his help to overcome a mid-project crisis.

I cannot thank enough all of my good friends and family for supporting me on this challenging way; I would not have made it without you. Last but not least my biggest thanks go to my love Samsara (you know why!).

Abstract

Domes of high-grade metamorphic rocks are found in recent and ancient orogens alike. They commonly expose parts of the deep interior of mountain belts, the so-called orogenic infrastructure. This thesis explores the controversial topic of infrastructure exhumation in two different ways: First, through reviewing the history of tectonic research leading to the concept of metamorphic core complexes (MCCs). Second, in a case study of basement windows in the deeply eroded Paleozoic Caledonian orogen of West Norway. Including the (ultra)high-pressure Western Gneiss Region, these domal windows record Caledonian continental subduction of the Baltic Shield and controversial exhumation mechanisms.

Paper 1 explores the lithological and structural composition of the Baltic Shield in the eastern part of the Øygarden Complex, which represents the westernmost Caledonian basement window. Secondary-ion mass spectrometry (SIMS) U-Pb zircon geochronology constrains two pulses of voluminous Sveconorwegian intrusions into a Telemarkian (1506 ± 5 Ma) granitic basement. Bimodal magmatism at 1041 ± 3 Ma, followed by leucogranite magmatism at 1027-1022 Ma, correlate the Øygarden Complex with the Sirdal Magmatic Belt in South Norway. A low-temperature resetting of metamict grains at ~482 Ma is the only Caledonian record in zircon. The Sveconorwegian intrusions were strongly reworked by Caledonian ductile deformation. Starting at amphibolite facies conditions, retrograde top-to-E shearing involved fluid-induced phyllonitization that localized ductile-to-brittle low-angle shear zones. Structural features of the Øygarden Complex are discussed in the light of MCC exhumation.

Paper 2 investigates the southernmost culmination of the eclogite-bearing Western Gneiss Region in the footwall of the Nordfjord-Sogn detachment (Gulen dome). Semi-quantitative mapping of ductile strain along glacier-polished fjords reveals two distinct structural levels. The amphibolite-facies core domain involved fluid-controlled eclogite retrogression and records coaxial E-W stretching in subvertical shear zones and vast extension-perpendicular shortening in upright folds. Detachment

mylonites wrap around the core and record amphibolite-facies to semi-brittle, non-coaxial deformation. Our reconstruction constrains dome formation through extension-perpendicular inward flow of solid-state material in the deep crust isostatically compensating upper crustal thinning. Differential folding within solid-state MCCs can resemble the dynamics of migmatite-cored MCCs and exhume deep parts of the crust.

Paper 3 provides the first comprehensive study of the Øygarden Complex with a focus on ductile-to-brittle Caledonian structures. The comparison of 23 classified shear zones and a structural dataset comprising >4500 data constrain pervasive E-W stretching with distinct deformation styles at three structural levels. The upper unit shows localized ductile deformation and top-to-E kinematics, in contrast to distributed flow and top-to-W kinematics in the middle unit. The lower unit consists of migmatites, which define a double-dome in the core of the complex. Retrograde shearing affected all levels and localized ductile-to-brittle shear zones through fluid-induced weakening (phyllonitization). We suggest exhumation of a bivergent MCC in two stages. Extension-perpendicular flow of partially molten crust formed the migmatite dome in response to intra-crustal necking. Fluid-induced retrograde weakening feedbacks occurred in a wide zone and facilitated detachment formation and rapid exhumation of previously ductile crust.

Paper 4 presents new geochronology from the previously poorly dated Gulen and Øygarden domes and integrates them in an orogen-scale synthesis of infrastructure exhumation. Three of four SIMS U-Pb zircon migmatite samples from the Øygarden Complex date melt crystallization at 405 ± 3 Ma. This result conforms to dated melts in other parts of the Western Gneiss Region, but largely expands the known spatial extent of Devonian melting. Most of the 28 new Ar-Ar white mica and biotite dates from shear zones in the Øygarden and Gulen domes record short-lived MCC exhumation in between 405 and 399 Ma, in accordance with previously published ages. We compiled a database comprising >450 U-Pb zircon, monazite, titanite and rutile as well as Ar-Ar white mica, biotite and hornblende ages. The intermingled spatial distribution of different chronometers suggests that ages cannot be assigned to

simple cooling histories. On the other hand, various chronometers robustly constrain the duration of ductile stretching in each segment of the infrastructure, with significant variations between different segments (~10-30 Myr). We combine our new geochronological insights with structural geometries, inferred from large-scale foliation-trace mapping and previous descriptions of the windows. Temperature-pressure-time-deformation discontinuities within the Caledonian infrastructure are explained in a model of segmented transtensional MCC exhumation.

Paper 5 combines field observations from onshore West Norway with new 3D seismic data revealing deep structures underneath the northern North Sea rift. We correlate two distinct structural units from the Gulen dome to corresponding seismic facies in the acoustic basement offshore. Our interpretation reveals an offshore dome, which resembles the onshore dome in size, geometry and kilometer-scale, upright folds. Both domes are connected by a >100 km long, shallowly W-dipping, extensional detachment zone with a non-planar, hyperbolic geometry. Devonian collapse formed dome and detachment, which were reactivated during Permian-Triassic North Sea rifting. Brittle reactivation of steep detachment segments resulted in strongly deviating rift fault orientations at the eastern margin of the rift around 61°N.

This study highlights large spatial and temporal variations in the evolution of the Caledonian infrastructure, intimately linked to preceding and subsequent tectonic events. During Caledonian collision the infrastructure represented a cold and rigid slab that allowed continental subduction. During Devonian transtensional collapse, in contrast, it represented a variably mobile substrate that could flow in response to pressure gradients. Structural inheritance might have controlled along-strike segmentation of the Caledonian orogen. During North Sea rifting it behaved rigid again, but inherited weak zones were inevitably reactivated.

The conceptual focus of this study may be its biggest limitation. On the other hand, it highlights the usefulness of the paradigm of extensional MCCs: It is a paradigm that raises many, testable questions.

List of Publications

Wiest, J. D., Jacobs, J., Ksienzyk, A. K., and Fossen, H., 2018,
Sveconorwegian vs. Caledonian orogenesis in the eastern Øygarden Complex, SW Norway – Geochronology, structural constraints and tectonic implications:
Precambrian Research, v. 305, p. 1-18,
https://doi.org/10.1016/j.precamres.2017.11.020.

Wiest, J. D., Osmundsen, P. T., Jacobs, J., and Fossen, H., 2019,
Deep Crustal Flow Within Postorogenic Metamorphic Core Complexes: Insights From the Southern Western Gneiss Region of Norway:
Tectonics, v. 38, p. 4267-4289, https://doi.org/10.1029/2019TC005708.

Wiest, J. D., Fossen, H., and Jacobs, J.,
Rheological Evolution of Ductile Crust Exhumed in a Metamorphic Core Complex:
Manuscript submitted to *Journal of Structural Geology*

Wiest, J. D., Jacobs, J., Fossen, H., Ganerød, M. and Osmundsen, P. T.,
Melting, flow and post-orogenic exhumation of the Caledonian infrastructure, W Norway:
Manuscript submitted to *Geosphere*

Wiest, J. D., Wrona, T., Bauck, M. S., Fossen, H., Gawthorpe, R.L., Osmundsen, P. T. and Faleide, J. I.
From Caledonian Collapse to North Sea Rift – The Extended History of a Metamorphic Core Complex:
Manuscript submitted to *Tectonics*

Contents

1. Introduction

South Tibetan Detachment System, Nepal (view towards east).
Peak of Machhapuchare is 6,993 m, bottom of photo is ~3,700 m.

Mountains have always played a central role for humans' attitude towards the planet (Macfarlane, 2008). The sublime intrigues our minds and only mountain landscapes provide extensive (vertical) exposure of rocks that record Earth's dynamic history. Research on mountain belts reveals intimate links between different systems such as tectonics, erosion and climate (Beaumont et al., 2001; Hoorn et al., 2018; Molnar et al., 2010; Willett, 1999). However, the very nature of mountains makes access and direct observation challenging or sometimes even impossible. Deeply eroded ancient orogens, on the other hand, can provide accessible exposure and represent invaluable analogues for recent orogens (Hodges, 2006).

Each orogen has its individual characteristics and distinct styles governed orogenesis at various stages of Earth's evolution (Chardon et al., 2009; Gerya, 2014; Rey and Houseman, 2006). Still, there are many similarities between recent and ancient orogens. In both cases, domes expose parts of the deep interior, the so-called orogenic infrastructure (Eskola, 1948; Hodges, 2016; Teyssier and Whitney, 2002; Vanderhaeghe, 2012; Wegmann, 1935; Whitney et al., 2004). It is often controversial whether it is contraction or extension that drives doming and exhumation of high-grade metamorphic rocks (Ring et al., 1999; Warren, 2013). Examples of this controversy are found in most recent and ancient orogens around the world, such as the Himalayas (Chen et al., 1990; Hodges, 2006; Jessup et al., 2008; Searle and Lamont, 2020), Alps (Frisch et al., 2000; Ratschbacher et al., 1991b; Rosenberg et al., 2018), Cyclades (Jolivet and Brun, 2010; Kruckenberg et al., 2011; Lamont et al., 2019; Vanderhaeghe et al., 2004), Variscides (Aerden, 1998; Brun and Van den Driessche, 1994; Roger et al., 2015) or the North American Cordillera (Gordon et al., 2008; Norlander et al., 2002; Simony and Carr, 2011; Vanderhaeghe and Teyssier, 1997).

In recent years, quantitative approaches have allowed physical proof of tectonic concepts (Jamieson and Beaumont, 2013). Still, geological concepts are observation-based and depend on the paradigms of our research. Kuhn (1962, p. viii) defined paradigms as *"universally recognized scientific achievements that, for a time, provide model problems and solutions for a community of researchers"*. As such, the

importance of paradigms is that they determine the questions a scientific community raises.

The ~200 year short history of serious geological research is marked by fundamental debates (e.g. age of the Earth, neptunism vs. plutonism, catastrophism vs. uniformitarianism) and paradigm shifts (Rudwick, 2014). The most dramatic among them is probably the change from fixism to mobilism, which fundamentally altered the role of orogenic infrastructures in tectonic research. Long-held fixist views withheld the suggestion of continental drift and were only swept away by the plate tectonic revolution in the late 1960s. Together with simultaneous geochronologic advances, the scientific revolution turned orogenic infrastructures from hot and mobile, vertically moving substrates into laterally moving, cold and rigid slabs (Wernicke, 2009) and shifted research focus towards far-travelled allochthonous units. As continents evolve through cyclic phases that influence each other (Wilson, 1966), however, contrasting interpretations of orogenic infrastructures imply a large uncertainty for tectonic reconstructions. Therefore, this thesis seeks to address some aspects of the overarching question: *How does the orogenic infrastructure behave during, at the end and after orogenesis?*

As the past is the key to the present, Section 1.1 takes a look back at the development of major tectonic paradigms from contractionism over geosynclines to plate tectonics. *How did the geoscientific community view the interiors of mountain belts historically?* And *how did previous paradigm changes affect modern tectonic concepts?* This thesis focuses on the concept of **metamorphic core complexes** (MCCs) because it has been instrumental in revolutionizing 20th-century tectonic research (Wernicke, 2009). Section 1.2 reviews the discovery of MCCs in the light of the historic context and presents definitions that reflect the evolution of a field-based concept to a geodynamic paradigm. To find out *what is the essence of a core complex,* we discuss models, conditions and dynamics of core-complex formation.

The main body of this thesis is a case study of a deeply eroded Paleozoic orogen, the **Norwegian Caledonides**. Using excellently exposed basement windows along the west coast of Norway, we test MCC models to better understand the tectonic evolution of the Caledonian infrastructure. Furthermore, we investigate the relation of (post-)Caledonian features to later and earlier tectonic phases. Section 1.4 introduces the tectonic setting and main characteristics of the Caledonian and Sveconorwegian orogenic infrastructures. More detailed descriptions of the setting and the applied methods are found in the individual papers, which address the following questions:

What constitutes the Baltic Shield basement in West Norway and how did it deform during the Caledonian orogenic cycle?

Published in *Precambrian Research*, Paper 1 presents a high-resolution study of the mountain Lyderhorn in the eastern Øygarden Complex, exploring the lithological and structural inventory of the Baltic Shield basement in the Bergen area. Field mapping and secondary-ion mass spectrometry (SIMS) U-Pb zircon geochronology were conducted during my Master studies at UiB, while the paper was written during the PhD and represents the starting point for following investigations.

How does the deep crust flow below extensional detachments and contribute to exhumation of high-pressure rocks?

Paper 2 is published in *Tectonics* and provides a detailed study of the Gulen MCC, the southernmost culmination of the eclogite-hosting Western Gneiss Region. Numerous glacier-polished fjords transect the gneiss dome and provide continuous, excellent exposures that can be easily accessed by boat. To exploit these conditions, we developed a novel semi-quantitative mapping scheme for ductile strain.

How does the rheology of ductile crust evolve during exhumation and what are the implications for large-magnitude extensional detachments?

Paper 3 has been submitted to *Journal of Structural Geology* and investigates shear zones in the Øygarden Complex building upon Paper 1. The complex is easily

accessible from Bergen and was mapped continuously over the entire project period, resulting in an extensive documentation of retrograde shear zone structures.

How and when was the Caledonian orogenic infrastructure exhumed?

Paper 4 has been submitted to *Geosphere*. It presents SIMS U-Pb zircon ages of four late Caledonian migmatite samples from the Øygarden Complex and 28 Ar-Ar mica dates of shear zones in the Øygarden Complex and the Gulen MCC. The new ages are integrated in a geochronological and structural synthesis of Caledonian basement windows including different segments of the Western Gneiss Region.

What was the influence of the inherited Caledonian infrastructure on North Sea rifting?

Paper 5 has been submitted to *Tectonics* and expands Paper 2 from the onshore to the offshore. Combining new 3D seismic data with field observations of the Gulen MCC, we correlate 3D seismic basement facies offshore with units mapped in the field onshore. The onshore-offshore correlation constrains dome and detachment geometries formed during the Devonian and their relation to Permian-Triassic rift faults.

1.1 A Short History of Tectonics

Glarus Thrust, Switzerland, drawn by H.C. Escher von der Linth (1812). *Downloaded from https://en.wikipedia.org/wiki/Glarus_thrust#/media/File:Escher_Martinsloch.jpg*

1.1.1 Contractionism, Geosynclines and Orogenic Infrastructures

Early geological research emancipated Earth's deep history from scriptural interpretation (Rudwick, 2014). Biblical heritage still influenced geological reasoning in the 19th century, when the theory of a cooling and contracting Earth became universally accepted (Oreskes, 1988, 1999). Contractionism was practiced in two independent schools, which reflected controversial paradigms (catastrophism vs. uniformitarianism). The European version (E. Suess, published 1883 - 1904), explained global tectonics through catastrophic events that turned continents into oceans and vice versa. The American school, in contrast, followed J. Dana theory of stable continents and permanent oceans. The geosyncline theory (suggested by J. Hall in 1859 and J. Dana in 1873) sought to explain the structure of mountain belts with sediments overlaying crystalline rocks (Knopf, 1948). The basic idea of the geosyncline (Fig. 1) was a trough at the edge of a continent (the geanticline) that is filled with sediments in cyclic episodes. Accommodation space is provided by lateral flow of a mobile substrate from below the subsiding basin, while lateral pressure gradients fold the sedimentary rocks. Huge piles of sediments can be accumulated, however, heating progressively weakens the most deeply buried layers. At some stage, the weakened root rises buoyantly and forms a mountain belt with a crystalline core mantled by sediments.

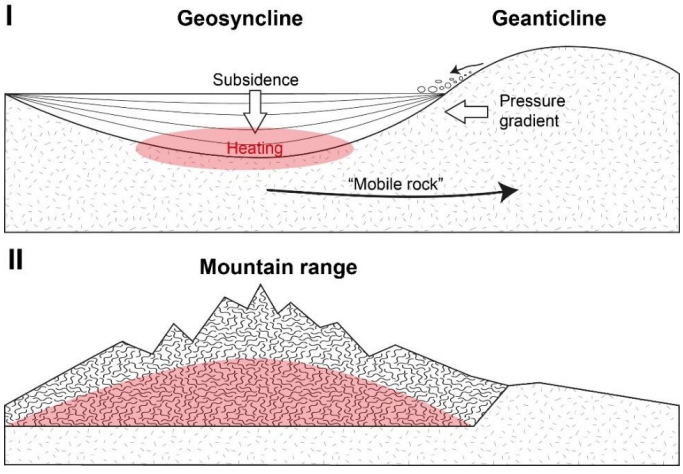

Fig. 1: Schematic illustration of mountain building in two stages according to the 19th century geosyncline theory (based on description by Knopf, 1948).

The demise of contractionism

At the turn of the 20th century, important discoveries caused serious issues for the contractionist paradigm (Oreskes, 1988).

I) Thrusts were first observed in the early 1800s, but not publicly interpreted before the 1880s. Thirty years later, the concept of thrusting was firmly established and implied large amounts of horizontal shortening in mountain belts (Trümpy, 2001).
II) Isostasy required a mobile substrate below Earth's rigid crust to explain the gravitational signature of mountain belts and post-glacial rebound. Furthermore, it showed that oceans and continents are made of different materials, disproving Suess' collapsing Earth theory.
III) The discovery of radioactivity disproved Earth's secular cooling, the basic assumption of contractionism, and allowed the absolute dating of rocks and thereby the age of the Earth.

Thus, contractionism was proven incompatible with 20th century physical principles and the amount of shortening observed in mountain belts. Nevertheless, the geosyncline theory gained global popularity and became the principal tectonic paradigm, although without a functioning global geodynamic framework (Oreskes, 1999).

The rejection of continental drift

Around the same time, Alfred Wegener published the first edition of "Die Entstehung der Kontinente und der Ozeane" (1915). Although not the first mobilist, Wegener was the first to propose a unified theory of continental drift, which was based on multidisciplinary evidence including the fossil record, stratigraphy, paleoclimate and continental fits. In 1929, Arthur Holmes published a speculative mantle convection model, which provided the missing driving mechanism of Wegener's drift theory. Nevertheless, continental drift was mostly rejected and after Wegener died in 1930, the theory lost its strongest proponent.

The infrastructure-superstructure concept (stockwerk-folding)

While a school of Alpine geologists developed mobilist syntheses on mountain building (Trümpy, 2001), mainstream tectonic research upheld fixist paradigms and continued to elaborate the geosyncline theory. New models were based on field observations in deeply eroded ancient orogens and focused on the genesis of migmatites and granites (Wegmann, 1935). In particular the spectacular exposures of the Greenland Caledonides should turn out to be highly influential (Hodges, 2016; Wernicke, 2009). The elaboration of the geosyncline theory led to the infrastructure-superstructure concept or "stockwerk-folding hypothesis" (Fig. 2), which explained contrasting deformation styles observed at different crustal levels (in German: "Stockwerk").

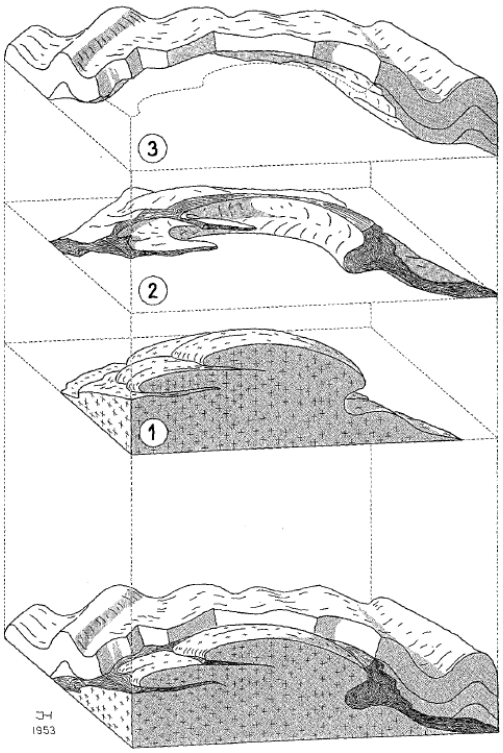

Fig. 2: Illustration of the infrastructure-superstructure concept ("stockwerk-folding") based on field observations from the Greenland Caledonides from Haller (1956). (1) Migmatite domes (the infrastructure) are separated through (2) a detachment zone ("Abscherungszone") from (3) low-grade metamorphic and weakly deformed sedimentary rocks (the superstructure).

While largely based on vertical tectonic movements (Haller, 1956), this concept explained the formation of a migmatized and "granitized" infrastructure through the metasomatic influx of material ("Stoffzufuhr"). When the buoyant infrastructure becomes mobile, it rises into domes with complex internal fold patterns (Fig. 2) that fold the overlaying low-grade sedimentary rocks of the superstructure. The distinct crustal levels are separated by a tectonic decoupling horizon, the so called "Abscherungszone" (German for: detachment zone). These deformation zone comprise mylonites, cataclasites and other fault rocks that formed through minor lateral displacements (Wegmann, 1935). As buoyantly rising domes were seen as the main driving force of nappe displacements (see review by Rey et al., 2001), they were a principal focus of research (Eskola, 1948).

1.1.2 The Plate Tectonic Revolution

In 1948, the retiring President of the Geological Society of America wrote enthusiastically: "*the geosynclinal doctrine is likely to prove to be a great unifying principle, possibly one of the greatest in geologic science*" (Knopf, 1948, p. 667). After the second World War, however, geophysical data was drawing a whole new picture of the ocean floors that inevitably re-opened fixism vs. mobilism debate. The new form of geophysical evidence quickly decided the debate in favor of mobilism (Oreskes, 1999), while tectonic research of mountain belts played no active role in the scientific revolution (Trümpy, 2001). Developed in the 1960s, plate tectonics was established within a few years as the great unifying geodynamic paradigm.

What became of the orogenic infrastructure?

At the time of the plate tectonic revolution, rapid advances in the field of geochronology allowed absolute dating of rocks in large numbers. In the 1970s, Rb-Sr whole rock dating was widely applied to ancient mountain belts around the world. The resulting ages commonly turned out to be much older than predicted by the infrastructure-superstructure concept (e.g. Higgins et al., 1978). In the words of Wernicke (2009): "*The stockwerk hypothesis for East Greenland did not survive geochronological testing*". Based on the geochronology and shallow-dipping reflections observed in seismic profiles, orogenic infrastructures were reinterpreted as

cold and rigid crystalline thrust sheets. Yet, the Rb-Sr whole rock method proved unsuited to date high-grade metamorphism and partial melting in polyorogenic continental basements constituting orogenic infrastructures (Jäger, 1979). High-precision in-situ analytical techniques and in particular zircon geochronology turned out to be indispensable for this purpose (Rubatto, 2017).

1.1.3 The Legacy of Fixist vs. Mobilist Debate

From today's perspective it seems that – in the heat of the plate tectonic revolution – the tectonic community was (understandably) overeager in sweeping away "fixist" ideas. More differentiated views in recent years give credit to previously discarded observations and new roles for old ideas.

I) The geosyncline theory and the stockwerk folding hypothesis contained the important idea that downward increasing temperatures permit **ductile flow** at depth (compare to "mobile rock" in Fig. 1), while upper crustal rocks deform brittlely (Wernicke, 2009). Later, rock deformation experiments quantified rheological behavior and constrained flow laws for different materials (Brace and Kohlstedt, 1980). Depending on mineralogy, deformation mechanism, thermal state, fluids and other parameters, the crust contains several rheological transitions (Cooper et al., 2017).

II) The **infrastructure-superstructure concept** was resurrected within the plate tectonic framework (Culshaw et al., 2006). These authors argue that thrusting alone cannot explain the structure of most orogenic belts, in particular not for large hot orogens (Fig. 3). Mobilist and fixist ideas are reconciled by considering that orogens can undergo substantial changes in their lifetime (Jamieson and Beaumont, 2013). Lateral growth and crustal thickening form mobile ductile infrastructures, allowing channel flow and extrusion of low-viscosity material below orogenic plateau (e.g. Beaumont et al., 2001; Beaumont et al., 2006; Bird, 1991; Grujic, 2006; Hodges, 2006; Royden et al., 1997; Teyssier et al., 2005; Vanderhaeghe, 2009; Vanderhaeghe, 2012; Vanderhaeghe and Teyssier, 2001; Williams et al., 2006). For the representative case of the Greenland Caledonides, Hodges (2016) suggests to

rehabilitate the infrastructure-superstructure terminology as it highlights the importance of crustal decoupling.

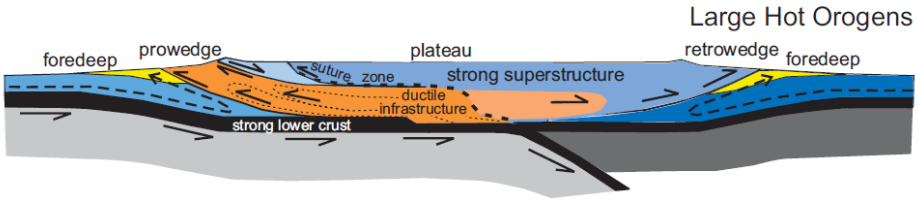

Fig. 3: Schematic diagram of the modern infrastructure-superstructure concept applied to large hot orogens from Jamieson and Beaumont (2013).

III) Pioneering work on **gravity tectonics** considered gravity as the main driver of all tectonic movements (see review by Rey et al., 2001). Following a "plate-tectonic hiatus", the role of gravity in orogenic belts was reconsidered after the discovery of surface extension in active orogens (e.g. Burchfiel and Royden, 1985) and the reappraisal of basement domes in ancient orogens (e.g. Ramberg, 1981). In the modern tectonic context, gravitational collapse is defined as "*the gravity-driven ductile flow that effectively reduces lateral contrasts in gravitational potential energy*" (Rey et al., 2001). These authors distinguish two fundamental regimes of gravitational collapse: *Divergent collapse* removes excess gravitational potential (thickened crust), while *convergent collapse* compensates a deficit in gravitational potential energy (thinned crust). An example of divergent gravitational collapse is orogen-parallel extension (Burchfiel and Royden, 1985; Chen et al., 1990; Jessup et al., 2008). It can be difficult, however, to distinguish gravity-driven lateral extrusion from escape tectonics (Molnar and Tapponnier, 1975; Ratschbacher et al., 1991b).

IV) The combination of fixist ideas and mobilist views led **to the discovery of extensional detachments and metamorphic core complexes**.

1.2 Metamorphic Core Complexes (MCCs)

Boudinage/fold patterns in gneiss, Øygarden Complex.

1.2.1 History of the Concept

Following the plate tectonic revolution, large horizontal movements needed to be considered not only for convergent but also extensional settings (Wernicke, 2009). This new perspective led to the discovery of large-magnitude low-angle normal faults in the North American Cordillera. Structures previously mapped as thrusts, were now reinterpreted as extensional faults (Anderson, 1971; Armstrong, 1972) because I) they placed younger onto older rocks and II) high-angle normal faults, which distended Tertiary rocks, rooted in these "décollement zones" (Fig. 4). Wright et al. (1974) interpreted domical fault surfaces in the Death Valley (so-called "turtlebacks") as phenomena of extensional tectonics. Soon after, characteristic dome-shaped basement uplifts of high-grade metamorphic rocks were discovered in the footwalls of low-angle faults along the entire North American Cordillera. While high-grade metamorphism and ductile deformation were traditionally associated with contractional tectonics, the 1977 Penrose Conference established their extensional nature in the basement uplifts (Crittenden et al., 1978) that Coney (1980) termed "Cordilleran metamorphic core complexes". The most important implications of the new-born concept were: I) low-angle faults can accommodate large magnitudes of continental extension; II) high-grade metamorphic and plutonic rocks can form and exhume during extension (Wernicke, 2009).

The systematic interpretation of kinematic indicators (Berthé et al., 1979; Lister and Snoke, 1984) furthermore cemented the extensional nature of detachments and MCCs (Fossen, 2010) and helped to recognize extensional features in many orogens around the world, such as the Aegean (Lister et al., 1984) and western Norway (Hossack, 1984; McClay et al., 1986; Seranne and Seguret, 1987). Insights from MCCs inspired new models of passive margins (e.g. Lister et al., 1986; Wernicke, 1985) and established the concept as a fundamental mode of continental lithosphere extension (Buck, 1991). The comparison with slow spreading ridges furthermore led to the discovery of oceanic detachments and core complexes (e.g. Tucholke et al., 1997) and provides a tight link between continental and oceanic tectonic research (Whitney et al., 2013). Still, some workers question a major role of continental extension and favor a compressional origin for most MCCs (Searle and Lamont, 2020).

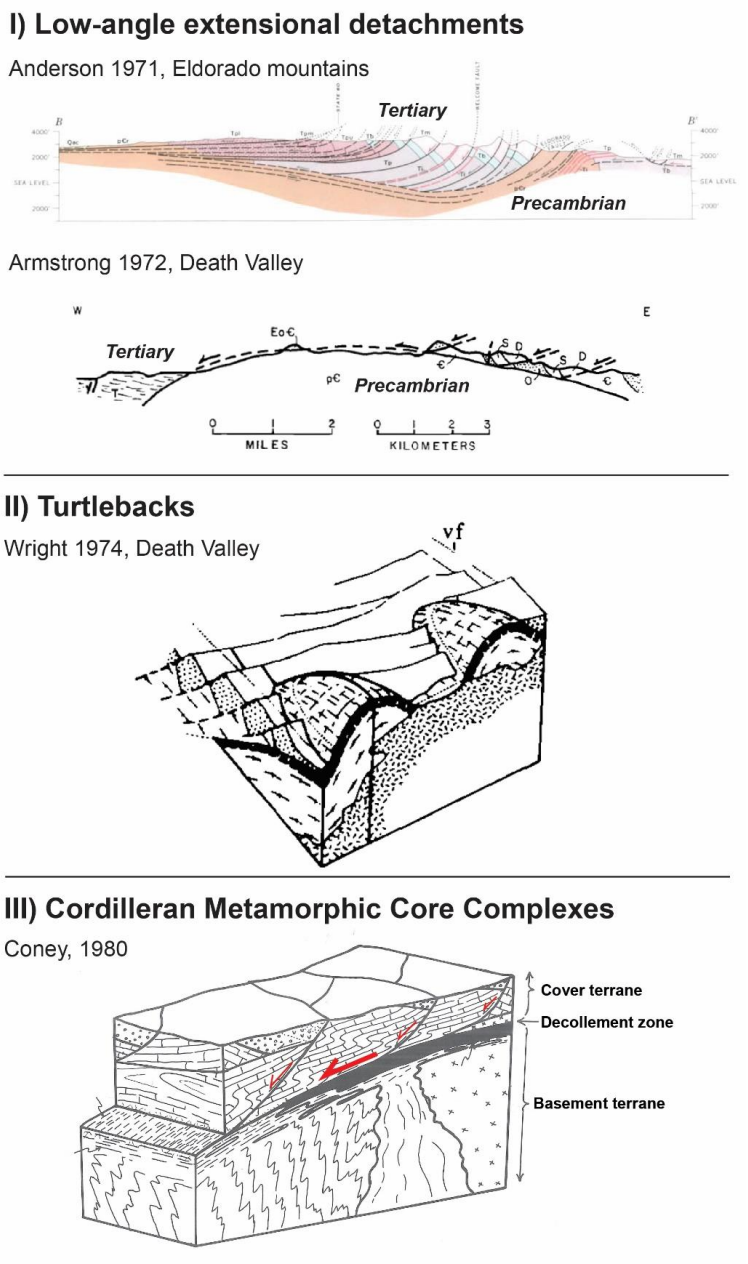

Fig. 4: Three landmarks in the discovery of MCCs: I) Early cross sections of low-angle normal faults (detachments) from Anderson (1971) and Armstrong (1972). Note that these faults place younger rocks on older rocks and extend layers (unlike thrusts). II) Wright et al. (1974) interpreted Death Valley turtlebacks as giant extensional fault mullions. III) Coney (1980) synthesized the concept of Cordilleran metamorphic core complexes. Note the threefold unit distinction, which is similar to the infrastructure-superstructure concept (Fig. 2).

1.2.2 Definitions

Definitions of MCCs (Table 1) reflect an evolution from a field-based concept to a tectonic paradigm.

Table 1: Definitions of MCCs sorted by year of publication.

Coney (1980)	Cordilleran metamorphic core complexes, […], are a group of generally domal or archlike, isolated uplifts of anomalously deformed, metamorphic and plutonic rocks overlain by a tectonically detached and distended unmetamorphosed cover.
Armstrong (1982)	A core complex can be described in a few words: it is an exposure of rocks that were once ductile lower crust, on which shallow brittle extensional features have been superimposed.
Lee et al. (1987)	In recent years considerable attention has focused on metamorphic core complexes […]. These highly extended areas are characterized by an upper plate that has been brittlely attenuated by normal faults separated by a sub-horizontal detachment surface from a lower plate that has been ductilely thinned and stretched.
Lister and Davis (1989)	Cordilleran metamorphic core complexes appear to be bodies from the middle crust that have been dragged out from beneath fracturing and extending upper crustal rocks, and exposed beneath shallow-dipping (normal slip) faults of large areal extent.
Buck (1991)	Core complexes are areas in which high-grade metamorphic rocks originating in the middle to lower crust are exposed at the surface, surrounded and overlain by lower-grade rocks [see Coney, 1980].
Whitney et al. (2013)	A core complex is a domal or arched geologic structure composed of ductilely deformed rocks and associated intrusions underlying a ductile-to-brittle high-strain zone that experienced tens of kilometers of normal-sense displacement in response to lithospheric extension.
Platt et al. (2015)	A metamorphic core complex comprises three essential elements […]. From bottom to top these are as follows. (1) A core of metamorphic rock, commonly 10 km or more across, affected by ductile deformation and associated metamorphic recrystallization, and derived from the mid-crust or deeper. (2) The metamorphic core is overlain by a regionally gently dipping to subhorizontal tectonic discontinuity, commonly referred to as a detachment, comprising a discrete brittle fault surface, several metres to tens of metres of cataclastic rocks in its immediate footwall, underlain in turn by a zone of ductile mylonite and ultramylonite, which may be hundreds to thousands of metres in thickness, grading downwards into the main metamorphic core (Davis et al. 1980, 2004). (3) The detachment is overlain by hanging-wall rocks that are either unmetamorphosed or of significantly lower grade than the metamorphic core, and that are commonly strongly disrupted and attenuated by normal faulting. The detachment places upper crustal rocks against metamorphic or plutonic rocks exhumed from beneath the BDT [brittle-ductile transition], and hence produces vertical thinning and horizontal extension. It is now universally accepted that MCCs are the product of a distinctive style of extensional tectonics.
Brun et al. (2018)	MCC correspond to dome shaped structures inside which deep crust or mantle rocks, mylonitized at least at their top, are separated from lower-grade or non-metamorphosed rocks seated above by a shallow-dipping extensional detachment zone.

We suggest a generic definition of MCCs that is illustrated in Fig. 5.

Metamorphic core complexes are kilometer-scale geological structures that form through localized thinning of brittle crust associated with exhumation of ductile crust. They comprise the following features (from bottom to top):

(1) A dome-shaped or arched core of metamorphic rocks (± migmatites ± plutonic rocks) that were ductilely flowing (± emplaced) during formation of the structure.

(2) Overlying the core, a large-magnitude shallow-dipping extensional high-strain zone (detachment zone), which gives evidence for ductile and brittle deformation during formation of the structure. The detachment zone consists commonly of a brittle fault zone on top of mylonitic rocks.

(3) On top of the detachment zone, a distended upper plate that was significantly lower grade than the core during formation of the structure. This may include syntectonic sediments.

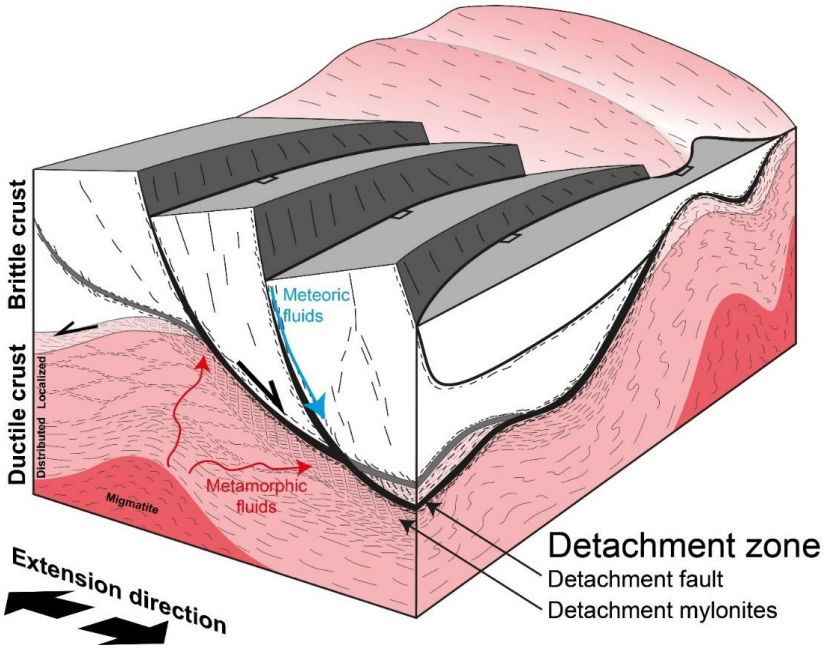

Fig. 5: Schematic illustration showing key elements of an MCC.

The characteristic parts of MCCs are described in detail by Whitney et al. (2013) and Platt et al. (2015). A few additional remarks on our definition:

I) To constrain an MCC, it is critical to establish the synchronicity of upper plate thinning, detachment formation and footwall ductile flow.

II) Upper crustal thinning can result from plate divergence and convergence, including gravitational collapse/lateral escape and focused erosion. In syn-convergent settings, it can be difficult to distinguish whether lower plate shortening or upper plate extension are cause or effect.

III) In an ideal MCC, upper crustal thinning is entirely compensated by viscous crustal flow so that the Moho remains flat (Block and Royden, 1990).

IV) MCCs form commonly in areas or preceding crustal thickening (see below). The effects of contractional and extensional tectonics are often controversial. In many cases, MCCs comprise different units assembled during convergence, which can end up in different parts of the MCC:

   a. If metamorphism and cooling precede MCC formation, high-grade metamorphic rocks can become part of the upper plate. This would be documented by pre-MCC mineral ages.
   b. Lithologies that are particularly weak (e.g. schists) are predestined to become part of the detachment zones.
   c. Syn-MCC metamorphism and ductile behavior makes candidates for the lower plate.
   d. In the dynamic evolution of an MCC, the same unit can go through different stages. Through progressive exhumation, cooling and embrittlement, originally ductile material can become part of the detachment or hanging wall.

V) The detachment zone commonly represents a barrier (Fig. 5) between meteoric and metamorphic fluid regimes (Siebenaller et al., 2012; Whitney et al., 2013). This might be important for isotopic homogenization.

VI) Depending on the erosion level, not all parts of the MCC must be exposed.

1.2.3 Models and Conditions of MCC Formation

Since their discovery, various models have been proposed to explain the development of MCCs and detachments in response to large-magnitude continental extension (see review by Brun et al., 2018). The first conceptual models focused on explaining the basement uplifts (Davis and Coney, 1979), while successive field-based and analytical models addressed the formation, mechanics and isostasy of low-angle normal faults (Buck, 1988; Lister and Davis, 1989; Spencer, 1984; Wernicke and Axen, 1988). Analogue and numerical models provided a different perspective and established MCCs as the result of intra-crustal boudinage, where viscous flow isostatically compensates localized thinning of the upper plate (Block and Royden, 1990; Brun and Van den Driessche, 1994; Tirel et al., 2004; Tirel et al., 2008; Tirel et al., 2006). In essence, MCCs portray non-uniform stretching of a rheologically layered crust resulting in exhumation of previously ductile material. This idea implies that their formation depends on the viscosity of the ductile crust and does not necessarily require a low-density anomaly (see dome-forming mechanisms below).

In contrast to narrow rifts (whole-crust necking) and wide rifts (no localization), intra-crustal necking is a prerequisite for exhuming the ductile crust (Brun et al., 2018). Therefore, the formation of MCCs requires a large volume of low-viscosity crustal material, which can flow efficiently, and a high intra-crustal strength contrast (Labrousse et al., 2016; Wijns et al., 2005). Elevated Moho temperatures (Tirel et al., 2008), overthickened lithospheres, low strain-rates (Tirel et al., 2006), inherited rheological layering due to nappe-stacking (Huet et al., 2011), partial melting (Schenker et al., 2012), metamorphic reactions and fluids (Mezri et al., 2015) facilitate MCC formation. While the intra-crustal strength contrast is important to initiate intra-crustal necking, a strong (thick) brittle crust can prevent localization on a single large-magnitude detachment (Lavier and Buck, 2002). Therefore, hydrothermal circulation, fault-weakening chemo-mechanical processes (Grasemann and Tschegg, 2012) and ductile-brittle energy feedbacks (Regenauer-Lieb et al., 2006) need to be considered.

The idea of MCCs might be simple (Tirel et al., 2008), but their unambiguous identification is not. As their formation requires specific conditions, it is a key constraint for tectonic reconstructions. The role and mechanics of low-angle normal faults remain a widely debated issue (Axen, 2007).

1.2.4 MCC Types and Core-Complex Dynamics

The MCC paradigm promotes the comparison of field structures and geodynamic models, to relate MCC features to generic parameters (Fig. 6). The **rocks in the metamorphic core** (Fig. 6A) can be entirely **solid-state** or contain a second **melt** phase, which has significantly lower viscosity (Rosenberg and Handy, 2005). Furthermore, **localized** and **distributed** types can be distinguished in both cases. While core rocks represent to some extent the geological setting and the pre-MCC history, they are also a function of temperature, extension rate, melting reactions and strain-weakening mechanisms (Rey et al., 2009a, b; Rosenbaum et al., 2005).

Asymmetric MCCs have only **one major detachment**, some have an **antithetic detachment**, while **symmetric** MCCs have two **bivergent detachments** of equal magnitude (Fig. 6B). Detachment (a)symmetry can relate to laterally variable boundary conditions, the finite amount of extension, structural inheritance or buoyancy of the core due to melting (Rey et al., 2009a).

The **3D geometries** of MCCs (Fig. 6C) reflect kinematic boundary conditions (Le Pourhiet et al., 2012). End members are elongated domes in **extension-perpendicular (b-type)** and **extension-parallel (a-type)** direction (Jolivet et al., 2004). A-type domes are bound by strike-slip detachment segments and host contractional structures (upright folds) formed by transtensional boundary conditions (Le Pourhiet et al., 2012; Rey et al., 2017).

The distinction of **dome-forming mechanisms** (Fig. 6D) is mostly of theoretical nature, yet highly illustrative and indispensable to understand MCCs (Kruckenberg et al., 2011). Followers of Ramsay (1967) consider most domes as the product of **refolding** around perpendicular sets of fold axes. The characteristic of fold interference is that if affects all layers in an area (Fig. 6D), while second order

variations relate to competence contrasts between layers. Also folding in a constrictional strain field (Fossen et al., 2013) and necking instabilities (Schmalholz and Mancktelow, 2016) can result in domal and basinal geometries. **Density-driven, buoyancy-dominated flow** (Rayleigh-Taylor instabilities) includes diapirism or crustal convection (Kruckenberg et al., 2011; Ramberg, 1981). The buoyancy of low-density material drives mainly vertical movements, which are independent of the regional kinematic boundary conditions. Dense mantling units are folded into pinched synclines (Fig. 6D), resulting in classical mantled gneiss dome structures (Brun et al., 1981; Eskola, 1948; Whitney et al., 2004).

Isostasy-dominated flow of low-viscosity material, on the other hand, is driven by **pressure gradients** induced by tectonics or surface processes (Block and Royden, 1990; Kruckenberg et al., 2011). Upper crustal extension, for example, can drive convergent flow of low-viscosity material in the deep crust (Brun et al., 2018; Rey et al., 2001; Rey et al., 2017; Rey et al., 2011; Rey et al., 2009b; Tirel et al., 2004; Tirel et al., 2008). Isostasy-dominated flow includes horizontal and vertical components depending on the orientation of gradients in gravitational potential energy (Rey et al., 2001). Pressure-driven flow is controlled by the viscosity of the flowing medium and therefore does <u>not</u> require density contrasts, as sometimes mistakenly assumed. In nature, low-viscosity materials have commonly (but not necessarily) lower densities (particularly in the case of partial melting), obscuring differences between buoyancy- and isostasy-driven flow. If extension creates space, however, buoyancy plays a subordinate role for migmatite domes (Rey et al., 2009a) and core-complex dynamics are controlled by isostasy-dominated flow.

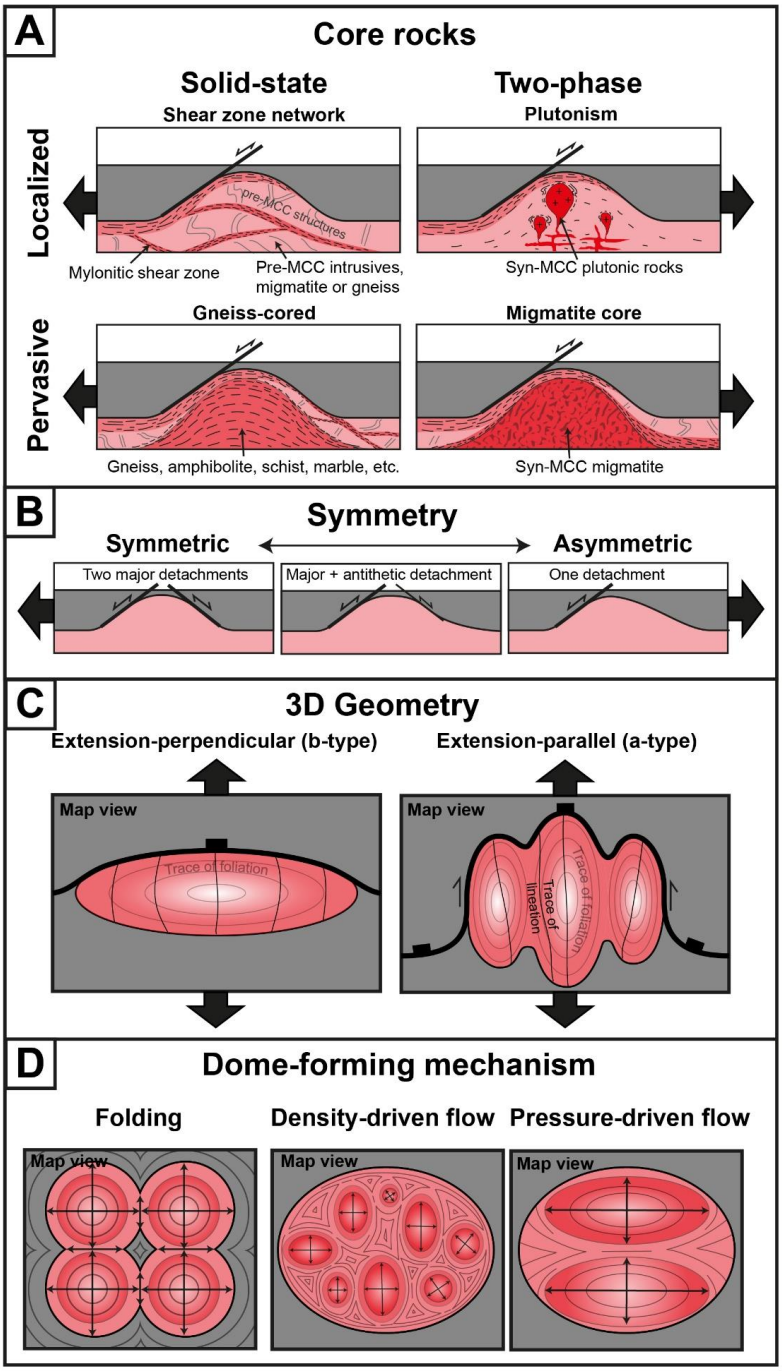

Fig. 6: Classification of MCCs based on: A: core rocks; B: symmetry; C: 3D geometry (based on Jolivet et al., 2004); D: dome-forming mechanism (based on Kruckenberg et al., 2011).

1.2.5 Core Complexes and Geodynamics

Continental extension

The rheological (and thermal) properties of an extending continental lithosphere determine three end-members of continental extension: the MCC, wide rift and narrow rift modes. As these properties are subject to change, the same area can pass through different modes in a progressive temporal evolution, as exemplified by the classical Basin and Range province (Buck, 1991). The MCC mode, typical for post-orogenic extension of thick and hot lithospheres, differs from wide rift mode through a high intra-crustal strength contrast, while lithosphere-scale necking leads to narrow rifting and continental break up (Brun et al., 2018). An important difference between (narrow) rift and MCC mode is the density of the ductile material (Fig. 7). In the case of rifting, ductilely flowing mantle replaces lower-density crustal material. In consequence, rift basins subside and can accumulate large amounts of sediments (McKenzie, 1978). In the MCC mode, on the other hand, the flowing crustal material has the same (or in case of melting even lower) density than the extended brittle crust. Hence, no topographic low develops in the area of upper crustal thinning, rather, crustal flow and sediments compete for accommodation space (Teyssier et al., 2018). Because of the inertia of crustal flow, initially developing sedimentary basins can be displaced by rising metamorphic domes and will be restricted to their flanks (Kapp et al., 2008; Le Pourhiet et al., 2012; Osmundsen and Péron-Pinvidic, 2018).

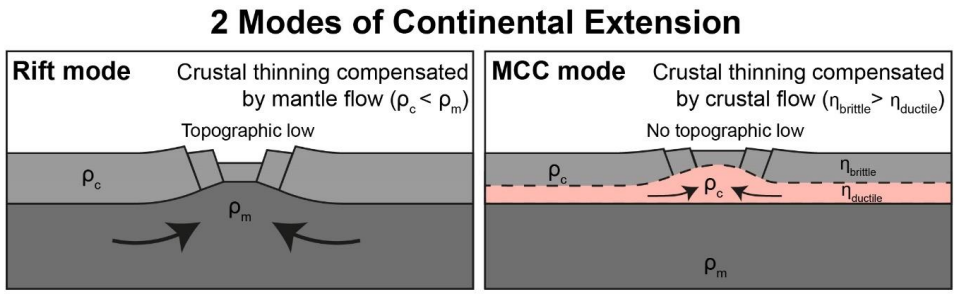

Fig. 7: Contrasting topographic evolutions of extended continents due to contrasting densities of the flowing material in rift mode and MCC mode.

Continental vs. oceanic extension

Research on MCCs has greatly contributed to understand processes at slow spreading ridges and passive margins (Whitney et al., 2013). Brun et al. (2018) point out that oceanic core complexes, magma-poor passive margins and continental metamorphic core complexes can be seen as a spectrum of structures and processes (Fig. 8). The difference between the different types is the nature of the lithosphere (oceanic vs. continental) and the ductilely flowing material that is exhumed in the core (crust vs. mantle). Passive margin core complexes represent an intermediate case, with successive stages of crustal flow and whole-crust necking (Peron-Pinvidic et al., 2013). However, such structures must be discerned from pre-existing MCCs that formed during previous tectonic phases such as post-orogenic collapse (Osmundsen and Péron-Pinvidic, 2018).

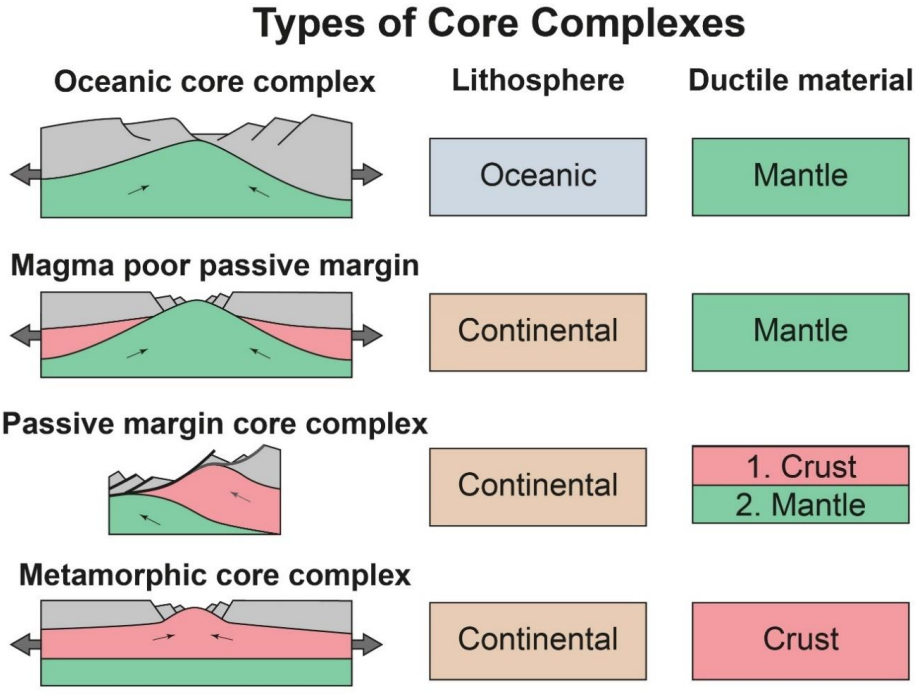

Fig. 8: Types of core complexes, modified from Brun et al. (2018) and Osmundsen and Péron-Pinvidic (2018).

1.3 Tectonic Setting of W Norway – Intersecting Orogens and Extensional Provinces

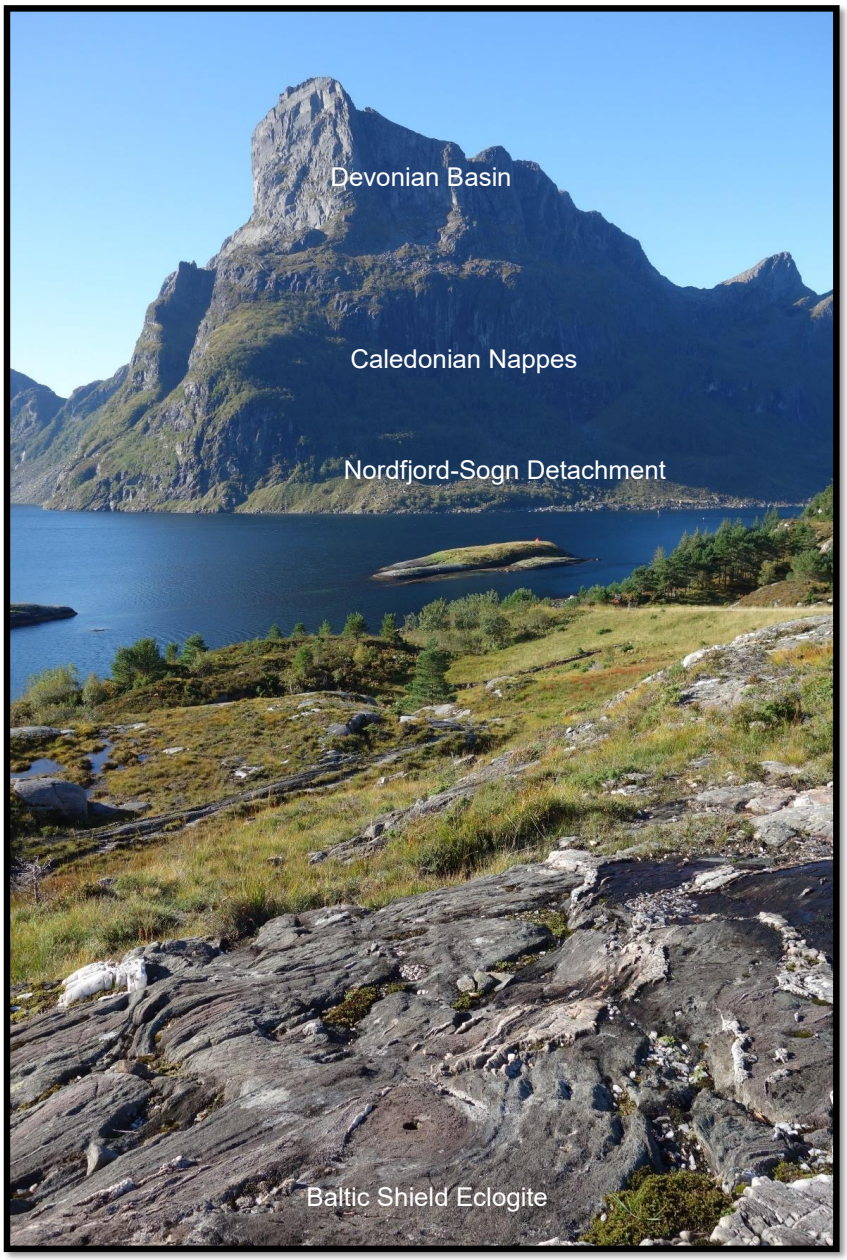

Earth history condensed into 860 vertical meters of the Hornelen cliff (view towards west).

The tectonic history of West Norway (Fig. 9) comprises two major orogenies and a long history of extensional events, uplift and erosion. This makes it an ideal natural laboratory for the behavior of orogenic infrastructures in contrasting tectonic settings.

The ~1.2 – 0.9 Ga **Sveconorwegian orogeny** (Fig. 9a) assembled various older crustal blocks and built the main crustal architecture of the western Baltic Shield (Bingen et al., 2008b; Bingen et al., 2005). The orogeny is part of Grenvillian orogenic activity leading to Rodinia assembly (Cawood and Pisarevsky, 2017; Li et al., 2008). However, it is controversially argued whether the Sveconorwegian orogen represents continent collision or an active margin (Möller et al., 2015; Möller et al., 2013; Slagstad et al., 2013). Besides its long duration, this orogenic period is marked by multiple contractional and extensional phases (Bingen and Viola, 2018; Spencer et al., 2014), voluminous magmatism and (ultra-)high-temperature metamorphism (Bingen and Solli, 2009; Coint et al., 2015; Roberts and Slagstad, 2015; Slagstad et al., 2018; Vander Auwera et al., 2003). Break-up of Rodinia at the end of the Proterozoic opened the Iapetus ocean and formed a **rifted margin** (Fig. 9b) with magma-rich/-poor and hyperextended segments (Andersen et al., 2012; Jakob et al., 2019; Kjøll et al., 2019). The Sveconorwegian infrastructure was uplifted, deeply eroded and transgressed (Gee et al., 2008; Slama and Pedersen, 2015).

During the Silurian-Devonian **Caledonian orogeny** (Fig. 9c), Baltica "soft-docked" with Avalonia before it collided with Laurentia (Fossen et al., 2017; Gee, 1975; Gee et al., 2008; Roberts, 2003; Torsvik, 2019). The Baltican margin was subducted to mantle depth, while a large pile of nappes was thrust onto the Baltic Shield. The nappe pile contains rifted fragments of the Baltic Shield, remnants of the former Iapetus ocean and parts of the overriding Laurentian plate (Jakob et al., 2019). **Devonian post-orogenic collapse** (Fig. 9d) overprinted large parts of the Caledonian orogen (Fossen, 2010). Extensional detachments and associated supra-detachment basins formed in a regime of sinistral transtension while the Baltican basement was exhumed in large windows (Krabbendam and Dewey, 1998; Osmundsen et al., 2005). Multiple phases of **Permian-Mesozoic rifting** opened the North Sea, followed by

Paleogene (ca. 55 Ma) **continental break-up** and opening of the North Atlantic (Faleide et al., 2010).

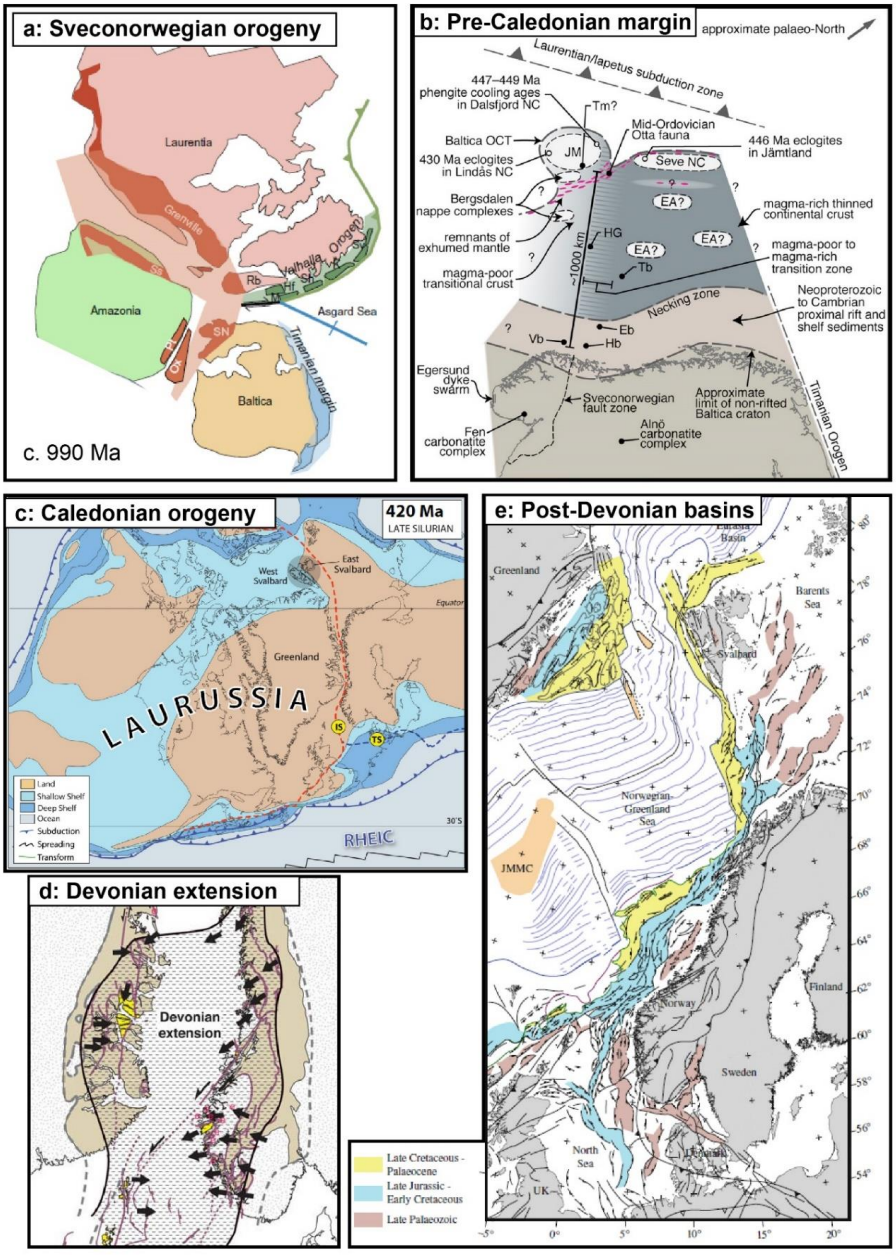

Fig. 9: Snapshots of Norway's tectonic evolution. Modified from: a - Cawood and Pisarevsky (2017), b - Jakob et al. (2019), c - Torsvik (2019), d - Fossen (2010), e - Faleide et al. (2010).

1.3.1 Orogenic Infrastructures

Figure 10 shows a newly compiled tectonic map of southern Norway based on extensive literature review and new results from this study. Large-scale foliation traces were mapped using the digital structural database of bedrock maps by the Norwegian Geological Survey (NGU) with ca. 85,000 measurements in the shown area. Lithological boundaries on bedrock maps, satellite images and topographic maps were consulted where data coverage was sparse or inconclusive. It is noted that foliation traces are non-unique solutions, as there are many ways to connect neighboring data points. The first-order consistency of the foliation-trace interpretation was assessed by comparison with interpolated foliation dip values (Fig. 11), magnetic (Fig. 12) and gravity anomalies (Fig. 13). The combination of foliation traces and dip interpolation allows a systematic comparison of structural domains, however, here it is only used to outline main differences between the Sveconorwegian and Caledonian infrastructures.

The Sveconorwegian Infrastructure

The Sveconorwegian province in southern Norway (Fig. 10) is characterized by mainly NNW – SSE-trending domain boundaries, shallow domes and N-S trending corridors of steep foliations (Fig. 11). Gneiss domes are ubiquitous and commonly cored by late Sveconorwegian magmatic rocks (Barnichon et al., 1999; O'Nions and Baadsgaard, 1971; Smithson, 1965; Sylvester, 1998). Their diameters range from a few to ~50 kilometers (e.g. Rogaland Anorthosite Province). However, also 100-km-scale gneiss domains define shallow domiform geometries. The domes are commonly juxtaposed against supracrustal sequences or large undeformed batholiths (Sirdal Magmatic Belt, Slagstad et al., 2018), yet, many contacts are enigmatic. The timing of high-grade metamorphism in different segments of the Sveconorwegian infrastructure is well documented in some segments (e.g. Bamble, Rogaland), while metamorphic and exhumation histories of large gneiss domains are poorly constrained (Bingen et al., 2008a). Orogen-wide gravitational collapse occurred presumably after 970 Ma (Bingen et al., 2006). Some domains were exhumed below extensional detachments, most of which reactivated previous thrusts (Mulch et al., 2005; Scheiber et al., 2015; Viola et al., 2011). A particularly interesting relationship

is found on the eastern Hardangervidda in the footwall of the Mandal-Ustaoset lineament (marked with MU on Fig. 10). The Kalhovd segment is a E-dipping low-angle ductile-to-brittle fault zone (Sigmond, 1985). In its footwall, E-W oriented (a-type) granite-migmatite-gneiss domes show 1066 ± 14 Ma zircon overgrowth on early Mesoproterozoic to Archean cores (Birkeland et al., 1997). The hanging wall is occupied by an intra-continental basin (Kalhovd Formation) with detrital zircons as young as 1065 ± 11 Ma (Bingen et al., 2003). This situation strongly resembles core-complex/detachment scenarios, which could have important bearings for the tectonic regime of this time, yet, detailed investigations await.

The Caledonian Infrastructure

The Caledonian thrust front (Fig. 10) shows that most of the Sveconorwegian province in South Norway was involved in the Caledonian orogeny, yet, with highly variable effects. Deformational, metamorphic and geochronological evidence for Caledonian overprinting are absent in southernmost Norway, but "Caledonization" increases gradually towards the NW, reflecting Scandian subduction of the Baltican margin (Hacker et al., 2010; Milnes et al., 1997). Allochthons separate the undeformed Baltic Shield from windows exposing variably "caledonized" basement, which is variably considered as allochthon or autochthon (Corfu et al., 2014; Gee et al., 2010). The Caledonian infrastructure consists of basement windows, whose diameters range from 10s to 100s of kilometers. Internally they contain mostly shallow dipping foliations and E-W or NE-SW trending steep zones (Fig. 11). In recent years, the Caledonides have been used as a geochronological test ground, revealing that different geochronometers record a complex relationship between mineral (re-) crystallization, fluid and melt chemistry, and thermal diffusion (e.g. Gasser et al., 2015; Gordon et al., 2016; Hacker et al., 2015; Holder et al., 2015; Kohn et al., 2015; McDonald et al., 2016; Schneider et al., 2008; Spencer et al., 2016; Warren et al., 2012). This study investigates the Øygarden Complex and the Gulen MCC (Fig. 10), which represents the southernmost culmination of the Western Gneiss Region (WGR). Detailed descriptions of the individual windows are given in the research papers.

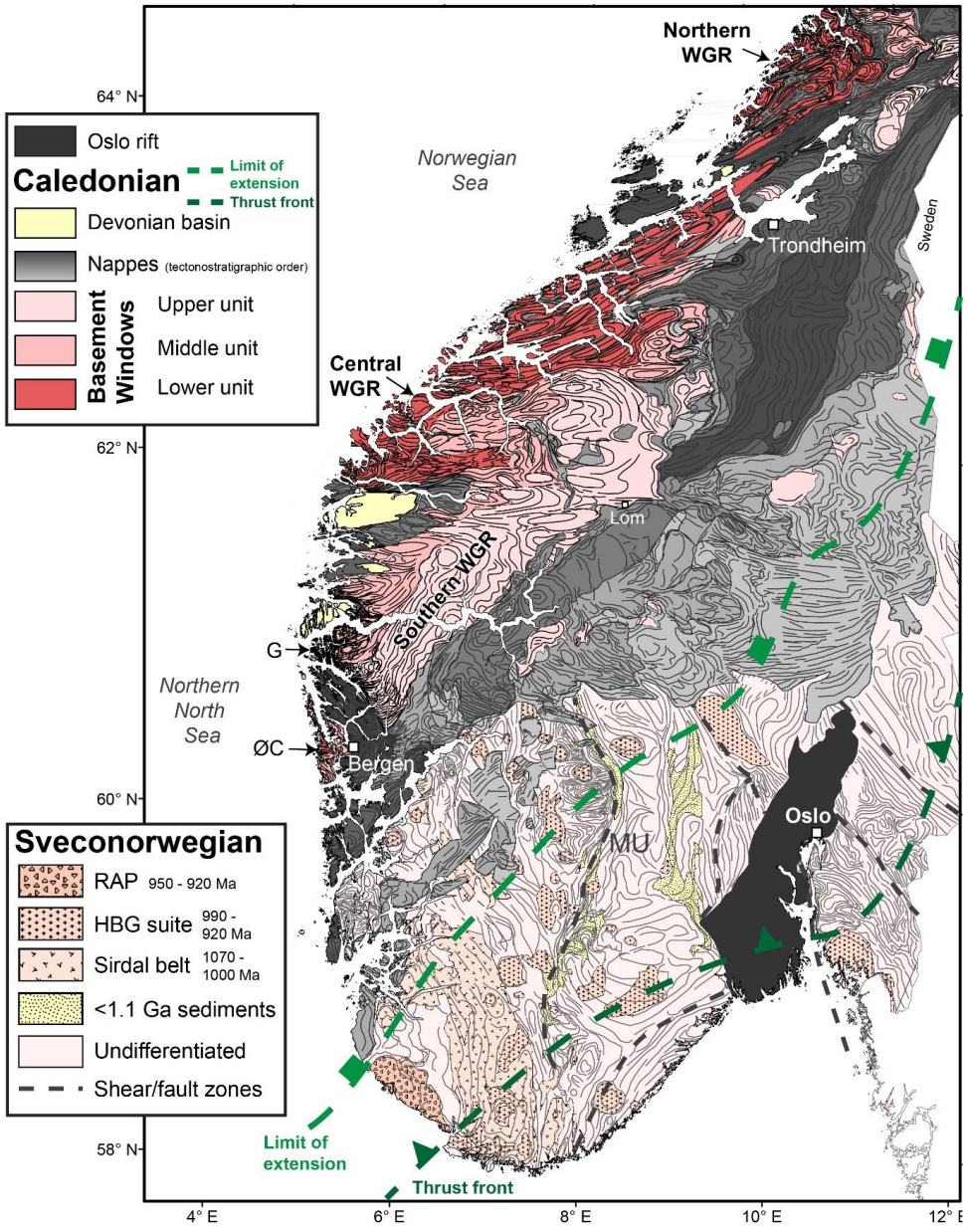

Fig. 10: Tectonic map of southern Norway showing newly interpreted foliation traces in the Caledonian and Sveconorwegian provinces. Sveconorwegian units based on Bingen and Viola (2018) and Slagstad et al. (2018). HBG – Hornblende biotite granites, RAP – Rogaland Anorthosite Province, MU – Mandal-Ustaoset shear/fault zone. Caledonian nappe tectonostratigraphy based on Jakob et al. (2019). Thrust front and limit of post-orogenic extension from Fossen et al. (2017). Main study areas: WGR – Western Gneiss Region, G – Gulen MCC, ØC – Øygarden Complex. See paper 4 for details of the Caledonian province.

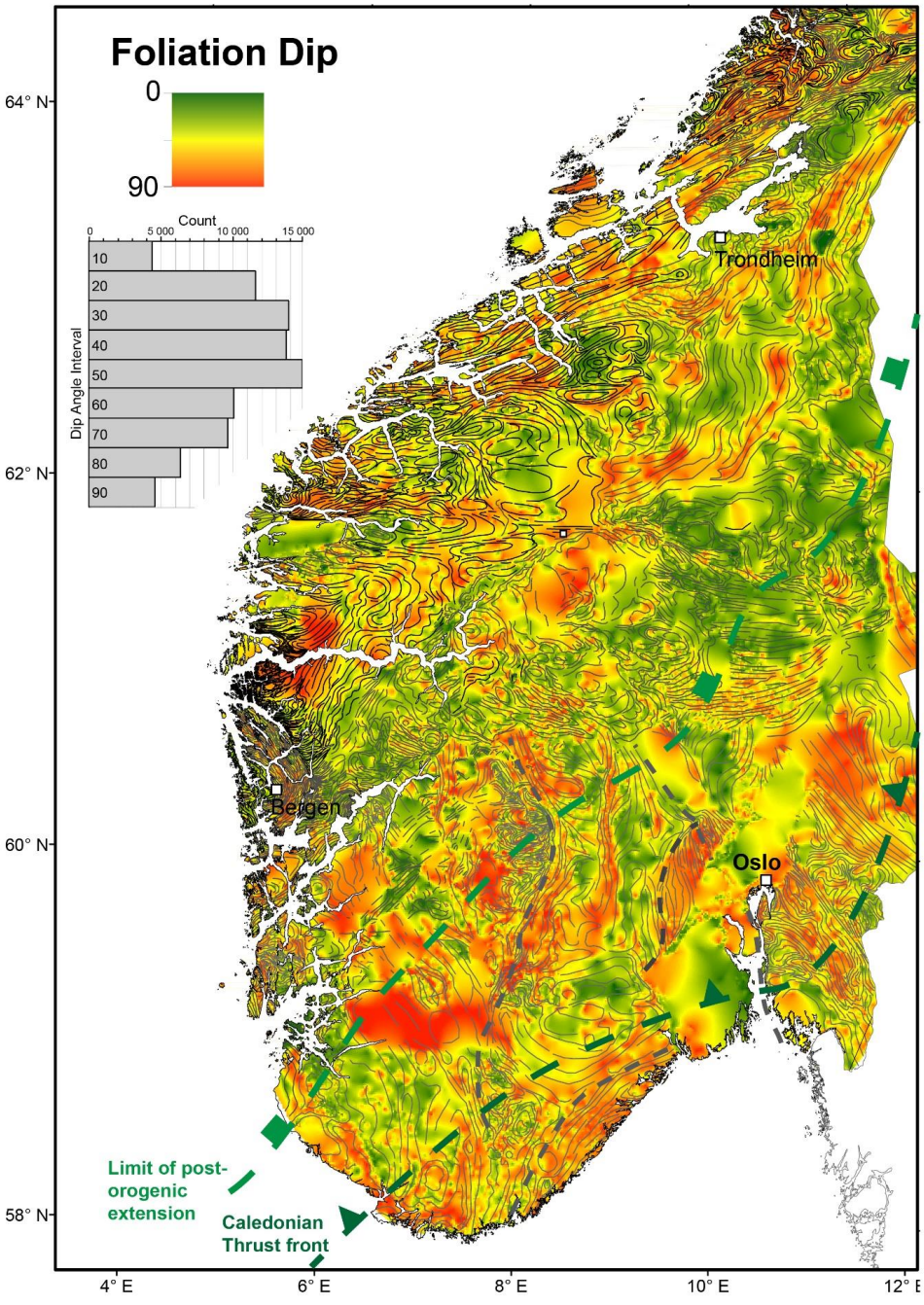

Fig. 11: Nearest-neighbor interpolation of foliation dip values from the digital structural database of NGU bedrock maps (n ≈ 85,000 (see included histogram), 1 km^2 cell size). Lineaments and place names are indicated as reference to unit boundaries in Fig. 10.

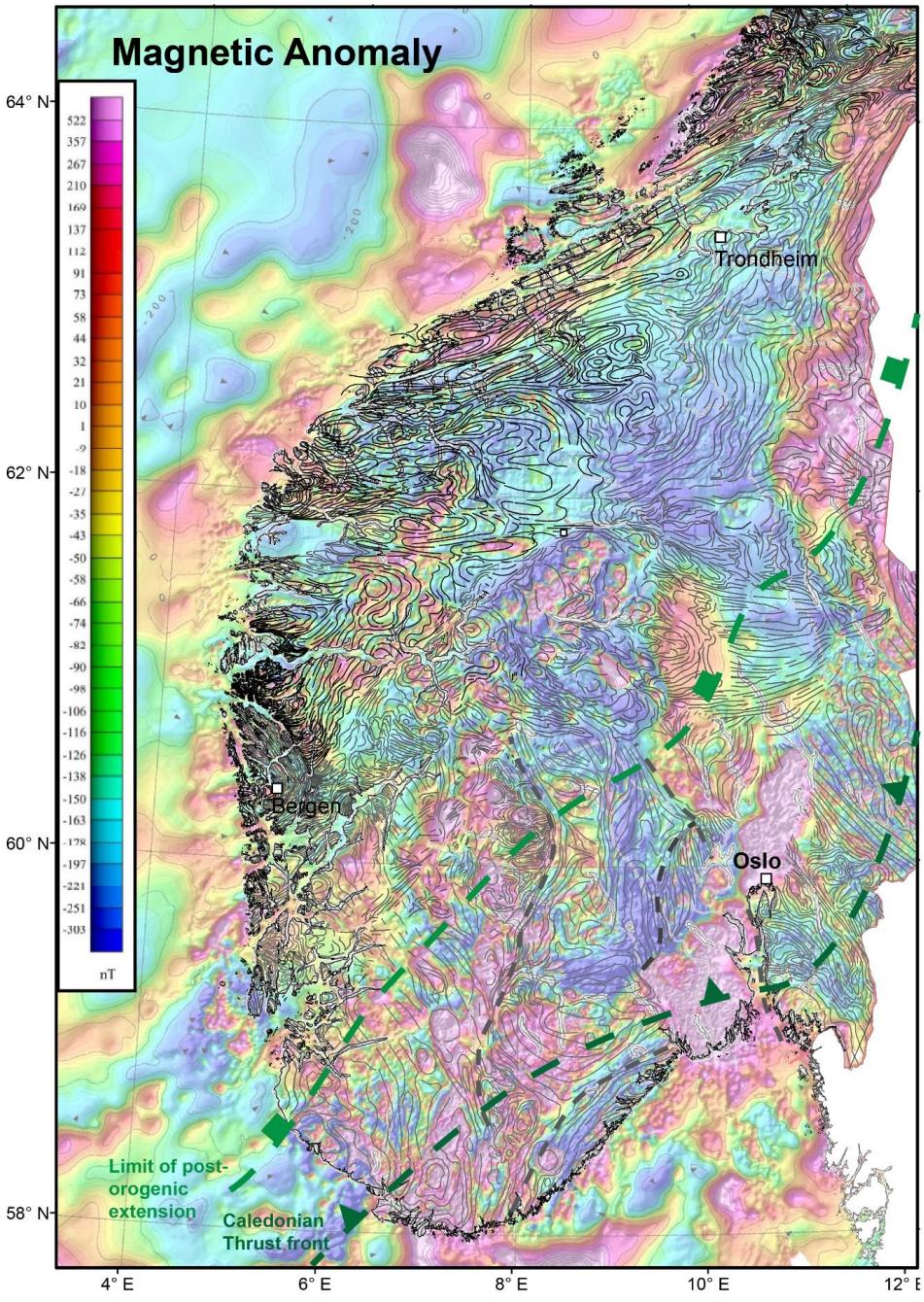

Fig. 12: Foliation-traces overlaying magnetic anomaly map (Olesen et al., 2010b).

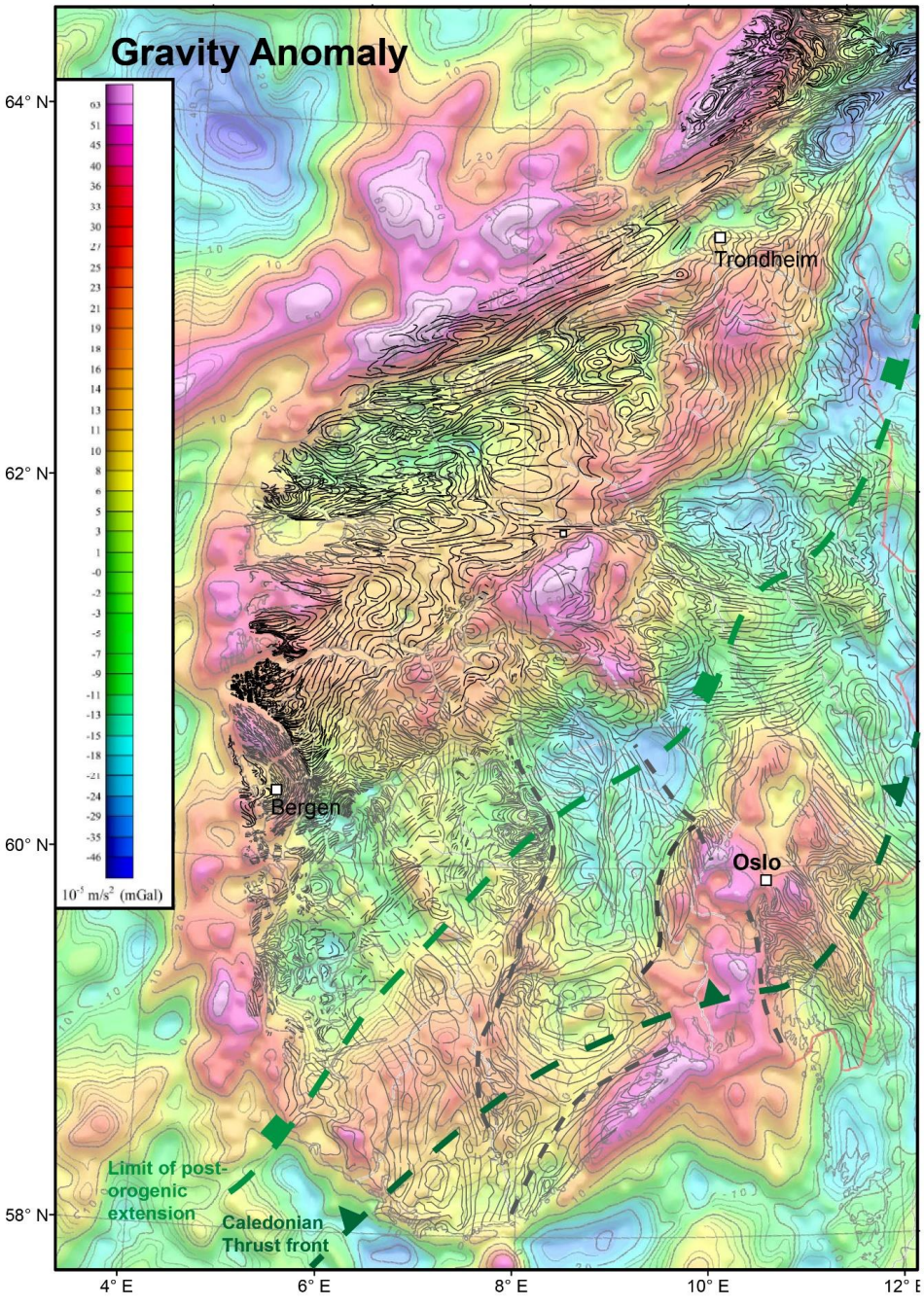

Fig. 13: Foliation-traces overlaying gravity anomaly map (Olesen et al., 2010a).

1.3.2 Few Thoughts on Infrastructure Reactivation

Sveconorwegian domain-bounding shear zones demonstratable influenced formation of the Oslo rift (Sundvoll and Larsen, 1994) and the evolution of the late Proterozoic Baltican margin (Jakob et al., 2019). It seems therefore likely that the pre-existing structural template also affected Caledonian reworking of the Baltic Shield. Besides tabular zones, the Sveconorwegian infrastructure is dominantly characterized by large shallow domes. We can distinguish a number of possible effects of these kinds of structures.

I) As argued in Paper 5 below, the combination of crystalline cores and weak bounding fault/shear zones or mantling units makes domes predestined to form structural highs during rifting. During subsequent convergence, these isolated highs are vulnerable to be turned into nappes (see Eskola (1948) for examples from the Alps). Slagstad et al. (2019) presented such a model for the Jotun/Lindås Nappes based on comparison with the Rogaland anorthosite province.

II) If domes are associated with low-density granitic intrusions, they can induce gravitational instabilities into the overthickened orogenic wedge (Cooper and Bradshaw, 1980).

III) Pre-existing domal geometries at layer boundaries can induce necking instabilities (Schmalholz and Mancktelow, 2016) leading to dome amplification.

The combination of II) and III) suggests that inherited Sveconorwegian basement domes may have influenced the locations and sizes of Caledonian basement windows.

2. Synthesis and Outlook

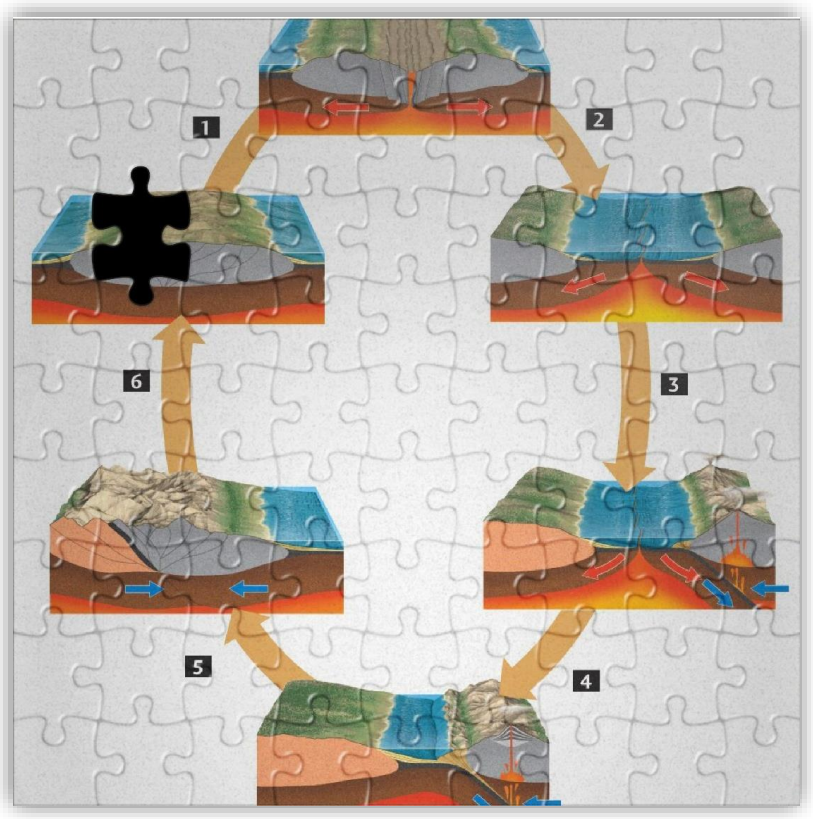

Geology can be puzzling.

Image modified from: https://geology-fundamentals.fandom.com/wiki/4244396/wilson-cycle

2.1 Insights from the Caledonian Infrastructure

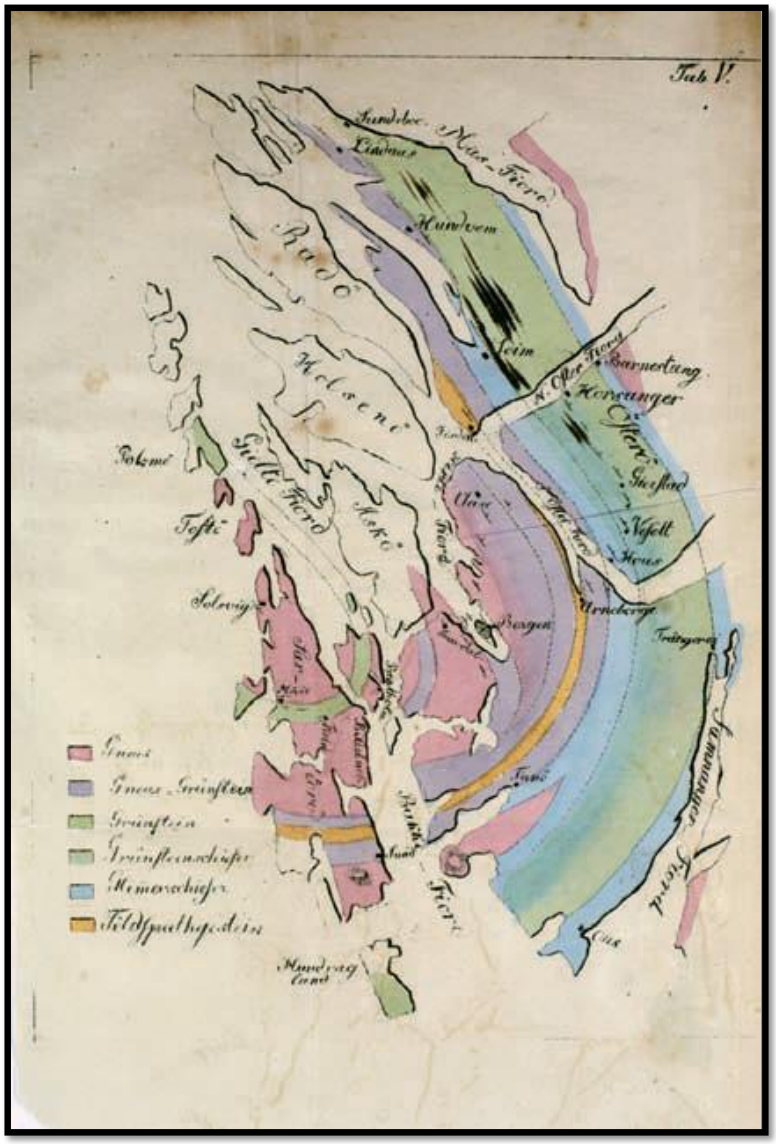

First geological map of the Bergen area from C.F. Naumann, 1824

We have found Sveconorwegian rocks in basement windows of West Norway that were deformed during the Caledonian orogeny. The before and after comparison with genetically related, but undeformed equivalents in South Norway allows to precisely constrain reworking of continental crust in the root zone of a large collisional orogen. The recognition of domal structures and ductile-to-brittle shear zones directed investigation of MCC exhumation models. The MCC paradigm transformed gneiss domains, which previously got little scientific attention, into interesting subjects of research. The Gulen MCC, for example, turned out to be more than a gneissic antiform. In fact, it contains an excellently exposed record of deformation processes and kinematics from different levels of the crust. Similarly to the Tonale fault zone (Stipp et al., 2002), the Øygarden Complex can be considered as a natural laboratory for crustal deformation. In the latter case, continuous high-quality exposures allowed us to constrain weakening-feedbacks in the exhuming ductile crust, which may play a fundamental role for detachment formation. The MCC paradigm was invaluable in searching and finding Caledonian migmatites in this part of the basement, which was previously unexpected. Furthermore, it provides a genetic framework for different types of shear zones, which can clearly improve our understanding of their brittle reactivation during rifting (Paper 5).

Paper 4 provides a regional synthesis of our findings and their extrapolation to larger parts of the orogen. We found that the Caledonian infrastructure underwent drastic rheological changes during orogenic evolution and, therefore, played distinct roles at different stages. During post-orogenic collapse, the state of the infrastructure was highly variable, both across- and along-strike of the orogen. Depending on the segment of the orogen, variable metamorphic and deformational gradients distinguished the foreland from the hinterland. The segmentation across orogen-scale transfer zones appears as a first-order feature in the evolution of the Caledonian orogen. Yet, to resolve the contrasting roles of structural inheritance and dynamic instabilities, we first need to better constrain the role of each segment at different stages of orogenic evolution. Just alone extensional collapse was certainly more complex than presented in our models. Hypothetically, convergent and divergent gravitational collapse (*sensu* Rey et al., 2001) may have occurred simultaneously

depending on the gravitational potential of each segment. In the case of excess gravitational potential, gravity indeed could have driven thrusting at least in parts of the foreland (Andersen and Jamtveit, 1990; Eskola, 1948; Ramberg, 1981). Another uncertainty in our model is the role of syn-contractional doming, e.g. due to orogen-parallel lateral extrusion (Braathen et al., 2002; Kirkland et al., 2006). To address this issue, we need to systematically constrain kinematics, conditions and timing of infrastructure deformation along the entire length of the Scandinavian Caledonides. New insights from basement windows in North Norway (Braathen et al., 2018; Froitzheim et al., 2016; Steltenpohl et al., 2011) require updated investigations to constrain their relation to the structures in southern Norway. Further synthesis with the Greenland Caledonides (Andresen et al., 1998; Andresen et al., 2007; Gilotti et al., 2014; Hartz and Andresen, 1997; Hodges, 2016; Johnston et al., 2010; McClelland and Gilotti, 2003; White et al., 2002) and the orogenic evolution of the Appalachians (Steltenpohl et al., 2013) would certainly enhance our understanding of the orogenic system as a whole.

Looking back at contrasting views on the orogenic infrastructure in the research history of the Scandinavian Caledonides (compare Gee, 1975; Hurich et al., 1989; Krill, 1985; Krill and Griffin, 1981; Wegmann, 1935), it seems that all sides were right in some aspects, while each position had also its limitations. Since research focus has shifted from regional field mapping campaigns to detailed, process-oriented investigations, however, the old field descriptions are indispensable documentations that should be acknowledged and guide modern research. For example, Eskola (1948 pp. 472 - 473) summarized a section through the northern Scandinavian Caledonides (Stora Lulevattnet – Ofoten area) by Kautsky (1946), which gives a remarkable complete picture of Caledonian tectonic evolution and asks to be tested with modern methods.

2.2 Temporal-Spatial Evolution of Orogenic Infrastructures

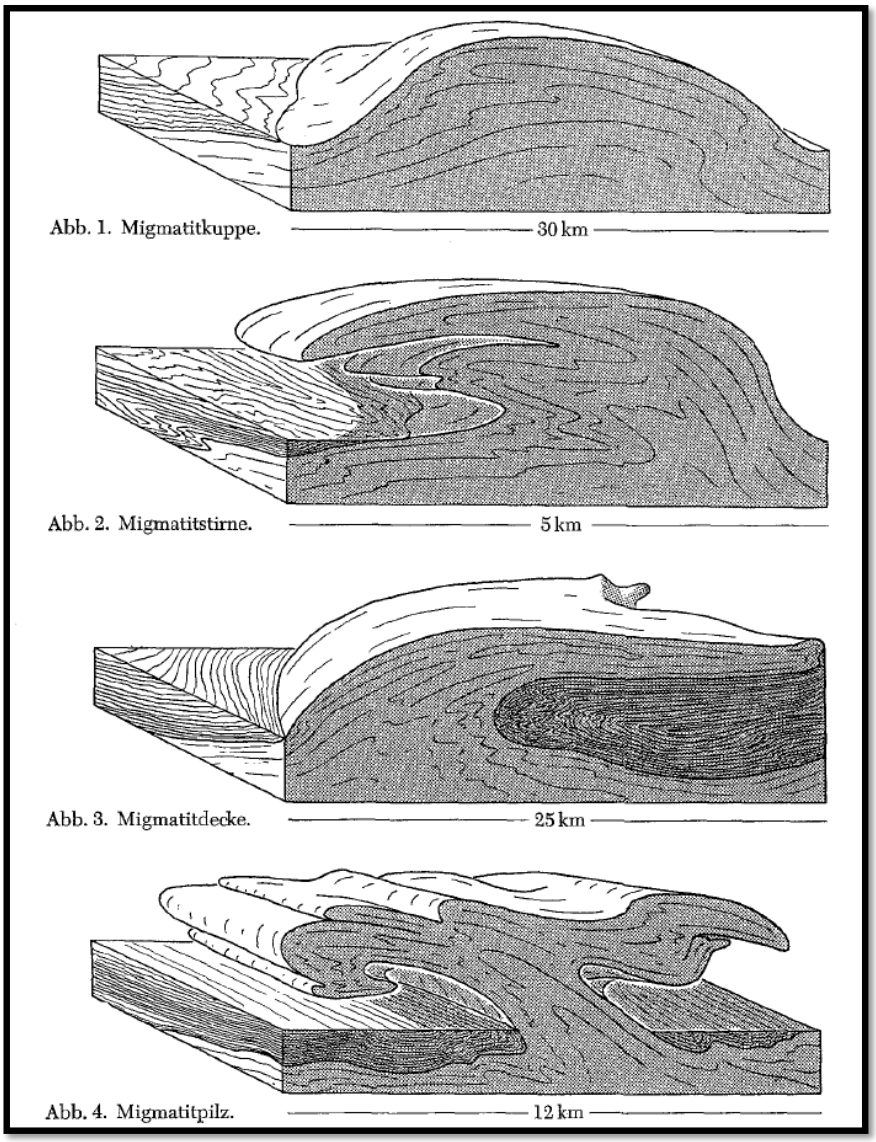

Schematic sketches of 3D shapes observed in the infrastructure of the Greenland Caledonides. From Haller (1956).

The temporal evolution of the rheological state of the lithosphere is now widely appreciated in the dynamics of convergent (Vanderhaeghe, 2012) and divergent tectonic systems (Buck, 1991). Our insights from the Scandinavian Caledonides fit well in the quantitative framework of the orogenic main sequence (Beaumont et al., 2006; Jamieson and Beaumont, 2013), while highlighting the importance of post-convergent collapse. We argue that most of the ductile structures we find "frozen" inside orogenic infrastructures formed during the last phase of orogenic evolution and overprinted or even entirely annealed previous features. This implies that our understanding of orogenic collapse largely determines the successful reconstruction of earlier and subsequent tectonic phases.

Besides the temporal evolution, the main insight from this study is the spatial variability of infrastructure deformation. Major recent orogens, for example the Andes (Jordan et al., 1983; Riller and Oncken, 2003), the Alps (Lacombe and Mouthereau, 2002; Ratschbacher et al., 1991a), and the Himalayas (Hubbard et al., 2016; Royden et al., 1997; van der Beek et al., 2016) show significant along-strike tectonic segmentation, influencing topography, surface processes and climate. Similarly, along-strike segmentation is common in ancient orogens (Slagstad et al., 2017), subduction zones (Faccenna et al., 2004; Jolivet et al., 2015; Saleeby, 2003), passive margins (Osmundsen and Péron-Pinvidic, 2018; Péron-Pinvidic et al., 2017) and mid-oceanic ridges (Carbotte et al., 2016; Macdonald et al., 1988).

In contrast to the temporal evolution of orogens, however, there is yet no general framework for their 3D evolution. Even in the case of inherently three-dimensional structures, such as domes and MCCs, there is a surprisingly small number of studies that focus on their 3D nature (e.g. Jolivet et al., 2004; Kruckenberg et al., 2011; Le Pourhiet et al., 2012; Osmundsen et al., 2005; Rey et al., 2017). Of course, it is challenging to visualize, draw and model three dimensions, but to rely on 2D approaches assuming cylindricality, fundamentally hampers our understanding of orogen dynamics. This might be one of the reasons for the unresolved origin of infrastructure domes. Most constraints are inconclusive and can be reconciled with contraction as well as extension. In the end, the tectonic model depends on the

interpreted lithosphere-scale 3D kinematic boundary conditions. The Caledonides appear to be a rare case where evidence speaks quite clearly for plate divergence during most of the Devonian (Fossen, 2010). In other cases, especially in areas of active convergence, the origin of domes remains much more ambiguous. Maybe, the distinction of contraction and extension as driving force is not that important after all. Many long-lasting binary debates in the history of Earth science show that both sides hold part of "the truth" (Rudwick, 2014). In the case of domes in orogens, it seems that only contraction provides the conditions for doming, while only extension (in one direction or the other) provides the necessary space for their exhumation.

2.3 Closing Remarks

Old woman or young woman? Observational bias is inevitable, so why not deal with it?

Image from https://www.researchgate.net/figure/The-optical-illusion-The-Young-Girl-Old-Woman_fig1_233626368

In the history of Earth science, continental tectonic research was not able to provide unambiguous evidence for global geodynamic paradigms (Oreskes, 1999; Trümpy, 2001). Due to its complexity, the geological record of continents could be reconciled with one interpretation or the other. In her analysis, Oreskes (1988) argues that fundamentally different types of evidence distinguished the stubborn rejection of continental drift from the quick acceptance of plate tectonics. Evidences for Wegener's drift theory were mainly **homologies**: "*similarities of patterns and forms based on direct observation of rocks in the field*" (Oreskes, 1988, p. 340), e.g. fossil, stratigraphic or paleoclimatic records. Plate tectonics, on the other hand, was based on de-personalized geophysical measurements.

The focus of modern research on numerical modelling and quantitative analytical techniques may reflect an amplification of this development. However, the gap between micro- to nano-scale constraints and the scale of tectonic plates poses an inevitable challenge. Homologies are difficult to handle within a quantitative framework and will always be biased by the observer's views, opinions and interests. In continental research, homologies still appear as the only mean to fill the gap between the scales of observations and models. In the age of digitalization, we can develop new (semi)quantitative field mapping techniques and integrate big data geology with geophysics to scale our observations. We can compare continental and oceanic tectonics, which seems beneficial for both sides. The oceans provide better geophysical coverage and a simpler system not complicated by repetitive life cycles. If we furthermore accept that observational bias is inevitable, we can develop ways to deal with it. The history of research paradigms and the uncertainty induced by of scientist's gender, status, background, etc. needs to be analyzed through meta-research (e.g. Bond, 2015). Last but not least, we need paradigms that make us go into the field to challenge established ideas. In the end, the real value of a paradigm is found in the questions it raises.

References Cited

Aerden, D. G. A. M., 1998, Tectonic evolution of the Montagne Noire and a possible orogenic model for syncollisional exhumation of deep rocks, Variscan belt, France: Tectonics, v. 17, no. 1, p. 62-79.

Andersen, T. B., Corfu, F., Labrousse, L., and Osmundsen, P. T., 2012, Evidence for hyperextension along the pre-Caledonian margin of Baltica: Journal of the Geological Society, v. 169, no. 5, p. 601-612.

Andersen, T. B., and Jamtveit, B., 1990, Uplift of Deep Crust during Orogenic Extensional Collapse - a Model Based on Field Studies in the Sogn-Sunnfjord Region of Western Norway: Tectonics, v. 9, no. 5, p. 1097-1111.

Anderson, R. E., 1971, Thin Skin Distension in Tertiary Rocks of Southeastern Nevada: Geological Society of America Bulletin, v. 82, no. 1, p. 43-58.

Andresen, A., Hartz, E. H., and Vold, J., 1998, A late orogenic extensional origin for the infracrustal gneiss domes of the East Greenland Caledonides (72–74°N): Tectonophysics, v. 285, no. 3, p. 353-369.

Andresen, A., Rehnström, E. F., and Holte, M., 2007, Evidence for simultaneous contraction and extension at different crustal levels during the Caledonian orogeny in NE Greenland: Journal of the Geological Society, v. 164, no. 4, p. 869-880.

Armstrong, R. L., 1972, Low-Angle (Denudation) Faults, Hinterland of Sevier Orogenic Belt, Eastern Nevada and Western Utah: Geological Society of America Bulletin, v. 83, no. 6, p. 1729-1754.

-, 1982, CORDILLERAN METAMORPHIC CORE COMPLEXES - FROM ARIZONA TO SOUTHERN CANADA: Annual Review of Earth and Planetary Sciences, v. 10, p. 129-154.

Axen, G. J., 2007, Research Focus: Significance of large-displacement, low-angle normal faults: Geology, v. 35, no. 3, p. 287-288.

Barnichon, J. D., Havenith, H., Hoffer, B., Charlier, R., Jongmans, D., and Duchesne, J. C., 1999, The deformation of the Egersund–Ogna anorthosite massif, south Norway: finite-element modelling of diapirism: Tectonophysics, v. 303, no. 1, p. 109-130.

Beaumont, C., Jamieson, R. A., Nguyen, M. H., and Lee, B., 2001, Himalayan tectonics explained by extrusion of a low-viscosity crustal channel coupled to focused surface denudation: Nature, v. 414, no. 6865, p. 738-742.

Beaumont, C., Nguyen, M. H., Jamieson, R. A., and Ellis, S., 2006, Crustal flow modes in large hot orogens: Geological Society, London, Special Publications, v. 268, no. 1, p. 91-145.

Berthé, D., Choukroune, P., and Jegouzo, P., 1979, Orthogneiss, mylonite and non coaxial deformation of granites: the example of the South Armorican Shear Zone: Journal of Structural Geology, v. 1, no. 1, p. 31-42.

Bingen, B., Davis, W. J., Hamilton, M. A., Engvik, A. K., Stein, H. J., Skar, O., and Nordgulen, O., 2008a, Geochronology of high-grade metamorphism in the Sveconorwegian belt, S. Norway: U-Pb, Th-Pb and Re-Os data: Norwegian Journal of Geology, v. 88, no. 1, p. 13-42.

Bingen, B., Nordgulen, O., and Viola, G., 2008b, A four-phase model for the Sveconorwegian orogeny, SW Scandinavia: Norwegian Journal of Geology, v. 88, no. 1, p. 43-72.

Bingen, B., Nordgulen, Ø., Sigmond, E. M. O., Tucker, R., Mansfeld, J., and Högdahl, K., 2003, Relations between 1.19–1.13 Ga continental magmatism, sedimentation and metamorphism, Sveconorwegian province, S Norway: Precambrian Research, v. 124, no. 2, p. 215-241.

Bingen, B., Skar, O., Marker, M., Sigmond, E. M. O., Nordgulen, O., Ragnhildstveit, J., Mansfeld, J., Tucker, R. D., and Liegeois, J. P., 2005, Timing of continental building in the Sveconorwegian orogen, SW Scandinavia: Norwegian Journal of Geology, v. 85, no. 1-2, p. 87-116.

Bingen, B., and Solli, A., 2009, Geochronology of magmatism in the Caledonian and Sveconorwegian belts of Baltica: synopsis for detrital zircon provenance studies: Norwegian Journal of Geology, v. 89, no. 4, p. 267-290.

Bingen, B., Stein, H. J., Bogaerts, M., Bolle, O., and Mansfeld, J., 2006, Molybdenite Re–Os dating constrains gravitational collapse of the Sveconorwegian orogen, SW Scandinavia: Lithos, v. 87, no. 3, p. 328-346.

Bingen, B., and Viola, G., 2018, The early-Sveconorwegian orogeny in southern Norway: Tectonic model involving delamination of the sub-continental lithospheric mantle: Precambrian Research, v. 313, p. 170-204.

Bird, P., 1991, Lateral extrusion of lower crust from under high topography in the isostatic limit: Journal of Geophysical Research: Solid Earth, v. 96, no. B6, p. 10275-10286.

Birkeland, A., Sigmond, E., Whitehouse, M., and Vestin, J., 1997, From archaean to proterozoic on hardangervidda, South Norway: Norges geologiske undersøkelse Bulletin, v. 433, p. 4-5.

Block, L., and Royden, L. H., 1990, Core Complex Geometries and Regional Scale Flow in the Lower Crust: Tectonics, v. 9, no. 4, p. 557-567.

Bond, C. E., 2015, Uncertainty in structural interpretation: Lessons to be learnt: Journal of Structural Geology, v. 74, p. 185-200.

Braathen, A., Osmundsen, P. T., Maher, H., and Ganerød, M., 2018, The Keisarhjelmen detachment records Silurian–Devonian extensional collapse in Northern Svalbard: Terra Nova, v. 30, no. 1, p. 34-39.

Braathen, A., Osmundsen, P. T., Nordgulen, Ø., Roberts, D., and Meyer, G. B., 2002, Orogen-parallel extension of the Caledonides in northern Central Norway: an overview: Norwegian Journal of Geology, v. 82, no. 4, p. 225-241.

Brace, W. F., and Kohlstedt, D. L., 1980, Limits on lithospheric stress imposed by laboratory experiments: Journal of Geophysical Research: Solid Earth, v. 85, no. B11, p. 6248-6252.

Brun, J.-P., Sokoutis, D., Tirel, C., Gueydan, F., Van Den Driessche, J., and Beslier, M.-O., 2018, Crustal versus mantle core complexes: Tectonophysics, v. 746, p. 22-45.

Brun, J. P., Gapais, D., and Le Theoff, B., 1981, The mantled gneiss domes of Kuopio (Finland): Interfering diapirs: Tectonophysics, v. 74, no. 3, p. 283-304.

Brun, J. P., and Van den Driessche, J., 1994, Extensional Gneiss Domes and Detachment Fault Systems - Structure and Kinematics: Bulletin De La Societe Geologique De France, v. 165, no. 6, p. 519-530.
Buck, W. R., 1988, Flexural Rotation of Normal Faults: Tectonics, v. 7, no. 5, p. 959-973.
-, 1991, Modes of Continental Lithospheric Extension: Journal of Geophysical Research-Solid Earth, v. 96, no. B12, p. 20161-20178.
Burchfiel, B. C., and Royden, L. H., 1985, North-south extension within the convergent Himalayan region: Geology, v. 13, no. 10, p. 679-682.
Carbotte, S. M., Smith, D. K., Cannat, M., and Klein, E. M., 2016, Tectonic and magmatic segmentation of the Global Ocean Ridge System: a synthesis of observations: Geological Society, London, Special Publications, v. 420, no. 1, p. 249-295.
Cawood, P. A., and Pisarevsky, S. A., 2017, Laurentia-Baltica-Amazonia relations during Rodinia assembly: Precambrian Research, v. 292, p. 386-397.
Chardon, D., Gapais, D., and Cagnard, F., 2009, Flow of ultra-hot orogens: A view from the Precambrian, clues for the Phanerozoic: Tectonophysics, v. 477, no. 3, p. 105-118.
Chen, Z., Liu, Y., Hodges, K. V., Burchfiel, B. C., Royden, L. H., and Deng, C., 1990, The Kangmar Dome: A Metamorphic Core Complex in Southern Xizang (Tibet): Science, v. 250, no. 4987, p. 1552-1556.
Coint, N., Slagstad, T., Roberts, N. M. W., Marker, M., Rohr, T., and Sorensen, B. E., 2015, The Late Mesoproterozoic Sirdal Magmatic Belt, SW Norway: Relationships between magmatism and metamorphism and implications for Sveconorwegian orogenesis: Precambrian Research, v. 265, p. 57-77.
Coney, P. J., 1980, Cordilleran metamorphic core complexes: An overview: Geological Society of America Memoirs, v. 153, p. 7-31.
Cooper, F. J., Platt, J. P., and Behr, W. M., 2017, Rheological transitions in the middle crust: insights from Cordilleran metamorphic core complexes: Solid Earth, v. 8, no. 1, p. 199-215.
Cooper, M. A., and Bradshaw, R., 1980, The significance of basement gneiss domes in the tectonic evolution of the Salta Region, Norway: Journal of the Geological Society, v. 137, no. 3, p. 231-240.
Corfu, F., Andersen, T., and Gasser, D., 2014, The Scandinavian Caledonides: main features, conceptual advances and critical questions: Geological Society, London, Special Publications, v. 390, no. 1, p. 9-43.
Crittenden, M., Coney, P. J., and Davis, G., 1978, Tectonic Significance of Metamorphic Core Complexes in North-American Cordillera: Geology, v. 6, no. 2, p. 79-80.
Culshaw, N. G., Beaumont, C., and Jamieson, R. A., 2006, The orogenic superstructure-infrastructure concept: Revisited, quantified, and revived: Geology, v. 34, no. 9, p. 733-736.
Davis, G. H., and Coney, P. J., 1979, Geologic development of the Cordilleran metamorphic core complexes: Geology, v. 7, no. 3, p. 120-124.
Eskola, P. E., 1948, The problem of mantled gneiss domes: Quarterly Journal of the Geological Society, v. 104, no. 1-4, p. 461-476.

Faccenna, C., Piromallo, C., Crespo-Blanc, A., Jolivet, L., and Rossetti, F., 2004, Lateral slab deformation and the origin of the western Mediterranean arcs: Tectonics, v. 23, no. 1.

Faleide, J. I., Bjørlykke, K., and Gabrielsen, R. H., 2010, Geology of the Norwegian Continental Shelf, *in* Bjorlykke, K., ed., Petroleum Geoscience: From Sedimentary Environments to Rock Physics: Berlin, Heidelberg, Springer Berlin Heidelberg, p. 467-499.

Fossen, H., 2010, Extensional tectonics in the North Atlantic Caledonides: a regional view: Geological Society, London, Special Publications, v. 335, no. 1, p. 767-793.

Fossen, H., Cavalcante, G. C., and de Almeida, R. P., 2017, Hot Versus Cold Orogenic Behavior: Comparing the Araçuaí-West Congo and the Caledonian Orogens: Tectonics, v. 36, p. 2159– 2178.

Fossen, H., Teyssier, C., and Whitney, D. L., 2013, Transtensional folding: Journal of Structural Geology, v. 56, p. 89-102.

Frisch, W., Dunkl, I., and Kuhlemann, J., 2000, Post-collisional orogen-parallel large-scale extension in the Eastern Alps: Tectonophysics, v. 327, no. 3, p. 239-265.

Froitzheim, N., Miladinova, I., Janák, M., Kullerud, K., Ravna, E. K., Majka, J., Fonseca, R. O. C., Münker, C., and Nagel, T. J., 2016, Devonian subduction and syncollisional exhumation of continental crust in Lofoten, Norway: Geology, v. 44, no. 3, p. 223-226.

Gasser, D., Jeřábek, P., Faber, C., Stünitz, H., Menegon, L., Corfu, F., Erambert, M., and Whitehouse, M. J., 2015, Behaviour of geochronometers and timing of metamorphic reactions during deformation at lower crustal conditions: phase equilibrium modelling and U–Pb dating of zircon, monazite, rutile and titanite from the Kalak Nappe Complex, northern Norway: Journal of Metamorphic Geology, v. 33, no. 5, p. 513-534.

Gee, D. G., 1975, A tectonic model for the central part of the Scandinavian Caledonides: American Journal of Science, v. 275A, p. 468-515.

Gee, D. G., Fossen, H., Henriksen, N., and Higgins, A. K., 2008, From the early Paleozoic platforms of Baltica and Laurentia to the Caledonide orogen of Scandinavia and Greenland: Episodes, v. 31, no. 1, p. 44-51.

Gee, D. G., Juhlin, C., Pascal, C., and Robinson, P., 2010, Collisional Orogeny in the Scandinavian Caledonides (COSC): GFF, v. 132, no. 1, p. 29-44.

Gerya, T., 2014, Precambrian geodynamics: Concepts and models: Gondwana Research, v. 25, no. 2, p. 442-463.

Gilotti, J. A., McClelland, W. C., and Wooden, J. L., 2014, Zircon captures exhumation of an ultrahigh-pressure terrane, North-East Greenland Caledonides: Gondwana Research, v. 25, no. 1, p. 235-256.

Gordon, S. M., Whitney, D. L., Teyssier, C., Fossen, H., and Kylander-Clark, A., 2016, Geochronology and geochemistry of zircon from the northern Western Gneiss Region: Insights into the Caledonian tectonic history of western Norway: Lithos, v. 246-247, p. 134-148.

Gordon, S. M., Whitney, D. L., Teyssier, C., Grove, M., and Dunlap, W. J., 2008, Timescales of migmatization, melt crystallization, and cooling in a Cordilleran

gneiss dome: Valhalla complex, southeastern British Columbia: Tectonics, v. 27, no. 4.

Grasemann, B., and Tschegg, C., 2012, Localization of deformation triggered by chemo-mechanical feedback processes: GSA Bulletin, v. 124, no. 5-6, p. 737-745.

Grujic, D., 2006, Channel flow and continental collision tectonics: an overview: Geological Society, London, Special Publications, v. 268, no. 1, p. 25-37.

Hacker, B. R., Andersen, T. B., Johnston, S., Kylander-Clark, A. R. C., Peterman, E. M., Walsh, E. O., and Young, D., 2010, High-temperature deformation during continental-margin subduction & exhumation: The ultrahigh-pressure Western Gneiss Region of Norway: Tectonophysics, v. 480, no. 1-4, p. 149-171.

Hacker, B. R., Kylander-Clark, A. R. C., Holder, R., Andersen, T. B., Peterman, E. M., Walsh, E. O., and Munnikhuis, J. K., 2015, Monazite response to ultrahigh-pressure subduction from U–Pb dating by laser ablation split stream: Chemical Geology, v. 409, p. 28-41.

Haller, J., 1956, Probleme der Tiefentektonik Bauformen im Migmatit Stockwerk der Ostgrönländischen Kaledoniden: Geologische Rundschau, v. 45, no. 2, p. 159-167.

Hartz, E. H., and Andresen, A., 1997, From collision to collapse: Complex strain permutations in the hinterland of the Scandinavian Caledonides: Journal of Geophysical Research: Solid Earth, v. 102, no. B11, p. 24697-24711.

Higgins, A. K., Friderichsen, J. D., Rex, D. C., and Gledhill, A. R., 1978, Early Proterozoic isotopic ages in the East Greenland Caledonian fold belt: Contributions to Mineralogy and Petrology, v. 67, no. 1, p. 87-94.

Hodges, K. V., 2006, A synthesis of the Channel Flow-Extrusion hypothesis as developed for the Himalayan-Tibetan orogenic system: Geological Society, London, Special Publications, v. 268, no. 1, p. 71-90.

Hodges, K. V., 2016, Crustal Decoupling in Collisional Orogenesis: Examples from the East Greenland Caledonides and Himalaya: Annual Review of Earth and Planetary Sciences, v. 44, no. 1, p. 685-708.

Holder, R. M., Hacker, B. R., Kylander-Clark, A. R. C., and Cottle, J. M., 2015, Monazite trace-element and isotopic signatures of (ultra)high-pressure metamorphism: Examples from the Western Gneiss Region, Norway: Chemical Geology, v. 409, p. 99-111.

Hoorn, C., Perrigo, A., and Antonelli, A., 2018, Mountains, Climate and Biodiversity: An Introduction, *in* Hoorn, C., Perrigo, A., and Antonelli, A., eds., Mountains, Climate and Biodiversity: Hoboken, New Jersey, Wiley-Blackwell, p. 1-13.

Hossack, J. R., 1984, The geometry of listric growth faults in the Devonian basins of Sunnfjord, W Norway: Journal of the Geological Society, v. 141, no. 4, p. 629-637.

Hubbard, J., Almeida, R., Foster, A., Sapkota, S. N., Bürgi, P., and Tapponnier, P., 2016, Structural segmentation controlled the 2015 Mw 7.8 Gorkha earthquake rupture in Nepal: Geology, v. 44, no. 8, p. 639-642.

Huet, B., Le Pourhiet, L., Labrousse, L., Burov, E., and Jolivet, L., 2011, Post-orogenic extension and metamorphic core complexes in a heterogeneous crust: the role of crustal layering inherited from collision. Application to the

Cyclades (Aegean domain): Geophysical Journal International, v. 184, no. 2, p. 611-625.
Hurich, C. A., Palm, H., Dyrelius, D., and Kristoffersen, Y., 1989, Deformation of the Baltic continental crust during Caledonide intracontinental subduction: Views from seismic reflection data: Geology, v. 17, no. 5, p. 423-425.
Jakob, J., Andersen, T. B., and Kjøll, H. J., 2019, A review and reinterpretation of the architecture of the South and South-Central Scandinavian Caledonides—A magma-poor to magma-rich transition and the significance of the reactivation of rift inherited structures: Earth-Science Reviews, v. 192, p. 513-528.
Jamieson, R. A., and Beaumont, C., 2013, On the origin of orogens: Geological Society of America Bulletin, v. 125, no. 11-12, p. 1671-1702.
Jessup, M. J., Newell, D. L., Cottle, J. M., Berger, A. L., and Spotila, J. A., 2008, Orogen-parallel extension and exhumation enhanced by denudation in the trans-Himalayan Arun River gorge, Ama Drime Massif, Tibet-Nepal: Geology, v. 36, no. 7, p. 587-590.
Johnston, S. M., Hartz, E. H., Brueckner, H. K., and Gehrels, G. E., 2010, U–Pb zircon geochronology and tectonostratigraphy of southern Liverpool Land, East Greenland: Implications for deformation in the overriding plates of continental collisions: Earth and Planetary Science Letters, v. 297, no. 3, p. 512-524.
Jolivet, L., and Brun, J.-P., 2010, Cenozoic geodynamic evolution of the Aegean: International Journal of Earth Sciences, v. 99, no. 1, p. 109-138.
Jolivet, L., Famin, V., Mehl, C., Parra, T., Aubourg, C., Hebert, R., and Philippot, P., 2004, Strain localization during crustal-scale boudinage to form extensional metamorphic domes in the Aegean Sea: Gneiss Domes in Orogeny, v. 380, p. 185-210.
Jolivet, L., Menant, A., Sternai, P., Rabillard, A., Arbaret, L., Augier, R., Laurent, V., Beaudoin, A., Grasemann, B., Huet, B., Labrousse, L., and Le Pourhiet, L., 2015, The geological signature of a slab tear below the Aegean: Tectonophysics, v. 659, p. 166-182.
Jordan, T. E., Isacks, B. L., Allmendinger, R. W., Brewer, J. A., Ramos, V. A., and Ando, C. J., 1983, Andean tectonics related to geometry of subducted Nazca plate: GSA Bulletin, v. 94, no. 3, p. 341-361.
Jäger, E., Introduction to Geochronology, *in* Proceedings Lectures in Isotope Geology, Berlin, Heidelberg, 1979// 1979, Springer Berlin Heidelberg, p. 1-12.
Kapp, P., Stockli, D., Taylor, M., and Ding, L., 2008, Development of active low-angle normal fault systems during orogenic collapse: Insight from Tibet: Geology, v. 36, no. 1, p. 7-10.
Kautsky, G., 1946, Neue Gesichtspunkte zu einigen nordskandinavischen Gebirgsproblemen: Geologiska Föreningen i Stockholm Förhandlingar, v. 68, no. 4, p. 589-602.
Kirkland, C. L., Daly, J. S., Eide, E. A., and Whitehouse, M. J., 2006, The structure and timing of lateral escape during the Scandian Orogeny: A combined strain and geochronological investigation in Finnmark, Arctic Norwegian Caledonides: Tectonophysics, v. 425, no. 1, p. 159-189.

Kjøll, H. J., Andersen, T. B., Corfu, F., Labrousse, L., Tegner, C., Abdelmalak, M. M., and Planke, S., 2019, Timing of Breakup and Thermal Evolution of a Pre-Caledonian Neoproterozoic Exhumed Magma-Rich Rifted Margin: Tectonics, v. 38, no. 6, p. 1843-1862.

Knopf, A., 1948, THE GEOSYNCLINAL THEORY: GSA Bulletin, v. 59, no. 7, p. 649-670.

Kohn, M. J., Corrie, S. L., and Markley, C., 2015, The fall and rise of metamorphic zircon: American Mineralogist, v. 100, no. 4, p. 897-908.

Krabbendam, M., and Dewey, J. F., 1998, Exhumation of UHP rocks by transtension in the Western Gneiss Region, Scandinavian Caledonides: Geological Society, London, Special Publications, v. 135, no. 1, p. 159-181.

Krill, A., 1985, Relationships between the Western Gneiss Region and the Trondheim Region – Stockwerk-Tectonics reconsidered, *in* Gee, D. G., and Sturt, B. A., eds., The Caledonide Orogen - Scandinavia and Related Areas: Chichester, Wiley, p. 475-483.

Krill, A. G., and Griffin, W. L., 1981, Interpretation of Rb-Sr dates from the Western Gneiss Region: a cautionary note: Nor. Geol. Tidsskr., v. 61, p. 83-86.

Kruckenberg, S. C., Vanderhaeghe, O., Ferre, E. C., Teyssier, C., and Whitney, D. L., 2011, Flow of partially molten crust and the internal dynamics of a migmatite dome, Naxos, Greece: Tectonics, v. 30.

Kuhn, T. S., 1962, The structure of scientific revolutions, *in* Neurath, O., ed., INTERNATIONAL ENCYCLOPEDIA of UNIFIED SCIENCE, Volume 2: Chicago, The university of Chicago press, p. 1 - 210.

Labrousse, L., Huet, B., Le Pourhiet, L., Jolivet, L., and Burov, E., 2016, Rheological implications of extensional detachments: Mediterranean and numerical insights: Earth-Science Reviews, v. 161, p. 233-258.

Lacombe, O., and Mouthereau, F., 2002, Basement-involved shortening and deep detachment tectonics in forelands of orogens: Insights from recent collision belts (Taiwan, Western Alps, Pyrenees): Tectonics, v. 21, no. 4, p. 12-11-12-22.

Lamont, T. N., Searle, M. P., Waters, D. J., Roberts, N. M. W., Palin, R. M., Smye, A., Dyck, B., Gopon, P., Weller, O. M., and St-Onge, M. R., 2019, Compressional origin of the Naxos metamorphic core complex, Greece: Structure, petrography, and thermobarometry: GSA Bulletin, v. 132, no. 1-2, p. 149-197.

Lavier, L. L., and Buck, W. R., 2002, Half graben versus large-offset low-angle normal fault: Importance of keeping cool during normal faulting: Journal of Geophysical Research: Solid Earth, v. 107, no. B6, p. ETG 8-1-ETG 8-13.

Le Pourhiet, L., Huet, B., May, D. A., Labrousse, L., and Jolivet, L., 2012, Kinematic interpretation of the 3D shapes of metamorphic core complexes: Geochemistry Geophysics Geosystems, v. 13, no. 9, p. 1-17.

Lee, J., Miller, E. L., and Sutter, J. F., 1987, Ductile strain and metamorphism in an extensional tectonic setting: a case study from the northern Snake Range, Nevada, USA: Geological Society, London, Special Publications, v. 28, no. 1, p. 267-298.

Li, Z. X., Bogdanova, S. V., Collins, A. S., Davidson, A., De Waele, B., Ernst, R. E., Fitzsimons, I. C. W., Fuck, R. A., Gladkochub, D. P., Jacobs, J., Karlstrom, K. E., Lu, S., Natapov, L. M., Pease, V., Pisarevsky, S. A., Thrane, K., and Vernikovsky, V., 2008, Assembly, configuration, and break-up history of Rodinia: A synthesis: Precambrian Research, v. 160, no. 1-2, p. 179-210.

Lister, G. S., Banga, G., and Feenstra, A., 1984, Metamorphic core complexes of Cordilleran type in the Cyclades, Aegean Sea, Greece: Geology, v. 12, no. 4, p. 221-225.

Lister, G. S., and Davis, G. A., 1989, The Origin of Metamorphic Core Complexes and Detachment Faults Formed during Tertiary Continental Extension in the Northern Colorado River Region, USA: Journal of Structural Geology, v. 11, no. 1-2, p. 65-94.

Lister, G. S., Etheridge, M. A., and Symonds, P. A., 1986, Detachment faulting and the evolution of passive continental margins: Geology, v. 14, no. 3, p. 246-250.

Lister, G. S., and Snoke, A. W., 1984, S-C Mylonites: Journal of Structural Geology, v. 6, no. 6, p. 617-638.

Macdonald, K. C., Fox, P. J., Perram, L. J., Eisen, M. F., Haymon, R. M., Miller, S. P., Carbotte, S. M., Cormier, M. H., and Shor, A. N., 1988, A new view of the mid-ocean ridge from the behaviour of ridge-axis discontinuities: Nature, v. 335, no. 6187, p. 217-225.

Macfarlane, R., 2008, Mountains of the Mind: A History of a Fascination, Granta.

McClay, Norton, M. G., Coney, P., and Davis, G. H., 1986, Collapse of the Caledonian orogen and the Old Red Sandstone: Nature, v. 323, no. 6084, p. 147-149.

McClelland, W. C., and Gilotti, J. A., 2003, Late-stage extensional exhumation of high-pressure granulites in the Greenland Caledonides: Geology, v. 31, no. 3, p. 259-262.

McDonald, C. S., Warren, C. J., Mark, D. F., Halton, A. M., Kelley, S. P., and Sherlock, S. C., 2016, Argon redistribution during a metamorphic cycle: Consequences for determining cooling rates: Chemical Geology, v. 443, p. 182-197.

McKenzie, D., 1978, Some remarks on the development of sedimentary basins: Earth and Planetary Science Letters, v. 40, no. 1, p. 25-32.

Mezri, L., Le Pourhiet, L., Wolf, S., and Burov, E., 2015, New parametric implementation of metamorphic reactions limited by water content, impact on exhumation along detachment faults: Lithos, v. 236-237, p. 287-298.

Milnes, A., Wennberg, O., Skår, Ø., and Koestler, A., 1997, Contraction, extension and timing in the South Norwegian Caledonides: the Sognefjord transect: Geological Society, London, Special Publications, v. 121, no. 1, p. 123-148.

Molnar, P., Boos, W. R., and Battisti, D. S., 2010, Orographic Controls on Climate and Paleoclimate of Asia: Thermal and Mechanical Roles for the Tibetan Plateau: Annual Review of Earth and Planetary Sciences, v. 38, no. 1, p. 77-102.

Molnar, P., and Tapponnier, P., 1975, Cenozoic Tectonics of Asia: Effects of a Continental Collision: Features of recent continental tectonics in Asia can be

interpreted as results of the India-Eurasia collision, v. 189, no. 4201, p. 419-426.

Mulch, A., Cosca, M. A., Andresen, A., and Fiebig, J., 2005, Time scales of deformation and exhumation in extensional detachment systems determined by high-spatial resolution in situ UV-laser 40Ar/39Ar dating: Earth and Planetary Science Letters, v. 233, no. 3, p. 375-390.

Möller, C., Andersson, J., Dyck, B., and Antal Lundin, I., 2015, Exhumation of an eclogite terrane as a hot migmatitic nappe, Sveconorwegian orogen: Lithos, v. 226, p. 147-168.

Möller, C., Bingen, B., Andersson, J., Stephens, M. B., Viola, G., and Schersten, A., 2013, A non-collisional, accretionary Sveconorwegian orogen - Comment: Terra Nova, v. 25, no. 2, p. 165-168.

Norlander, B. H., Whitney, D. L., Teyssier, C., and Vanderhaeghe, O., 2002, Partial melting and decompression of the Thor-Odin dome, Shuswap metamorphic core complex, Canadian Cordillera: Lithos, v. 61, no. 3-4, p. 103-125.

O'Nions, R. K., and Baadsgaard, H., 1971, A radiometric study of polymetamorphism in the Bamble region, Norway: Contributions to Mineralogy and Petrology, v. 34, no. 1, p. 1-21.

Olesen, O., Ebbing, J., Gellein, J., Kihle, O., Myklebust, R., Sand, M., Skilbrei, J., Solheim, D., and Usov, S., 2010a, Gravity anomaly map, Norway and adjacent areas: Geological Survey of Norway.

Olesen, O., Gellein, J., Gernigon, L., Kihle, O., Koziel, J., Lauritsen, T., Mogaard, J., Myklebust, R., Skilbrei, J., and Usow, S., 2010b, Magnetic anomaly map, Norway and adjacent ocean areas. Scale 1: 3 million: Geological Survey of Norway.

Oreskes, N., 1988, The Rejection of Continental Drift: Historical Studies in the Physical and Biological Sciences, v. 18, no. 2, p. 311-348.

-, 1999, The rejection of continental drift: Theory and method in American earth science, Oxford University Press, 432 p.:

Osmundsen, P. T., Braathen, A., Sommaruga, A., Skilbrei, J. R., Nordgulen, O., Roberts, D., Andersen, T. B., Olesen, O., and Mosar, J., 2005, Metamorphic core complexes and gneiss-cored culminations along the Mid-Norwegian margin: an overview and some current ideas.: Norwegian Petroleum Society Special Publications, v. 12, p. 29 - 41.

Osmundsen, P. T., and Péron-Pinvidic, G., 2018, Crustal-Scale Fault Interaction at Rifted Margins and the Formation of Domain-Bounding Breakaway Complexes: Insights From Offshore Norway: Tectonics, v. 37, no. 3, p. 935-964.

Péron-Pinvidic, G., Manatschal, G., Masini, E., Sutra, E., Flament, J. M., Haupert, I., and Unternehr, P., 2017, Unravelling the along-strike variability of the Angola–Gabon rifted margin: a mapping approach: Geological Society, London, Special Publications, v. 438, no. 1, p. 49-76.

Peron-Pinvidic, G., Manatschal, G., and Osmundsen, P. T., 2013, Structural comparison of archetypal Atlantic rifted margins: A review of observations and concepts: Marine and Petroleum Geology, v. 43, p. 21-47.

Platt, J. P., Behr, W. M., and Cooper, F. J., 2015, Metamorphic core complexes: windows into the mechanics and rheology of the crust: Journal of the Geological Society, v. 172, no. 1, p. 9-27.
Ramberg, H., 1981, The role of gravity in orogenic belts: Geological Society, London, Special Publications, v. 9, no. 1, p. 125-140.
Ramsay, J. G., 1967, Folding and fracturing of rocks, New York, Mc Graw Hill Book Company, 568 p.:
Ratschbacher, L., Frisch, W., Linzer, H.-G., and Merle, O., 1991a, Lateral extrusion in the eastern Alps, Part 2: Structural analysis: Tectonics, v. 10, no. 2, p. 257-271.
Ratschbacher, L., Merle, O., Davy, P., and Cobbold, P., 1991b, Lateral extrusion in the eastern Alps, Part 1: Boundary conditions and experiments scaled for gravity: Tectonics, v. 10, no. 2, p. 245-256.
Regenauer-Lieb, K., Weinberg, R. F., and Rosenbaum, G., 2006, The effect of energy feedbacks on continental strength: Nature, v. 442, no. 7098, p. 67-70.
Rey, P., Vanderhaeghe, O., and Teyssier, C., 2001, Gravitational collapse of the continental crust: definition, regimes and modes: Tectonophysics, v. 342, no. 3-4, p. 435-449.
Rey, P. F., and Houseman, G., 2006, Lithospheric scale gravitational flow: the impact of body forces on orogenic processes from Archaean to Phanerozoic: Geological Society, London, Special Publications, v. 253, no. 1, p. 153-167.
Rey, P. F., Mondy, L., Duclaux, G., Teyssier, C., Whitney, D. L., Bocher, M., and Prigent, C., 2017, The origin of contractional structures in extensional gneiss domes: Geology, v. 45, no. 3, p. 263-266.
Rey, P. F., Teyssier, C., Kruckenberg, S. C., and Whitney, D. L., 2011, Viscous collision in channel explains double domes in metamorphic core complexes: Geology, v. 39, no. 4, p. 387-390.
Rey, P. F., Teyssier, C., and Whitney, D. L., 2009a, Extension rates, crustal melting, and core complex dynamics: Geology, v. 37, no. 5, p. 391-394.
-, 2009b, The role of partial melting and extensional strain rates in the development of metamorphic core complexes: Tectonophysics, v. 477, no. 3-4, p. 135-144.
Riller, U., and Oncken, O., 2003, Growth of the Central Andean Plateau by Tectonic Segmentation Is Controlled by the Gradient in Crustal Shortening: The Journal of Geology, v. 111, no. 3, p. 367-384.
Ring, U., Brandon, M. T., Willett, S. D., and Lister, G. S., 1999, Exhumation processes: Geological Society, London, Special Publications, v. 154, no. 1, p. 1-27.
Roberts, D., 2003, The Scandinavian Caledonides: event chronology, palaeogeographic settings and likely, modern analogues: Tectonophysics, v. 365, no. 1-4, p. 283-299.
Roberts, N. M. W., and Slagstad, T., 2015, Continental growth and reworking on the edge of the Columbia and Rodinia supercontinents; 1.86-0.9 Ga accretionary orogeny in southwest Fennoscandia: International Geology Review, v. 57, no. 11-12, p. 1582-1606.
Roger, F., Teyssier, C., Respaut, J. P., Rey, P. F., Jolivet, M., Whitney, D. L., Paquette, J. L., and Brunel, M., 2015, Timing of formation and exhumation of

the Montagne Noire double dome, French Massif Central: Tectonophysics, v. 640, p. 53-69.
Rosenbaum, G., Regenauer-Lieb, K., and Weinberg, R., 2005, Continental extension: From core complexes to rigid block faulting: Geology, v. 33, no. 7, p. 609-612.
Rosenberg, C. L., and Handy, M. R., 2005, Experimental deformation of partially melted granite revisited: implications for the continental crust: Journal of Metamorphic Geology, v. 23, no. 1, p. 19-28.
Rosenberg, C. L., Schneider, S., Scharf, A., Bertrand, A., Hammerschmidt, K., Rabaute, A., and Brun, J. P., 2018, Relating collisional kinematics to exhumation processes in the Eastern Alps: Earth-Science Reviews, v. 176, p. 311-344.
Royden, L. H., Burchfiel, B. C., King, R. W., Wang, E., Chen, Z., Shen, F., and Liu, Y., 1997, Surface Deformation and Lower Crustal Flow in Eastern Tibet: Science, v. 276, no. 5313, p. 788-790.
Rubatto, D., 2017, Zircon: The Metamorphic Mineral: Reviews in Mineralogy and Geochemistry, v. 83, no. 1, p. 261-295.
Rudwick, M. J., 2014, Earth's Deep History: How it was Discovered and why it Matters, Chicago, University of Chicago Press, 392 p.:
Saleeby, J., 2003, Segmentation of the Laramide Slab—evidence from the southern Sierra Nevada region: GSA Bulletin, v. 115, no. 6, p. 655-668.
Scheiber, T., Viola, G., Bingen, B., Peters, M., and Solli, A., 2015, Multiple reactivation and strain localization along a Proterozoic orogen-scale deformation zone: The Kongsberg-Telemark boundary in southern Norway revisited: Precambrian Research, v. 265, p. 78-103.
Schenker, F. L., Gerya, T., and Burg, J. P., 2012, Bimodal behavior of extended continental lithosphere: Modeling insight and application to thermal history of migmatitic core complexes: Tectonophysics, v. 579, p. 88-103.
Schmalholz, S. M., and Mancktelow, N. S., 2016, Folding and necking across the scales: a review of theoretical and experimental results and their applications: Solid Earth, v. 7, no. 5, p. 1417-1465.
Schneider, J., Bosch, D., and Monié, P., 2008, Individualization of textural and reactional microdomains in eclogites from the Bergen Arcs (Norway): Consequences for Rb/Sr and Ar/Ar radiochronometer behavior during polymetamorphism: Geochemistry, Geophysics, Geosystems, v. 9, no. 12, p. 1-28.
Searle, M. P., and Lamont, T. N., 2020, Compressional metamorphic core complexes, low-angle normal faults and extensional fabrics in compressional tectonic settings: Geological Magazine, v. 157, no. 1, p. 101-118.
Seranne, M., and Seguret, M., 1987, The Devonian basins of western Norway: tectonics and kinematics of an extending crust: Geological Society, London, Special Publications, v. 28, no. 1, p. 537-548.
Siebenaller, L., Boiron M, C., Vanderhaeghe, O., Hibsch, C., Jessell M, W., Andre-Mayer A, S., France-Lanord, C., and Photiades, A., 2012, Fluid record of rock exhumation across the brittle–ductile transition during formation of a

Metamorphic Core Complex (Naxos Island, Cyclades, Greece): Journal of Metamorphic Geology, v. 31, no. 3, p. 313-338.
Sigmond, E. M. O., 1985, The Mandal — Ustaoset Line, A Newly Discovered Major Fault Zone in South Norway, *in* Tobi, A. C., and Touret, J. L. R., eds., The Deep Proterozoic Crust in the North Atlantic Provinces: Dordrecht, Springer Netherlands, p. 323-331.
Simony, P. S., and Carr, S. D., 2011, Cretaceous to Eocene evolution of the southeastern Canadian Cordillera: Continuity of Rocky Mountain thrust systems with zones of "in-sequence" mid-crustal flow: Journal of Structural Geology, v. 33, no. 9, p. 1417-1434.
Slagstad, T., Roberts, N. M. W., Coint, N., Høy, I., Sauer, S., Kirkland, C. L., Marker, M., Røhr, T. S., Henderson, I. H. C., Stormoen, M. A., Skår, Ø., Sørensen, B. E., and Bybee, G., 2018, Magma-driven, high-grade metamorphism in the Sveconorwegian Province, southwest Norway, during the terminal stages of Fennoscandian Shield evolution: Geosphere, v. 14, no. 2, p. 861-882.
Slagstad, T., Roberts, N. M. W., Ganerød, M., and Henderson, I. H. C., Ultrahigh-temperature metamorphic rocks in Rogaland, SW Norway exposed, *in* Proceedings 33rd Geological winter meeting, Bergen, 2019, Norsk Geologisk Forening
Slagstad, T., Roberts, N. M. W., and Kulakov, E., 2017, Linking orogenesis across a supercontinent; the Grenvillian and Sveconorwegian margins on Rodinia: Gondwana Research, v. 44, p. 109-115.
Slagstad, T., Roberts, N. M. W., Marker, M., Rohr, T. S., and Schiellerup, H., 2013, A non-collisional, accretionary Sveconorwegian orogen: Terra Nova, v. 25, no. 1, p. 30-37.
Slama, J., and Pedersen, R. B., 2015, Zircon provenance of SW Caledonian phyllites reveals a distant Timanian sediment source: Journal of the Geological Society, v. 172, no. 4, p. 465-478.
Smithson, S. B., 1965, The nature of the "granitic" layer of the crust in the southern Norwegian Precambrian: Norsk Geol. Tidsskr, v. 45, p. 113-133.
Spencer, C. J., Kirkland, C. L., and Taylor, R. J. M., 2016, Strategies towards statistically robust interpretations of in situ U-Pb zircon geochronology: Geoscience Frontiers, v. 7, no. 4, p. 581-589.
Spencer, C. J., Roberts, N. M. W., Cawood, P. A., Hawkesworth, C. J., Prave, A. R., Antonini, A. S. M., and Horstwood, M. S. A., 2014, Intermontane basins and bimodal volcanism at the onset of the Sveconorwegian Orogeny, southern Norway: Precambrian Research, v. 252, p. 107-118.
Spencer, J. E., 1984, Role of Tectonic Denudation in Warping and Uplift of Low-Angle Normal Faults: Geology, v. 12, no. 2, p. 95-98.
Steltenpohl, M. G., Moecher, D., Andresen, A., Ball, J., Mager, S., and Hames, W. E., 2011, The Eidsfjord shear zone, Lofoten–Vesterålen, north Norway: An Early Devonian, paleoseismogenic low-angle normal fault: Journal of Structural Geology, v. 33, no. 5, p. 1023-1043.

Steltenpohl, M. G., Schwartz, J. J., and Miller, B. V., 2013, Late to post-Appalachian strain partitioning and extension in the Blue Ridge of Alabama and Georgia: Geosphere, v. 9, no. 3, p. 647-666.

Stipp, M., Stünitz, H., Heilbronner, R., and Schmid, S. M., 2002, The eastern Tonale fault zone: a 'natural laboratory' for crystal plastic deformation of quartz over a temperature range from 250 to 700 °C: Journal of Structural Geology, v. 24, no. 12, p. 1861-1884.

Sundvoll, B., and Larsen, B. T., 1994, Architecture and early evolution of the Oslo Rift: Tectonophysics, v. 240, no. 1, p. 173-189.

Sylvester, A. G., 1998, Magma mixing, structure, and re-evaluation of the emplacement mechanism of Vrådal pluton, central Telemark, southern Norway: Norsk Geologisk Tidsskrift, v. 78, no. 4, p. 259-276.

Teyssier, C., Ferré, E. C., Whitney, D. L., Norlander, B., Vanderhaeghe, O., and Parkinson, D., 2005, Flow of partially molten crust and origin of detachments during collapse of the Cordilleran Orogen: Geological Society, London, Special Publications, v. 245, no. 1, p. 39-64.

Teyssier, C., Korchinski, M., Whitney, D. L., and Rey, P., 2018, Evolution of the geotherm during extension as sedimentation and deep crustal flow compete for space, EGU General Assembly Conference Abstracts, p. 11439.

Teyssier, C., and Whitney, D. L., 2002, Gneiss domes and orogeny: Geology, v. 30, no. 12, p. 1139-1142.

Tirel, C., Brun, J.-P., and Burov, E., 2004, Thermomechanical modeling of extensional gneiss domes: Geological Society of America Special Papers, v. 380, p. 67-78.

Tirel, C., Brun, J. P., and Burov, E., 2008, Dynamics and structural development of metamorphic core complexes: Journal of Geophysical Research-Solid Earth, v. 113, no. B4.

Tirel, C., Brun, J. P., and Sokoutis, D., 2006, Extension of thickened and hot lithospheres: Inferences from laboratory modeling: Tectonics, v. 25, no. 1.

Torsvik, T. H., 2019, Earth history: A journey in time and space from base to top: Tectonophysics, v. 760, p. 297-313.

Trümpy, R., 2001, Why plate tectonics was not invented in the Alps: International Journal of Earth Sciences, v. 90, no. 3, p. 477-483.

Tucholke, B. E., Lin, J., Kleinrock, M. C., Tivey, M. A., Reed, T. B., Goff, J., and Jaroslow, G. E., 1997, Segmentation and crustal structure of the western Mid-Atlantic Ridge flank, 25 degrees 25'-27 degrees 10'N and 0-29 m.y.: Journal of Geophysical Research-Solid Earth, v. 102, no. B5, p. 10203-10223.

van der Beek, P., Litty, C., Baudin, M., Mercier, J., Robert, X., and Hardwick, E., 2016, Contrasting tectonically driven exhumation and incision patterns, western versus central Nepal Himalaya: Geology, v. 44, no. 4, p. 327-330.

Vander Auwera, J., Bogaerts, M., Liégeois, J.-P., Demaiffe, D., Wilmart, E., Bolle, O., and Duchesne, J. C., 2003, Derivation of the 1.0–0.9 Ga ferro-potassic A-type granitoids of southern Norway by extreme differentiation from basic magmas: Precambrian Research, v. 124, no. 2–4, p. 107-148.

Vanderhaeghe, O., 2009, Migmatites, granites and orogeny: Flow modes of partially-molten rocks and magmas associated with melt/solid segregation in orogenic belts: Tectonophysics, v. 477, no. 3-4, p. 119-134.

Vanderhaeghe, O., 2012, The thermal–mechanical evolution of crustal orogenic belts at convergent plate boundaries: A reappraisal of the orogenic cycle: Journal of Geodynamics, v. 56-57, p. 124-145.

Vanderhaeghe, O., and Teyssier, C., 1997, Formation of the Shuswap metamorphic core complex during late-orogenic collapse of the Canadian Cordillera: Role of ductile thinning and partial melting of the mid- to lower crust: Geodinamica Acta, v. 10, no. 2, p. 41-58.

-, 2001, Partial melting and flow of orogens: Tectonophysics, v. 342, no. 3-4, p. 451-472.

Vanderhaeghe, O., Whitney, D. L., Teyssier, C., and Siddoway, C. S., 2004, Structural development of the Naxos migmatite dome, Gneiss Domes in Orogeny, Volume 380, Geological Society of America, p. 211-228.

Viola, G., Henderson, I. H. C., Bingen, B., and Hendriks, B. W. H., 2011, The Grenvillian–Sveconorwegian orogeny in Fennoscandia: Back-thrusting and extensional shearing along the "Mylonite Zone": Precambrian Research, v. 189, no. 3–4, p. 368-388.

Warren, C. J., 2013, Exhumation of (ultra-)high-pressure terranes: concepts and mechanisms: Solid Earth, v. 4, no. 1, p. 75-92.

Warren, C. J., Kelley, S. P., Sherlock, S. C., and McDonald, C. S., 2012, Metamorphic rocks seek meaningful cooling rate: Interpreting 40Ar/39Ar ages in an exhumed ultra-high pressure terrane: Lithos, v. 155, p. 30-48.

Wegmann, C. E., 1935, Zur Deutung der Migmatite: Geologische Rundschau, v. 26, no. 5, p. 305-350.

Wernicke, B., 1985, Uniform-sense normal simple shear of the continental lithosphere: Canadian Journal of Earth Sciences, v. 22, no. 1, p. 108-125.

Wernicke, B., 2009, The detachment era (1977–1982) and its role in revolutionizing continental tectonics: Geological Society, London, Special Publications, v. 321, no. 1, p. 1-8.

Wernicke, B., and Axen, G. J., 1988, On the Role of Isostasy in the Evolution of Normal-Fault Systems: Geology, v. 16, no. 9, p. 848-851.

White, A. P., Hodges, K. V., Martin, M. W., and Andresen, A., 2002, Geologic constraints on middle-crustal behavior during broadly synorogenic extension in the central East Greenland Caledonides: International Journal of Earth Sciences, v. 91, no. 2, p. 187-208.

Whitney, D. L., Teyssier, C., Rey, P., and Buck, W. R., 2013, Continental and oceanic core complexes: Geological Society of America Bulletin, v. 125, no. 3-4, p. 273-298.

Whitney, D. L., Teyssier, C., and Vanderhaeghe, O., 2004, Gneiss domes and crustal flow: Geological Society of America Special Papers, v. 380, p. 15-33.

Wijns, C., Weinberg, R., Gessner, K., and Moresi, L., 2005, Mode of crustal extension determined by rheological layering: Earth and Planetary Science Letters, v. 236, no. 1, p. 120-134.

Willett, S. D., 1999, Orogeny and orography: The effects of erosion on the structure of mountain belts: Journal of Geophysical Research: Solid Earth, v. 104, no. B12, p. 28957-28981.

Williams, P. F., Jiang, D., and Lin, S., 2006, Interpretation of deformation fabrics of infrastructure zone rocks in the context of channel flow and other tectonic models: Geological Society, London, Special Publications, v. 268, no. 1, p. 221-235.

Wilson, J. T., 1966, Did the Atlantic close and then re-open?: Nature, v. 211, no. 5050, p. 676-681.

Wright, L. A., Otton, J. K., and Troxel, B. W., 1974, Turtleback Surfaces of Death Valley Viewed as Phenomena of Extensional Tectonics: Geology, v. 2, no. 2, p. 53-54.

3. Research Articles

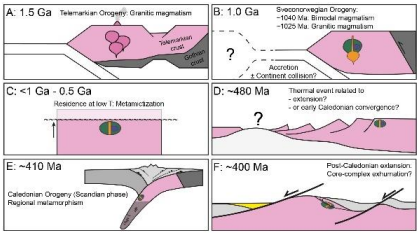

Paper 1: Sveconorwegian vs. Caledonian orogenesis in the eastern Øygarden Complex, SW Norway – Geochronology, structural constraints and tectonic implications.

Wiest, J. D., Jacobs, J., Ksienzyk, A. K., and Fossen, H., 2018:
Precambrian Research, v. 305, p. 1-18

Paper 2: Deep crustal flow within postorogenic metamorphic core complexes – Insights from the southern Western Gneiss Region of Norway.

Wiest, J. D., Osmundsen, P. T., Jacobs, J., and Fossen, H., 2019
Tectonics, v. 38, p. 4267-4289

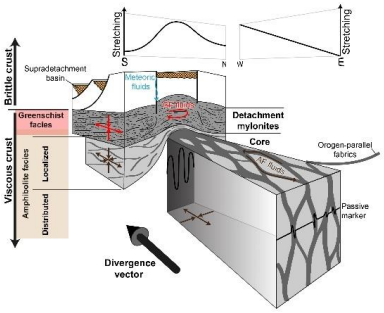

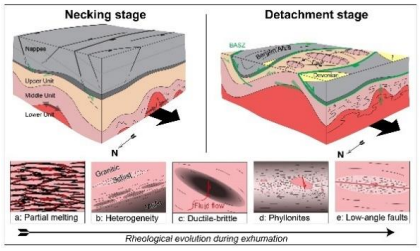

Paper 3: Rheological evolution of ductile crust exhumed in a metamorphic core complex.

Wiest, J. D., Fossen, H., and Jacobs, J.
Manuscript submitted to *Journal of Structural Geology*

Paper 4: Melting, flow and post-orogenic exhumation of the Caledonian infrastructure, W Norway

Wiest, J. D., Jacobs, J., Fossen, H., Ganerød, M, and Osmundsen, P. T.
Manuscript submitted to *Geosphere*

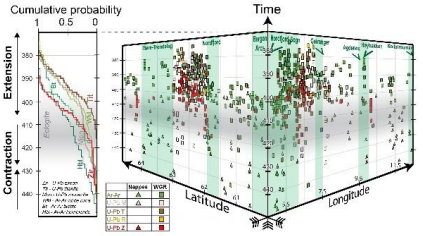

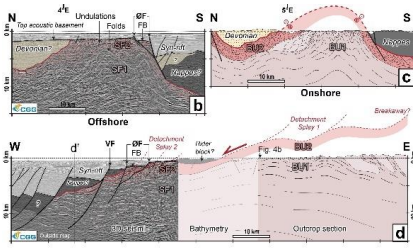

Paper 5: From Caledonian Collapse to North Sea Rift – The Extended History of a Metamorphic Core Complex:

Wiest, J. D., Wrona, T., Bauck, M. S., Fossen, H., Gawthorpe, R.L., Osmundsen, P. T. and Faleide, J. I.
Manuscript submitted to *Tectonics*

Paper 1:
Sveconorwegian vs. Caledonian orogenesis in the eastern Øygarden Complex, SW Norway – Geochronology, structural constraints and tectonic implications.

Wiest, J. D., Jacobs, J., Ksienzyk, A. K., and Fossen, H., 2018:
Precambrian Research, v. 305, p. 1-18

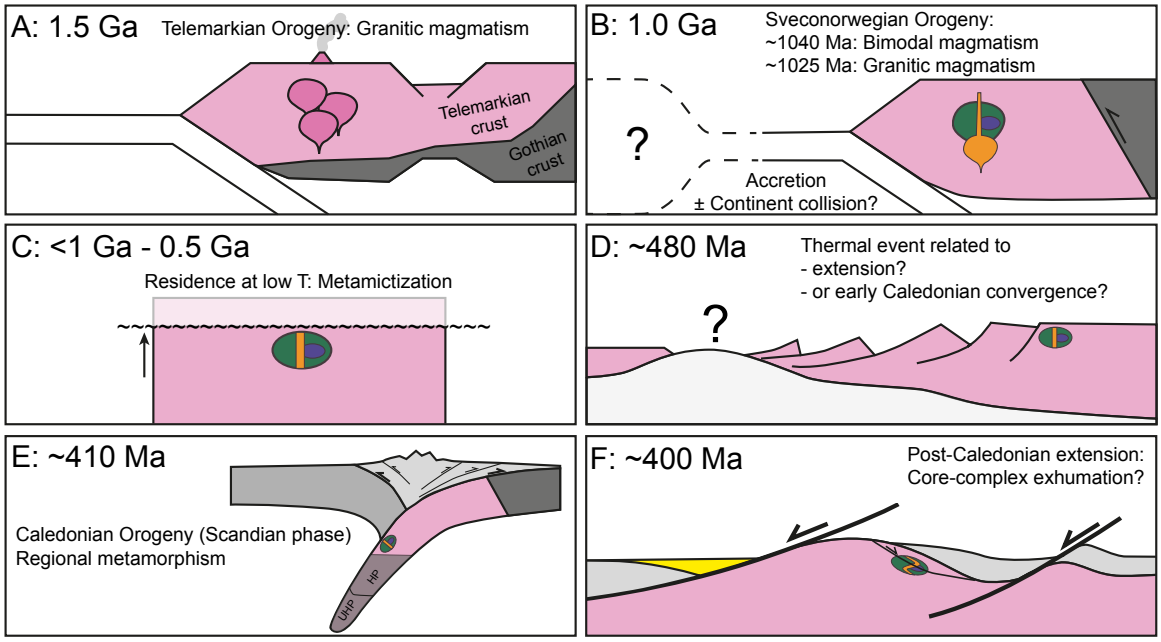

Precambrian Research 305 (2018) 1–18

Contents lists available at ScienceDirect

Precambrian Research

journal homepage: www.elsevier.com/locate/precamres

Sveconorwegian vs. Caledonian orogenesis in the eastern Øygarden Complex, SW Norway – Geochronology, structural constraints and tectonic implications

Johannes D. Wiest[a,*], Joachim Jacobs[a,b], Anna K. Ksienzyk[a], Haakon Fossen[a,c]

[a] Department of Earth Science, University of Bergen, P.O. Box 7803, 5007 Bergen, Norway
[b] Norwegian Polar Institute, Fram Centre, P.O. Box 6606 Langnes, 9296 Tromsø, Norway
[c] Museum of Natural History, University of Bergen, P.O. Box 7803, 5007 Bergen, Norway

ARTICLE INFO

Keywords:
Baltica
Telemarkia
Sirdal Magmatic Belt
SIMS U–Pb zircon geochronology
Western Gneiss Region
Metamorphic core complex

ABSTRACT

The Øygarden Complex is the westernmost basement window in the Norwegian Caledonides, yet, the age and evolution of this part of the Baltic Shield is largely unknown. We examined the eastern part of the window by detailed field mapping and SIMS U–Pb zircon geochronology, to disentangle the record of Caledonian and Sveconorwegian orogenesis and to constrain the long-term crustal evolution. The eastern Øygarden Complex comprises mainly Sveconorwegian metaigneous rocks, which intrude Telemarkian granitic basement, dated at 1506 ± 5 Ma. Sveconorwegian magmatism occurred in two distinct phases: Contemporaneous hornblende biotite granite and gabbro intrusions revealed crystallization ages of 1042 ± 3 Ma and 1041 ± 3 Ma, respectively. We dated younger leucogranitic intrusions at 1027 ± 4 Ma, 1024 ± 6 Ma and ca. 1022 Ma. The new ages clearly identify the Øygarden Complex as a part of Telemarkia and correlate it with the Sirdal Magmatic Belt. Furthermore, they show that the Precambrian evolution of the Øygarden Complex is distinctly different from the Western Gneiss Region. Bimodal magmatism at 1041 Ma and the absence of Sveconorwegian high-grade metamorphism in the eastern Øygarden Complex support the idea of an accretionary Sveconorwegian orogen. Following long-term residence at low temperatures, a temperature increase caused resetting of high-U metamict zircons at ca. 482 Ma. This early Ordovician thermal event might reflect extension of the Baltican margin or early Caledonian convergence. Caledonian ductile reworking involved top-to-E shearing and recumbent lineation-parallel folding followed by the formation of ductile-to-brittle normal-sense shear zones. We discuss this structural evolution in the light of existing and new tectonic models, including early Devonian core-complex exhumation of the Øygarden Complex.

1. Introduction

Grenville-age orogens (1.3–1.0 Ga) are found on all continents and indicate a very important period of continental crust formation (Rino et al., 2008) that finally led to the formation of Rodinia (Li et al., 2008). Across the planet, the style of Grenville-age orogens ranges from large and hot continent-continent collision orogens to variably sized accretionary orogens (Cawood and Pisarevsky, 2017; Roberts et al., 2015). The Sveconorwegian orogen in southern Baltica is traditionally seen as a direct continuation of the Grenvillian continent-continent collision (e.g. Bingen et al., 2008b; Bingen et al., 2005; Möller et al., 2015). However, since the recent recognition of the late Mesoproterozoic (1050–1020 Ma) Sirdal Magmatic Belt in southern Norway (Coint et al., 2015; Slagstad et al., 2013a) the style of Sveconorwegian orogenesis has become a matter of controversy (Möller et al., 2013; Slagstad et al., 2013b). Previously, calc-alkaline 1040–1020 Ma granitoids in Telemarkia were interpreted as evidence of syn-collisional magmatism caused by crustal thickening (Bingen et al., 1993; Bingen and Van Breemen, 1998). Slagstad et al. (2013a,b), however, point out the subduction-related geochemical signatures of 1050–1020 Ma granitoids and the widespread absence of regional metamorphism and deformation after 1020 Ma in the Sirdal Magmatic Belt. Emplacement of the major granitic batholith was contemporary with mafic magmatism and voluminous mafic underplating (Bybee et al., 2014; Slagstad et al., 2017 and b). Based on these findings, Slagstad et al. (2013a) proposed a non-collisional and rather accretionary style of the Sveconorwegian orogen. Slagstad et al. (2017) argue that the Sveconorwegian province represents the lateral termination of the Grenvillian continent-continent

* Corresponding author.
E-mail address: johannes.wiest@uib.no (J.D. Wiest).

https://doi.org/10.1016/j.precamres.2017.11.020
Received 27 April 2017; Received in revised form 22 November 2017; Accepted 27 November 2017
Available online 27 November 2017

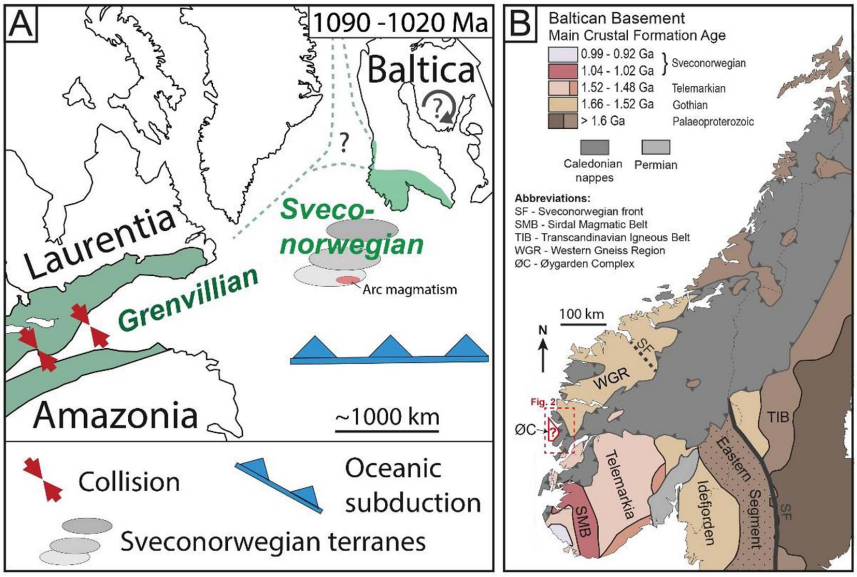

Fig. 1. A: Schematic paleogeography of Laurentia, Baltica and Amazonia for the period 1090–1020 Ma, showing the Sveconorwegian orogen as a lateral termination of the Grenville continent-continent collision modified from Slagstad et al. (2017). Possible clockwise rotation of Baltica (Cawood and Pisarevsky, 2017) is shown symbolically and a possible northward continuation of the Sveconorwegian belt (Gee et al., 2017) is indicated by green dashed lines. B: Simplified geologic map showing major tectonic units and crustal formation ages of the Baltic Shield. After Bingen and Solli (2009) and Slagstad et al. (2013a). Red rectangle marks extend of Fig. 2A. (For interpretation of the references to colour in this figure legend, the reader is referred to the web version of this article.)

collision, related to the spatially limited extent of the Amazonian continent (Fig. 1A). Cawood and Pisarevsky (2017) suggested a more dynamic model that is based on clockwise rotation of Baltica related to the opening of the Asgard Sea. In this alternative scenario, the southern margin of Baltica collided softly with Amazonia. However, the relationship between the Grenvillian and Sveconorwegian orogens is obscured by the loss or extensive tectonic reworking of vast parts of continental crust, which were originally linking the two orogenic belts (e.g. Gee et al., 2017). Large parts of the Sveconorwegian crust were strongly overprinted by the Caledonian orogeny (e.g. Gee et al., 2008). Therefore, tectonic models for the Sveconorwegian orogeny are based on a limited belt of preserved Precambrian crust as well as allochthonous fragments of Baltican crust (e.g. Roffeis et al., 2013). The Precambrian evolution of large parts of the 'caledonized' Baltican basement, on the other hand, remains poorly understood.

We address this problem by taking a closer look at the Øygarden Complex, the westernmost basement window in the Norwegian Caledonides (Fig. 2). The window exposes Precambrian rocks that experienced strong Caledonian reworking (Fossen and Rykkelid, 1992b; Sturt et al., 1975), but the precise age and origin of the pre-Caledonian protoliths are still unknown. The Øygarden Complex is located alongstrike of the Sirdal Magmatic Belt in the direction towards the Grenvillian orogen (Fig. 1), making it a key area for our understanding of Sveconorwegian orogenesis. In this study, we test a possible Grenville-age affinity of the Øygarden Complex after carefully disentangling its strong Caledonian overprint. Thereby, we try to clarify the relationship between the Øygarden Complex and adjacent basement provinces as well as the Sirdal Magmatic Belt. Detailed field mapping in the eastern Øygarden Complex constrained igneous and metamorphic as well as structural relationships, and formed the basis for Secondary Ion Mass Spectrometry (SIMS) U-Pb zircon geochronology. This paper presents a detailed geologic description of the eastern Øygarden Complex and the first high-resolution U–Pb zircon geochronological data from the entire Øygarden Complex.

2. Geologic setting

2.1. Precambrian evolution of SW Norway

Most of the Baltican continental crust formed in the Proterozoic at the long-lived (1.9–0.9 Ga) accretionary margin of Fennoscandia (Bingen and Solli, 2009; Roberts and Slagstad, 2015; Torsvik and Cocks, 2005). This evolution is reflected in the distribution of main crustal formation ages in Scandinavia, getting generally younger from E towards W (Fig. 1B). In SW Norway, the basement can be principally subdivided into a Gothian (1.66–1.52 Ga) and a Telemarkian (1.52–1.48 Ga) domain (Bingen et al., 2005). The Gothian-Telemarkian orogenic episode marks a distinct period of spatially and temporally variable arc magmatism, sedimentation and accretion in a subduction-zone environment at the long-lived accretionary margin of Fennoscandia (Roberts and Slagstad, 2015). Gothian crust constitutes the Western Gneiss Region (WGR) and the Idefjorden Terrane (e.g. Rohr et al., 2013; Skår, 2000; Skår et al., 1994; Skår and Pedersen, 2003). In contrast, 1.52–1.48 Ga crust and a significant volume of Sveconorwegian intrusives (1.15–0.9 Ga) define Telemarkia and the Bamble-Kongsberg terrane (e.g. Bingen et al., 2008a,b; Bingen and Solli, 2009; Coint et al., 2015; Slagstad et al., 2013a). The Sveconorwegian orogeny marks the final episode of the long-lived accretionary history at the active SW margin of Fennoscandia (Roberts and Slagstad, 2015). Sveconorwegian tectonics juxtaposed different crustal blocks and largely formed the internal structure of the Baltican basement (Bingen et al., 2005), yet, the style of the Sveconorwegian orogeny remains controversial (e.g. Bingen et al., 2008b; Möller et al., 2013; Slagstad et al., 2017; Slagstad et al., 2013a,b). Rodinia's break up around 800 Ma was followed by the opening of the Iapetus Ocean from around 550 Ma, with Baltica emerging as an independent continent (Cocks and Torsvik, 2005; Li et al., 2008; Pease et al., 2008; Torsvik and Cocks, 2005). Multiple phases of extension apparently led to the formation of a hyperextended margin of Baltica (Abdelmalak et al., 2015; Andersen

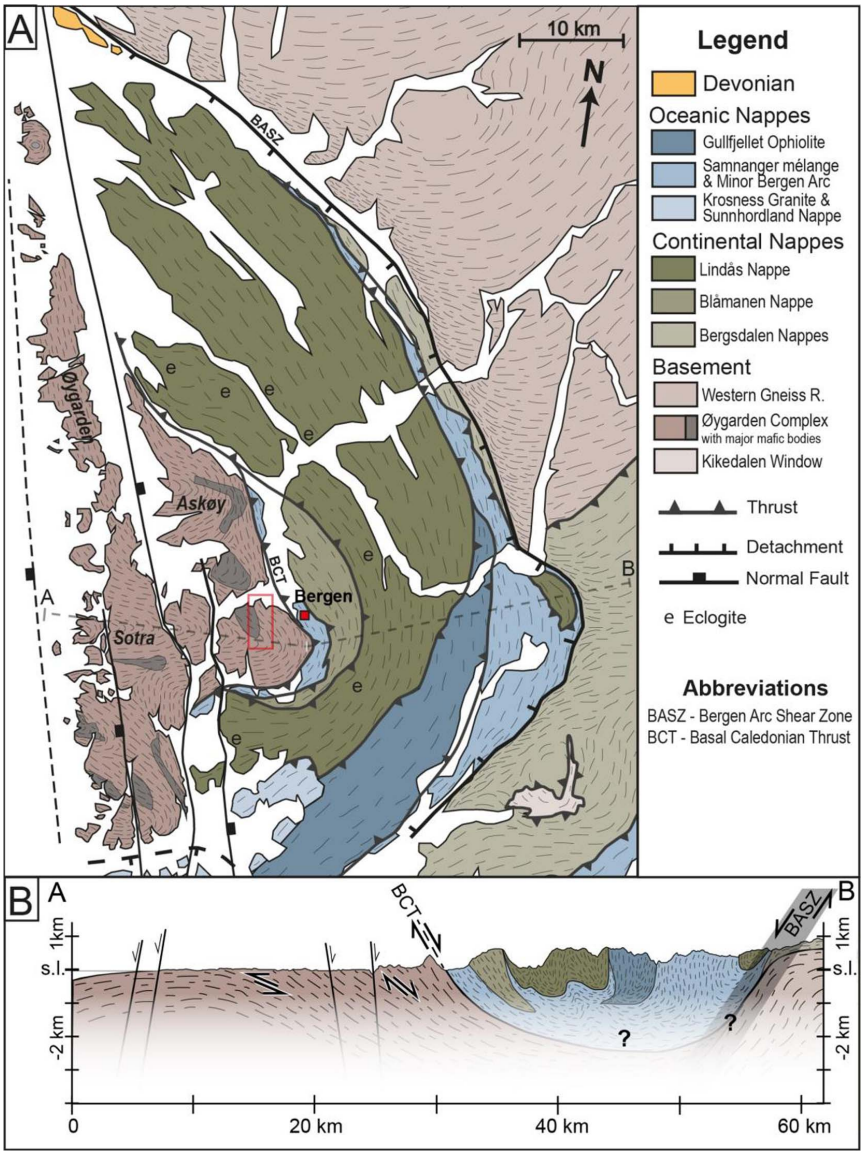

Fig. 2. A: Simplified geologic map of the Bergen Arc System based on Ragnhildstveit and Helliksen (1997). Dashes indicate the trace of foliation and the red rectangle marks the study area around Mt. Lyderhorn. B: Schematic E-W cross section through the Bergen Arc System based on Ragnhildstveit and Helliksen (1997) and Fossen (1998). The present geometry of the Basal Caledonian Thrust (BCT), which separates the Øygarden Complex from the overlaying nappes, could be explained either by passive rotation or by reactivation as a detachment. (For interpretation of the references to colour in this figure legend, the reader is referred to the web version of this article.)

et al., 2012; Jakob et al., 2017).

2.2. Paleozoic evolution of the Baltoscandian margin

From around 480 Ma, the Caledonian orogeny evolved around the closure of the Iapetus Ocean and resulted in Scandian (Silurian) oblique continent-continent collision between Laurentia and Baltica (Gee, 1975; Gee et al., 2008; Roberts, 2003; Torsvik and Cocks, 2005). Various early Caledonian events are recorded in different allochthonous units, but their allocation to either the Baltican or the Laurentian margin is in many cases controversial (e.g. Corfu et al., 2014; Faerseth et al., 2011; Roberts, 2003; Sturt et al., 1978). At the Laurentian margin, several Ordovician ophiolite complexes were emplaced in a suprasubduction setting, accompanied by arc magmatism, accretion and subduction of transitional Laurentian crust (Taconic orogeny; e.g. Andresen and Steltenpohl, 1994; Augland et al., 2014; Dunning and Pedersen, 1988; Furnes et al., 2012; Pedersen and Dunning, 1997; Slagstad et al., 2014; Steltenpohl et al., 2003). Early subduction of previously rifted parts of

the Baltoscandian margin is recorded in Ordovician ultra-high pressure rocks in some Caledonian thrust nappes (e.g. Brueckner et al., 2004; Essex et al., 1997; Gee et al., 2013; Hacker and Gans, 2005; Klonowska et al., 2014; Root and Corfu, 2012).

During the Scandian phase, the Baltican margin was deeply subducted below Laurentia, reaching ultra-high pressure conditions in parts of the WGR (Hacker et al., 2010; Root et al., 2004). The metasedimentary basement cover acted as the basal décollement for a wedge-shaped pile of nappes that was thrust onto the Baltoscandian margin to the SE (Gee, 1975; Gee et al., 2008). Post-orogenic extensional deformation strongly affected the Scandinavian Caledonides (Fossen, 2010). During Mode I extension, the basal décollement zone was reactivated with top-to-the-hinterland (NW) transport (Fossen, 1992, 2000; Fossen and Dunlap, 1998), corresponding to eduction of the Baltican slab (Andersen et al., 1991). Subsequent Mode II extension formed steeper hinterland-dipping extensional shear zones that cut through the orogenic wedge and the inactivated décollement zone and rapidly exhumed the basement to shallow crustal depths (e.g. Andersen and Jamtveit, 1990; Fossen, 1992; Fossen and Hurich, 2005; Milnes et al., 1997; Norton, 1987) . Intermontane basins filled with Middle Devonian conglomerates and sandstones formed in the hanging wall of the Nordfjord-Sogn Detachment Zone (Johnston et al., 2007; Seranne and Seguret, 1987; Steel et al., 1985; Vetti and Fossen, 2012) and the Bergen Arc Shear Zone (Wennberg et al., 1998). The detachments, high-grade footwall gneisses as well as the supra-detachment basins were folded into E-W-trending upright folds in a transtensional regime (Chauvet and Seranne, 1994; Fossen et al., 2016; Fossen et al., 2013; Krabbendam and Dewey, 1998; Osmundsen and Andersen, 2001). The onset of brittle extensional deformation (Mode III) has been dated in the Bergen area to 396 Ma (Larsen et al., 2003). At the same time, partial melting continued in the WGR (Gordon et al., 2013). Brittle conditions were reached in parts of the WGR as late as the Permian, according to Eide et al. (1997).

2.3. The Øygarden Complex

The Øygarden Complex forms a tectonic window occupying the core and the western part of the Bergen Arc System (Fig. 2; Johns, 1981; Kolderup and Kolderup, 1940). The Bergen Arcs consist of a series of Caledonian nappes with different origins and tectonic histories, which are synclinally folded and refolded into a large-scale arc structure (Fossen, 1989; Kvale, 1960; Sturt and Thon, 1978). The allochthons occupy a major depression in the basement (Fig. 2B; Fossen and Dunlap, 2006) which is related to the Bergen Arc Shear Zone (BASZ), a Devonian extensional shear zone (Fossen and Rykkelid, 1992a; Wennberg and Milnes, 1994; Wennberg et al., 1998). Basement rocks in the footwall of the concave-shaped BASZ are considered part of the southern WGR. The Øygarden Complex comprises (par)autochthonous basement in the hanging wall of the shear zone (Kvale, 1960; Ragnhildstveit and Helliksen, 1997; Sturt et al., 1975). However, due to strong penetrative deformation of the Øygarden Complex, an allochthonous state has also been suggested (Bering, 1985).

The rocks in the Øygarden Complex are mainly granitic, granodioritic and tonalitic gneisses as well as several bodies of gabbroic rocks, which are mostly transformed into amphibolites (Johns, 1981). The only published geochronological ages, so far, are Rb/Sr whole rock ages that show a large scatter ranging from 1750 to 473 Ma (Sturt et al., 1975). SIMS U–Pb analysis of three single zircon grains revealed a poorly constrained upper intercept age of 1620 ± 120 Ma (Knudsen and Fossen, 2001). Johns (1981) suggested that most gneisses and amphibolites in the Øygarden Complex are Pre-Svecofennian (> 1800 Ma) and represent a meta-volcanic-sedimentary succession. Gabbroic and granitic rocks in the Haganes gneissose granite suite on Sotra (Fig. 2A) partially preserve intrusive relationships and revealed Sveconorwegian Rb–Sr ages (Johns, 1981; Sturt et al., 1975). These rocks have been correlated with a large gabbroic pluton on Askøy (Askvik, 1971) and the arc-shaped belt of augen gneisses that forms the eastern limit of the Øygarden Complex (Weiss, 1977). In some of the granitic rocks within the latter group, exceptionally high radiogenic heat production values have been recently discovered (Pascal and Rudlang, 2016; Schulze, 2014).

Thermochronological studies in the western part of the Øygarden Complex showed that Scandian peak metamorphism reached upper amphibolite facies conditions with temperatures in excess of 650 °C at 7–8 kbar (Boundy et al., 1996). They were followed by rapid exhumation in the early Devonian through lower amphibolite facies at 408–404 Ma and greenschist facies at 401 Ma to the brittle-plastic transition at 396 Ma (Boundy et al., 1996; Fossen and Dunlap, 1998; Larsen et al., 2003). Besides basic field studies conducted by Askvik (1971) and Weiss (1977), neither detailed structural nor thermochronological constraints are available from the eastern Øygarden Complex so far. Generally, the mylonitic contact between the Øygarden Complex and the Paleozoic rocks of the Minor Bergen Arc is considered as the basal Caledonian thrust (Fossen, 1989; Kvale, 1960) and top-to-E fabrics in the eastern Øygarden Complex are accordingly interpreted to reflect Scandian southeastward thrusting (Fossen and Dunlap, 1998; Larsen et al., 2003; Wennberg, 1996). In contrast to the basal décollement of the SW Norwegian Caledonides farther east, this segment of the basal thrust was not reactivated with top-to-NW deformation corresponding to Mode I extension (Fossen, 1993; Fossen and Dunlap, 1998). Structurally lower levels in the western part of the Øygarden Complex, on the other hand, record strong ductile top-to-W shearing related to early Devonian crustal extension (Fossen and Rykkelid, 1992a; Rykkelid and Fossen, 1992). The main composite gneissic fabric in the Øygarden Complex is folded into a series of upright E-plunging syn- and antiforms (Fig. 2A), including top-to-W fabrics (Fossen and Rykkelid, 1990). The general eastward dip of the gneissic fabrics becomes progressively shallower towards the west and rotates into shallow westward dip at the westernmost shoreline, reflecting a large N–S-trending anticline (Fig. 2C; Fossen, 1998; Larsen, 1996; Larsen et al., 2003). Steep brittle faulting and the intrusion of N–S-trending basaltic dykes are related to various phases of Mesozoic rifting (e.g. Fossen, 1998; Fossen et al., 2016; Ksienzyk et al., 2014; Ksienzyk et al., 2016; Larsen et al., 2003).

3. High-resolution field mapping of the eastern Øygarden Complex

Directly west of the city of Bergen, the mountains Lyderhorn, Damsgårdsfjellet and Løvstakken form a horseshoe-shaped belt, mostly consisting of granitic rocks (sometimes referred to as the “Løvstakken granite”) that follows the contact between Øygarden Complex and Minor Bergen Arc (Weiss, 1977). The 400 m-high mountain Lyderhorn (Figs. 2 and 3) forms an N–S-elongated ridge with steep eastern and western flanks, which offer excellent and easily accessible exposures. Based on lithological differences, five metaigneous lithological units have been identified (Table 1) and are shown on the newly compiled detailed geologic map (Fig. 3).

3.1. Lithological field relationships

The northern ridge of the mountain consists of a layered sequence of granitic, granodioritic and tonaltitic gneisses that are variably deformed, ranging from coarse-grained granites to mylonites. Local amphibolite dykes are concordant to the foliation without clear cross-cutting relationships. A major body of gabbroic rocks that has been mostly metamorphosed and transformed into metagabbros and amphibolites occupies the central part of the study area. Minor lenses that escaped deformation show an original noritic composition, indicating that the basic body can be correlated with the nearby norite pluton on Askøy (Fig. 2A; Askvik, 1971). Different types of granites intrude the gabbroic rocks. Hornblende biotite granite gneiss forms two confined

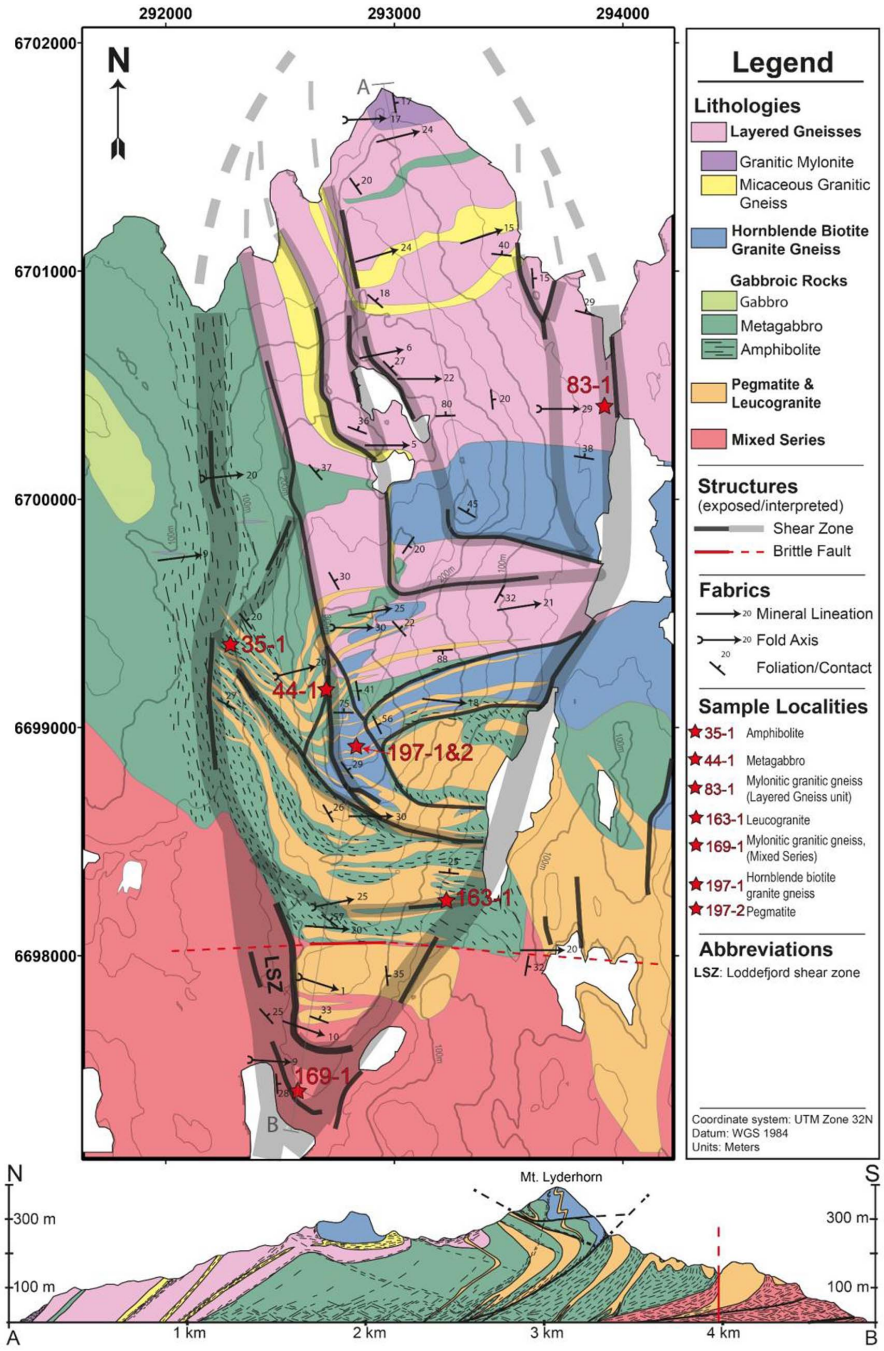

Fig. 3. Newly compiled geologic map and N–S cross section of the Lyderhorn area in the eastern Øygarden Complex showing sample localities for U–Pb zircon geochronology. Note that the shear zone pattern reflects the topography of the mountain, which relates to shallowly E-dipping shear zones and steep N–S- and E–W-trending brittle faults.

Table 1
Lithological units and SIMS U–Pb zircon geochronology samples.

Unit	Lithologies	Sample	Igneous Age	GPS Position
Layered gneisses	**Mylonitic granitic gneiss** Granitic augen gneiss Micaceous granit. gneiss Tonalitic gneiss	LYD-83-1	1506 ± 5 Ma	5°15′35,7″E, 60°23′14,5″N
Gabbroic rocks	Gabbro **Metagabbro** **Amphibolite**	 LYD-44-1 LYD-35-1	 1041 ± 3 Ma 1040 ± 11 Ma	 5°14′20,9″E, 60°22′31,9″N 5°13′53,6″E, 60°22′37,7″N
Hornblende biotite granite gneiss	**Hornblende biotite granite gneiss**	LYD-197-1	1041 ± 3 Ma	5°14′30,7″E, 60°22′24,9″N
Pegmatite and leucogranite	**Leucogranitic pegmatite** **Gneissic leucogranite**	LYD-197-2 LYD-163-1	1022 ± 11 Ma 1022 ± 11 Ma	5°14′30,7″E, 60°22′24,9″N 5°14′58,5″E, 60°22′4,5″N
Mixed Series	Leucogranitic pegmatite **Mylonitic granitic gneiss** Amphibolite Hornblende biotite granite gneiss	LYD-169-1	1027 ± 4 Ma	5°14′18,8″E, 60°21′37,5″N

bodies and show a gradual transition towards tonalite at the margins of the intrusions. Locally, hornblende biotite granite clearly intrudes gabbroic rocks (Fig. 4A), but more commonly the contacts are interlayered zones with ambiguous relationships, which imply that the granite intruded the gabbro before the latter was entirely crystallized. Leucogranites and pegmatites intrude all the previously described units and form E-W striking dykes that get increasingly more voluminous towards the south. Compositions range from alkali feldspar granite to monzogranite, and textures vary gradually from pegmatitic to medium-grained granitic gneiss. The mapped occurrence of the leucogranites and pegmatites coincides precisely with high concentrations of radioactive elements, found through gamma-spectrometry measurements carried out by Schulze (2014). In the southernmost part of the study area, the previously described lithologies alternate on a meter-scale with the dominant leucogranitic gneisses. Lenses of amphibolite and metagabbro are contained within layers of hornblende biotite granite gneiss and banded mylonitic granitic gneisses. Abundant K-feldspar-rich leucogranitic pegmatites show clear intrusive relationships with the other lithologies. The unit is here termed Mixed Series, following Weiss (1977) who mapped the unit as 'layered series'. The strong mixing of lithologies appears to be related to intrusive relationships in combination with strong tectonic transposition.

3.2. Metamorphic fabrics and mineralogy

To various degrees, all the magmatic lithologies were affected by metamorphic recrystallization and transformed into L, L > S or L = S tectonites. Metamorphosed and deformed gabbroic rocks clearly show that peak metamorphism reached amphibolite facies conditions. Metagabbros consist mostly of plagioclase and green hornblende overgrowing relict orthopyroxene, with minor amounts of biotite, titanite-rutile aggregates and epidote. In areas of higher strain, metagabbros grade into amphibolites, which are mineralogically similar but characterized by finer grain size, the absence of pyroxenes and the local occurrence of garnet. Recrystallized plagioclase and aligned growth of hornblende form a pronounced E-plunging mineral lineation in mylonitic amphibolites (Fig. 4B).

Metagranitic rocks range from protomylonites to ultramylonites and show heterogeneous, but generally, strong dynamic recrystallization of quartz and feldspar. Elongated rods of recrystallized quartz and feldspar form a well-defined shallowly E-plunging linear fabric in most granitic rocks while the development of a mylonitic foliation is more heterogeneous (Fig. 4C): Foliations are well developed within anastomosing shear zones and in mica-rich lithologies, however, augen gneisses with a dominant L fabric are abundant. Microfabrics in metagranitic rocks show mostly deformation at greenschist facies conditions, but amphibolite facies fabrics occur in banded gneisses. Metamorphic index minerals that could constrain peak metamorphic conditions more precisely are absent. Leucogranites and pegmatites are commonly rich in K-feldspar and exhibit heterogeneous mineral-dependent deformation at greenschist facies conditions (Fig. 4D), i.e. quartz domains show strong dynamic recrystallization, while K-feldspar crystals are only marginally recrystallized and deform mainly by brittle fracturing. In places, feldspathic pegmatites appear to have escaped ductile deformation probably due to strain partitioning into more quartz- or mica-rich lithologies.

A characteristic feature of the area is the intensity of low-grade deformation and alteration. Cataclastic fabrics are abundant in shallowly E-dipping high-strain zones, which exhibit a strong brittle overprint on previously ductile fabrics (see section 3.4). Within this ductile-to-brittle shear zones retrograde hydration mineral reactions indicate the presence of fluids during deformation at greenschist facies and even lower metamorphic grades (Wintsch et al., 1995). Chlorite phyllonites formed from mafic rocks, where biotite replaced amphibole and was itself altered into chlorite (Fig. 4E). In felsic phyllonites that formed from granitic rocks, K-feldspar was largely replaced by muscovite and quartz (Fig. 4G–H). The strain weakening that is associated with these retrograde mineral reactions (Bos and Spiers, 2002) enhanced the localization of low-grade deformation in discrete shear zones. Further evidence for hydrothermal activity at greenschist facies conditions in high-strain zones can be found at several locations. In a mylonitic to cataclastic granitic fault rock, garnet porphyroblasts overgrow muscovite and quartz, which themselves replace K-feldspar (Fig. 4F). Radial aggregates of actinolite have been found overgrowing granitic fragments in a chlorite breccia and in most thin section samples abundant saussuritization of plagioclase and kaolinitization of K-feldspar can be observed.

3.3. Fabric orientation, kinematic indicators and fold geometries

Shallow eastward dipping planar fabrics and ENE-plunging linear fabrics characterize the structural geometry of the study area with a distinct appearance of E–W and N–S outcrop faces (Fig. 5A). In sections parallel to the E-plunging mineral stretching lineations, fabrics appear with mostly subhorizontal preferred orientations and are rotated into parallelism. On the other hand, sections perpendicular to the lineation exhibit contrasting domains with predominant linear or planar fabrics, respectively. L > S domains are characterized by prolate feldspar augen as well as ribbons of recrystallized quartz and feldspar that could indicate constriction. The preservation of primary intrusive

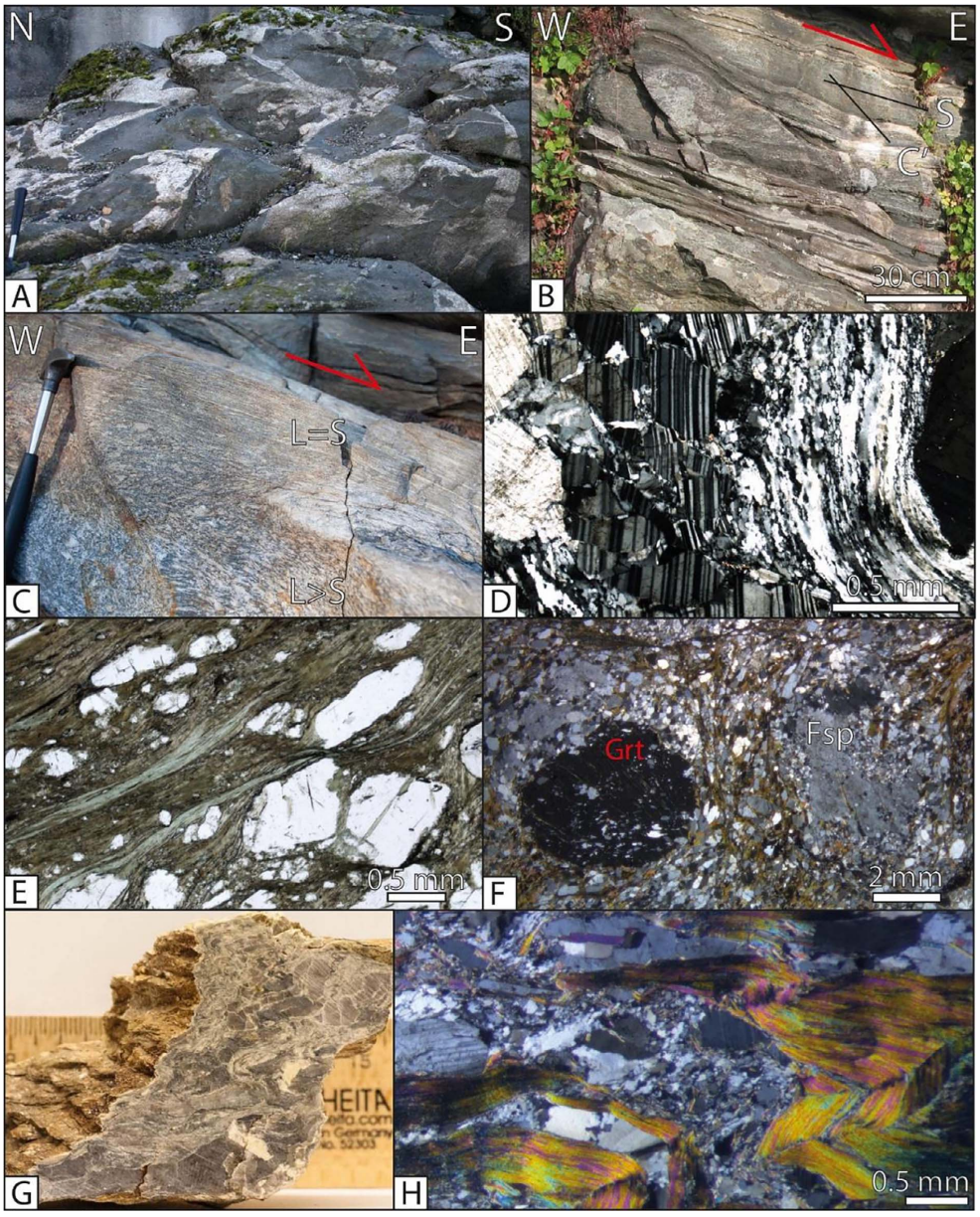

Fig. 4. Photographs of field relationships and metamorphic fabrics. A: Bright hornblende biotite granite veins intruding amphibolite (60°22′55.58″N; 5°13′56.30″E) seen in section perpendicular to mineral lineation. B: Mylonitic amphibolite in section parallel to the mineral lineation (60°21′34.07″N; 5°14′27.75″E). C′-shear bands deflect the mylonitic foliation (S) and indicate top-to-E sense of shear. C: Mesoscale shear zone in mylonitic granitic gneiss (60°23′18.11″N; 5°14′24.57″E). A mylonitic foliation is well developed within the shear zone (L = S), while the gneiss in the footwall has a dominant L fabric. Deflection of the foliation and asymmetrically sheared feldspar clasts indicate top-to-E sense of shear. D: Photomicrograph (crossed polarized light) of granite pegmatite showing strong dynamic recrystallization of quartz and brittle fracturing of plagioclase. E: Photomicrograph (plain polarized light) of chlorite phyllonite (same as Fig. 6E). F: Photomicrograph (crossed polarized light) of granitic fault rock (60°23′6.92″N; 5°14′56.96″E) showing unstable K-feldspar being replaced by quartz and muscovite close to a large garnet porphyroblast. G: Cut hand specimen of felsic phyllonite (60°22′17.74″N; 5°14′34.86″E), showing almost complete replacement of K-feldspar (yellowish-white) by muscovite and quartz. H: Photomicrograph (crossed polarized light) of the same fault rock. (For interpretation of the references to colour in this figure legend, the reader is referred to the web version of this article.)

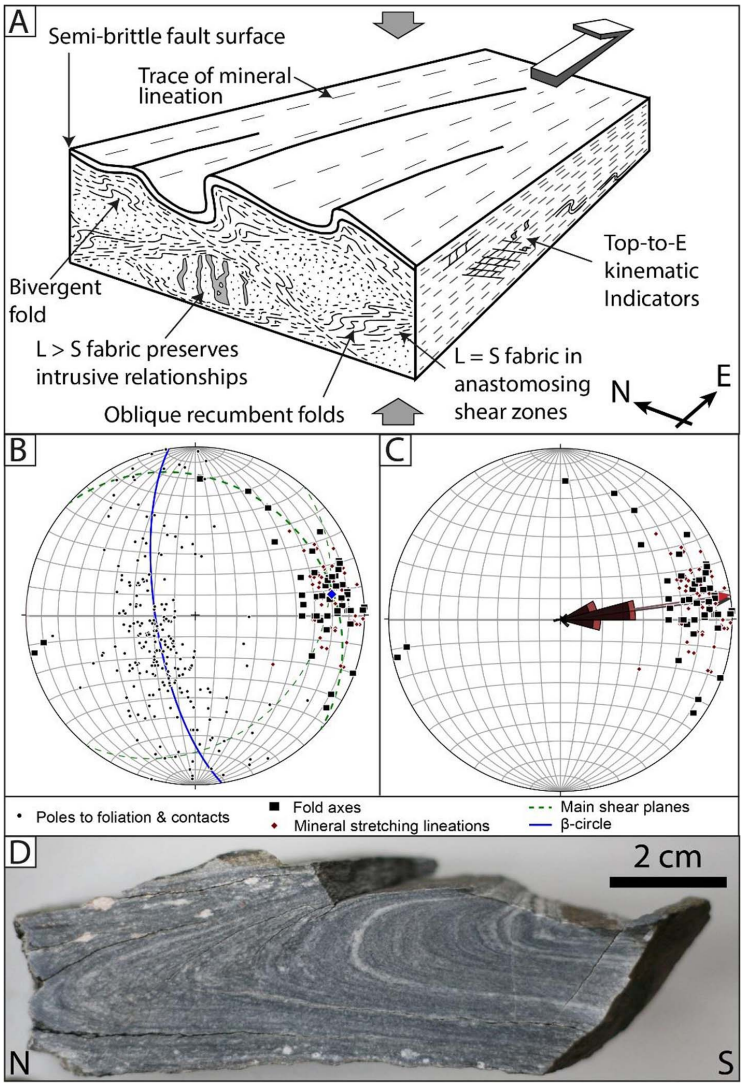

Fig. 5. A: Schematic drawing illustrating the style of ductile deformation. See text for discussion B: Lower hemisphere equal-area plot of measured linear and planar fabrics. The plot was created with Stereoplot (Allmendinger et al., 2011). C: Lower hemisphere equal-area plot of mineral lineations (red, n = 64) and fold axes (black, n = 52) showing rose diagrams and calculated mean trends (arrows). Both populations have an identical mean trend of 82°. D: Cut hand specimen of a cylindrical isoclinal recumbent fold in mylonitic granitic gneiss. The orientation of the fold axis (15 → 074) is parallel to the mineral lineation defined by elongated rods of recrystallized quartz and feldspar. (For interpretation of the references to colour in this figure legend, the reader is referred to the web version of this article.)

relationships in the L > S domains and the geometric relationship between all measured fabric elements with consistent orientations indifferent of metamorphic grade (Fig. 5B) indicate that all of the fabrics seem to be related to one main deformation event. In outcrop sections parallel to the mineral lineation, abundant kinematic indicators are well developed. S-C′ type structures (Figs. 4B and 6D), deflected mylonitic foliations (Fig. 4C), asymmetrically sheared clasts (Fig. 6C) as well as E-vergent isoclinal folds show without exception non-coaxial strain with top-to-E(NE) sense of shear from amphibolite facies to lowest greenschist facies conditions.

The mylonitic foliation and contacts between all the different lithologies exhibit strong folding on various scales. Planar fabrics exhibit folding around an ENE-plunging fold axis (Fig. 5B), and the general NE-dip reflects the position of the study area on the northern limb of an upright, E-plunging megafold (Weiss, 1977). Observable meso- and macrofolds can be grouped into two sets based on different geometries and orientations. A minor set of N–S-trending, E-vergent, isoclinal recumbent folds are commonly non-cylindrical with strongly curved hinge lines and non-planar axial surfaces. Far more abundant are ENE-plunging tight to isoclinal recumbent folds that are mostly cylindrical on the outcrop scale and classify as parallel folds with attenuated limbs and thickened hinge areas (Fig. 5D). This set of folds has subhorizontal axial surfaces that dip to the North, as well as the South, creating in places bivergent fold patterns in single layers (Fig. 5A). Statistically, the orientation of the acquired fold axes and mineral stretching lineations is identical; both have a mean trend of 82° (Fig. 5C). Folded mylonitic foliations, which are cut by discrete top-to-E shear zones with lower greenschist facies fabrics (see below), indicate that the recumbent lineation-parallel folds formed most likely simultaneously with amphibolite to upper-greenschist facies top-to-E shearing. Assuming that the recumbent mesofolds and the upright megafold (Weiss, 1977) formed at the same time, their relationship

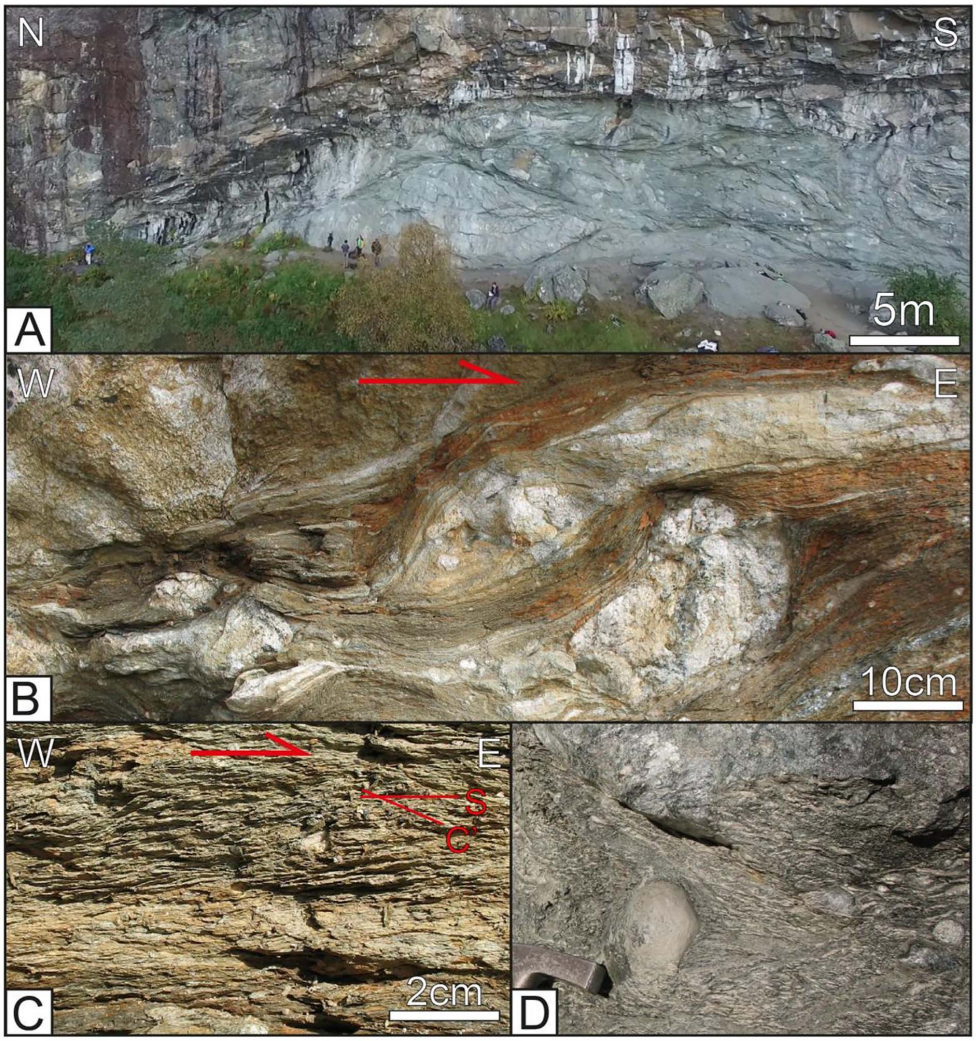

Fig. 6. Loddefjord shear zone: A: View of the main deformation zone in section perpendicular to the mineral lineation (60°21′46.50″N; 5°14′17.10″E). Within the deformation zone, granitic fragments float in a matrix of chlorite phyllonite. Drone image from Robert Sasak. B and C: Field photographs of shallowly E-dipping fabrics in section parallel to the mineral lineation (60°21′42.69″N; 5°14′19.39″E). Asymmetrically sheared granitic clasts and C′-S structures within the phyllonitic matrix indicate top-to-E sense of shear. D: Strongly rounded granitic clasts in the "tectonic conglomerate".

corresponds to the geometry of cascading folds (Whitney et al., 2004) and indicates that the area was affected by vertical shortening on a regional scale.

3.4. Ductile-to-brittle low-angle shear zones

Numerous shallowly NE- and SE-dipping shear zones with top-to-E displacement dissect the entire study area and cut earlier formed fold structures (Fig. 3). The pattern of shear zones on the geologic map is caused by the intersection of E-dipping shear zones with subvertical N–S- and E–W-striking brittle faults. High-strain zones exhibit relict amphibolite facies fabrics, but most deformation occurred at greenschist facies conditions and continued, enhanced by retrograde strain-weakening hydration reactions (section 3.2), to semi-brittle conditions.

The Loddefjord Shear Zone, which consists of several anastomosing branches at the western base of the mountain Lyderhorn (Fig. 3), provides excellent exposures to study shear zone evolution (Fig. 6). Strain localization at amphibolite and upper greenschist facies deformation was facilitated by abundant intrusive contacts in the Mixed Series, which are associated with strong rheological contrasts. The alteration of amphibolites into chlorite phyllonites allowed strain localization into mafic layers at lower metamorphic grades. The deformation zone of the Loddefjord Shear Zone is of variable thickness, reaching up to 10 m, and contains fragments of granitic and tonalitic gneiss floating in a matrix of greenish-grey chlorite phyllonite (Fig. 6A). Linear fabrics are defined by the preferred orientation of amphiboles in mylonitic amphibolite, quartz-feldspar rods in granitic gneiss as well as biotite and chlorite in the phyllonitic matrix and plunge consistently shallowly to the East. In

Fig. 7. Geochronology sample lithologies and representative CL images of analyzed zircon grains. Note the distinct textures of zircons from granitic (A, D, E), gabbroic (B, C) as well as highly radioactive leucogranitic samples (A, F), respectively. Analyzed spots (15 µm diameter) are shown by red circles together with resulting single grain Concordia ages. Note that discordant ages (grey) are not geologically significant. (For interpretation of the references to colour in this figure legend, the reader is referred to the web version of this article.)

addition, quartz-striations on corrugated shallowly E-dipping brittle fault surfaces show an identical orientation. In sections parallel to the lineation, asymmetrically sheared granitic clasts, E-vergent folding of the mylonitic foliation, as well as S-C structures in the phyllonitic matrix indicate uniformly top-to-E sense of shear (Fig. 6B and C). In other exposures, ductile flow of the phyllonitic matrix caused brecciation of granitic fragments and created a peculiar-looking fault rock with strongly rounded clasts, which consist of isolated fold hinges (Fig. 6D). Kolderup and Kolderup (1940) coined the term 'tectonic conglomerate' that has been used to describe similar fault rocks from various parts of the Øygarden Complex (Johns, 1981; Weiss, 1977).

4. SIMS U–Pb zircon geochronology

4.1. Samples and methods

Seven metaigneous samples were collected from key localities to represent the previously identified lithological units, as well as different states of deformation, comprising orthogneisses, gneissic leucogranite, pegmatite, metagabbro and amphibolite (Table 1; Figs. 3 and 7). Mineral separation at the University of Bergen followed standard procedures. Separated zircon grains were handpicked, mounted in epoxy and polished prior to cathodoluminescence (CL) imaging using a ZEISS SUPRA 55VP SEM (scanning electron microscope) at the University of Bergen. U–Pb geochronology was performed using a CAMECA IMS1280 large-geometry ion microprobe at the NordSIMS facility, Stockholm, following routine procedures outlined by Whitehouse et al. (1999) and Whitehouse and Kamber (2005): A ca. 6 nA, −13 kV O_2^- primary beam (imaged aperture of 150 µm corresponding to a spot diameter on the sample of ca. 15 µm) was used to sputter +10 kV secondary ions, which were admitted to the mass spectrometer and detected in a peak-hopping sequence using a single ion-counting electron multiplier (EM). The mass spectrometer was operated at a mass resolution (M/ΔM) of 5400, sufficient to separate all species of interest from molecular interferences. Each analysis comprised a 70 s pre-sputter to remove the Au coating and allow the secondary beam to stabilize, centering of the secondary beam in the field aperture, energy optimization in the 45 eV energy window, mass calibration adjustment using the $^{90}Zr_2{}^{16}O$ peak, and 12 cycles through the species of interest. Groups of analyses were performed in fully automated sequences, regularly interspersing reference

material analyses with those of the sample zircon grains. Data reduction utilized an in-house developed suite of software. Pb-isotope ratios were corrected for common Pb estimated from measured ^{204}Pb assuming the present-day terrestrial Pb isotope composition calculated with the model of Stacey and Kramers (1975), except where the ^{204}Pb count was statistically insignificant relative to the long-term background on the EM, in which case no correction was applied. U/Pb ratios were calibrated using a Pb/UO–UO_2/UO calibration (Jeon and Whitehouse, 2015) from regular measurements of the 1065 Ma 91500 zircon (Wiedenbeck et al., 1995). Age calculations assume the decay constant recommendations of Steiger and Jäger (1977) and utilize the routines of Isoplot-Ex (Ludwig, 2003). All age uncertainties include uncertainties on the decay constants as well as propagation of the error on the Pb/UO–UO_2/UO calibration (Jeon and Whitehouse, 2015; Whitehouse et al., 1997), and are reported at 2σ if not further specified. For Concordia ages, the mean square of weighted deviates (MSWD) on combined equivalence and concordance is reported following the recommendation of Ludwig (1998). Zircon U–Pb data are presented in Appendix A: Table S1.

4.2. U–Pb geochronology results

4.2.1. Hornblende biotite granite gneiss (LYD-197-1)

Weakly foliated hornblende biotite granite gneiss was sampled at the peak of Lyderhorn (Fig. 3) where it is intruded by a subvertical pinkish pegmatite dike that constitutes sample LYD-197-2 (Fig. 7A). The rock consists mostly of coarse grained K-feldspar augen surrounded by a matrix of fine grained, dynamically recrystallized quartz, plagioclase and biotite. Large blueish-green hornblende phenocrysts form mafic clusters together with biotite and rutile. The analyzed zircon crystals are large (100–300 μm), idiomorphic (aspect ratio 3–4), transparent and show oscillatory zoning in CL images, as is typical for zircon crystallized from granitic melts (Corfu et al., 2003). Twenty-six analyses with Th/U ratios typical for magmatic zircon (~0.3) give a Concordia age of 1041.6 ± 2.9 Ma (Fig. 8A) that is interpreted as the igneous crystallization age of the granitic protolith. One outlier analysis with a lower age from an U-rich spot was excluded from the age calculation.

4.2.2. Metagabbro (LYD-44-1)

Metagabbro was sampled in a weakly foliated outcrop that is intruded by a subvertical granitic pegmatite sheet (Fig. 7B). The main mineral constituents are blueish-green amphiboles, which have almost completely replaced primary orthopyroxene, and plagioclase. Minor components are biotite, commonly altered to chlorite, and titanite as well as opaque minerals and zircon as accessory phases. Zircon crystals vary in size (up to 300 μm in length) and are subhedral, elongated (aspect ratios 2–5), colorless and transparent. In CL images, they show oscillatory zoning with broad zones parallel to the c-axis that are typical for magmatic zircons from gabbroic melts. Eighteen analyses with Th/U ratios typical for magmatic zircon (0.6–1.05) give a common Concordia age of 1041.3 ± 3.3 Ma (Fig. 8B) that is interpreted as the igneous crystallization age of the gabbro. One reversely discordant outlier analysis has been excluded from the age calculation.

4.2.3. Amphibolite (LYD-35-1)

The sampled amphibolite is intruded by subvertical pinkish pegmatites and contains minor white granitic veins that are concordant with the foliation (Fig. 7C). The sampled rock consists almost entirely of hornblende, plagioclase and minor opaque minerals. Aligned amphiboles and dynamically recrystallized plagioclase form a pronounced L-S-fabric. Zircon occurs as a very rare accessory phase and can be divided into two subpopulations: The first consists of fragments of relatively large, subhedral to anhedral crystals that are colorless and show oscillatory zoning or more complex textures in CL. The second group consists of smaller brownish metamict grains with rounded corners. The comparison with other samples analyzed in this study suggests that the first subpopulation represents the gabbroic protolith and the latter the intrusive granitic veins. Zircons from both populations show thin discontinuous high-luminescent rims and revealed Th/U-ratios in the typical range for magmatic zircon. Analyses from the first zircon population are mostly concordant and give a Concordia age of 1040 ± 11 Ma (Fig. 8C) that is interpreted as the igneous crystallization age of the gabbroic protolith. Metamict zircons from the second subpopulation revealed high U concentrations and generally discordant analyses that define a discordia. The upper intercept age of 1024 ± 10 Ma (Fig. 8C) is interpreted as the crystallization age of the granitic vein that is probably related to the nearby intrusion of granitic pegmatites.

4.2.4. Mylonitic granitic gneiss, mixed series (LYD-169-1)

The sample locality exposes all the different lithologies that constitute the mixed series. The sampled mylonitic gneiss has a leucogranitic composition and is intruded by granite pegmatites with heterogeneous shapes and dimensions. All lithologies in the sampled outcrop are strongly ductilely deformed and folded around moderately E-plunging fold axes. The sampled gneiss has a prominent L-S fabric and consists of finely laminated layers of recrystallized quartz and feldspar and coarser grained pinkish K-feldspar bands, respectively (Fig. 7D). Biotite is the only mafic component and is commonly replaced by chlorite. The analyzed zircons are mostly 100–150 μm in length, brownish, euhedral or subhedral with stubby crystal shapes (aspect ratio ≈ 2) and subrounded corners. In CL images, zircon crystals show oscillatory zoning as well as thin irregular high-luminescent rims. All analyses revealed high U concentrations (800–2000 ppm) and Th/U-ratios typical for magmatic rocks (0.6–1.2). Out of eighteen analyzed grains, four slightly discordant analyses have been excluded to calculate a Concordia age of 1027.1 ± 4.1 Ma (Fig. 8D) that is interpreted as the igneous crystallization age of the granitic protolith.

4.2.5. Mylonitic granitic gneiss, layered gneisses (LYD-83-1)

The sample locality represents the lower limb of a tight, E-plunging fold in mylonitic granitic gneiss with a moderately N-dipping axial surface. Finely laminated layers of recrystallized quartz, feldspar and biotite alternating with coarse-grained pinkish K-feldspar bands (Fig. 7E) constitute the gneissic banding. Elongated rods of quartz and feldspar define an L-S fabric with a shallowly ENE-plunging mineral stretching lineation. The analyzed zircon crystals are slightly brownish, mostly around 100 μm in length, euhedral to subhedral and have stubby shapes (aspect ratio 2–4) with commonly rounded corners. In CL images, most of the zircons show oscillatory zoning typical for magmatic zircons, but also convolute zoning and sector zoning occur. Xenocrystic cores and rims with high U concentrations and diffuse textures are found, but most of the grains have thin discontinuous high-luminescent rims. All of the 22 analyzed spots have Th/U ratios between 0.2–0.4. The oldest and most concordant analyses come from 13 euhedral grains with clear oscillatory zoning and relatively low U (< 400 ppm), and give a Concordia age of 1506.0 ± 4.8 Ma (Fig. 8E) that is interpreted as the igneous crystallization age of the granitic protolith. Rims and diffuse textural domains revealed analyses with high U (400–1600 ppm) that are slightly or strongly discordant and define a Discordia with a lower intercept age of 482 ± 25 Ma, interpreted to reflect metamictization and partial resetting due to a thermal event.

4.2.6. Leucogranite (LYD-163-1)

Gneissic leucogranite (LYD-163-1) was sampled from a 20 m wide, NE–SW-striking, subvertical body that intrudes amphibolite. Inside the body, textures vary diffusively between pegmatitic and medium-grained granite. The sampled rock (Fig. 7F) is mostly equigranular, medium grained and consists of K-feldspar, plagioclase, quartz as well as minor white mica and biotite, which is mostly altered to chlorite.

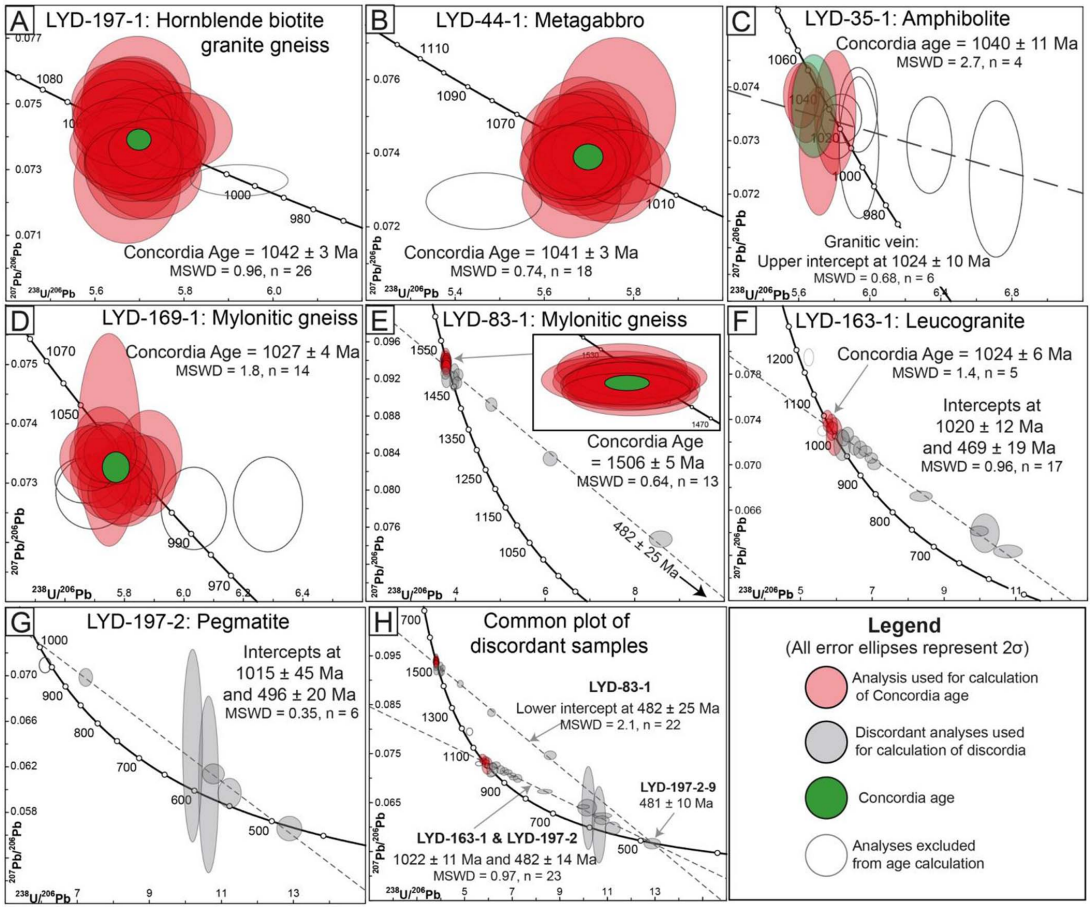

Fig. 8. A–G: Tera-Wasserburg Concordia diagrams of SIMS U–Pb zircon geochronology results. See text for explanation of the age calculations. H: Tera-Wasserburg Concordia diagram of discordant samples LYD-83-1, LYD-163-1 and LYD-197-2. A common Discordia has been calculated for samples LYD-163-1 and LYD-197-2, which represent the same lithological unit. Note that the lower intercept ages from different samples are identical with a concordant analysis from the pegmatite (LYD-197-2).

Quartz and feldspar are partially dynamically recrystallized into a weak L-S-fabric while flame perthites and myrmekites in feldspar appear to represent preserved magmatic textures. The zircon population consists of mostly idiomorphic grains of 100–200 µm in length, which are brown and opaque due to very strong metamictization. Remnants of oscillatory zoning are visible in CL images and some grains exhibit xenocrystic cores, but most internal textures have been obliterated by metamictization. Sixteen analyses of the least metamict grains revealed very high U concentrations reaching up to 4500 ppm and Th/U ratios typical for magmatic zircons (0.4–0.7). The resulting ages show a large scatter along a Discordia line, but a Concordia age of 1024.4 ± 6.3 Ma can be calculated for the most concordant analyses (Fig. 8F) and is interpreted as the igneous crystallization age of the leucogranite. The discordance of U-rich analyses reflects episodic Pb-loss due to thermal resetting and is best constrained by the common lower intercept age of samples LYD-163-1 and LYD-197-2 at 482 ± 14 Ma (Fig. 7H), which represent the same lithological unit. A single older analysis is discordant and most likely represents an inherited core.

4.2.7. Pegmatite (LYD-197-2)

Pegmatite was sampled from a 1 m-wide, subvertical NE–SW-striking dyke that intrudes hornblende biotite granite gneiss (sample LYD-197-1; Fig. 7A). The pegmatite has alkali feldspar granite composition and consists mostly of large pinkish K-feldspar, white plagioclase, grey quartz and subordinate red garnet. Quartz is dynamically recrystallized into elongated rods while large feldspar crystals are only marginally recrystallized and deform mostly by brittle fracturing. The zircon population is characterized by extreme metamictization and consists of brown, non-transparent and commonly idiomorphic crystals, 100–200 µm in length. Due to the extreme metamictization, internal textures are largely obliterated and only eight grains could be analyzed from a large number of picked zircons. All spots revealed very high U concentrations between 1000 and 3500 ppm with Th/U ratios below 0.05. The resulting ages have a large scatter but correlate strongly with U concentrations and define a Discordia line with poorly constrained intercepts at 1015 ± 45 Ma and 496 ± 20 Ma (Fig. 8G). The discordance pattern with one concordant analysis at 481 ± 10 Ma suggests that the strongly metamict grains were partially or completely reset by a thermal event. The pegmatite sample represents the same lithological unit as the leucogranite sample LYD-163-1 and both samples revealed similar zircon populations and resulting ages. Therefore, we assume that the best constraint on the intrusion age of the pegmatite

and the age of the thermal resetting is given by the common discordia line calculated for samples LYD-163-1 and LYD-197-2 together (Fig. 8H) with intercepts at ca. 1022 Ma and 482 Ma, respectively.

4.2.8. Summary of U–Pb zircon geochronology

The oldest rock found in this study is a layer of granitic gneiss (LYD-83-1) with an igneous crystallization age of 1506 ± 5 Ma. The sampled hornblende biotite granite (LYD-197-1) and metagabbro (LYD-44-1) revealed within uncertainties identical crystallization ages of 1042 ± 3 Ma and 1041 ± 3 Ma, which overlap with the crystallization age of the amphibolite (LYD-35-1) at 1040 ± 11 Ma. The granitic protolith of a mylonitic gneiss (LYD-169-1) crystallized at 1027 ± 4 Ma. The intrusion age of gneissic leucogranite (LYD-163-1) is 1024 ± 6 Ma and a related leucogranitic pegmatite (LYD-197-2) is best constrained by a common upper intercept age to ca. 1022 Ma. Three independent samples (LYD-83-1, LYD-163-1 and LYD-197-2) revealed a partial to complete resetting of strongly metamict zircon at ca. 482 Ma.

5. Discussion of U–Pb zircon geochronology

The U–Pb zircon ages acquired in this study range over more than 1000 Ma from ca. 1506 to 482 Ma. The following discussion will show that concordant ages represent the Telemarkian, Sveconorwegian and Caledonian orogenic periods, respectively, but also highlight a major difference between Proterozoic and Paleozoic orogenesis: Proterozoic ages in this dataset represent magmatic activity, while the Caledonian orogeny is only represented by reseting of strongly metamict zircons.

5.1. Magmatic formation history of the eastern Øygarden Complex

The new geochronological data in combination with the results from detailed field mapping allow us to establish the first precise magmatic formation history for the eastern Øygarden Complex. Telemarkian granitoids crystallized at 1506 ± 5 Ma and have lithological compositions resembling the Suldal Arc (Roberts et al., 2013). Sveconorwegian magmatism occurred in two distinct phases; contemporary gabbro and hornblende biotite granite magmatism at ca. 1041 Ma was followed by leucogranitic magmatism in between 1027 ± 4 Ma and ca. 1022 Ma, with leucogranitic pegmatites being the latest intrusives. Field relationships, implying that hornblende biotite granite intruded the gabbro before the latter was entirely crystallized and the observed transition from tonalite to hornblende biotite granite imply a genetic link between gabbroic and granitic magmatism at 1041 Ma. Bimodal magmatism in the eastern Øygarden Complex resembles pre-Sveconorwegian bimodal magmatism in the Telemarkia terrane (Brewer et al., 2004; Spencer et al., 2014). A late- to post-Sveconorwegian (990–920 Ma) Hornblende–Biotite Granite suite in southern Norway might have evolved by extreme magmatic differentiation from mafic magmas (Auwera et al., 2003; Bogaerts et al., 2003), however, contrasting models involve crustal anatexis (c.f. Andersen et al., 2009). In the eastern Øygarden Complex, 1027–1022 Ma leucogranitic magmatism shows a striking contrast in composition to the preceding magmatic phase, yet, it is not clear whether this reflects evolved differentiation of the same parent magma or a different magmatic source.

5.2. Correlating the Øygarden Complex with Telemarkia and the Sirdal magmatic Belt

To constrain the tectonostratigraphic position of the Øygarden Complex, we compared the ages acquired in this study with the occurrence of magmatism in adjacent domains of Baltican basement and Caledonian nappes of continental origin. The two main events dated at around 1500 Ma and 1040 Ma (Fig. 9A) represent distinct magmatic episodes that correspond precisely to the Telemarkian and Sveconorwegian orogenic periods. Igneous rocks of these ages occur in several of the Sveconorwegian domains of southern Norway, but the combination of 1500 Ma and 1040 Ma ages has not been reported from the Caledonian continental nappes (Roffeis and Corfu, 2014). An important finding of this study is that the Øygarden Complex has a distinct Precambrian evolution that is different from that of the WGR. The latter is characterized by Gothian protholiths (1650–1600 Ma) overprinted by late Sveconorwegian (< 1000 Ma) high-grade metamorphism and associated intrusives (e.g. Bingen and Solli, 2009; Roffeis and Corfu, 2014; Rohr et al., 2013; Skår, 2000; Skår et al., 1994; Skår and Pedersen, 2003; Tucker et al., 1987). By contrast, the combination of 1500 Ma and 1040 Ma ages clearly correlates the Øygarden Complex with Telemarkia (Fig. 9A). Furthermore, the newly acquired Sveconorwegian crystallization ages show a precise overlap with emplacement ages of the Sirdal Magmatic Belt in southern Norway (Fig. 9B). Ages of Sirdal Magmatic Belt granites form two clusters around 1050 and 1030 Ma (Coint et al., 2015) which resemble two distinct magmatic phases recorded in the eastern Øygarden Complex around 1040 Ma and 1027–1022 Ma. Nevertheless, it is interesting to note that 1040 Ma bimodal magmatism in the Øygarden Complex falls within a period of relatively low magmatic activity in the Sirdal Magmatic Belt (Fig. 9B). Both areas have a number of common features, such as leucogranites with diffuse textural variations and xenolith-rich zones (Mixed Series in the eastern Øygarden Complex). Large parts of the Sirdal Magmatic Belt are virtually undeformed (Slagstad et al., 2013a), in contrast to the strong deformation that overprinted the eastern Øygarden Complex. Yet we argue, that the ductile deformation described in this study is entirely Caledonian (see section 6 for discussion), highlighting the absence of Sveconorwegian deformation as an important similarity between the Øygarden Complex and the Sirdal Magmatic Belt. Our results suggest that the Øygarden Complex is part of the Telemarkia domain of the autochthonous Baltican basement that has been subject to strong Caledonian deformation. Based on similar ages and the geographic relationship between the two areas (Fig. 9C), we furthermore propose that the Øygarden Complex represents a northern, “caledonized” continuation of the Sirdal Magmatic Belt.

5.3. Implications for Sveconorwegian orogeny in SW Norway and reconstructions of the pre-Caledonian architecture of the Baltican margin

The newly acquired Sveconorwegian ages from the eastern Øygarden Complex are very relevant with respect to the lively debate about the style of the Sveconorwegian orogeny. The contemporaneous occurrence of gabbroic and granitic magmatism at 1041 Ma found in this study, is more in accordance with arc-magmatism in an accretionary setting (Slagstad et al., 2013a) than with syn-collisional magmatism caused by crustal thickening (Bingen et al., 2008b). Furthermore, we found no record of Sveconorwegian high-grade metamorphism or deformation in the eastern Øygarden Complex. This is consistent with interpretations of the Sirdal Magmatic Belt in the context of an accretionary Sveconorwegian orogen (Coint et al., 2015; Slagstad et al., 2013a). Based on findings from the Caledonian Hardanger-Ryfylke Nappe Complex, Roffeis et al. (2013) argue that Gothian rocks were thrust on top of Telemarkian rocks around 1000 Ma, but it is not clear where this tectonism took place and whether it represents accretion or continental collision. As large parts of the pre-Caledonian basement in southern Norway remain poorly studied, we believe that the spatiotemporal evolution of the Sveconorwegian orogeny, which spans more than 200 m.y. (Bingen et al., 2008b), could be more complex than hitherto resolved by available data. In the light of our results, however, we favor an accretionary model (Slagstad et al., 2017). Clockwise rotation and soft collision of Baltica’s southern margin with Amazonia is an alternative scenario that cannot be ruled out based on presently available data (Cawood and Pisarevsky, 2017).

Our finding of Telemarkian crust in the Øygarden Complex and its interpretation as a northern continuation of the Sirdal Magmatic Belt contradicts the orientation and location of previously proposed terrane

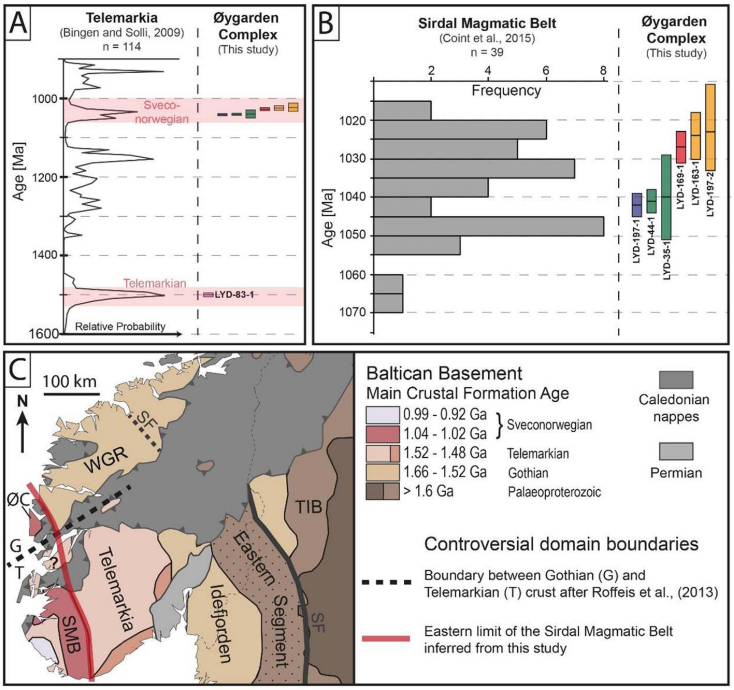

Fig. 9. A: Comparison of magmatic ages from this study with the relative probability of magmatic ages in the Telemarkia domain (Bingen and Solli, 2009). Error bars represent 2σ and colors correspond to the legend in Fig. 3. B: Comparison of Sveconorwegian igneous ages from this study and the Sirdal Magmatic Belt (Coint et al., 2015). Error bars represent 2σ and colors correspond to the legend in Fig. 3. C: Schematic map proposing the Øygarden Complex (ØC) as a northern continuation of the Sirdal Magmatic Belt (SMB). The suggested NNW-trending domain boundary highlights the difference between Øygarden Complex and Western Gneiss Region (WGR) and contradicts the inferred border of Gothian and Telemarkian crust proposed by Roffeis et al. (2013).

boundaries in SW Norway (Fig. 9C). Roffeis et al. (2013) and Roffeis and Corfu (2014) suggested a ENE–WSW-trending terrane boundary to explain different ages of the crust in Telemarkia (< 1.52 Ga) and the Gothian crust (1.66–1.52 Ga) in the WGR. In contrast, our interpretation of a continuous NNW-trend of Sveconorwegian domain boundaries into the 'caledonized' part of the Baltican basement is consistent with the NW-trending limit of Sveconorwegian overprint in the WGR (Bingen et al., 2008a) and the general strike of domain boundaries in the entire Sveconorwegian province (Fig. 9C). The distinction between Øygarden Complex and WGR found in this study suggests that the northern branch of the Bergen Arc Shear Zone separates different crustal domains (Fig. 2). Possibly, this crustal lineament originated during the Sveconorwegian orogeny and was later reactivated by post-Caledonian extensional deformation (Wennberg et al., 1998). Even though we reject the reconstruction of the pre-Caledonian architecture proposed by Roffeis et al. (2013), we agree that the obvious difference in crustal formation ages between the WGR and Telemarkia (including Øygarden Complex) needs to be explained. In our opinion, the relation between these domains is still an open question with great significance for the Sveconorwegian crustal assembly of Baltica as well as Caledonian tectonic reconstructions.

5.4. Significance of the early Ordovician (482 Ma) lower intercept age

None of the three samples with discordant zircon data (LYD-83-1, LYD-163-1 & LYD-197-2) revealed zircon textures that could relate the lower intercept ages to metamorphic recrystallization. The discordant analyses are associated with idiomorphic magmatic zircons with very high U concentrations. In these samples, a strong correlation between U concentration and resulting age is observed. The most discordant analyses and youngest ages come from the highly radioactive leucogranite and pegmatite samples that are the least deformed of the analyzed samples. The samples that show the strongest state of dynamic recrystallization at amphibolite and greenschist facies conditions (LYD-35-1, LYD-83-1 & LYD-169-1) revealed zircons with thin discontinuous U-poor rims, which were too thin to analyze. Therefore, we interpret the ca. 482 Ma lower intercept age as a partial to complete resetting of metamict grains caused by a rapid temperature increase from low temperatures to above the 'critical amorphization temperature' of ~360 °C, as demonstrated by diffusion experiments (Cherniak and Watson, 2003). The intense ductile deformation of the eastern Øygarden Complex related to a regional amphibolite facies metamorphic event might be recorded in the thin U-poor rims, but their age was not determined. In our geochronological dataset, the early Ordovician (ca. 482 Ma) resetting of strongly metamict zircons is the only record of the entire Caledonian orogenic cycle. This result seems surprising only at first sight, as it actually reflects the typical behavior of the U–Pb zircon system with its robustness to high temperatures and vulnerability to diffusional Pb-loss at low temperatures because of metamictization (Mezger and Krogstad, 1997). Residence at low temperatures over several hundred million years is necessary for U-rich grains to accumulate enough metamictization to allow the strong or complete resetting through Pb-diffusion that is recorded in our dataset (Cherniak and Watson, 2003). Thus, this part of the Baltoscandian platform must have been exhumed soon after the Sveconorwegian orogeny and resided at shallow crustal levels through most of the Neoproterozoic and early Paleozoic. This thermal history likely reflects the Cryogenian to Cambrian rift to drift history of Baltica related to the break-up of Rodinia and the opening of the Iapetus Ocean (Abdelmalak et al., 2015; Andersen et al., 2012; Gee et al., 2017; Torsvik et al., 1996). The suggested temperature increase in the Øygarden Complex at 482 Ma, on the other hand, falls into the poorly understood early Caledonian period. Early Ordovician ages of magmatism and metamorphism are very common in the Upper Allochthon of the Caledonian orogenic wedge. They imply considerable tectonic activity in the early Ordovician in outboard terranes and at the Laurentian margin (e.g.

Corfu et al., 2014; Dunning and Pedersen, 1988; Gee et al., 2013; Hacker and Gans, 2005; Klonowska et al., 2014; Pedersen et al., 1992; Pedersen and Dunning, 1997; Root and Corfu, 2012; Slagstad et al., 2014). In contrast, early Ordovician ages have not yet been reported from rocks that are clearly part of the autochthonous Baltican basement, as is the case with the eastern Øygarden Complex, although Ordovician intrusive rocks are intricately folded into the basement gneisses of the northern WGR (e.g. Tucker et al., 2004). Recently, Jakob et al. (2017) presented new evidence for early Ordovician magmatic activity in the Samnanger mélange, which rests now in the Caledonian nappe pile above the Øygarden Complex (Fig. 2). These authors interpret the mélange to represent the Pre-Caledonian hyperextended margin of Baltica and suggest two possible tectonic scenarios for the early Ordovician: 1. The hyperextended margin formed in the Ediacaran and experienced latest Cambrian–early Ordovician tectonomagmatic activity related to shortening of transitional crust. 2. The mélange formed entirely through latest Cambrian–early Ordovician (back-arc) extension. In an alternative model, Slama and Pedersen (2015) argue that the mélange represents an Ordovician arc located in between Baltica and an outboard microcontinent. Our results cannot confirm or contradict any of these models. However, they show that Ordovician tectonothermal activity seems to have affected the proximal domain of the Baltican margin, as represented by the Øygarden Complex. Furthermore, this thermal event seems to have been strong enough to anneal metamictization completely, as no Pb-loss occurred during subsequent Scandian metamorphism.

6. Caledonian tectonic evolution of the eastern Øygarden Complex

As previously discussed (section 5.1), U–Pb zircon geochronology could not constrain the timing of the ductile reworking of the eastern Øygarden Complex. In the context of regional geologic models, however, this deformation must have occurred during the Caledonian orogenic cycle (e.g. Fossen and Dunlap, 1998; Johns, 1981; Rykkelid and Fossen, 1992). Structural analysis showed a geometric relationship between all fabrics and structures with consistent fabric orientations indifferent of metamorphic grade, including widespread low-grade deformation. We have not identified distinct fabrics that could represent a Precambrian deformation history. Previous thermochronological studies in the western Øygarden Complex found early Devonian ages for amphibolite facies metamorphism and subsequent cooling to the brittle-ductile transition (Boundy et al., 1996; Fossen and Dunlap, 1998; Larsen et al., 2003). These ages represent the best available constraints on the timing of ductile reworking in the eastern Øygarden Complex, as they correspond well to the metamorphic sequence found in this study. Yet, the absence of top-to-W kinematics and the abundance of ductile-to-brittle top-to-E low-angle shear zones with intensive low-grade deformation in the eastern Øygarden Complex require further discussion. There are two plausible scenarios that could explain the absence of top-to-W deformation: (I) the eastern Øygarden Complex and the basal contact of the nappes comprise a large tectonic lens that escaped post-orogenic top-to-W shearing and preserves Scandian contractional deformation. (II) At least to some degree, the top-to-E deformation in the eastern Øygarden Complex is also extensional (post-orogenic). As extensional top-to-W shearing affected structurally lower levels, the latter case would imply bi-directional extension in the Øygarden Complex.

Since precise thermochronological constraints on the age of the deformation are lacking, it is difficult to distinguish between contractional and extensional deformation. However, the ENE-plunge of linear fabrics in the eastern Øygarden Complex, is slightly oblique to the regional direction of Scandian thrusting (e.g. Fossen, 2000). Furthermore, the occurrence of constrictional fabrics as well as the abundance of lineation-parallel folds seem to be structurally better compatible with a Devonian transtensional system (Fossen et al., 2013; Krabbendam and Dewey, 1998; Osmundsen and Andersen, 2001) than with Scandian thrusting. More importantly, however, the progressive overprinting of brittle structures on previously ductile fabrics in low-angle shear zones with top-to-E kinematics, such as the Loddefjord shear zone, records exhumation during shearing. The phyllonites that formed in these shear zones are comparable to similar fault rocks in the Nordfjord Sogn detachment zone and have arguably an extraordinarily low shear strength (Braathen et al., 2004). If one assumes that these phyllonitic top-to-E fabrics formed during Scandian thrusting, they should have become overprinted by the intense extensional top-to-W deformation that overprinted gneisses with similar fabric orientation nearby (Rykkelid and Fossen, 1992). This implies that the phyllonitic top-to-E shear zones presumably formed during post-orogenic extension. Based on the identical orientation of amphibolite and upper greenschist facies fabrics it cannot be ruled out that also higher-grade mylonitic top-to-E deformation could have been extensional. Comparing the structure of the Øygarden Complex with similar basement windows in the central Norwegian Caledonides (Braathen et al., 2000; Osmundsen et al., 2005), we speculate that the Øygarden Complex could represent an early Devonian core complex. We believe that such a model could explain the occurrence of opposed shear-senses within the mylonitic foliation, constrictional fabrics with lineation parallel folds as well as low-angle normal-sense shear zones recording fluid-related strain weakening facilitating deformation at the brittle-ductile transition (Whitney et al., 2013).

7. Summary and conclusions

The evolution of continental crust in the eastern Øygarden Complex through three distinct orogenic periods as well as intermittent episodes of extension and tectonic quiescence is summarized in Fig. 10.

- The eastern Øygarden Complex consists of Telemarkian (1506 ± 5 Ma) granitic basement that was intruded by voluminous Sveconorwegian melts. These Grenville-age rocks formed through two distinct magmatic events: Bimodal gabbro and hornblende biotite granite magmatism at ca. 1041 Ma was followed by leucogranitic magmatism at ca. 1027–1022 Ma.
- The Precambrian evolution of the Øygarden Complex is distinct from that of the WGR. The Øygarden Complex rather represents a part of Telemarkia and a northern continuation of the Sirdal Magmatic Belt, but with a strong Caledonian overprint. Our results contradict previously proposed terrane boundaries (Roffeis and Corfu, 2014; Roffeis et al., 2013) separating Gothian and Telemarkian crust.
- Careful ion microprobe dating did not reveal any record of Sveconorwegian tectono-metamorphism in the eastern Øygarden Complex. In accordance with the undeformed Sirdal Magmatic Belt further south, our results support an accretionary Sveconorwegian orogen (e.g. Slagstad et al., 2013a), rather than involvement in a major continent-continent collision in the period 1040–1020 Ma.
- Resetting of strongly metamict zircons at ca. 482 Ma indicates an early Ordovician thermal event, reflecting either extension of the Baltican margin or early Caledonian convergence. Scandian regional metamorphism left no measurable record in the U-Pb zircon system.
- Caledonian ductile reworking involved east-directed shearing and recumbent lineation-parallel folding, followed by the formation of ductile-to-brittle top-to-E shear zones. Whether these E-directed fabrics/structures relate to Caledonian thrusting or post-Caledonian extension needs to be resolved by careful thermochronological dating. However, based on field observations, we currently favor an extensional origin related to the exhumation of the Øygarden Complex, possibly as an early Devonian core complex.

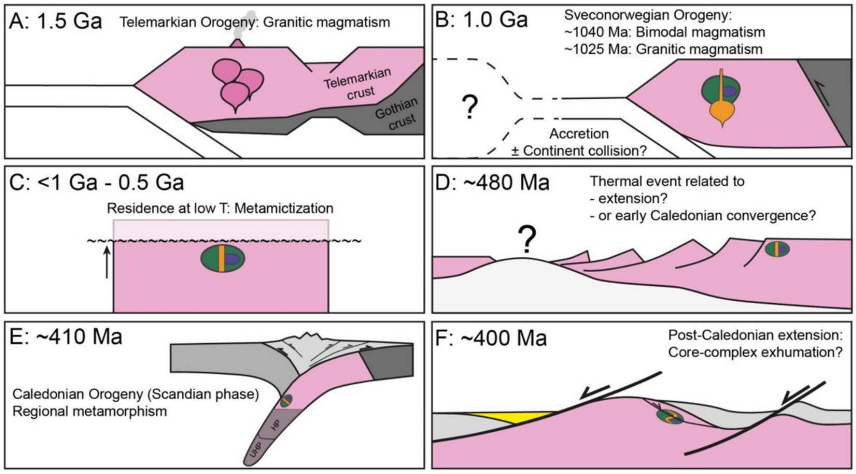

Fig. 10. Cartoon illustrating the geologic evolution of the eastern Øygarden Complex from the Mesoproterozoic to the early Devonian. Note that the colors correspond to the map units in Fig. 3. A, B are modified from (Roberts and Slagstad (2015)). D is based on (Andersen et al., 2012). E, F are modified from Fossen et al. (2017).

Acknowledgements

We thank Irina Dumitru, Martina Suppersberger Hamre, Egil Erichsen and Irene Heggstad at UiB for help with sample preparation and CL imaging. Martin Whitehouse, Lev Ilinsky and Kerstin Lindén at NordSIMS, Stockholm are thanked for great help with geochronology. We thank Fernando Corfu and one anonymous reviewer for thorough reviews that helped to improve the manuscript. JDW was supported by a DAAD student grant; and VISTA – a basic research program in collaboration between The Norwegian Academy of Science and Letters, and Statoil [grant number 6271]. The NordSIMS facility is supported by the research funding agencies of Denmark, Iceland, Norway and Sweden, and the Swedish Museum of Natural History. This is NordSIMS contribution number 534.

Appendix A. Supplementary data

Supplementary data associated with this article can be found, in the online version, at http://dx.doi.org/10.1016/j.precamres.2017.11.020.

References

Abdelmalak, M.M., Andersen, T.B., Planke, S., Faleide, J.I., Corfu, F., Tegner, C., Shephard, G.E., Zastrozhnov, D., Myklebust, R., 2015. The ocean-continent transition in the mid-Norwegian margin: insight from seismic data and an onshore Caledonian field analogue. Geology 43, 1011–1014. http://dx.doi.org/10.1130/G37086.1.

Allmendinger, R.W., Cardozo, N., Fisher, D.M., 2011. Structural Geology Algorithms: Vectors and Tensors. Cambridge University Press, Cambridge, pp. 302.

Andersen, T.B., Jamtveit, B., 1990. Uplift of deep crust during orogenic extensional collapse – a model based on field studies in the Sogn-Sunnfjord Region of Western Norway. Tectonics 9, 1097–1111. http://dx.doi.org/10.1029/TC009i005p01097.

Andersen, T.B., Jamtveit, B., Dewey, J.F., Swensson, E., 1991. Subduction and eduction of continental-crust – major mechanisms during continent-continent collision and orogenic extensional collapse, a model based on the South Norwegian Caledonides. Terra Nova 3, 303–310. http://dx.doi.org/10.1111/j.1365-3121.1991.tb00148.x.

Andersen, T., Graham, S., Sylvester, A.G., 2009. The geochemistry, Lu–Hf isotope systematics, and petrogenesis of Late Mesoproterozoic A-type granites in southwestern Fennoscandia. Can. Mineral. 47, 1399–1422. http://dx.doi.org/10.3749/canmin.47.6.1399.

Andersen, T.B., Corfu, F., Labrousse, L., Osmundsen, P.T., 2012. Evidence for hyperextension along the pre-Caledonian margin of Baltica. J. Geol. Soc. 169, 601–612. http://dx.doi.org/10.1144/0016-76492012-011.

Andresen, A., Steltenpohl, M.G., 1994. Evidence for ophiolite obduction, terrane accretion and polyorogenic evolution of the north Scandinavian Caledonides. Tectonophysics 231, 59–70. http://dx.doi.org/10.1016/0040-1951(94)90121-X.

Askvik, H., 1971. Gabbroic and Quartz Dioritic Intrusions in Gneisses on Southern Askoy, West Norwegian Caledonides. Norges Geologiske Undersøkelse 270, 3–38.

Augland, L.E., Andresen, A., Gasser, D., Steltenpohl, M.G., 2014. Early Ordovician to Silurian evolution of exotic terranes in the Scandinavian Caledonides of the Ofoten-Troms area – terrane characterization and correlation based on new U-Pb zircon ages and Lu–Hf isotopic data. Geol. Soc. London Spec. Publ. 390, 655–678. http://dx.doi.org/10.1144/sp390.19.

Auwera, J.V., Bogaerts, M., Liégeois, J.-P., Demaiffe, D., Wilmart, E., Bolle, O., Duchesne, J.C., 2003. Derivation of the 1.0–0.9 Ga ferro-potassic A-type granitoids of southern Norway by extreme differentiation from basic magmas. Precambr. Res. 124, 107–148. http://dx.doi.org/10.1016/S0301-9268(03)00084-6.

Bering, D.H., 1985. Tektonometamorf Utvikling Av Det Vestlige Gneiskompleks I Sund. University of Bergen, Sotra, pp. 367.

Bingen, B., Solli, A., 2009. Geochronology of magmatism in the Caledonian and Sveconorwegian belts of Baltica: synopsis for detrital zircon provenance studies. Norw. J. Geol. 89, 267–290.

Bingen, B., Van Breemen, O., 1998. Tectonic regimes and terrane boundaries in the high-grade Sveconorwegian belt of SW Norway, inferred from U-Pb zircon geochronology and geochemical signature of augen gneiss suites. J. Geol. Soc. 155, 143–154. http://dx.doi.org/10.1144/gsjgs.155.1.0143.

Bingen, B., Demaiffe, D., Hertogen, J., Weis, D., Michot, J., 1993. K-rich calc-alkaline Augen Gneisses of Grenvillian age in Sw Norway – mingling of mantle-derived and crustal components. J. Geol. 101, 763–778.

Bingen, B., Skar, O., Marker, M., Sigmond, E.M.O., Nordgulen, O., Ragnhildstveit, J., Mansfeld, J., Tucker, R.D., Liegeois, J.P., 2005. Timing of continental building in the Sveconorwegian orogen, SW Scandinavia. Norw. J. Geol. 85, 87–116.

Bingen, B., Davis, W.J., Hamilton, M.A., Engvik, A.K., Stein, H.J., Skar, O., Nordgulen, O., 2008a. Geochronology of high-grade metamorphism in the Sveconorwegian belt, S. Norway: U-Pb, Th-Pb and Re-Os data. Norw. J. Geol. 88, 13–42.

Bingen, B., Nordgulen, O., Viola, G., 2008b. A four-phase model for the Sveconorwegian orogeny, SW Scandinavia. Norw. J. Geol. 88, 43–72.

Bogaerts, M., Scaillet, B., Liégeois, J.-P., Vander Auwera, J., 2003. Petrology and geochemistry of the Lyngdal granodiorite (Southern Norway) and the role of fractional crystallisation in the genesis of Proterozoic ferro-potassic A-type granites. Precambr. Res. 124, 149–184. http://dx.doi.org/10.1016/S0301-9268(03)00085-8.

Bos, B., Spiers, C.J., 2002. Frictional-viscous flow of phyllosilicate-bearing fault rock: microphysical model and implications for crustal strength profiles. J. Geophys. Res. Solid Earth 107http://dx.doi.org/10.1029/2001jb000301. ECV 1-1-ECV 1-13.

Boundy, T.M., Essene, E.J., Hall, C.M., Austrheim, H., Halliday, A.N., 1996. Rapid exhumation of lower crust during continent-continent collision and late extension: evidence from Ar-40/Ar-39 incremental heating of hornblendes and muscovites, Caledonian orogen, western Norway. Geol. Soc. Am. Bull. 108, 1425–1437. http://dx.doi.org/10.1130/0016-7606(1996) 108.

Braathen, A., Nordgulen, O., Osmundsen, P.T., Andersen, T.B., Solli, A., Roberts, D., 2000. Devonian, orogen-parallel, opposed extension in the Central Norwegian Caledonides. Geology 28, 615–618. http://dx.doi.org/10.1130/0091-7613(2000) 28.

Braathen, A., Osmundsen, P.T., Gabrielsen, R.H., 2004. Dynamic development of fault rocks in a crustal-scale detachment: an example from western Norway. Tectonics 23. http://dx.doi.org/10.1029/2003tc001558.

Brewer, T.S., Åhäll, K.I., Menuge, J.F., Storey, C.D., Parrish, R.R., 2004. Mesoproterozoic bimodal volcanism in SW Norway, evidence for recurring pre-Sveconorwegian continental margin tectonism. Precambr. Res. 134, 249–273. http://dx.doi.org/10.1016/j.precamres.2004.06.003.

Brueckner, H.K., Van Roermund, H.L.M., Pearson, N.J., 2004. An archean(?) to paleozoic evolution for a garnet peridotite lens with sub-baltic shield affinity within the Seve Nappe Complex of Jamtland, Sweden, central Scandinavian Caledonides. J. Petrol.

45, 415–437. http://dx.doi.org/10.1093/petrology/egg088.
Bybee, G.M., Ashwal, L.D., Shirey, S.B., Horan, M., Mock, T., Andersen, T.B., 2014. Pyroxene megacrysts in Proterozoic anorthosites: implications for tectonic setting, magma source and magmatic processes at the Moho. Earth Planet. Sci. Lett. 389, 74–85. http://dx.doi.org/10.1016/j.epsl.2013.12.015.
Cawood, P.A., Pisarevsky, S.A., 2017. Laurentia-Baltica-Amazonia relations during Rodinia assembly. Precambr. Res. 292, 386–397. http://dx.doi.org/10.1016/j.precamres.2017.01.031.
Chauvet, A., Seranne, M., 1994. Extension-parallel folding in the Scandinavian Caledonides – implications for Late-Orogenic processes. Tectonophysics 238, 31–54. http://dx.doi.org/10.1016/0040-1951(94)90048-5.
Cherniak, D.J., Watson, E.B., 2003. Diffusion in zircon. Rev. Mineral. Geochem. 53, 113–143. http://dx.doi.org/10.2113/0530113.
Cocks, L.R.M., Torsvik, T.H., 2005. Baltica from the late Precambrian to mid-Palaeozoic times: the gain and loss of a terrane's identity. Earth Sci. Rev. 72, 39–66. http://dx.doi.org/10.1016/j.earscirev.2005.04.001.
Coint, N., Slagstad, T., Roberts, N.M.W., Marker, M., Rohr, T., Sorensen, B.E., 2015. The Late Mesoproterozoic Sirdal Magmatic Belt, SW Norway: relationships between magmatism and metamorphism and implications for Sveconorwegian orogenesis. Precambr. Res. 265, 57–77. http://dx.doi.org/10.1016/j.precamres.2015.05.002.
Corfu, F., Hanchar, J.M., Hoskin, P.W., Kinny, P., 2003. Atlas of zircon textures. Rev. Mineral. Geochem. 53, 469–500. http://dx.doi.org/10.2113/0530469.
Corfu, F., Andersen, T., Gasser, D., 2014. The Scandinavian Caledonides: main features, conceptual advances and critical questions. Geol. Soc. London Spec. Publ. 390, 9–43. http://dx.doi.org/10.1144/SP390.25.
Dunning, G.R., Pedersen, R.B., 1988. U/Pb ages of ophiolites and arc-related plutons of the Norwegian Caledonides – implications for the development of Iapetus. Contrib. Miner. Petrol. 98, 13–23. http://dx.doi.org/10.1007/Bf00371904.
Eide, E.A., Torsvik, T.H., Andersen, T.B., 1997. Absolute dating of brittle fault movements: Late Permian and late Jurassic extensional fault breccias in western Norway. Terra Nova 9, 135–139.
Essex, R.M., Gromet, L.P., Andreasson, P.G., Albrecht, L., 1997. Early Ordovician U-Pb metamorphic ages of the eclogite-bearing Seve Nappes, northern Scandinavian Caledonides. J. Metamorph. Geol. 15, 665–676. http://dx.doi.org/10.1111/j.1525-1314.1997.00048.x.
Faerseth, R.B., Gjelberg, J., Martinsen, O.J., 2011. Structural geology and sedimentology of Silurian metasediments in the Ulven area, Major Bergen Arc, SW Norway. Norw. J. Geol. 91, 19–33.
Fossen, H., 1989. Geology of the minor Bergen arc, West Norway. Norges Geologiske Undersøkelse Bull. 416, 47–62.
Fossen, H., 1992. The role of extensional tectonics in the Caledonides of South Norway. J. Struct. Geol. 14, 1033–1046. http://dx.doi.org/10.1016/0191-8141(92)90034-T.
Fossen, H., 1993. Linear fabrics in the bergsdalen nappes, southwest Norway – implications for deformation history and fold development. Nor. Geol. Tidsskr. 73, 95–108.
Fossen, H., 1998. Advances in understanding the post-Caledonian structural evolution of the Bergen Area, West Norway. Nor. Geol. Tidsskr. 78, 33–46.
Fossen, H., 2000. Extensional tectonics in the Caledonides: synorogenic or postorogenic? Tectonics 19, 213–224. http://dx.doi.org/10.1029/1999tc900066.
Fossen, H., 2010. Extensional tectonics in the North Atlantic Caledonides: a regional view. Geol. Soc. London Spec. Publ. 335, 767–793. http://dx.doi.org/10.1144/SP335.31.
Fossen, H., Dunlap, W.J., 1998. Timing and kinematics of Caledonian thrusting and extensional collapse, southern Norway: evidence from Ar-40/Ar-39 thermochronology. J. Struct. Geol. 20, 765–781. http://dx.doi.org/10.1016/S0191-8141(98)00007-8.
Fossen, H., Dunlap, W.J., 2006. Age constraints on the late Caledonian (Scandian) deformation in the major Bergen Arc, SW Norway. Norw. J. Geol. 86, 59–70.
Fossen, H., Hurich, C.A., 2005. The Hardangerfjord Shear Zone in SW Norway and the North Sea: a large-scale low-angle Shear Zone in the Caledonian crust. J. Geol. Soc. 162, 675–687. http://dx.doi.org/10.1144/0016-764904-136.
Fossen, H., Rykkelid, E., 1990. Shear zone structures in the Oygarden Area, West Norway. Tectonophysics 174, 385–397. http://dx.doi.org/10.1016/0040-1951(90)90333-4.
Fossen, H., Rykkelid, E., 1992a. The Interaction between oblique and layer-parallel shear in high-strain zones – observations and experiments. Tectonophysics 207, 331–343. http://dx.doi.org/10.1016/0040-1951(92)90394-L.
Fossen, H., Rykkelid, E., 1992b. Postcollisional extension of the caledonide orogen in Scandinavia – structural expressions and tectonic significance. Geology 20, 737–740. http://dx.doi.org/10.1130/0091-7613(1992) 020∗0737:Peotco > 2.3.Co;2.
Fossen, H., Teyssier, C., Whitney, D.L., 2013. Transtensional folding. J. Struct. Geol. 56, 89–102. http://dx.doi.org/10.1016/j.jsg.2013.09.004.
Fossen, H., Khani, H.F., Faleide, J.I., Ksienzyk, A.K., Dunlap, W.J., 2016. Post-Caledonian extension in the West Norway–northern North Sea region: the role of structural inheritance. Geol. Soc. London Spec. Publ. 439. http://dx.doi.org/10.1144/SP439.6.
Fossen, H., Cavalcante, G.C., de Almeida, R.P., 2017. Hot versus cold orogenic behavior: comparing the araçuaí-West Congo and the Caledonian Orogens. Tectonics. http://dx.doi.org/10.1002/2017TC004743. n/a–n/a.
Furnes, H., Dilek, Y., Pedersen, R.B., 2012. Structure, geochemistry, and tectonic evolution of trench-distal backarc oceanic crust in the western Norwegian Caledonides, Solund-Stavfjord ophiolite (Norway). Geol. Soc. Am. Bull. 124, 1027–1047. http://dx.doi.org/10.1130/B30561.1.
Gee, D.G., 1975. A tectonic model for the central part of the Scandinavian Caledonides. Am. J. Sci. A275, 468–515.
Gee, D.G., Fossen, H., Henriksen, N., Higgins, A.K., 2008. From the early Paleozoic platforms of Baltica and Laurentia to the Caledonide orogen of Scandinavia and Greenland. Episodes 31, 44–51.
Gee, D.G., Janak, M., Majka, J., Robinson, P., van Roermund, H., 2013. Subduction along and within the Baltoscandian margin during closing of the Iapetus Ocean and Baltica-Laurentia collision. Lithosphere 5, 169–178. http://dx.doi.org/10.1130/L220.1.
Gee, D.G., Andréasson, P.-G., Li, Y., Krill, A., 2017. Baltoscandian margin, Sveconorwegian crust lost by subduction during Caledonian collisional orogeny. GFF 139, 36–51. http://dx.doi.org/10.1080/11035897.2016.1200667.
Gordon, S.M., Whitney, D.L., Teyssier, C., Fossen, H., 2013. U-Pb dates and trace-element geochemistry of zircon from migmatite, Western Gneiss Region, Norway: significance for history of partial melting in continental subduction. Lithos 170, 35–53. http://dx.doi.org/10.1016/j.lithos.2013.02.003.
Hacker, B.R., Gans, P.B., 2005. Continental collisions and the creation of ultrahigh-pressure terranes: petrology and thermochronology of nappes in the central Scandinavian Caledonides. Geol. Soc. Am. Bull. 117, 117–134. http://dx.doi.org/10.1130/B25549.1.
Hacker, B.R., Andersen, T.B., Johnston, S., Kylander-Clark, A.R.C., Peterman, E.M., Walsh, E.O., Young, D., 2010. High-temperature deformation during continental-margin subduction & exhumation: the ultrahigh-pressure Western Gneiss Region of Norway. Tectonophysics 480, 149–171. http://dx.doi.org/10.1016/j.tecto.2009.08.012.
Jakob, J., Alsaif, M., Corfu, F., Andersen, T.B., 2017. Age and origin of thin discontinuous gneiss sheets in the distal domain of the magma-poor hyperextended pre-Caledonian margin of Baltica, southern Norway. J. Geol. Soc. http://dx.doi.org/10.1144/jgs2016-049.
Jeon, H., Whitehouse, M.J., 2015. A critical evaluation of U-Pb calibration schemes used in SIMS zircon geochronology. Geostand. Geoanal. Res. 39, 443–452. http://dx.doi.org/10.1111/j.1751-908X.2014.00325.x.
Johns, C.C., 1981. The Geology of Northern Sotra: Precambrian Gneisses West of the Bergen Arcs. University of London, Norway, Bedford College, pp. 397.
Johnston, S., Hacker, B.R., Ducea, M.N., 2007. Exhumation of ultrahigh-pressure rocks beneath the Hornelen segment of the Nordfjord-Sogn Detachment Zone, western Norway. Geol. Soc. Am. Bull. 119, 1232–1248. http://dx.doi.org/10.1130/B26172.1.
Klonowska, I., Majka, J., Janák, M., Gee, D.G., Ladenberger, A., 2014. Pressure–temperature evolution of a kyanite–garnet pelitic gneiss from Åreskutan: evidence of ultra-high-pressure metamorphism of the Seve Nappe Complex, west-central Jämtland, Swedish Caledonides. Geol. Soc. London Spec. Publ. 390, 321–336. http://dx.doi.org/10.1144/SP390.7.
Knudsen, T.L., Fossen, H., 2001. The Late Jurassic Bjoroy Formation: a provenance indicator for offshore sediments derived from SW Norway as based on single zircon (SIMS) data. Nor. Geol. Tidsskr. 81, 283–292.
Kolderup, C.F., Kolderup, N.H., 1940. Geology of the Bergen Arc System. Bergen Museums Skrifter 20, 137.
Krabbendam, M., Dewey, J.F., 1998. Exhumation of UHP rocks by transtension in the Western Gneiss Region, Scandinavian Caledonides. Geol. Soc. London Spec. Publ. 135, 159–181.
Ksienzyk, A.K., Dunkl, I., Jacobs, J., Fossen, H., Kohlmann, F., 2014. From orogen to passive margin: constraints from fission track and (U–Th)/He analyses on Mesozoic uplift and fault reactivation in SW Norway. Geol. Soc. London Spec. Publ. 390, 679–702. http://dx.doi.org/10.1144/SP390.27.
Ksienzyk, A.K., Wemmer, K., Jacobs, J., Fossen, H., Schomberg, A.C., Sussenberger, A., Lunsdorf, N.K., Bastesen, E., 2016. Post-Caledonian brittle deformation in the Bergen area, West Norway: results from K-Ar illite fault gouge dating. Norw. J. Geol. 96, 275–299. https://doi.org/10.17850/njg96-3-06.
Kvale, A., 1960. The nappe area of the Caledonides in western Norway. Norges Geologiske Undersøkelse Bull. 21–43 212e.
Larsen, O., 1996. Fedjedomens tektoniske utvikling (Øygarden gneiskompleks, vest Norge) – en alternative model for dannelse av gneisdomer (MSc thesis). University of Bergen.
Larsen, O., Fossen, H., Langeland, K., Pedersen, R.B., 2003. Kinematics and timing of polyphase post-Caledonian deformation in the Bergen area, SW Norway. Norw. J. Geol. 83, 149–165.
Li, Z.X., Bogdanova, S.V., Collins, A.S., Davidson, A., De Waele, B., Ernst, R.E., Fitzsimons, I.C.W., Fuck, R.A., Gladkochub, D.P., Jacobs, J., Karlstrom, K.E., Lu, S., Natapov, L.M., Pease, V., Pisarevsky, S.A., Thrane, K., Vernikovsky, V., 2008. Assembly, configuration, and break-up history of Rodinia: a synthesis. Precambr. Res. 160, 179–210. http://dx.doi.org/10.1016/j.precamres.2007.04.021.
Ludwig, K.R., 1998. On the treatment of concordant uranium-lead ages. Geochim. Cosmochim. Acta 62, 665–676. http://dx.doi.org/10.1016/S0016-7037(98)00059-3.
Ludwig, K.R., 2003. User's Manual For Isoplot 3.00: A Geochronological Toolkit for Microsoft Excel. Kenneth R. Ludwig.
Mezger, K., Krogstad, E.J., 1997. Interpretation of discordant U-Pb zircon ages: an evaluation. J. Metamorph. Geol. 15, 127–140. http://dx.doi.org/10.1111/j.1525-1314.1997.00008.x.
Milnes, A., Wennberg, O., Skår, Ø., Koestler, A., 1997. Contraction, extension and timing in the South Norwegian Caledonides: the Sognefjord transect. Geol. Soc. London Spec. Publ. 121, 123–148.
Möller, C., Bingen, B., Andersson, J., Stephens, M.B., Viola, G., Schersten, A., 2013. A non-collisional, accretionary Sveconorwegian orogen – comment. Terra Nova 25, 165–168. http://dx.doi.org/10.1111/ter.12029.
Möller, C., Andersson, J., Dyck, B., Antal Lundin, I., 2015. Exhumation of an eclogite terrane as a hot migmatitic nappe, Sveconorwegian orogen. Lithos 226, 147–168. http://dx.doi.org/10.1016/j.lithos.2014.12.013.
Norton, M.G., 1987. The Nordfjord-Sogn Detachment, W Norway. Nor. Geol. Tidsskr. 67, 93–106.
Osmundsen, P.T., Andersen, T.B., 2001. The middle Devonian basins of western Norway: sedimentary response to large-scale transtensional tectonics? Tectonophysics 332, 51–68. http://dx.doi.org/10.1016/S0040-1951(00)00249-3.
Osmundsen, P.T., Braathen, A., Sommaruga, A., Skilbrei, J.R., Nordgulen, O., Roberts, D., Andersen, T.B., Olesen, O., Mosar, J., 2005. Metamorphic core complexes and gneiss-cored culminations along the Mid-Norwegian margin: an overview and some current

ideas. Norw. Petrol. Soc. Spec. Publ. 12, 29–41. http://dx.doi.org/10.1016/S0928-8937(05)80042-6.
Pascal, C., Rudlang, T., 2016. Discovery of highly radioactive granite in the Bergen Region. Norw. J. Geol. 96, 319–328. https://doi.org/10.17850/njg96-4-03.
Pease, V., Daly, J.S., Elming, S.Å., Kumpulainen, R., Moczydlowska, M., Puchkov, V., Roberts, D., Saintot, A., Stephenson, R., 2008. Baltica in the Cryogenian, 850–630Ma. Precambr. Res. 160, 46–65. http://dx.doi.org/10.1016/j.precamres.2007.04.015.
Pedersen, R.B., Dunning, G.R., 1997. Evolution of arc crust and relations between contrasting sources: U-PL (age), Nd and Sr isotope systematics of the ophiolitic terrain of SW Norway. Contrib. Miner. Petrol. 128, 1–15. http://dx.doi.org/10.1007/s004100050289.
Pedersen, R.B., Bruton, D.L., Furnes, H., 1992. Ordovician Faunas, Island Arcs and Ophiolites in the Scandinavian Caledonides. Terra Nova 4, 217–222. http://dx.doi.org/10.1111/j.1365-3121.1992.tb00475.x.
Ragnhildstveit, J., Helliksen, D., 1997. Geologisk Kart Over Norge, berggrunnskart Bergen – M 1:250.000. Norges Geologiske Undersøkelse.
Rino, S., Kon, Y., Sato, W., Maruyama, S., Santosh, M., Zhao, D., 2008. The Grenvillian and Pan-African orogens: world's largest orogenies through geologic time, and their implications on the origin of superplume. Gondwana Res. 14, 51–72. http://dx.doi.org/10.1016/j.gr.2008.01.001.
Roberts, D., 2003. The Scandinavian Caledonides: event chronology, palaeogeographic settings and likely, modern analogues. Tectonophysics 365, 283–299. http://dx.doi.org/10.1016/S0040-1951(03)00026-X.
Roberts, N.M.W., Slagstad, T., 2015. Continental growth and reworking on the edge of the Columbia and Rodinia supercontinents; 1.86-0.9 Ga accretionary orogeny in southwest Fennoscandia. Int. Geol. Rev. 57, 1582–1606. http://dx.doi.org/10.1080/00206814.2014.958579.
Roberts, N.M.W., Slagstad, T., Parrish, R.R., Norry, M.J., Marker, M., Horstwood, M.S.A., 2013. Sedimentary recycling in arc magmas: geochemical and U-Pb-Hf-O constraints on the Mesoproterozoic Suldal Arc, SW Norway. Contrib. Miner. Petrol. 165, 507–523. http://dx.doi.org/10.1007/s00410-012-0820-y.
Roberts, N.M.W., Slagstad, T., Viola, G., 2015. The structural, metamorphic and magmatic evolution of Mesoproterozoic orogens. Precambr. Res. 265, 1–9. http://dx.doi.org/10.1016/j.precamres.2015.05.031.
Roffeis, C., Corfu, F., 2014. Caledonian nappes of southern Norway and their correlation with Sveconorwegian basement domains. Geol. Soc. London Spec. Publ. 390, 193–221. http://dx.doi.org/10.1144/SP390.13.
Roffeis, C., Corfu, F., Gabrielsen, R.H., 2013. A Sveconorwegian terrane boundary in the Caledonian Hardanger-Ryfylke Nappe Complex: the lost link between Telemarkia and the Western Gneiss Region? Precambr. Res. 228, 20–35. http://dx.doi.org/10.1016/j.precamres.2013.01.008.
Rohr, T.S., Bingen, B., Robinson, P., Reddy, S.M., 2013. Geochronology of Paleoproterozoic Augen Gneisses in the Western Gneiss Region, Norway: evidence for Sveconorwegian Zircon Neocrystallization and Caledonian Zircon Deformation. J. Geol. 121, 105–128. http://dx.doi.org/10.1086/669229.
Root, D., Corfu, F., 2012. U-Pb geochronology of two discrete Ordovician high-pressure metamorphic events in the Seve Nappe Complex, Scandinavian Caledonides. Contrib. Miner. Petrol. 163, 769–788. http://dx.doi.org/10.1007/s00410-011-0698-0.
Root, D.B., Hacker, B.R., Mattinson, J.M., Wooden, J.L., 2004. Zircon geochronology and ca. 400 Ma exhumation of Norwegian ultrahigh-pressure rocks: an ion microprobe and chemical abrasion study. Earth Planet. Sci. Lett. 228, 325–341. http://dx.doi.org/10.1016/j.epsl.2004.10.019.
Rykkelid, E., Fossen, H., 1992. Composite fabrics in Midcrustal Gneisses – observations from the Oygarden complex, West Norway Caledonides. J. Struct. Geol. 14, 1–9. http://dx.doi.org/10.1016/0191-8141(92)90139-N.
Schulze, K., 2014. Radiogenic Heat Production in the Bed Rock of Bergen, Norway with Gamma-Spectrometry and its Relevance for Geothermal Energy (MSc thesis). Christian-Albrechts Universität Kiel, pp. 108.
Seranne, M., Seguret, M., 1987. The Devonian basins of western Norway: tectonics and kinematics of an extending crust. Geol. Soc. London Spec. Publ. 28, 537–548.
Skår, Ø., 2000. Field relations and geochemical evolution of the Gothian rocks in the Kvamsoy area, southern Western Gneiss Complex, Norway. Norges Geologiske Undersøkelse Bulletin 437, 5–24.
Skår, Ø., Pedersen, R.B., 2003. Relations between granitoid magmatism and migmatization: U-Pb geochronological evidence from the Western Gneiss Complex, Norway. J. Geol. Soc. 160, 935–946. http://dx.doi.org/10.1144/0016-764901-121.
Skår, Ø., Furnes, H., Claesson, S., 1994. Proterozoic orogenic magmatism within the Western Gneiss Region, Sunnfjord, Norway. Nor. Geol. Tidsskr. 74, 114–126.
Slagstad, T., Roberts, N.M.W., Marker, M., Rohr, T.S., Schiellerup, H., 2013a. A non-collisional, accretionary Sveconorwegian orogen. Terra Nova 25, 30–37. http://dx.doi.org/10.1111/ter.12001.
Slagstad, T., Roberts, N.M.W., Marker, M., Rohr, T.S., Schiellerup, H., 2013b. A non-collisional, accretionary Sveconorwegian orogen – reply. Terra Nova 25, 169–171. http://dx.doi.org/10.1111/ter.12028.
Slagstad, T., Pin, C., Roberts, D., Kirkland, C.L., Grenne, T., Dunning, G., Sauer, S., Andersen, T., 2014. Tectonomagmatic evolution of the Early Ordovician supra-subduction-zone ophiolites of the Trondheim Region, Mid-Norwegian Caledonides. Geol. Soc. London Spec. Publ. 390, 541–561. http://dx.doi.org/10.1144/SP390.11.
Slagstad, T., Roberts, N.M.W., Kulakov, E., 2017. Linking orogenesis across a supercontinent; the Grenvillian and Sveconorwegian margins on Rodinia. Gondwana Res. 44, 109–115. http://dx.doi.org/10.1016/j.gr.2016.12.007.
Slama, J., Pedersen, R.B., 2015. Zircon provenance of SW Caledonian phyllites reveals a distant Timanian sediment source. J. Geol. Soc. 172, 465–478. http://dx.doi.org/10.1144/jgs2014-143.
Spencer, C.J., Roberts, N.M.W., Cawood, P.A., Hawkesworth, C.J., Prave, A.R., Antonini, A.S.M., Horstwood, M.S.A., 2014. Intermontane basins and bimodal volcanism at the onset of the Sveconorwegian Orogeny, southern Norway. Precambr. Res. 252, 107–118. http://dx.doi.org/10.1016/j.precamres.2014.07.008.
Stacey, J.S., Kramers, J.D., 1975. Approximation of Terrestrial Lead Isotope Evolution by a 2-Stage Model. Earth Planet. Sci. Lett. 26, 207–221. http://dx.doi.org/10.1016/0012-821x(75)90088-6.
Steel, R., Siedlecka, A., Roberts, D., 1985. The Old Red Sandstone basins of Norway and their deformation: a review. In: Gee, D.G., Sturt, B.A. (Eds.), The Caledonide Orogen – Scandinavia and Related Areas. Wiley, Chichester, pp. 293–315.
Steiger, R.H., Jäger, E., 1977. Subcommission on geochronology – convention on use of decay constants in geochronology and cosmochronology. Earth Planet. Sci. Lett. 36, 359–362. http://dx.doi.org/10.1016/0012-821x(77)90060-7.
Steltenpohl, M., Hames, W., Andresen, A., Markl, G., 2003. New Caledonian eclogite province in Norway and potential Laurentian (Taconic) and Baltic links. Geology 31, 985–988. http://dx.doi.org/10.1130/g19744.1.
Sturt, B.A., Thon, A., 1978. Caledonides of southern Norway. Caledonian-Appalachian orogen of the North Atlantic region, IGCP project 27, pp. 39–47.
Sturt, B.A., Skarpenes, O., Ohanian, A.T., Pringle, I.R., 1975. Reconnaissance Rb-Sr Isochron Study in Bergen Arc System and Regional Implications. Nature 253, 595–599. http://dx.doi.org/10.1038/253595a0.
Sturt, B., Pringle, I., Ramsay, D., 1978. The Finnmarkian phase of the Caledonian orogeny. J. Geol. Soc. 135, 597–610.
Torsvik, T.H., Cocks, L.R.M., 2005. Norway in space and time: a centennial cavalcade. Norw. J. Geol. 85, 73–86.
Torsvik, T.H., Smethurst, M.A., Meert, J.G., VanderVoo, R., McKerrow, W.S., Brasier, M.D., Sturt, B.A., Walderhaug, H.J., 1996. Continental break-up and collision in the Neoproterozoic and Palaeozoic – a tale of Baltica and Laurentia. Earth Sci. Rev. 40, 229–258. http://dx.doi.org/10.1016/0012-8252(96)00008-6.
Tucker, R.D., Raheim, A., Krogh, T.E., Corfu, F., 1987. Uranium-lead zircon and titanite ages from the northern portion of the Western Gneiss Region, South-Central Norway. Earth Planet. Sci. Lett. 81, 203–211. http://dx.doi.org/10.1016/0012-821x(87)90156-7.
Tucker, R.D., Robinson, P., Solli, A., Gee, D.G., Thorsnes, T., Krogh, T.E., Nordgulen, O., Bickford, M.E., 2004. Thrusting and extension in the Scandian hinterland, Norway: new U-Pb ages and tectonostratigraphic evidence. Am. J. Sci. 304, 477–532. http://dx.doi.org/10.2475/ajs.304.6.477.
Vetti, V.V., Fossen, H., 2012. Origin of contrasting Devonian supradetachment basin types in the Scandinavian Caledonides. Geology 40, 571–574. http://dx.doi.org/10.1130/G32512.1.
Weiss, L.E., 1977. Structural features of the Laksevåg Gneiss, Bergen, Norway. Norges Geologiske Undersøkelse 334, 1–17.
Wennberg, O.P., 1996. Superimposed fabrics due to reversal of shear sense: an example from the Bergen Arc Shear Zone, western Norway. J. Struct. Geol. 18http://dx.doi.org/10.1016/0191-8141(96)00014-4. 871-&.
Wennberg, O.P., Milnes, A.G., 1994. Interpretation of kinematic indicators along the northeastern margin of the bergen arc system – a preliminary field-study. Nor. Geol. Tidsskr. 74, 166–173.
Wennberg, O.P., Milnes, A.G., Winsvold, I., 1998. The northern Bergen Arc Shear Zone – an oblique-lateral ramp in the Devonian extensional detachment system of western Norway. Nor. Geol. Tidsskr. 78, 169–184.
Whitehouse, M.J., Kamber, B.S., 2005. Assigning dates to thin gneissic veins in high-grade metamorphic terranes: a cautionary tale from Akilia, southwest Greenland. J. Petrol. 46, 291–318. http://dx.doi.org/10.1093/petrology/egh075.
Whitehouse, M.J., Claesson, S., Sunde, T., Vestin, J., 1997. Ion microprobe U–Pb zircon geochronology and correlation of Archaean gneisses from the Lewisian Complex of Gruinard Bay, northwestern Scotland. Geochim. Cosmochim. Acta 61, 4429–4438. http://dx.doi.org/10.1016/S0016-7037(97)00251-2.
Whitehouse, M.J., Kamber, B.S., Moorbath, S., 1999. Age significance of U-Th-Pb zircon data from early Archaean rocks of west Greenland – a reassessment based on combined ion-microprobe and imaging studies. Chem. Geol. 160, 201–224. http://dx.doi.org/10.1016/S0009-2541(99)00066-2.
Whitney, D.L., Teyssier, C., Vanderhaeghe, O., 2004. Gneiss domes and crustal flow. Geol. Soc. Am. Spec. Papers 380, 15–33. http://dx.doi.org/10.1130/0-8137-2380-9.15.
Whitney, D.L., Teyssier, C., Rey, P., Buck, W.R., 2013. Continental and oceanic core complexes. Geol. Soc. Am. Bull. 125, 273–298. http://dx.doi.org/10.1130/B30754.1.
Wiedenbeck, M., Alle, P., Corfu, F., Griffin, W., Meier, M., Oberli, F., Quadt, A.V., Roddick, J., Spiegel, W., 1995. Three natural zircon standards for U-Th-Pb, Lu-Hf, trace element and REE analyses. Geostand. Newslett. 19, 1–23. http://dx.doi.org/10.1111/j.1751-908X.1995.tb00147.x.
Wintsch, R.P., Christoffersen, R., Kronenberg, A.K., 1995. Fluid-rock reaction weakening of fault zones. J. Geophys. Res. Solid Earth 107http://dx.doi.org/10.1029/94jb02622. ECV 1-1-ECV 1-13.

Appendix

Table S1. SIMS U-Pb zircon data

Sample ID	Int.[1]	Concentration (ppm)						Total (uncorrected) ratio				Radiogenic (corrected) ratio[4]				Calculated age (Ma)				
		U	Th	Pb	Th/U [2]	$^{206}Pb/^{204}Pb$	f_{206} [3] (%)	$^{206}Pb/^{238}U$	±σ (%)	$^{207}Pb/^{206}Pb$	±σ (%)	$^{206}Pb/^{238}U$	±σ (%)	$^{207}Pb/^{206}Pb$	±σ (%)	$^{207}Pb/^{206}Pb$	±σ	$^{206}Pb/^{238}U$	±σ	Conc (%)
LYD-197-1: *Hornblende biotite granite gneiss; 5°14'30,7"E, 60°22'24,9"N*																				
n5416-01	I	230	76	47	0.33	252462	{0.01}	0.1747	0.83	0.07330	0.72	0.1747	0.83	0.07330	0.72	1022	14	1038	8	102
n5416-02	I	209	69	43	0.33	44154	{0.04}	0.1747	0.82	0.07280	0.75	0.1747	0.82	0.07280	0.75	1008	15	1038	8	103
n5416-03	I	150	61	31	0.41	62481	{0.03}	0.1740	0.88	0.07413	0.88	0.1740	0.88	0.07413	0.88	1045	18	1034	8	99
n5416-04	I	570	80	110	0.14	79916	0.02	0.1725	0.77	0.07435	0.64	0.1724	0.77	0.07417	0.64	1046	13	1026	7	98
n5416-05	I	151	47	31	0.31	38875	{0.05}	0.1744	0.83	0.07393	0.84	0.1744	0.83	0.07393	0.84	1039	17	1036	8	100
n5416-06	I	185	72	39	0.39	70701	{0.03}	0.1763	0.82	0.07347	0.72	0.1763	0.82	0.07347	0.72	1027	14	1047	8	102
n5416-07	I	170	55	35	0.33	92407	{0.02}	0.1759	0.86	0.07468	0.97	0.1759	0.86	0.07468	0.97	1060	19	1044	8	98
n5416-08	I	152	48	31	0.31	60603	{0.03}	0.1766	0.83	0.07463	0.79	0.1766	0.83	0.07463	0.79	1058	16	1048	8	99
n5416-09-1	I	195	62	40	0.32	58907	{0.03}	0.1750	0.83	0.07419	0.70	0.1750	0.83	0.07419	0.70	1047	14	1039	8	99
n5416-09-2	P	1399	43	256	0.03	64916	0.03	0.1688	0.76	0.07287	0.27	0.1688	0.76	0.07265	0.27	1004	5	1005	7	100
n5416-10	I	279	120	59	0.43	114366	{0.02}	0.1766	0.81	0.07413	0.58	0.1766	0.81	0.07413	0.58	1045	12	1048	8	100
n5416-11	I	206	60	42	0.29	150254	{0.01}	0.1759	0.80	0.07323	0.68	0.1759	0.80	0.07323	0.68	1020	14	1044	8	103
n5416-12	I	121	35	25	0.29	65275	{0.03}	0.1756	0.87	0.07542	0.89	0.1756	0.87	0.07542	0.89	1080	18	1043	8	96
n5416-13	I	211	68	43	0.32	28987	0.06	0.1760	0.80	0.07366	0.93	0.1759	0.80	0.07316	0.96	1019	19	1044	8	103
n5416-14	I	114	71	25	0.62	22520	{0.08}	0.1763	0.87	0.07256	1.04	0.1763	0.87	0.07256	1.04	1002	21	1047	8	105
n5416-15	I	194	70	41	0.36	226435	{0.01}	0.1760	0.80	0.07374	0.70	0.1760	0.80	0.07374	0.70	1034	14	1045	8	101
n5416-16	I	179	57	37	0.32	89744	{0.02}	0.1758	0.82	0.07394	0.76	0.1758	0.82	0.07394	0.76	1040	15	1044	8	100
n5416-17	I	360	113	73	0.31	110278	{0.02}	0.1743	0.78	0.07362	0.52	0.1743	0.78	0.07362	0.52	1031	10	1036	7	100
n5416-18-1	I	195	94	42	0.48	141587	{0.01}	0.1767	0.81	0.07449	0.68	0.1767	0.81	0.07449	0.68	1055	14	1049	8	99
n5416-18-2	I	413	121	85	0.29	56551	0.03	0.1760	0.78	0.07351	0.56	0.1759	0.78	0.07325	0.57	1021	12	1045	7	102
n5416-19-1	I	158	50	32	0.32	61678	{0.03}	0.1748	0.82	0.07361	0.87	0.1748	0.82	0.07361	0.87	1031	17	1039	8	101
n5416-19-2	I	100	41	21	0.41	33246	{0.06}	0.1759	0.91	0.07456	0.95	0.1759	0.91	0.07456	0.95	1057	19	1045	9	99
n5416-20	I	185	60	38	0.33	41137	{0.05}	0.1765	0.85	0.07501	0.71	0.1765	0.85	0.07501	0.71	1069	14	1048	8	98
n5416-21	I	194	65	40	0.33	45732	{0.04}	0.1768	0.82	0.07366	0.68	0.1768	0.82	0.07366	0.68	1032	14	1050	8	102
n5416-22	I	153	38	31	0.25	218947	{0.01}	0.1760	0.83	0.07499	0.77	0.1760	0.83	0.07499	0.77	1068	15	1045	8	98
n5416-23	I	141	49	29	0.35	23517	{0.08}	0.1750	0.85	0.07419	0.80	0.1750	0.85	0.07419	0.80	1047	16	1040	8	99
n5416-24	I	186	43	37	0.23	25209	0.07	0.1754	0.84	0.07416	0.70	0.1752	0.84	0.07360	0.74	1030	15	1041	8	101
LYD-44-1: *Metagabbro; 5°14'20,9"E, 60°22'31,9"N*																				
n5417-01	I	210	213	51	1.01	56358	{0.03}	0.1758	0.81	0.07447	0.66	0.1758	0.81	0.07447	0.66	1054	13	1044	8	99
n5417-02	I	174	138	40	0.79	14339	0.13	0.1741	0.81	0.07457	0.72	0.1739	0.81	0.07358	0.83	1030	17	1034	8	100
n5417-03	I	169	101	37	0.60	>1e6	{0.00}	0.1748	0.81	0.07464	0.72	0.1748	0.81	0.07464	0.72	1059	14	1039	8	98
n5417-04	I	138	68	29	0.49	>1e6	{0.00}	0.1735	0.93	0.07521	1.05	0.1735	0.93	0.07521	1.05	1074	21	1031	9	96
n5417-05	I	196	126	44	0.64	35219	0.05	0.1767	0.80	0.07335	0.68	0.1766	0.80	0.07294	0.70	1012	14	1048	8	104
n5417-06	I	167	121	38	0.72	235159	{0.01}	0.1764	0.85	0.07379	0.74	0.1764	0.85	0.07379	0.74	1036	15	1048	8	101
n5417-07	I	210	195	50	0.93	299077	{0.01}	0.1758	0.83	0.07440	0.92	0.1758	0.83	0.07440	0.92	1052	18	1044	8	99
n5417-08	I	290	233	66	0.80	76252	{0.02}	0.1732	0.78	0.07362	0.56	0.1732	0.78	0.07362	0.56	1031	11	1030	7	100
n5417-09	I	186	172	45	0.92	>1e6	{0.00}	0.1753	0.80	0.07410	0.70	0.1753	0.80	0.07410	0.70	1044	14	1041	8	100
n5417-10	I	291	265	70	0.91	90980	{0.02}	0.1762	0.77	0.07374	0.57	0.1762	0.77	0.07374	0.57	1034	11	1046	7	101
n5417-11	I	216	194	52	0.90	169740	{0.01}	0.1767	0.79	0.07444	0.64	0.1767	0.79	0.07444	0.64	1054	13	1049	8	100
n5417-12	I	296	240	69	0.81	236995	{0.01}	0.1759	0.78	0.07381	0.56	0.1759	0.78	0.07381	0.56	1036	11	1044	8	101
n5417-13	I	324	266	76	0.82	255534	{0.01}	0.1762	0.80	0.07357	0.56	0.1762	0.80	0.07357	0.56	1030	11	1046	8	102
n5417-14	I	150	116	35	0.77	59648	{0.03}	0.1752	0.83	0.07434	0.78	0.1752	0.83	0.07434	0.78	1051	16	1041	8	99
n5417-16	I	194	191	47	0.98	39704	{0.05}	0.1759	0.84	0.07354	0.69	0.1759	0.84	0.07354	0.69	1029	14	1045	8	102
n5417-15	I	293	274	71	0.94	151879	{0.01}	0.1769	0.78	0.07375	0.56	0.1769	0.78	0.07375	0.56	1035	11	1050	8	102
n5417-17	I	463	603	125	1.30	222877	{0.01}	0.1830	0.97	0.07269	0.43	0.1830	0.97	0.07269	0.43	1005	9	1083	10	108
n5417-18	I	367	381	90	1.04	28581	0.07	0.1747	0.81	0.07451	0.51	0.1746	0.81	0.07401	0.54	1042	11	1037	8	100
n5417-19	I	184	109	40	0.59	>1e6	{0.00}	0.1747	0.82	0.07346	0.73	0.1747	0.82	0.07346	0.73	1027	15	1038	8	101

LYD-169-1: *Mylonitic granitic gneiss; 5°14'18,8"E, 60°21'37,5"N*

n5418-01	I	2030	1331	457	0.66	154802	0.01	0.1765	0.72	0.07314	0.21	0.1765	0.72	0.07305	0.21	1015	4	1048	7	103
n5418-02	I	1100	858	251	0.78	129703	0.01	0.1734	0.76	0.07360	0.29	0.1734	0.76	0.07349	0.29	1027	6	1031	7	100
n5418-03	I	1330	1539	332	1.16	65561	0.03	0.1744	0.75	0.07370	0.26	0.1744	0.75	0.07348	0.27	1027	5	1036	7	101
n5418-04	I	1021	1011	247	0.99	25870	0.07	0.1750	0.73	0.07371	0.31	0.1749	0.73	0.07315	0.33	1018	7	1039	7	102
n5418-05	I	890	860	207	0.97	32713	0.06	0.1701	0.77	0.07387	0.42	0.1700	0.77	0.07344	0.44	1026	9	1012	7	99
n5418-06	I	1021	1031	242	1.01	9397	0.2	0.1719	0.74	0.07473	0.31	0.1716	0.74	0.07322	0.35	1020	7	1021	7	100
n5418-07	I	851	779	200	0.92	466635	{0.00}	0.1741	0.74	0.07295	0.33	0.1741	0.74	0.07295	0.33	1013	7	1035	7	102
n5418-08	I	1070	1259	271	1.18	39890	0.05	0.1761	0.73	0.07376	0.30	0.1760	0.73	0.07340	0.31	1025	6	1045	7	102
n5418-09	I	1480	1739	371	1.18	1695	1.1	0.1760	0.76	0.08212	0.55	0.1740	0.76	0.07372	1.00	1034	20	1034	7	100
n5418-10	I	1108	1036	260	0.94	33638	0.06	0.1725	0.78	0.07325	0.29	0.1724	0.78	0.07283	0.32	1009	7	1026	7	102
n5418-11	I	964	995	234	1.03	215928	{0.01}	0.1745	0.73	0.07371	0.31	0.1745	0.73	0.07371	0.31	1034	6	1037	7	100
n5418-12	P	1126	871	245	0.77	10650	0.18	0.1661	0.74	0.07391	0.35	0.1658	0.74	0.07257	0.39	1002	8	989	7	99
n5418-13	I	957	633	214	0.66	260988	{0.01}	0.1750	0.74	0.07346	0.31	0.1750	0.74	0.07346	0.31	1027	6	1039	7	101
n5418-14	I	1050	957	242	0.91	20139	0.09	0.1706	0.73	0.07381	0.36	0.1704	0.73	0.07310	0.38	1017	8	1014	7	100
n5418-15	I	850	686	194	0.81	82081	0.02	0.1728	0.73	0.07325	0.34	0.1728	0.73	0.07308	0.34	1016	7	1027	7	101
n5418-16	D	1140	1215	254	1.07	2314	0.81	0.1605	0.75	0.07881	0.29	0.1592	0.76	0.07264	0.45	1004	9	952	7	94
n5418-17	I	1055	810	243	0.77	35801	0.05	0.1758	0.89	0.07324	0.33	0.1757	0.89	0.07284	0.34	1009	7	1043	9	104
n5418-18	I	1105	973	257	0.88	94722	0.02	0.1730	0.76	0.07297	0.30	0.1730	0.76	0.07282	0.30	1009	6	1028	7	102

LYD-35-1: *Amphibolite; 5°13'53,6"E, 60°22'37,7"N*

n5419-01	I	1450	1525	350	1.05	11313	0.17	0.1725	0.75	0.07443	0.25	0.1722	0.75	0.07317	0.28	1019	6	1024	7	101
n5419-02	D	983	894	202	0.91	781	2.39	0.1527	0.91	0.09055	0.30	0.1490	0.92	0.07228	0.83	994	17	895	8	89
n5419-03	P	1124	969	255	0.86	82482	0.02	0.1685	0.74	0.07375	0.44	0.1685	0.74	0.07358	0.44	1030	9	1004	7	97
n5419-04	I	1584	713	330	0.45	123241	0.02	0.1713	0.80	0.07353	0.25	0.1712	0.80	0.07341	0.25	1025	5	1019	8	99
n5419-05	I	540	414	125	0.77	73666	0.03	0.1774	0.74	0.07390	0.41	0.1774	0.74	0.07371	0.42	1033	8	1053	7	102
n5419-06	I	816	350	175	0.43	186881	{0.01}	0.1782	0.73	0.07383	0.33	0.1782	0.73	0.07383	0.33	1037	7	1057	7	102
n5419-07	I	207	102	44	0.50	54462	{0.03}	0.1750	0.80	0.07280	0.68	0.1750	0.80	0.07280	0.68	1008	14	1040	8	103
n5419-08	D	429	235	85	0.55	47859	0.04	0.1579	0.82	0.07322	0.49	0.1578	0.82	0.07292	0.51	1012	10	945	7	93
n5419-09	P	339	214	72	0.63	15458	0.12	0.1686	0.77	0.07379	0.65	0.1684	0.77	0.07287	0.74	1010	15	1003	7	99
n5419-10	I	318	197	69	0.62	13222	0.14	0.1726	0.84	0.07459	0.59	0.1723	0.84	0.07352	0.65	1028	13	1025	8	100

LYD-163-1: *Gneissic Leucogranite; 5°14'58,5"E, 60°22'4,5"N*

n5420-01	D	1653	745	300	0.45	8607	0.22	0.1507	1.11	0.07295	0.32	0.1504	1.11	0.07128	0.44	966	9	903	9	93
n5420-02	P	1390	693	276	0.50	12267	0.15	0.1621	1.05	0.07347	0.34	0.1619	1.05	0.07231	0.39	995	8	967	9	97
n5420-03	D	1932	999	339	0.52	23128	0.08	0.1438	1.04	0.07116	0.26	0.1437	1.04	0.07054	0.27	944	6	865	8	91
n5420-04	D	3649	1229	427	0.34	6826	0.27	0.1004	1.05	0.06617	0.23	0.1001	1.05	0.06406	0.29	744	6	615	6	82
n5420-05	X	1133	387	255	0.34	31325	0.06	0.1921	1.05	0.07994	0.38	0.1920	1.05	0.07949	0.39	1184	8	1132	11	95
n5420-06	I	561	349	124	0.62	24143	{0.08}	0.1745	1.04	0.07403	0.42	0.1745	1.04	0.07403	0.42	1042	9	1037	10	99
n5420-07	I	635	725	137	1.14	2353	0.79	0.1722	1.10	0.07933	0.38	0.1708	1.10	0.07327	0.65	1021	13	1017	10	99
n5420-08	D	2146	1367	387	0.64	12314	0.15	0.1422	1.06	0.07115	0.24	0.1420	1.06	0.06998	0.27	928	6	856	8	92
n5420-09	D	940	439	182	0.47	24231	0.08	0.1589	1.11	0.07321	0.35	0.1588	1.11	0.07262	0.37	1003	7	950	10	94
n5420-10	D	1631	1187	324	0.73	7596	0.25	0.1544	1.04	0.07354	0.36	0.1541	1.04	0.07166	0.48	976	10	924	9	94
n5420-11	D	1973	917	352	0.46	35636	0.05	0.1472	1.09	0.07156	0.26	0.1472	1.09	0.07116	0.27	962	6	885	9	91
n5420-12	I	1086	463	223	0.43	57156	{0.03}	0.1705	1.04	0.07319	0.32	0.1705	1.04	0.07319	0.32	1019	6	1015	10	100
n5420-13	I	993	598	216	0.60	54970	{0.03}	0.1735	1.04	0.07344	0.33	0.1735	1.04	0.07344	0.33	1026	7	1032	10	101
n5420-14	D	2894	1551	428	0.54	11526	0.16	0.1199	1.54	0.06841	0.25	0.1197	1.54	0.06716	0.28	843	6	729	11	86
n5420-15	D	3703	1364	406	0.37	5082	0.37	0.0931	1.52	0.06510	0.30	0.0927	1.52	0.06225	0.38	683	8	572	8	83
n5420-16	D	4515	2032	542	0.45	1348	1.39	0.1000	1.61	0.07456	0.65	0.0986	1.61	0.06385	1.10	737	23	606	9	81
n5420-17-2	P	1060	546	213	0.51	853	2.19	0.1664	1.52	0.08845	0.35	0.1628	1.52	0.07170	0.79	977	16	972	14	99
n5420-17-1	I	322	331	75	1.03	2080	0.9	0.1702	1.58	0.07931	0.57	0.1686	1.58	0.07245	0.95	999	19	1005	15	101
n5420-18	I	1617	770	352	0.48	167914	{0.01}	0.1783	1.08	0.07295	0.26	0.1783	1.08	0.07295	0.26	1013	5	1058	11	105

LYD-197-2: *Leucogranitic pegmatite; 5°14'30,7"E, 60°22'24,9"N*

n5421-01	P	1076	31	190	0.03	7100	0.26	0.1642	1.09	0.07294	0.33	0.1637	1.09	0.07092	0.39	955	8	978	10	103
n5421-06	D	1747	42	260	0.02	4621	0.4	0.1392	1.08	0.07296	0.38	0.1386	1.08	0.06986	0.47	924	10	837	9	90
n5421-07	D	2838	121	304	0.04	474	3.95	0.0978	1.08	0.09099	2.03	0.0940	1.08	0.06039	5.28	618	110	579	6	93
n5421-08	D	2871	80	284	0.03	1663	1.12	0.0939	1.16	0.07003	0.33	0.0928	1.16	0.06132	0.59	650	13	572	6	87
n5421-09	P	3517	113	289	0.03	711	2.63	0.0797	1.11	0.07699	0.28	0.0776	1.11	0.05650	0.78	472	17	482	5	102
n5421-10	D	3233	96	306	0.03	1345	1.39	0.0904	1.18	0.07042	0.49	0.0891	1.18	0.05962	0.90	590	19	550	6	93
n5421-11	D	1988	335	210	0.17	381	4.91	0.1032	1.11	0.10173	2.04	0.0981	1.11	0.06382	5.44	736	111	603	6	81

LYD-83-1: *Mylonitic granitic gneiss; 5°15'35,7"E, 60°23'14,5"N*

n5422-01	I	353	153	114	0.43	26120	{0.07}	0.2634	1.10	0.09390	0.40	0.2634	1.10	0.09390	0.40	1506	8	1507	15	100
n5422-02	I	390	102	121	0.26	31434	{0.06}	0.2652	1.10	0.09357	0.42	0.2652	1.10	0.09357	0.42	1499	8	1516	15	101
n5422-03	P	399	84	115	0.21	2748	0.68	0.2540	1.11	0.09758	0.38	0.2522	1.11	0.09252	0.51	1478	10	1450	14	98
n5422-04	D	1235	208	160	0.17	2842	0.66	0.1172	1.21	0.07960	0.34	0.1165	1.21	0.07459	0.49	1058	10	710	8	65
n5422-05	I	288	79	89	0.27	22897	{0.08}	0.2641	1.11	0.09374	0.45	0.2641	1.11	0.09374	0.45	1503	8	1511	15	101
n5422-06	I	362	94	112	0.26	29567	{0.06}	0.2642	1.11	0.09339	0.40	0.2642	1.11	0.09339	0.40	1496	8	1511	15	101
n5422-07-1	I	337	91	105	0.27	59510	{0.03}	0.2644	1.11	0.09313	0.41	0.2644	1.11	0.09313	0.41	1491	8	1512	15	102
n5422-07-2	D	1627	570	314	0.35	4431	0.42	0.1645	1.07	0.08651	0.29	0.1638	1.07	0.08333	0.39	1277	8	978	10	75
n5422-08	P	463	74	132	0.16	14049	0.13	0.2530	1.09	0.09275	0.46	0.2526	1.09	0.09176	0.48	1462	9	1452	14	99
n5422-09	I	329	88	102	0.27	43302	{0.04}	0.2649	1.10	0.09362	0.41	0.2649	1.10	0.09362	0.41	1500	8	1515	15	101
n5422-10	I	293	86	92	0.29	61632	{0.03}	0.2655	1.11	0.09425	0.47	0.2655	1.11	0.09425	0.47	1513	9	1518	15	100
n5422-11	I	303	139	99	0.46	93427	{0.02}	0.2657	1.13	0.09404	0.43	0.2657	1.13	0.09404	0.43	1509	8	1519	15	101
n5422-12	D	923	160	220	0.17	6919	0.27	0.2094	1.09	0.09122	0.30	0.2088	1.09	0.08921	0.34	1409	7	1223	12	86
n5422-13	I	390	109	123	0.28	49562	{0.04}	0.2673	1.10	0.09377	0.44	0.2673	1.10	0.09377	0.44	1503	8	1527	15	102
n5422-14	I	272	67	84	0.25	128049	{0.01}	0.2660	1.11	0.09369	0.44	0.2660	1.11	0.09369	0.44	1502	8	1520	15	101
n5422-15	P	635	120	194	0.19	46118	{0.04}	0.2658	1.10	0.09262	0.30	0.2658	1.10	0.09262	0.30	1480	6	1519	15	103
n5422-16	P	880	217	253	0.25	14028	0.13	0.2474	1.10	0.09343	0.26	0.2471	1.10	0.09244	0.28	1477	5	1424	14	96
n5422-17	P	944	330	279	0.35	7439	0.25	0.2493	1.08	0.09346	0.25	0.2487	1.08	0.09159	0.29	1459	5	1432	14	98
n5422-18	I	495	127	154	0.26	58774	{0.03}	0.2651	1.09	0.09325	0.35	0.2651	1.09	0.09325	0.35	1493	7	1516	15	102
n5422-19	I	241	93	77	0.39	87625	{0.02}	0.2645	1.11	0.09372	0.45	0.2645	1.11	0.09372	0.45	1502	9	1513	15	101
n5422-20	I	309	61	94	0.20	26301	{0.07}	0.2645	1.10	0.09362	0.41	0.2645	1.10	0.09362	0.41	1500	8	1513	15	101
n5422-21	P	535	63	159	0.12	8284	0.23	0.2650	1.13	0.09362	0.31	0.2644	1.13	0.09194	0.40	1466	8	1512	15	104

Notes:

(1) Interpretation of ages: I = magmatic; P = concordant but interpreted to have undergone radiogenic-Pb loss;
D = outside discordance threshold or age information regarded as geologically meaningless; X = xenocryst/inheritance

(2) Based on measured Th and U signals.

(3) f_{206} is the percentage of common Pb estimated from 204Pb counts; in brackets where these are insignificant;

(4) Ratios after subtraction of common Pb (if detected)

Paper 2:
Deep crustal flow within postorogenic metamorphic core complexes – Insights from the southern Western Gneiss Region of Norway.

Wiest, J. D., Osmundsen, P. T., Jacobs, J., and Fossen, H., 2019
Tectonics, v. 38, p. 4267-4289

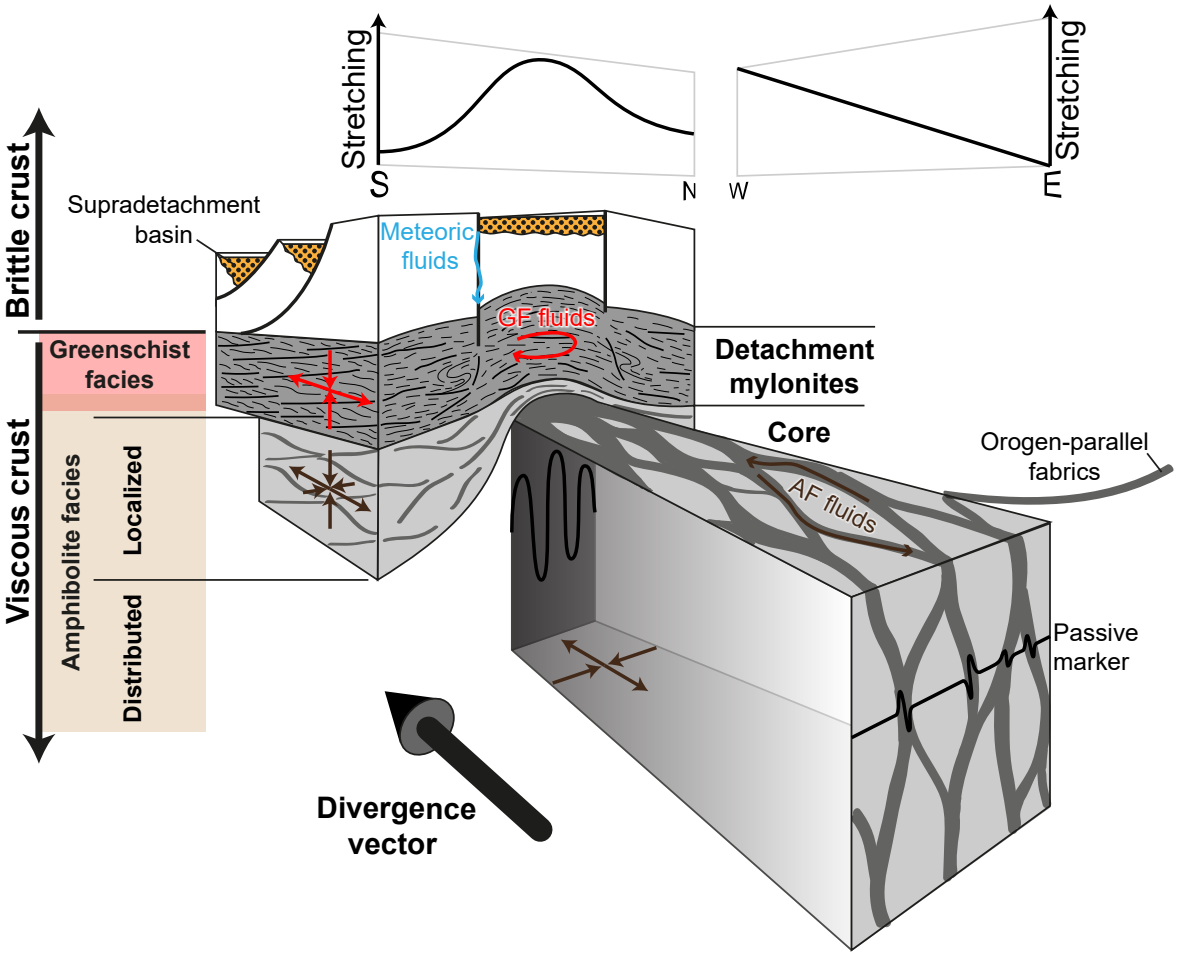

Tectonics

RESEARCH ARTICLE
10.1029/2019TC005708

Deep Crustal Flow Within Postorogenic Metamorphic Core Complexes: Insights From the Southern Western Gneiss Region of Norway

J. D. Wiest[1], P. T. Osmundsen[2,3], J. Jacobs[1], and H. Fossen[5]

[1]Department of Earth Science, University of Bergen, Bergen, Norway, [2]Department of Geoscience and Petroleum, Norwegian University of Science and Technology, Trondheim, Norway, [3]Department of Geosciences, University of Oslo, Oslo, Norway, [4]Museum of Natural History and Department of Earth Science, University of Bergen, Bergen, Norway

Key Points:

- A deeply eroded and particularly well-exposed transtensional core complex reveals mechanisms of solid-state viscous flow in the deep crust
- Vertical metamorphic variations and lateral strain gradients lead to differential folding of distinct crustal levels
- Solid-state flow mechanisms are similar to anatectic crust and can contribute to postorogenic exhumation of (ultra-)high-pressure rocks

Correspondence to:
J. D. Wiest,
johannes.wiest@uib.no

Citation:
Wiest, J. D., Osmundsen, P. T., Jacobs, J., & Fossen, H. (2019). Deep Crustal Flow Within Postorogenic Metamorphic Core Complexes: Insights From the Southern Western Gneiss Region of Norway. *Tectonics*, *38*. 4267–4289. https://doi.org/10.1029/2019TC005708

Received 5 JUN 2019
Accepted 6 NOV 2019
Accepted article online 11 NOV 2019
Published online 17 DEC 2019

Abstract Viscous crustal flow can exhume once deeply buried rocks in postorogenic metamorphic core complexes (MCCs). While migmatite domes record the flow dynamics of anatectic crust, the mechanics and kinematics of solid-state flow in the deep crust are poorly constrained. To address this issue, we studied a deeply eroded and particularly well-exposed MCC in the southern Western Gneiss Region of Norway. The Gulen MCC formed during Devonian transtensional collapse of the Caledonian orogeny in the footwall of the Nordfjord-Sogn detachment zone. We developed a semiquantitative mapping scheme for ductile strain to constrain micro- to megascale processes, which brought eclogite-bearing crust from the orogenic root into direct contact with Devonian supradetachment basins. The Gulen MCC comprises different structural levels with distinct metamorphic evolutions. In the high-grade core, amphibolite-facies structures record fluid-controlled eclogite retrogression and coaxial flow involving vast extension-perpendicular shortening. Detachment mylonites formed during ductile-to-brittle noncoaxial deformation and wrap around the core. We present a sequential 3-D reconstruction of MCC formation. In the detachment zone, the combined effects of simple shearing, incision/excision, and erosion thinned the upper crust. Internal necking of the ductile crust was compensated by extension-perpendicular shortening within the deep crust and resulted in differential folding of distinct crustal levels. We identify this differential folding as the main mechanism that can redistribute material within solid-state MCCs. Our interpretation suggests a continuum of processes from migmatite-cored to solid-state MCCs and has implications for postorogenic exhumation of (ultra-)high-pressure rocks.

Plain Language Summary The Earth's crust has different layers with contrasting mechanics. Rocks in the upper crust tend to break, while higher temperatures at depth make rocks flow, although very slowly. This contrast is important when continents collide forming mountain belts but also when plates drift apart and mountain ranges collapse. In SW Norway, hundreds of million years of erosion have exposed rocks that once were deep below a large mountain range (the Caledonides). Today, glacier-polished fjords reveal large dome structures that formed when the Caledonides collapsed. Inside such a dome, we find rocks originating from different levels of the crust. Rocks and structures in the core formed at high pressures and temperatures. Wrapped around, we find rocks that deformed while they cooled down, became more resistant to flow, and finally broke apart. Above the dome, we find remnants of the upper crust, which was broken up by faults, eroded, and deposited in sedimentary basins. We reconstruct how mechanical contrasts between crustal layers brought rocks from the root of the mountain belt in contact with sediments deposited at the surface. Understanding this process is important, because it can entirely transform the crust within a—geologically speaking—short period of time.

1. Introduction

Postorogenic metamorphic core complexes (MCCs) show that the crust reequilibrates after orogeny and an entirely new crustal template may be created (e.g., Brun et al., 2017 ; Buck, 1991 ; Coney, 1980 ; Osmundsen et al., 2005 ; Platt et al., 2015 ; Vanderhaeghe & Teyssier, 2001 ; Whitney et al., 2013). Since the classic paper by Block and Royden (1990), it seems widely accepted that MCCs form by viscous crustal flow as a mode of isostatic compensation in response to upper crustal thinning by extensional faulting. Block and Royden [1990] elegantly explain geophysical observations made around MCCs, suggesting that the flow of lower crustal material forms a dome, while the Moho remains flat. Yet, what is the actual mechanism of this

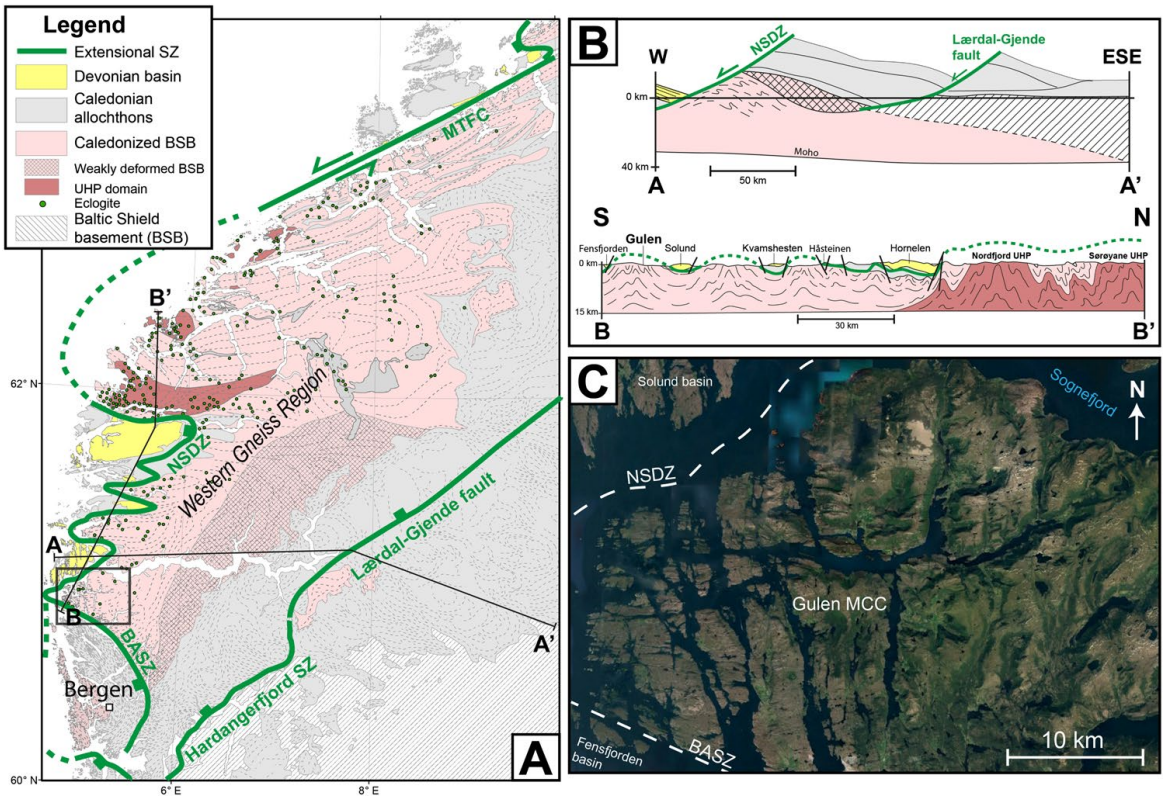

Figure 1. Overview of the study area. (a) Geologic map of the Western Gneiss Region. Ultrahigh-pressure domains after Hacker et al. (2010). Eclogite localities from Andersen et al. (1994), Krabbendam and Dewey (1998), Hacker et al. (2003), Hacker et al. (2010), and Hacker et al. (2015) and weakly deformed Baltic Shield basement (BSB) domain after Milnes et al. (1997). Structures of the extensional detachment system are shown in green. The location of cross sections in B is indicated, and the study area is marked by a rectangle. Abbreviations: BASZ = Bergen Arcs shear zone; MTFC = Møre-Trøndelag fault complex; NSDZ = Nordfjord-Sogn detachment zone. (b) Schematic cross sections of the WGR. A-A' redrawn from Milnes et al. (1997). B-B' based on Johnston, Hacker, and Ducea (2007b) and modified after Krabbendam and Dewey (1998), Braathen and Erambert (2014), this study and interpretation of regional structural data. (c) Satellite image of the Gulen MCC in between the Solund and Fensfjorden Devonian basins. Numerous islands in the western part of the area provide continuous and excellently exposed natural cross sections in E-W and N-S direction. Image from Google Earth.

flow that supposedly redistributes material within the deep crust? For hot lithospheres, it has been suggested that mid- to lower crustal channels of partially molten low-viscosity crust can form (e.g., Rey et al., 2009 ; Rey et al., 2011 ; Whitney et al., 2013). However, there are many examples of MCCs, including classical Cordilleran MCCs, where high-strain rocks are in solid state and no such channels are observed (e.g., Cooper et al., 2017; Platt et al., 2015). Further complexity arises if we consider MCCs as three-dimensional structures. In settings that involve a 3-D component of strain, like transtension, 3-D numerical experiments show extension-perpendicular flow of material (Le Pourhiet et al., 2012; Rey et al., 2017) instead of extension-parallel flow as it is commonly shown in schematic cross sections of MCCs. Therefore, we need detailed constraints on the internal architecture of deeply eroded MCCs that can help us to unravel the 3-D kinematics and mechanisms of postorogenic crustal flow.

The Western Gneiss Region (WGR) of the SW Scandinavian Caledonides (Figure 1) is an excellent place to do this. It represents the deeply eroded core of a Silurian continent-continent collision orogen where large parts of the crust were turned around during Devonian postorogenic transtension (e.g., Krabbendam & Dewey, 1998). Material metamorphosed in the orogenic root at high- or even ultrahigh-pressure

conditions was brought back to the surface in the time it took to deposit Devonian supradetachment basins (e.g., Eide et al., 2005; Templeton, 2015). The processes responsible for this crustal revolution are recorded in MCCs in the footwall of large-magnitude extensional detachments along the western coast of southern Norway (Figure 1b). The Gulen MCC, which is the southernmost of these structures, offers particular exposure conditions. Numerous islands with an orthogonal set of ideally oriented coastlines provide almost continuous high-quality exposures, which can be easily accessed by boat (Figure 1c). In this study, we provide a detailed look inside the anatomy of a particularly well-exposed postorogenic MCC in order to understand the viscous flow of the crust during transtension. We approach this issue from the micro- to the megascale to constrain the timing, quantity, and kinematics of ductile strain as well as the metamorphic conditions and deformation processes.

2. Geologic Setting

The WGR of southern Norway comprises Mesoproterozoic crust of the Baltic Shield that was subducted below Laurentia during Caledonian orogeny. The pre-Caledonian configuration of this part of the Baltic Shield was largely formed through the 1.2–0.9 Ga Sveconorwegian orogeny, involving widespread magmatism and migmatization (e.g., Bingen et al., 2005; Coint et al., 2015 ; Engvik et al., 2000 ; Kylander-Clark & Hacker, 2014 ; Røhr et al., 2004 ; Slagstad et al., 2018 ; Wiest et al., 2018).

NW-directed Caledonian subduction of the Baltican margin is reflected by increasing peak metamorphic conditions and deformation of Baltic Shield basement from SE to NW (e.g., Griffin & Brueckner, 1980; Hacker et al., 2010). Deep burial of the Baltican crust is witnessed by the widespread occurrence of high-pressure eclogites and externally derived mantle rocks, which have been inserted in the subducted continental crust from the overlying mantle wedge (e.g., Brueckner, 2018). Ultrahigh-pressure conditions are recorded in three distinct domains in the NW portion of the WGR (e.g., Cuthbert et al., 2000; Hacker et al., 2010 ; Root et al., 2005). Eclogite ages, which reflect subduction and peak metamorphism, range mostly from 430 to 395 Ma. They overlap in part with U-Pb zircon ages from granitic leucosomes (405–390 Ma; see compilation by Kylander-Clark & Hacker, 2014). Partial melting and local ultrahigh-temperature metamorphism occurred during high-temperature equilibration (e.g., Engvik et al., 2018; Ganzhorn et al., 2014; Gordon et al., 2013; Kylander-Clark & Hacker, 2014; Labrousse et al., 2011). Yet, it remains controversial to what extent melting initiated at ultrahigh-pressure conditions (e.g., Kohn et al., 2015) and whether pressure estimates reflect other processes than burial only (e.g., Vrijmoed et al., 2009). Amphibolite-facies reworking and exhumation of the WGR are dated by U-Pb monazite (410–390 Ma; Hacker et al., 2015; Holder et al., 2015), U-Pb titanite (405–385 Ma; Kylander-Clark et al., 2008; Spencer et al., 2013), U-Pb rutile (400–375 Ma; Butler et al., 2018; Cutts et al., 2019), and Ar-Ar white mica ages (405–375 Ma; Chauvet & Dallmeyer, 1992; Walsh et al., 2007; Young et al., 2011; Walsh et al., 2013). These ages show regional trends with younger ages toward the NW and imply progressive SE to NW unroofing of the WGR between 400 and 375 Ma.

Exhumation models of the WGR commonly involve two stages. The first stage is seen either as postorogenic eduction of the continental slab (Andersen et al., 1991; Fossen, 1992), gravity-driven ductile rebound of the orogenic root (Milnes et al., 1997; Milnes & Koyi, 2000), or flexural rebound and flattening of the slab (Cutts et al., 2019). A second phase comprising transtensional collapse of the overthickened crust and the formation of large-magnitude detachments is widely accepted (e.g., Butler et al., 2015; Fossen, 2010; Krabbendam & Dewey, 1998). Indeed, most structures in the WGR, from supradetachment basins to the ultrahigh-pressure domains, follow the trend of sinistral transtension (Dewey, 2002; Fossen et al., 2013; Krabbendam & Dewey, 1998; Osmundsen & Andersen, 2001). The felsic gneisses of the WGR were pervasively deformed during amphibolite-facies coaxial shear deformation with increasing intensity from E to W (Andersen et al., 1994; Hacker et al., 2010; Milnes et al., 1997). The gneisses are folded into tight, kilometer- to centimeter-scale, extension-parallel upright folds (Chauvet & Seranne, 1994). Large-magnitude, ductile-to-brittle detachments juxtapose the coaxially stretched, eclogite-bearing crust of the WGR with remnants of Caledonian allochthons and Devonian supradetachment basins (Andersen et al., 1994; Krabbendam & Dewey, 1998; Osmundsen & Andersen, 2001; Braathen et al., 2004; Johnston et al., 2007a; Johnston et al., 2007b).

The most important Devonian structure in SW Norway, the Nordfjord-Sogn detachment zone (NSDZ), is strongly undulating around E-W axes. Scoop-shaped Devonian basins occupy synformal positions, while

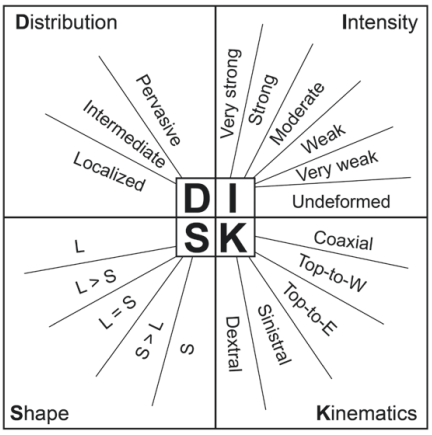

Figure 2. Schematic illustration of the DISK scheme for semiquantitative description of ductile deformation. The four parameters can be recorded as alphanumeric values, using mobile field mapping devices. See text for explanation of the parameters.

the WGR forms several E-W elongated culminations (antiforms) in the footwall of the undulating detachment. The portion of the WGR situated between the Møre-Trøndelag fault complex and the Hornelen basin (ca. 62° N, Figure 1a) can be seen as the largest culmination of the WGR. A magnitude smaller are the culminations in between the Devonian basins (Figure 1b). While the entire WGR can be seen as one giant MCC (Andersen & Jamtveit, 1990; Krabbendam & Dewey, 1998; McClay et al., 1986), we find it useful to apply the MCC concept (Brun et al., 2017; Platt et al., 2015; Whitney et al., 2013) also to the second-order antiformal culminations in the footwall of the NSDZ.

The Gulen MCC represents the southernmost culmination of the WGR and consists of strongly reworked Baltic Shield basement separated from overlying Devonian basins by the NSDZ and its southern continuation, the Bergen Arcs shear zone (BASZ; Wennberg et al., 1998). Precambrian protoliths were mainly formed during the 1.0 Ga Sveconorwegian orogeny as dated by U-Pb zircon ages of granitic leucosomes from migmatites (Wiest et al., 2019) and U-Pb zircon and monazite ages of local occurrences of granulite-facies rocks (Røhr et al., 2004). The area hosts the southernmost exposures of Caledonian eclogite in the Baltic Shield basement (Winsvold, 1996). Peak metamorphic conditions of the nearby Lavik eclogites have been constrained to 700°C, 2.3 GPa (Hacker et al., 2003). Previously published Ar-Ar ages group narrowly around 394 Ma (Boundy et al., 1996; Chauvet & Dallmeyer, 1992; Walsh et al., 2013), and Hacker et al. (2003) suggested rapid exhumation of the eclogite-bearing WGR along the southern segment of the NSDZ.

3. Semiquantitative Mapping of Ductile Strain

In order to reveal strain variations across a large area, we developed a scheme for the systematic description of ductile strain in outcrops, considering four main parameters: distribution, intensity, shape of the strain ellipsoid, and kinematics (Figure 2). The acronym DISK makes it easy to remember the parameters, which can be easily recorded in a numeric scheme for each visited locality. With the help of mobile mapping devices (e.g., Midland Valley Field Move Clino™), a large number of data points can be efficiently collected and exported to GIS software for data analysis and visualization.

The first parameter in the DISK scheme describes whether the deformation is localized, intermediate, or pervasive on the scale of 1–10 m. The intensity of the strain is recorded in five steps (very weak –very strong) plus an additional value for undeformed rocks. It should be noted that the intensity of the strain refers to the deformed portion of the outcrop, and hence, this parameter needs to be read together with the distribution parameter. For example, an outcrop with pervasive strong deformation records more bulk strain than an outcrop with localized strong deformation. The shape of the strain ellipsoid follows the common classification from L-tectonites to S-tectonites. Our classification includes coaxial deformation and noncoaxial deformation. Because shear sense indicators are sometimes ambiguous, this parameter can be furthermore improved by additionally recording the certainty of the observation with a second parameter (e.g., uncertain; certain; very certain).

3.1. Dataset Presentation

The collection of data presented in this study is prepared for use in GIS software and can be accessed online (https://doi.org/10.6084/m9.figshare.c.4697006.v1). Our field data comprise 36 eclogite localities, 1264 structural measurements, and 216 structural data that have been digitized from Winsvold (1996). Around 190 localities have been classified with the DISK scheme, and in addition we present more than 400 georeferenced and commented field photos. The trace of the foliation has been interpreted from structural measurements and high-resolution orthophotos. The same accounts for the boundaries of mapped units. Our field results are presented in a newly compiled geological map and accompanying cross sections (Figure 3). In addition, we present the results from DISK mapping in Figure 4 with symbols for each parameter overlaying the map.

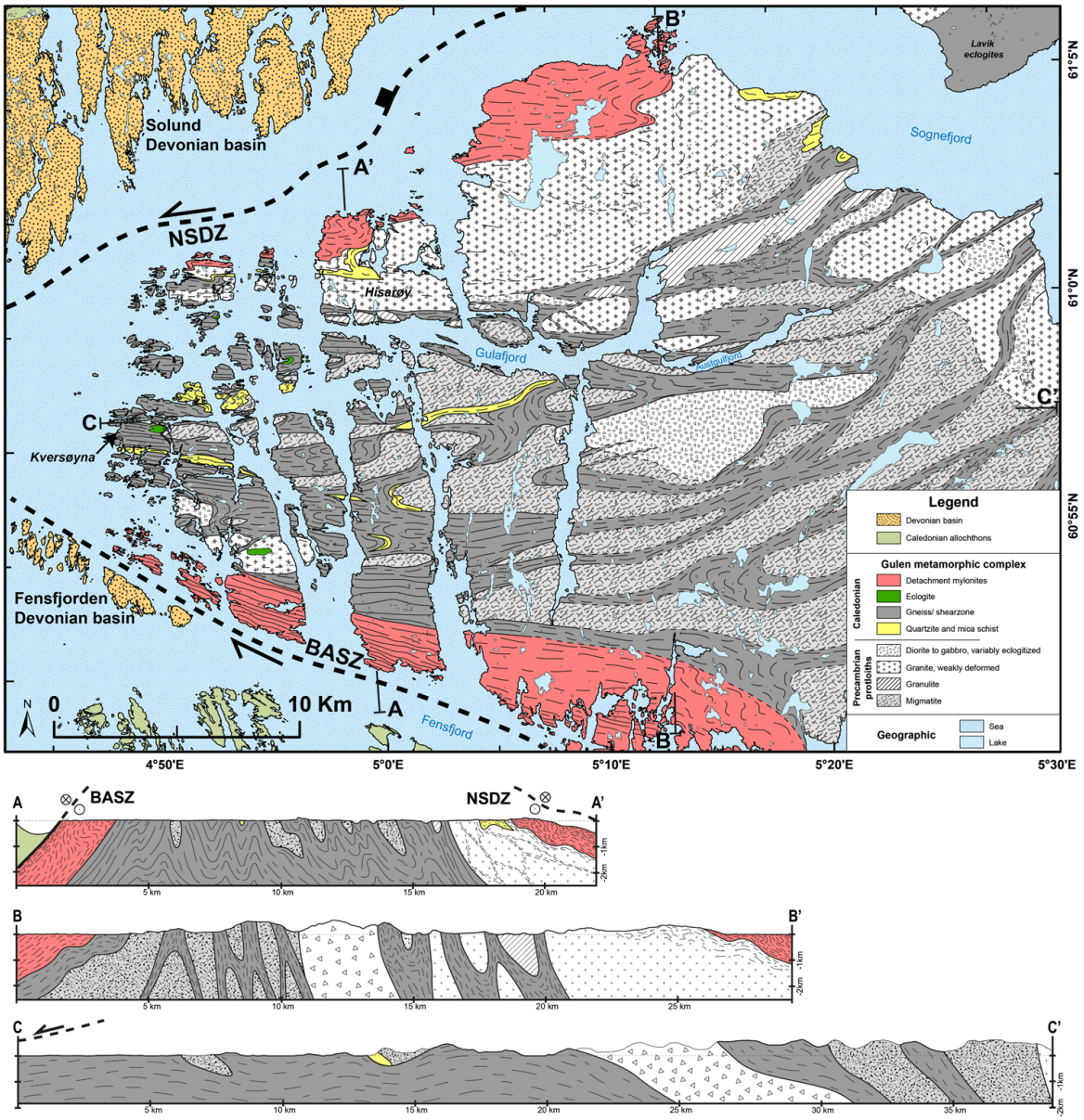

Figure 3. Newly compiled geologic map and cross sections of the Gulen area based on recent field mapping, Kildal (1970); Winsvold (1996); Ragnhildstveit and Helliksen (1997); Wennberg et al. (1998); Røhr et al. (2004). Abbreviations: BASZ = Bergen Arcs shear zone; NSDZ = Nordfjord-Sogn detachment zone.

4. Structural Architecture of the Gulen MCC

Our newly compiled geologic map and cross sections of the Gulen MCC are shown in Figure 3. The overarching structure of the MCC can be described as an open, south-verging antiform (Figure 3, cross

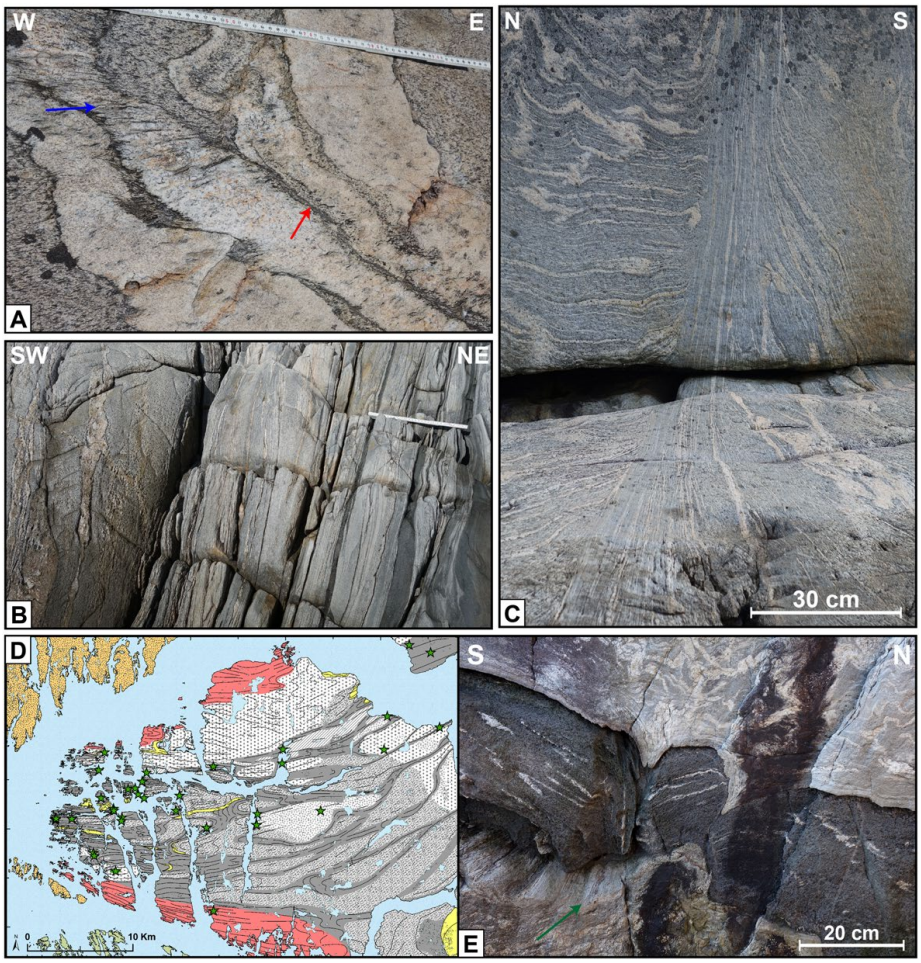

Figure 4. Distinguishing Precambrian protoliths from Caledonian shear zone rocks (a–c) and field occurrence of Caledonian eclogites (d and e). (a) Precambrian granodiorite intruded by granitic dykes. Weak Caledonian shear strain is localized at the dyke margins where they are preferentially oriented (red arrow). In case of less-suited orientations, the foliation transects the dyke (blue arrow). Ruler for scale. (b) Coarse-grained Precambrian migmatite (left side) is transformed into Caledonian banded gneiss in a meter-scale shear zone. The thin amphibolite layers represented originally mafic boudins in migmatite. Same locality as (a). Ruler is 40 cm. (c) Localized coaxial shear zone in Precambrian migmatite exposed in three dimensions. The straight trend and the sharp northern boundary may indicate that this shear zone has localized along a preexisting brittle feature. (d) The map of eclogite localities shows the highest concentration of eclogite bodies in the western core of the MCC. (e) Eclogitized mafic dyke in Precambrian migmatite. The dyke was boudinaged during migmatization, as boudin necks are filled with leucosomes. The protolith relationship was preserved because eclogitization was static and left the migmatite unchanged. However, eclogitization liberated fluids that were consumed by the host rock and led to garnet and white-mica growth in a narrow zone around the mafic body (green arrow). Note that minor shear deformation localized later at the hydrated contact zone.

section A) that plunges shallowly toward the west. The MCC is bound to the NW by the shallowly dipping NSDZ, which is overlain by the extensive Solund basin in the hanging wall. To the south, the MCC is bound by the steep northern BASZ. In contrast to the NSDZ, the hanging wall of the BASZ is occupied by large remnants of Caledonian allochthons of the Bergen Arcs and Devonian sediments are preserved only in an isolated fault-bounded block of the Fensfjorden basin. Bathymetric lineaments seem to indicate that the NSDZ and the BASZ merge offshore, just west of Figure 3, and form a well-defined western boundary of

the MCC. In contrast, there is no clear eastern boundary of the MCC, but rather a gradual transition into weaker deformed portions of the WGR (Figures 1a and 1b). This transition coincides with a rotation of structural trends from E-W in the MCC to NE-SW and the disappearance of eclogites toward the east. In E-W direction, the gneissic fabrics within the MCC appear shallowly undulating and rotate from generally easterly dip in the east to westerly dip in the west (Figure 3, cross section C). In three dimensions, thus, the shape of the Gulen MCC does not conform to a simple dome shape, but rather it must be described as a hyperbolic surface with marked N-S as well as E-W asymmetry.

Our mapping shows that the Gulen MCC comprises two fundamentally distinct structural units: first, mylonites that formed in relation to the extensional detachment system on the flanks of the MCC and, second, a high-grade metamorphic core. Low-grade retrogression overprinted higher-grade fabrics in the detachment mylonites. In contrast, the metamorphic core preserves amphibolite-facies fabrics, and low-grade retrogression is absent. The following sections will present detailed descriptions of how the crust was transforming inside this MCC.

4.1. How to Distinguish Precambrian Protoliths from Caledonian Shear Zones?

One of our main objectives was to quantify the amount of reworking of the Baltic Shield basement during the Caledonian orogeny. The distinctive feature of the Precambrian rocks is that they formed at high temperatures and involve large amounts of melt. Therefore, they are consistently coarse grained, which makes them easily discernible from rocks that experienced Caledonian solid-state shear deformation and associated grain size reduction (Figure 4). The oldest rocks are a metasedimentary sequence that has been intruded by a large gabbro and countless mafic dykes. The metasediments have been almost entirely migmatized, and only quartzites are preserved as relicts within the migmatites. Large granite plutons intruded in the northern half of the area. A distinct belt of coarse-grained gneissic rocks with granulite facies assemblages (Røhr et al., 2004) runs along the boundary of the largest of these plutons.

We find features that indicate a considerable time gap of cooling between Sveconorwegian migmatization and the initiation of solid-state shear deformation. In low-strain areas, shear deformation is commonly localized along primary lithological heterogeneities like dyke margins (Figure 4a) and probably preexisting brittle features (Figure 4c). With increasing strain, these shear zones grow in width and transform the coarse-grained Precambrian protoliths into medium-grained banded gneisses, where primary lithological relationships are obscured (Figure 4b).

4.2. Eclogites Record Processes in the Orogenic Root

Numerous eclogite localities (Figure 4d) demonstrate that the crust within the MCC represents parts of the former orogenic root. They occur dominantly in the core of the culmination, and the concentration of eclogite bodies and pods increases from E to W. The eclogites occur mostly as isolated lenses within felsic gneisses, as it is typical all throughout the WGR. In contrast to other portions of the WGR, however, eclogitization in the Gulen MCC appears to have been a static process. There are no eclogite-facies fabrics, but pre-eclogite textural relationships are preserved. Figure 4e shows a mafic dyke that has been boudinaged during Mesoproterozoic migmatization. Later, the mafic dyke has been entirely eclogitized, while the migmatite remained unaltered. However, there are several centimeter-thick zones around the eclogitized dyke where white mica and garnet overgrow the migmatite fabric. These observations suggest that the eclogitization of hydrous mafic rocks liberated fluids that were consumed by the immediate host rock leading to overgrowth of eclogite-facies minerals. Phengite-quartz veins, found in many eclogites, appear to be related to the same process. Almost all of the eclogites in the Gulen MCC were retrogressed to some extent. The relation between eclogite retrogression and deformation of felsic gneisses is explained in section 6 and discussed in section 7.1.

5. Caledonian Shear Strain

The width of gneissic shear zones ranges from the centimeter scale to the kilometer scale. The distribution of deformation at the mesoscale classified with the DISK scheme shows no systematic variations within the MCC (Figure 5). Localized mesoscale shear zones are restricted to low-strain domains, and most shear zones are tens of meters to kilometers wide. Therefore, variations in the distribution of shear zones become visible only at the map scale.

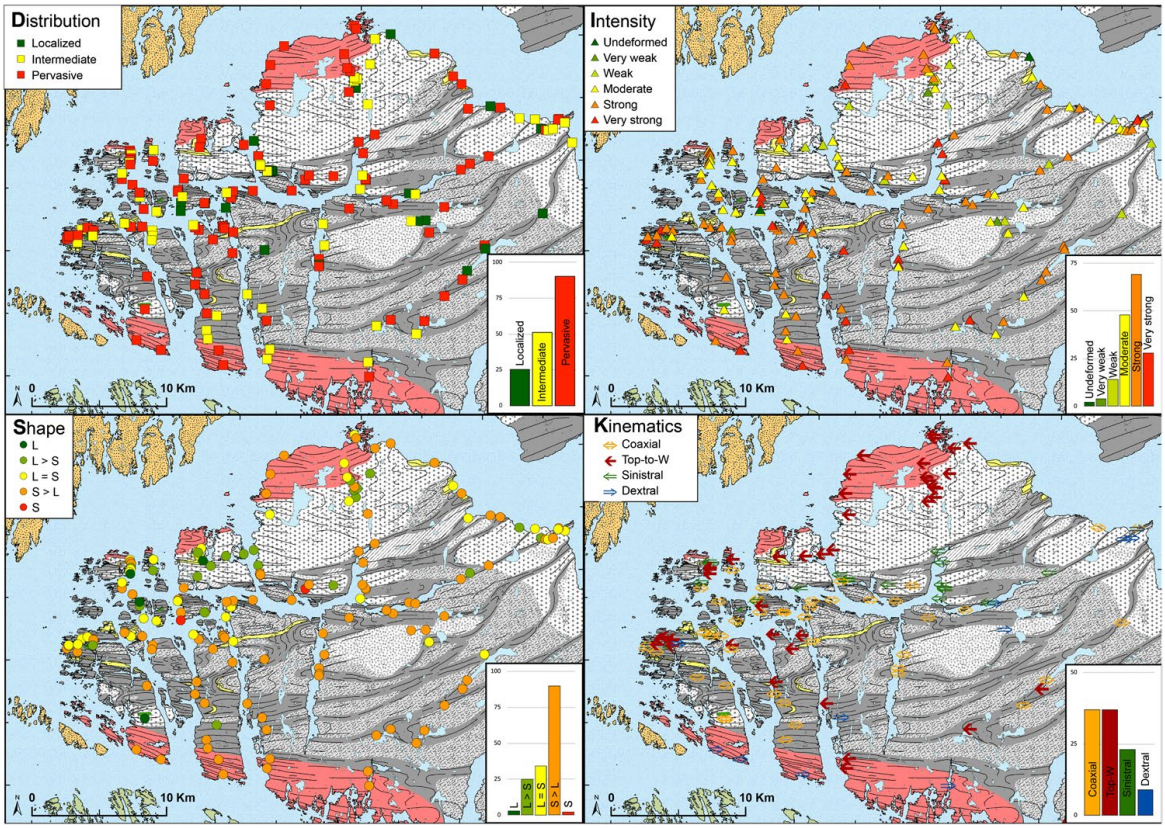

Figure 5. Results from DISK mapping: Each parameter is presented by symbols overlaying the geologic map and a histogram. Note that undeformed localities have usually not been recorded with the DISK scheme and, hence, are underrepresented.

In the eastern part of the area, shear deformation localized in an anastomosing network of discrete shear zones cutting through little deformed protoliths. Along the N-S cross section B (Figure 3), 45% of surface exposures are shear zone rocks, but within the core (excluding the detachment mylonites), only 25% of the protoliths have been significantly deformed. Toward the west, these isolated shear zones merge and form a coherent mass of highly sheared gneisses containing only isolated blocks of undeformed protolith. Along cross section A (Figure 3), >80% of the protoliths have been transformed into shear zone rocks, and this value increases even further toward the west.

The mesoscale classification of strain intensity, shape of the strain ellipsoid, and kinematics shows systematic variations that distinguish the detachment mylonites from the core (Figure 5). The detachment mylonites are dominated by noncoaxial top-W fabrics with a dominant S > L shape and strong deformation intensity. Strain intensity is generally increasing toward the top of the detachment. Large areas below the NSDZ mylonites are occupied by granite plutons with weak to moderate strain and a dominant L > S fabric.

Further away from the detachments, in the core of the culmination, the deformation intensity increases again and coaxial S > L fabrics dominate in strongly deformed domains. Strain intensity is mostly classified as strong, while very strong deformation is only found where rheological contrasts create particular conditions for strain localization (e.g., large eclogites contained in gneiss). Weakly deformed domains in the core show a dominant L-shape of the coaxial background strain. In general, stronger shearing appears to be

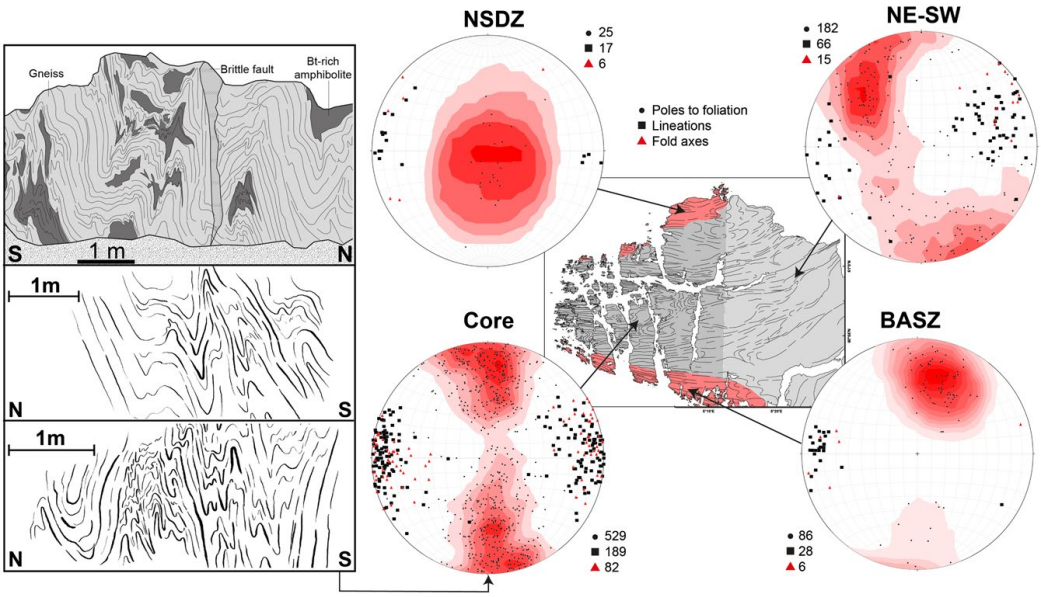

Figure 6. Lower hemisphere equal-area plots of structural data. Contours are plotted for poles to foliations. Four structural domains have been distinguished based on variations in fabric orientation. The inlet shows upright folds in gneisses of the core domain, redrawn from field photos. Most folds are tight to isoclinal. Multilayer buckling with small-scale parasitic folds occurs mostly in and around biotite-rich mafic layers.

associated with more planar fabrics, or in other words, the amount of E-W stretching correlates with N-S shortening. Noncoaxial fabrics occur to some extent also in the core of the MCC. They reflect overall top-to-W shearing by sinistral and dextral fabrics at the northward- and southward-dipping flanks of the culmination, respectively.

5.1. Fabric Orientations and Folding

Across the entire MCC, we find subhorizontal to moderately plunging lineations, lineation-parallel fold axes, and a corresponding girdle of foliations (Figure 6). For structural analysis, we distinguished four domains with distinct fabric orientations. Mylonites belonging to the NDSZ show WNW-plunging lineations and subhorizontal foliations. Mylonitic foliations are folded around NE-SW as well as NW-SE trending tight recumbent folds, consistent with vertical shortening. The mylonites of the BASZ show consistently WNW-plunging lineations and steeply SSW-dipping foliations. The mylonitic foliation is folded around isoclinal folds with SW-dipping axial planes that are parallel to the foliation. Lineations and fold axes in the core follow an E-W trend and plunge shallowly toward the east and the west. Foliations are mostly steep to subvertical and folded around E-W trending tight to isoclinal upright folds (Figure 6). These folds are observed from the outcrop scale to the map scale (compare Figure 3) and involve passive folding as well as active multilayer buckling. Fold tightness appears to be correlated to strain intensity, and fold amplitude seems to relate to shear zone width. However, it should be noted that even in an almost continuously exposed area like the one studied, the exact amplitude of such steep folds is practically impossible to constrain. Our cross section reconstruction implies amplitudes up to several kilometers in the most strongly deformed domain in the west of the MCC. It is also impossible to quantify the amount of E-W extension and N-S shortening in these kinds of rocks, but conservative estimates imply at least 70% of N-S shortening by upright folding in individual outcrops of strongly deformed gneisses.Toward the east, fabrics rotate into an orogen-parallel trend: lineations plunge mostly toward the NE and foliations dip mostly steeply toward the SE. Besides this change in orientation, the NE-SW-oriented shear zones show the same characteristics as the shear zones in the core domain.

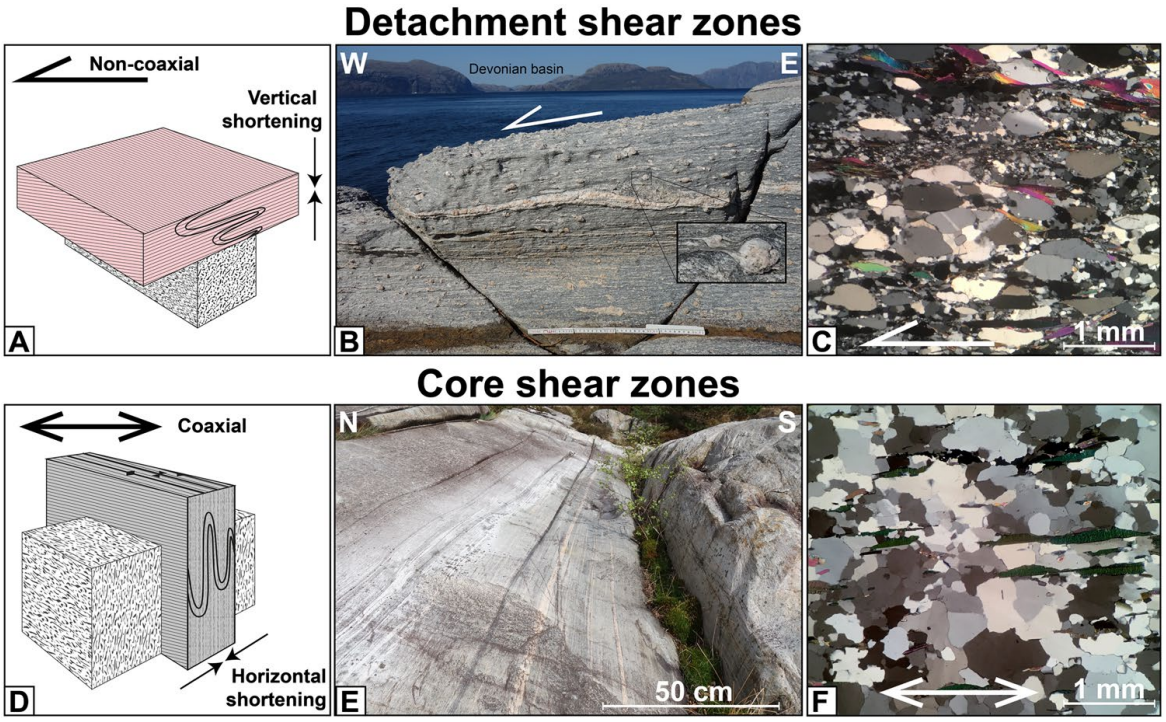

Figure 7. Two endmembers of shear zones developed in the detachment zone (a–c) and the core (d–f). (a) Schematic sketch of subhorizontal detachment shear zone with underlying constrictional domain. (b) Outcrop photo of typical rock in the detachment mylonites. This granitic mylonite contains large feldspar σ- and δ-porphyroclasts within a fine-grained phyllonitic matrix that indicate top-to-W noncoaxial deformation (see inlet). Contrasting rheological behavior of feldspar and the quartz-rich matrix, respectively, indicate lower greenschist facies deformation. The cliffs in the background on the other side of the Sognefjord are part of the Solund Devonian basin. (c) Photomicrograph (cross-polarized light) of quartzite from the detachment mylonites with a composite microstructure. Large grains showing grain boundary migration microstructures and indicate high-temperature low-stress recrystallization (Regime 3, Platt et al., 2015). The coarse-grained fabric is overprinted by fine-grained low-temperature, high-stress (Regimes 1–2) micro shear zones with bulging and subgrain rotation recrystallization. Both fabrics show asymmetry related to top-to-W shearing. (d) Schematic sketch of vertical and coaxial core shear zone, involving simultaneous N-S shortening and E-W extension. (e) Outcrop photo of a typical core shear zone. The mylonitic foliation is subvertical, fabrics are coaxial, and alternating feldspar- and quartz-rich layers show identical rheological behavior, indicative of high-temperature deformation. (f) Photomicrograph (cross-polarized light) of quartzite from a core shear zone with a simple microstructure of coarse-grained quartz. Grain boundary migration microstructures are observed, but most grains are strain-free and abundant 120° triple junctions indicate high-temperature recovery. The absence of a clear shape or crystallographic preferred orientation in quartz and parallel mica grains indicates coaxial deformation.

5.2. Shear Zone Endmembers: Detachment vs. Core Shear Zones

Systematic variations in fabric orientation, ductile strain characteristics, as well as distinct metamorphic evolutions suggest that the detachment mylonites of the NSDZ and the shear zones in the core represent endmembers of shear zones that formed at different structural levels of the MCC (Figure 7). The BASZ seems to be an intermediate case.

5.2.1. Endmember 1: Detachment Mylonites of the NSDZ

In the detachment mylonites, which belong to the NSDZ, foliations are shallowly dipping to subhorizontal, and folds have subhorizontal axial planes (Figure 7a). Most fabrics are noncoaxial and consistently show top-to-W transport (Figure 7b). Another striking characteristic of the detachment mylonites is their record of progressive retrograde deformation from high-grade to low-grade conditions. Amphibolite-facies fabrics are partly preserved as relicts and comprise coarse grain boundary migration fabrics in quartz-rich lithologies, which indicate high temperatures and low flow stresses (Regime 3 microstructures, Platt et al., 2015). Yet, most samples show complex microstructures with greenschist-facies fabrics overprinting higher-grade

fabrics (Figure 7c). Subgrain rotation and bulging recrystallization of quartz to very fine grain sizes indicate high flow stress and low-temperature deformation conditions (Regime 1–2 microstructures). Progressive retrograde deformation appears to lead to increasing strain localization that is strongly related to fluid-rock interaction. There are large tracts of phyllonitic shear zones, both in mafic and felsic lithologies, and chloritization, saussuritization, and epidotization are abundant. Embrittlement of feldspar-rich layers is recorded by greenschist-facies quartz veins. Layers of amorphous greenish cataclasites, with thicknesses up to several meters, are parallel to the shallow-dipping foliation and indicate a progressive fault rock evolution from ductile to brittle conditions.

5.2.2. Endmember 2: Core Shear Zones

Shear zones in the core of the MCC have distinct structures and record a different metamorphic evolution. Foliations are steep to vertical and folded into tight to isoclinal upright folds. Subhorizontal lineations and mostly coaxial fabrics indicate overall pure shear deformation with simultaneous E-W stretching and N-S shortening (Figure 7d). Core shear zones preserve amphibolite-facies fabrics without further retrogression. In quartz-rich lithologies, these commonly involve grain boundary migration recrystallization of quartz at high temperatures and low flow stresses resulting in large grain sizes (Regime 3 microstructures, Figure 7 f). Feldspar layers in the gneisses are behaving entirely viscously and show identical rheological behavior as quartz-dominated layers (Figure 7e). Even though the core shear zones do not show evidence for low-grade fluid-related retrogression, there is clear evidence that they represented important fluid conduits at amphibolite-facies conditions. Fractures occur at sites of rheological heterogeneity, commonly related to extension-parallel folding, and are mineralized as quartz-feldspar veins. The importance of fluids during amphibolite-facies deformation is furthermore recorded by the relationship between shearing and eclogite retrogression, which is presented in section 6.

5.2.3. The Intermediate Case: The BASZ

The detachment mylonites of the BASZ show noncoaxial deformation and a similar metamorphic fabric evolution to the ones from the NSDZ, with low-grade retrogression overprinting higher-grade fabrics. Yet, there are some important differences between these two segments of the detachment system.

The northern BASZ represents an oblique dextral strike-slip segment of the detachment system (Wennberg et al., 1998) and along the southern boundary of the Gulen MCC, the shear zone dips consistently with ca. 60° toward SSW. Large domains of weakly deformed rocks, as found below the NSDZ, are absent in the footwall of the BASZ. In contrast, the BASZ mylonites show a gradual transition into core shear zones, and their fabric orientation is more similar to those observed in the core than those in the NSDZ. Folds in the BASZ indicate N-S shortening and do not show vertical shortening like the NSDZ mylonites. No remnants of the Caledonian nappe pile are exposed in between the Fensfjorden basin and the BASZ mylonites, and the Devonian sediments appear directly juxtaposed to the eclogite bearing crust. These observations suggest that the amount of excision and incision was larger along the southern bounding fault of the Gulen MCC than along its northern boundary. Incision of the strike-slip segment of the detachment has allowed parts of the high-grade core to become overprinted by retrograde strike-slip shearing along the BASZ. Yet, the same may account for the westernmost part of the NSDZ mylonites that contain retrogressed eclogites (Figure 4d).

6. Amphibolite-Facies Reworking of the Exhuming Crust

Pristine eclogites are preserved only in undeformed protolith domains (e.g., Figure 4e). Most eclogites were variably retrogressed at amphibolite-facies conditions. Larger eclogites within shear zones show progressive retrogression from the rim, with amphibolitized margins and eclogite in the core. The state of retrogression appears to be related to the position of the eclogites with respect to shear zones, the availability of fluids, and the size of the eclogite body. A particularly well-exposed locality on Kversøyna at the western apex of the MCC (see Figure 3 for location) shows that eclogite retrogression was fluid induced and simultaneous with shearing and folding of felsic gneisses.

6.1. Structure of the Kversøyna Locality

The 200-m-long and 100 m-wide coastal section (Figure 8) exposes strongly pervasively sheared gneisses and eclogite bodies of variable size, ranging from few meters to >100 m. The gneisses are folded around E-W trending fold axes into tight to isoclinal upright folds with undulating hinge lines. The eclogite bodies are boudinaged, indicating E-W stretching, and occupy synformal positions within the folded gneisses. A

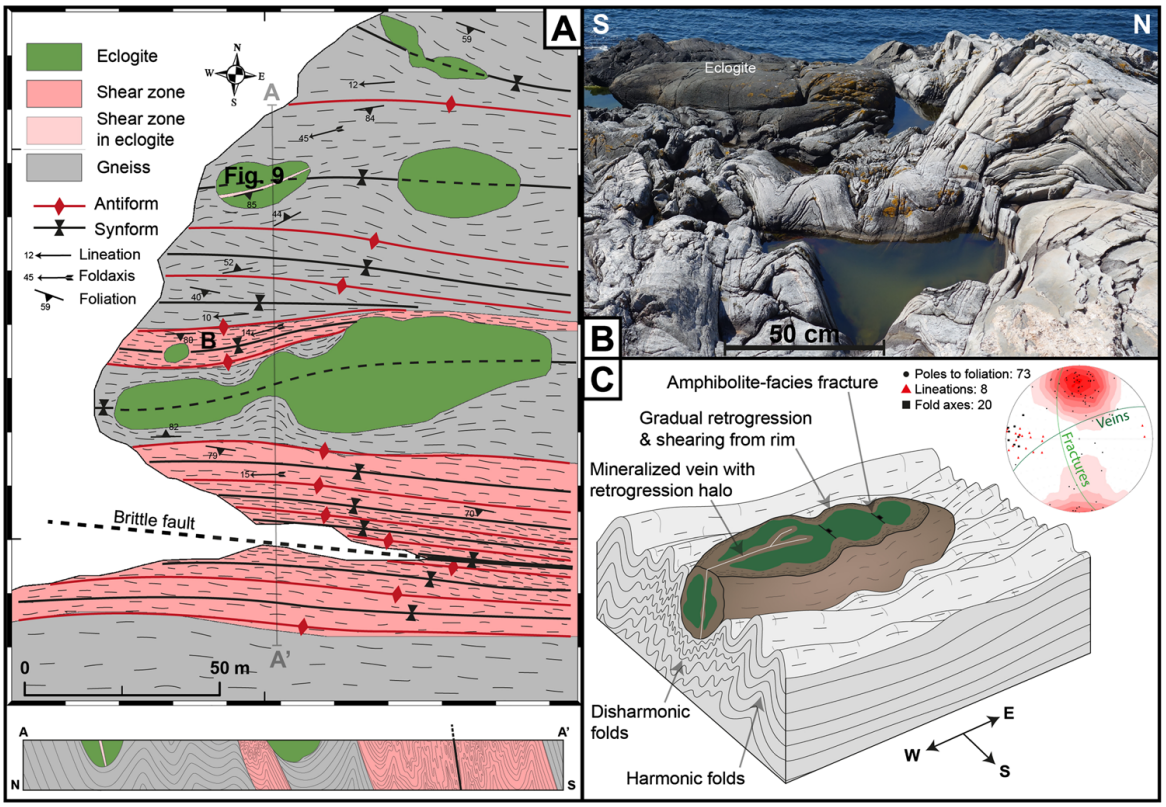

Figure 8. Overview of the Kversøyna locality (location marked on Figure 2). (a) Map and N-S cross section of the locality. Note the influence of dense and rigid eclogite lenses on the gneiss fabric and how fold tightness increases in high-strain zones. The strong fabric anisotropy in the larger shear zone has been exploited by a brittle fault, which is also marked in the coastline. (b) Outcrop photo of eclogite boudin in strongly folded gneiss. Location is marked in (a). (c) Schematic sketch illustrating the observed relationship between folding of gneiss and eclogite retrogression. The lower area equal-area plot shows structural data of the gneisses together with the mean orientation of amphibolite-facies fractures and mineralized veins in eclogite lenses.

weakly pronounced structural asymmetry could indicate a minor component of dextral simple shear, but the gneissic fabrics are symmetric and imply dominant coaxial deformation with synchronous E-W stretching and N-S shortening, like in the rest of the core domain. High-strain zones formed at the borders of the largest eclogite body and show a marked increase of fold tightness compared to the surrounding gneisses. The folded gneisses wrap around the eclogite lenses (Figures 8b and 8c). The folds in the gneisses are generally harmonic; however, in proximity to the eclogites, they get increasingly disharmonic (Figure 8c). The synformal positions of the eclogites within the gneisses, their boudinage, and their influence on folding as well as shear zone localization indicate that the eclogites formed rigid and dense anomalies that were perturbing the else homogeneous flow of the felsic gneisses.

6.2. Fluid-Induced Eclogite Retrogression and Rheological Weakening

Even though the eclogite lenses appear as homogeneous rigid blocks at first sight, a closer look reveals that their rheological behavior has been highly variable depending on their state of retrogression. The typical pattern of eclogite retrogression is a reaction front that moved from the rim of the body toward the core (Figure 8c). Retrogressed amphibolite margins have been sheared progressively together with the surrounding gneisses and indicate that rheological weakening accompanied retrogression.

The rheological contrast within the partially retrogressed mafic bodies leads to fracturing and boudinage of the eclogite domains (Figure 8c). Two conjugated sets of subvertical fractures strike roughly parallel and perpendicular to the maximum stretching direction, respectively. The extension-parallel set of fractures is mineralized with amphibole, plagioclase, and quartz (marked as veins in Figure 8c). In a large (> 20 m) eclogite, these veins are surrounded by decimeter-wide fluid alteration haloes. Within these fluid alteration zones, the eclogite has been retrogressed to undeformed amphibolite (Figure 9a). These mineralized fractures apparently represent corridors where fluids could enter the core of the eclogite and trigger retrogression, while dry domains of pristine eclogite, only centimeters apart, survived metastably until final exhumation.

On the microscale, retrogression is most advanced within fractures, where fluids have entered the rock (Figures 9b and 9c). From these fractures, the retrogression front spreads through the rock along microfractures and grain boundaries (Figure 9d). Microfractures and grain boundaries in omphacite show successive generations of symplectites with coarser symplectites in the core and finer symplectites at the rim. In some cases, symplectites are cut by fractures themselves and then replaced by amphibole (Figure 9c).

Like the retrogression at the rim of the eclogite bodies, retrogression in the core of the mafic lenses gives evidence for significant rheological weakening. The widest retrogression zone, measuring roughly 1 m in thickness, has been entirely transformed into an amphibolite-facies shear zone that cuts through the center of a large eclogite body (Figure 9a). Within this shear zone, not a single relict of the eclogite assemblage is preserved. The shear zone is cut itself by a mineralized fracture, giving evidence for brittle-ductile deformation cycles at amphibolite-facies conditions, probably caused by large rheological heterogeneity within the mafic body. This behavior is furthermore recorded by pseudotachylite formation in partially retrogressed and sheared domains of the eclogite.

Our observations show that the eclogite-bearing crust from the orogenic root was largely reworked at amphibolite-facies conditions. Shear zones appear to have served as conduits for amphibolite-facies fluids that entered undeformed domains through fractures. The availability of fluids clearly controlled the retrogression of eclogites and thereby rheological weakening that enabled viscous flow. These observations strongly resemble the processes observed in the famous Bergen Arcs eclogites (e.g., Austrheim et al., 1997), however, with the difference that they apply to retrogression and not during eclogitization.

7. Discussion: Crustal Flow Within the Gulen MCC

7.1. Eclogites as Time Markers of Postorogenic Viscous Flow

Eclogites within the Gulen MCC are robust time markers for processes that took place in the orogenic root as well as those associated with exhumation. Static eclogitization and the absence of eclogite-facies deformation fabrics indicate that the crust in the southernmost part of the Caledonian eclogite province was still relatively cold and rigid and did not deform pervasively during peak metamorphism. This is quite different from other parts of the WGR where eclogite-facies fabrics are well developed, probably because the crust was buried deeper and higher metamorphic grades were reached (e.g., Andersen et al., 1994; Braathen & Erambert, 2014).

In the Gulen MCC, extensive ductile deformation localized into shear zones and in broad zones of pervasive viscous flow. We find a consistent relationship pattern of eclogites being retrogressed in shear zones, while eclogites in undeformed domains remain mostly preserved. This indicates that the shear zones formed during the transtensional collapse of the overthickened crust (Mode II extension by Fossen, 1992) and after exhumation from eclogite facies conditions, possibly through eduction (Mode I extension). Obviously, we cannot exclude the possibility that some of the shear deformation may have occurred at an earlier stage. However, fabrics show a consistent orientation from the top of the detachment to the lowermost exposed parts of the metamorphic core. The rotation of fabrics from E-W into a more orogen-parallel trend toward the East represents an exception from the rule. Yet, shear zones in this domain show a metamorphic evolution similar to that in the rest of the core, the same relation between linear and planar fabrics and, most importantly, they also contain retrogressed eclogites. Hence, the NE-SW trending shear zones are likely to be postorogenic as well, and their orientation might relate to local orogen-parallel flow during unloading of the orogen (Duclaux et al., 2007). Our interpretation of postorogenic viscous flow in the Gulen MCC is supported by available thermochronological data (Boundy et al., 1996; Chauvet & Dallmeyer, 1992; Walsh

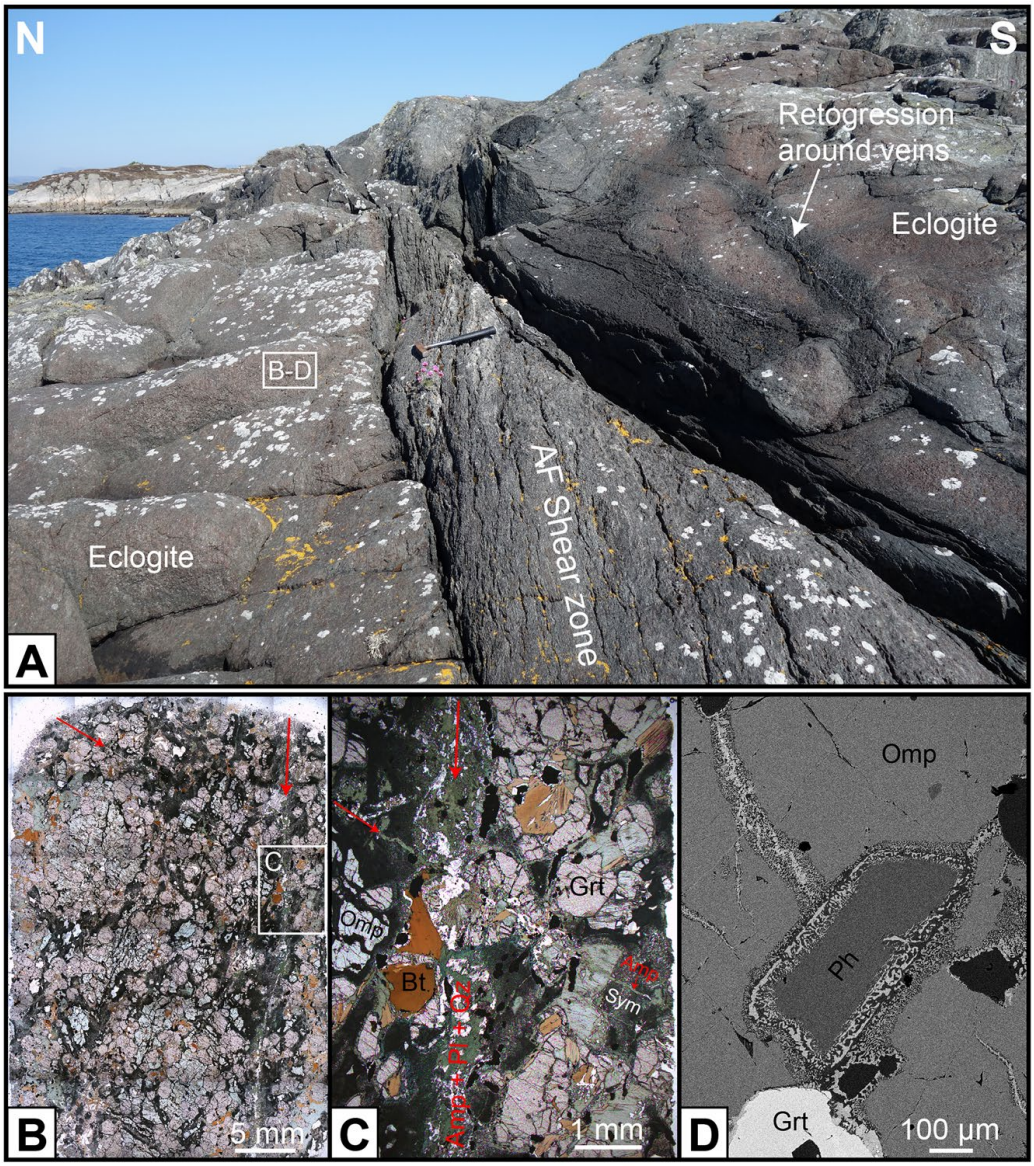

Figure 9. Fluid-induced eclogite retrogression from mesoscale to microscale. (a) Outcrop photo of fluid-induced retrogression in large eclogite body. Location is indicated in Figure 8a. Around mineralized veins, eclogite (red-green) was retrogressed statically to amphibolite (dark green to black). The largest retrogression zone in the center of the photo developed into an amphibolite-facies shear zone, which is cut again by a mineralized brittle fracture. Hammer for scale. (b) Thin section photomosaic (cross-polarized light) of partially retrogressed eclogite. Retrogression domains are easily recognized by the dark color of nontransparent symplectites and green amphiboles in contrast to the light-colored eclogite facies minerals. Retrogression is most advanced along a conjugate set of fractures (red arrows). Note how the retrogression front follows grain boundaries. (c) Close-up of the intersection of the mineralized fractures (red arrows). The larger fracture displays an amphibolite-facies mineralogy. Omphacite is surrounded by a rim of fine grained symplectites, which become coarser further away from the grain boundary and show progressive symplectite growth. Note how symplectites are transformed into amphibole, where they are cut by the small fracture. This relationship clearly demonstrates that even on the microscale, retrogression is a function of fluid availability. (d) Scanning electron microscope image of the least retrogressed eclogite domain. Retrogression advances along fractures and grain boundaries and leads to growth of submicrometer size symplectites.

et al., 2013) and interpretations of previous works in the surrounding areas (Andersen et al., 1994; Hacker et al., 2003; Milnes et al., 1997).

7.2. Viscous Flow at Distinct Structural Levels: Kinematically Linked, Mechanically Decoupled

Our results from the Gulen MCC fit very well within the general framework of postorogenic exhumation of the WGR by shearing along the NSDZ during sinistral transtension (e.g., Krabbendam & Dewey, 1998). Yet, our results are not fully explained neither by simple shear detachment models (e.g., Hacker et al., 2003; Souche et al., 2013), nor by homogeneous constriction as predicted from transtension (e.g., Dewey, 2002; Fossen et al., 2013; Krabbendam & Dewey, 1998), nor by simple vertical thinning of the overthickened crust (e.g., Andersen et al., 1994). All of these elements need to be integrated in a dynamic model of detachment and footwall evolution, to explain the distinct deformation that we observe at various levels of the extending crust.

At the presently exposed level, crustal flow within the Gulen MCC is entirely solid state. The crust appears to represent a coherently stretched block with significant strain variations in three dimensions (Figure 10). We find distinct structural levels that appear kinematically linked while mechanically decoupled. They formed within the same kinematic boundary conditions of sinistral transtension but represent different metamorphic conditions and hence different rheologies. On top, the detachment level shows simple shear with vertical thinning and the characteristic overprint of greenschist facies and semibrittle fabrics on higher-grade fabrics. In contrast, the lowest level shows pervasive coaxial amphibolite-facies viscous flow of the crust reaching extreme amounts of simultaneous E-W stretching and N-S shortening. A key finding of this study is that the coaxial high-grade fabrics in the core experienced no further low-grade overprint. As such, it must represent a structural level that is distinct from the noncoaxial detachment zone with its consistent retrograde overprinting relationships. In between these two levels, we find minor remnants of an intermediate domain of localized amphibolite-facies deformation, which involves constriction and minor vertical thinning. These distinct amphibolite-facies domains resemble the localized-distributed transition within the viscous crust postulated by Cooper et al. (2017). Today, we find all these different structural levels along the same exposure level as observed along cross section A (Figure 3). Their systematic variations in metamorphic conditions and strain characteristics imply, however, that they formed at different vertical levels of the crust and were later juxtaposed during core-complex exhumation.

7.3. Inward Flow Through Differential Folding ("Stockwerk Folding")

The N-S cross sections through the WGR and the Gulen MCC show intensive extension-parallel folding (compare Figure 1B and Figure 3) in contrast to shallowly undulating, parallel fabrics seen in E-W sections. According to our mapping in the Gulen MCC and the interpretation of large-scale fold patterns along the west coast of the WGR (Figure 1B), different crustal levels experienced apparently different amounts of N-S shortening. The detachment zone and the overlying basins show mostly open folds, although thrusts and reverse faults within the basins record locally larger amounts of syn-sedimentary N-S shortening (Osmundsen et al., 2019). The WGR footwall, however, is pervasively folded into tight to isoclinal upright folds from the scale of meters to tens of kilometers. Thus, the amount of N-S shortening in the footwall of the NSDZ appears to be significantly larger than in the overlying nappes and the detachment zone itself (Braathen & Erambert, 2014). These extension-parallel folds have been related to a distinct tectonic phase of regional N-S compression (e.g., Chauvet & Seranne, 1994), but they are also adequately explained as a result of transtension (Dewey, 2002; Fossen et al., 2013; Krabbendam & Dewey, 1998). However, our observations are not in agreement with a simple model of progressive transtensional folding during exhumation. The tight upright folds formed due to strong extension-perpendicular shortening during internal necking within the amphibolite-facies crust, while the upper crustal levels experienced only weak extension-perpendicular shortening. This differential folding might just represent the actual mechanism of extension-perpendicular crustal flow that is predicted from 3-D numerical models of transtensional core-complex formation (Le Pourhiet et al., 2012). We interpret the high-grade extension-parallel folds as the structural expression of isostasy-driven Poiseuille-type flow in the deep crust that moved low-viscosity solid-state material from the north and south into the dome and hence as a less drastic case of the mechanism postulated for migmatite-cored MCCs (e.g., Kruckenberg et al., 2011; Rey et al., 2017; Roger et al., 2015). As an interesting side note, this kind of differential folding was already described by Wegmann (1935) and Haller (1956) in the Greenland Caledonides. Distinct deformation regimes in relation to different metamorphic

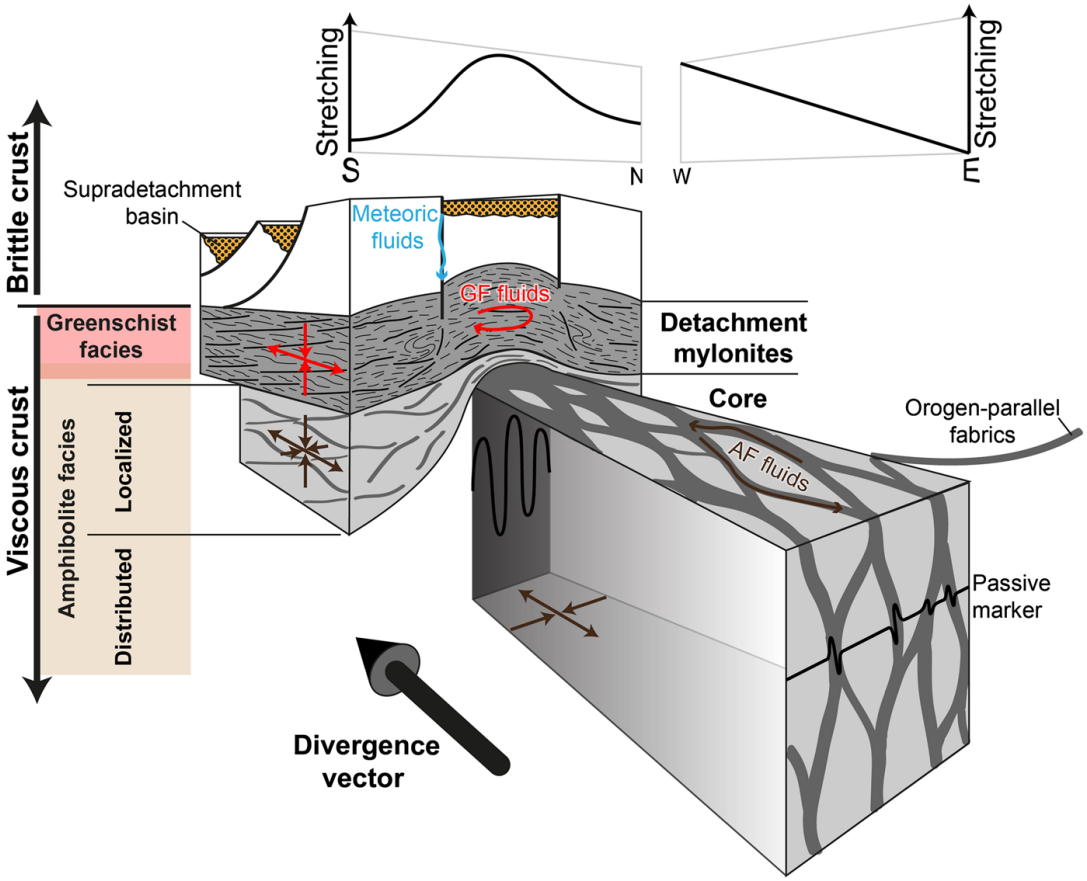

Figure 10. The internal structure of the Gulen MCC reveals a coherently stretched crustal section; however, distinct structural levels show very different deformation fabrics, kinematics, and fluids. Differences between these structural levels appear to relate to vertical metamorphic variations and horizontal strain gradients in N-S as well as E-W direction. Yet, they are all interpreted to have formed within the same kinematic boundary condition of sinistral transtension, which is represented by the divergence vector (Fossen et al., 2013). Below the brittle crust, the detachment mylonites show retrograde deformation from amphibolite-facies to semibrittle conditions, involving noncoaxial shearing and vertical shortening. The amphibolite-facies core consists of a domain of localized deformation, which is necked by pervasively sheared gneisses. The localized domain shows weak noncoaxial shearing and minor vertical shortening. In contrast, the distributed domain is characterized by coaxial shearing and N-S shortening.

conditions in vertical levels of the crust were the essence of the "stockwerk folding hypothesis." However, as pointed out by Wernicke (2009), these authors worked within a "fixist" paradigm that did not permit major horizontal movements. Therefore, it took many years until researchers realized that this "stockwerk folding" occurred in the footwall of massive extensional detachment shear zones (Hodges, 2016; White et al., 2002).

7.4. When Distant Relatives Become Close Neighbors: A Dynamic Model for Transtensional MCC Formation

During MCC exhumation, large parts of the original crust can be removed through the combination of incision, excision, and erosion. In the final structure of the Gulen MCC, syntectonic sedimentary rocks are directly juxtaposed with deep crustal levels, as demonstrated by the juxtaposition of the Fensfjorden Devonian basin with the eclogite-bearing crust across the BASZ. During the progressive evolution, material within the MCC is moving through different metamorphic conditions and deformation regimes, for

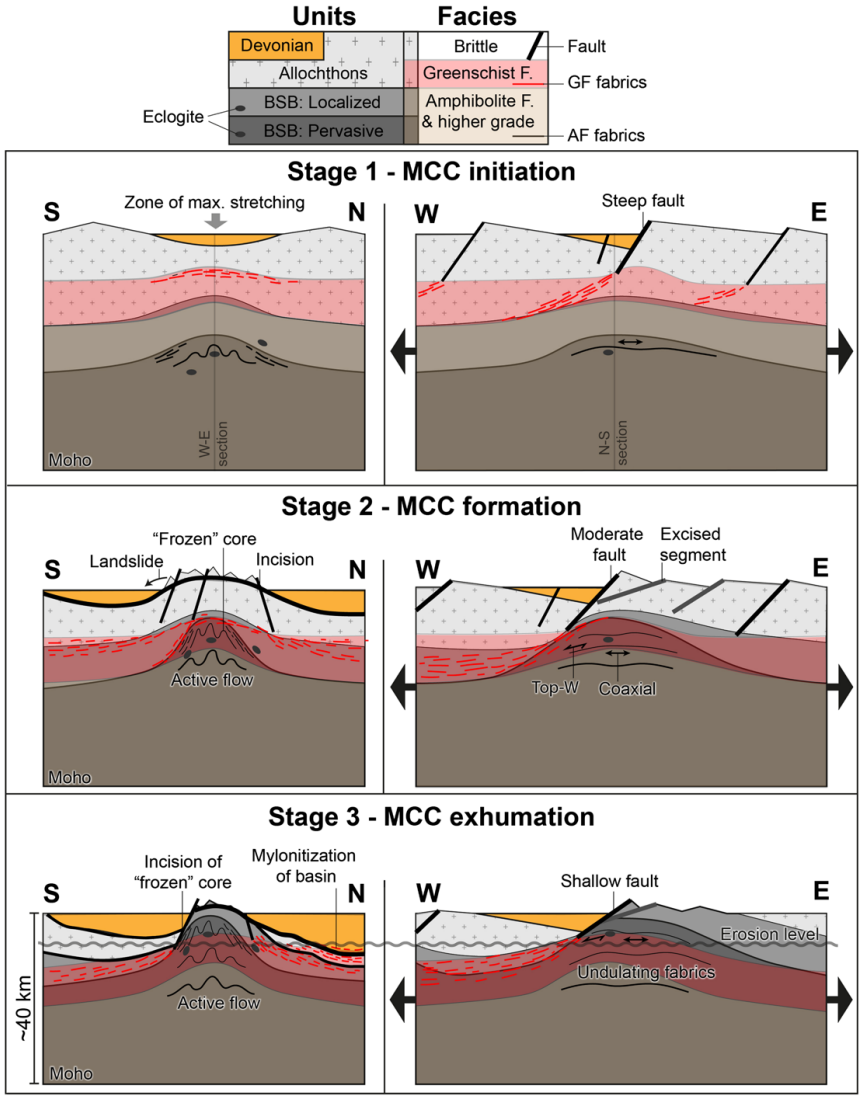

Figure 11. Sequential model for transtensional MCC formation in the footwall of the NSDZ. The evolution is illustrated in three stages with perpendicular cross sections that intersect each other in the center. The present erosion level is indicated in Stage 3. BSB = Baltic Shield basement (see text for discussion).

example, ductile rocks become brittle. In addition, the thermal conditions of the system are transient. Heat advection will change the geothermal gradient during MCC evolution (Whitney et al., 2013) and hence the spatial distribution of deformation regimes.

We incorporated these basic principles of MCC formation with existing models of postorogenic collapse of the Scandinavian Caledonides. Thereby we try to explain our field observations in accordance with the available information from other culminations of the WGR, the NSDZ, and recent work in the Devonian basins (Osmundsen & Péron-Pinvidic, 2018; Osmundsen et al., 2019). Our model is presented in Figure 11 as a

series of N-S and E-W cross sections to illustrate the 3-D kinematics. The time evolution is portrayed in three stages, which do not represent distinct phases but are an inevitable simplification made to illustrate the incremental evolution. The model that we come up with, of course, is highly simplified. We do not consider any internal structural geometries, rheological heterogeneities, or topographic variations that were possibly there at the end of Mode I extension. Our cross sections show neither E-W extension of the entire crust nor the associated extension-orthogonal shortening of the crustal section. Furthermore, we do not show the interference of different MCCs and the rotation of the divergence vector during progressive transtension.

Our model starts with a strongly thickened, horizontally layered crust. We show three rheological layers (Figure 11): brittle upper crust and the ductile crust separated between greenschist facies and amphibolite facies or higher grades. The crust consists of a thick pile of nappes overlaying the eclogite-bearing Baltic Shield basement (BSB). The unit boundaries serve only as passive markers for the structural evolution but do not represent rheological boundaries, except for the distinction between localized and pervasive deformation domains within the BSB. For reasons of simplicity, we overlap the greenschist-/amphibolite-facies boundary with the nappe-basement contact, but we note that extensional shearing in the lower nappes started at amphibolite-facies conditions (Johnston, Hacker, & Ducea, 2007b and references therein).

7.4.1. Stage 1: MCC Initiation

Initial extension formed steep, laterally limited normal faults that grade into mid-crustal shear zones at depth. Initial necking occurred at rheological transitions and involved extension-perpendicular folding within the amphibolite layer. It should be noted that both the depocenter of the initial basin and the future MCC formed in the center of the fault, because this is the zone of maximum stretching (e.g., Kapp et al., 2008; Osmundsen & Péron-Pinvidic, 2018; Osmundsen et al., 2019).

7.4.2. Stage 2: MCC Formation

During the main phase of MCC formation, the MCC started to rise in the zone of maximum stretching, and the basins were displaced to the flanks of the MCC as argued by Osmundsen et al. (2019). The synchronous formation of several MCCs along-strike (not shown in Figure 11) made the basins occupy synforms in between the rising antiforms. Different processes occurred at the different levels, which are still far apart from each other. The brittle crust, comprising the upper part of the nappe pile, was exposed, eroded, and deposited in the basins. Steep faults incised at the flanks of the MCC and form steep topography, which promoted catastrophic mass movements through large landslides as observed in the Solund and Kvamshesten basins (Hartz et al., 2002; Osmundsen et al., 1998). This shows that erosion can contribute significantly to upper crustal thinning during MCC exhumation.Greenschist facies top-to-W shearing within the detachment zone itself occurred mostly in the nappes, but as the upper crust was thinning progressively, also the BSB got involved. At the same time, at a deeper level, the amphibolite-facies crust was necking internally. Lateral inward flow occurred through extension-orthogonal shortening of the pervasively deforming low-viscosity crust. This process formed the high-grade core with steep strike-slip shear zones at its flanks. Differential exhumation at amphibolite-facies conditions is a consequence of this process. Rocks originating from different depths may be juxtaposed in relation to their position along major fold structures (compare position of eclogite bodies between stages 1 and 2). The high-grade core was exhumed progressively to greenschist facies conditions, but greenschist facies deformation was restricted to the top and the flanks of the culmination. Apparently, retrograde deformation stalled suddenly within the core, high-grade fabrics became “frozen-in,” and active flow moved to weaker layers.

A possible explanation for this may be that the internal necking of the ductile layer and the associated exhumation of the high-grade core represent a form of vertical heat advection. The rising core apparently contributed heat and fluids to the detachment system, which lead to weakening and increasing strain localization in the detachment layer. Furthermore, greenschist facies phyllonites, which formed previously through fluid-related retrogression within the detachment mylonites, are brought into the realm of brittle faulting. Such fault rocks with particularly low shear strength (Braathen et al., 2004), the abundance of fluids, and progressive heating within the detachment zone through head advection and possibly shear heating (Souche et al., 2013) imply that the brittle layer became weakened at this stage, promoting brittle faulting at progressively lower angles. At the same time, the rising core itself was cooling down, and therefore the active amphibolite-facies flow moved to a deeper and hotter level where the viscosity was lower. Furthermore, the possible occurrence of partial melting at a deeper, unexposed level of the MCC must be noted.

7.4.3. Stage 3: MCC Exhumation

The "frozen-in" high-grade core was exhumed progressively through localized deformation in the weakened detachment system. Brittle faulting occurred at progressively lower dips. At this stage, the deep crust had reached the surface and became eroded itself, as demonstrated by detrital Ar-Ar cooling ages from Hornelen basin (Templeton, 2015). The basins have reached a massive size at this stage, but only minor remnants are preserved at the present erosion level, which expose the oldest strata. Reconstructions imply a maximum basin depth between 9 and 13.5 km with a geothermal gradient of 38°C/km (Souche et al., 2012; Souche et al., 2013; Svensen et al., 2001). This implies that in parts of the system, the brittle crust had been entirely replaced by supradetachment basins. Devonian sediments were directly juxtaposed to detachment mylonites, and in the case of the Solund Basin, the lowest strata of the basin were even mylonitized themselves (Seranne & Seguret, 1987). At this stage, most of the nappe pile and even parts of the basement have been removed by ductile thinning, excision, and incision. The detachment system can be envisaged as a selective rock grinder: Weak rocks were smeared out ductilely in the detachment shear zone, while strong lithologies were removed through brittle faulting, footwall uplift, and erosion. In the synforms of the detachment zone, we find mostly weak rheologies like mica schists and phyllonites preserved. At the flank of the MCC, steep strike-slip faults incised the core and exploited previously formed ductile fabrics. In the case of the BASZ, the basin was directly juxtaposed to the deep crust. Further isostatic compensation may have occurred through folding at deeper amphibolite-facies levels.

At the end of this evolution, our reconstruction implies a crustal thickness of around 40 km (10 km thick basin fill + 30 km present crustal thickness). Final juxtaposition of the different units occurred through brittle fault reactivation during North Sea rifting (e.g., Eide et al., 1997; Torsvik et al., 1992).

8. Conclusions and Implications for Postorogenic Exhumation of (Ultra-)High-Pressure Rocks

Our study shows that vertical metamorphic variations and lateral strain gradients during postorogenic transtension may cause a highly variable behavior of the crust, leading to differential exhumation and the formation of MCCs. We think that our field-based model (Figure 11) encapsulates important general aspects of MCC formation in 3-D strain settings and can contribute to understand MCCs where the deep levels of the crust are not exposed. Large magnitudes of extension can amplify differential extension-orthogonal shortening of distinct crustal levels. This process results in characteristic fold structures, which resemble the historic "stockwerk folding hypothesis" (Wernicke, 2009) and might easily be mistaken for contractional structures formed during convergence. In the case of the WGR, however, they clearly formed during postorogenic transtension. Thus, like in the case of migmatite-cored MCCs (Rey et al., 2017), extension-orthogonal contraction within the deep crust is the main mechanism of isostasy-driven crustal flow also in solid-state MCCs.

This crustal flow mechanism has the potential to redistribute material within the extending crust (Figure 11). Hence, it might be highly important for the exhumation of (ultra-) high-pressure rocks in postorogenic settings. A comprehensive look at the WGR demonstrates that this might have been the case in the Caledonides. The Gulen MCC is the southernmost of a series of evenly spaced MCCs (Figures 1A and 1B); however, also the ultrahigh-pressure domains north of the Hornelen Basin have similar orientations, spacing, and wavelengths. If the pressure estimates from these rocks reflect burial depth, the occurrence of such discrete domains (e.g., Root et al., 2005) implies that the rocks inside these domains have been exhumed from greater depth than the rocks in the surrounding areas. We suggest that our model of crustal flow could offer a plausible explanation for this differential exhumation pattern. This would imply that the processes across the WGR have been self-similar over large areas of the giant high-pressure terrane.

Even if we zoom out to the scale of the entire orogen, we can find notable self-similarities. Already Ramberg (1981) pointed out the existence of two distinct belts of basement domes that run parallel along the entire length of the Scandinavian Caledonides. Osmundsen et al. (2005) showed that these domes can be seen as different types of MCCs. The belt in the foreland consists of cylindrical domes with long axes perpendicular to the extension direction, which comprise low-grade metamorphic rocks and record low amounts of exhumation. In contrast, the domes in the hinterland of the orogen are noncylindrical with long axes parallel to

the extension direction and expose high-grade metamorphic rocks, which were exhumed from great depth. The different shapes of these domes resemble exactly the a-type versus b-type classification that has been suggested for Aegean domes (Jolivet et al., 2004). Le Pourhiet et al. (2012) attributed the coeval formation of both dome types in the Cyclades to distinct kinematic boundary conditions related to a slab tear during rollback of the Aegean slab. In the case of the Scandinavian Caledonides, however, the different dome-types appear systematically with respect to their position toward the foreland or the hinterland of the orogen. Furthermore, as they occur along the entire length of the orogen, the domes in the Scandinavian Caledonides are likely to have formed within the same kinematic boundary conditions. Thus, the different dome types apparently relate to variations in metamorphic conditions at the onset of extension, as well as different amounts of crustal stretching and associated exhumation. At least in the case of the Scandinavian domes, noncylindricality appears to be a function of crustal stretching, but we speculate that this relationship might also apply universally. During the formation of large normal-fault systems, there will always be along-strike variations, which can trigger differential crustal flow in the deep crust. This creates a feedback loop that can be amplified during progressive crustal stretching. Hence, an alternative explanation for the coeval formation of a- and b-type domes might be that noncylindrical MCCs will be exhumed from the deep crust if a critical amount of extension is reached (Stage 2 in Figure 13). A way to test this hypothesis could be to analyze systematic variations in metamorphic grade and exhumation recorded in a- and b-type domes around the world, respectively.

Acknowledgments
The field data from this study can be accessed online (https://doi.org/10.6084/m9.figshare.c.4697006.v1). JDW thanks Sebastian Wolf, Arne Fuhrmann, Thilo Wrona, Theo Kassaras, and Anne Reiff for their company that made fieldwork possible. We thank Irina Dumitru and Irene Heggstad at UiB for help with sample preparation and BSE imaging. This research was funded by VISTA—a basic research program in collaboration between the Norwegian Academy of Science and Letters and Equinor [grant number 6271] as well as a student grant for JDW from the Meltzer fond at the University of Bergen. We thank C. Teyssier and P. Rey for constructive reviews and L. Jolivet and W. Behr for editorial handling.

References

Andersen, T. B., & Jamtveit, B. (1990). Uplift of deep crust during orogenic extensional collapse: A model based on field studies in the Sogn-Sunnfjord Region of Western Norway. *Tectonics*, *9*(5), 1097–1111. https://doi.org/10.1029/TC009i005p01097

Andersen, T. B., Jamtveit, B., Dewey, J. F., & Swensson, E. (1991). Subduction and eduction of continental crust: Major mechanisms during continent-continent collision and orogenic extensional collapse, a model based on the South Norwegian Caledonides. *Terra Nova*, *3*(3), 303–310. https://doi.org/10.1111/j.1365-3121.1991.tb00148.x

Andersen, T. B., Osmundsen, P. T., & Jolivet, L. (1994). Deep crustal fabrics and a model for the extensional collapse of the southwest Norwegian Caledonides. *Journal of Structural Geology*, *16*(9), 1191–1203. https://doi.org/10.1016/0191-8141(94)90063-9

Austrheim, H., Erambert, M., & Engvik, A. K. (1997). Processing of crust in the root of the Caledonian continental collision zone: The role of eclogitization. *Tectonophysics*, *273*(1-2), 129–153. https://doi.org/10.1016/S0040-1951(96)00291-0

Bingen, B., Skar, O., Marker, M., Sigmond, E. M. O., Nordgulen, O., Ragnhildstveit, J., et al. (2005). Timing of continental building in the Sveconorwegian orogen, SW Scandinavia. *Norwegian Journal of Geology*, *85*(1-2), 87–116.

Block, L., & Royden, L. H. (1990). Core complex geometries and regional scale flow in the lower crust. *Tectonics*, *9*(4), 557–567. https://doi.org/10.1029/TC009i004p00557

Boundy, T. M., Essene, E. J., Hall, C. M., Austrheim, H., & Halliday, A. N. (1996). Rapid exhumation of lower crust during continent-continent collision and late extension: Evidence from Ar-40/Ar-39 incremental heating of hornblendes and muscovites, Caledonian orogen, western Norway. *Geological Society of America Bulletin*, *108*(11), 1425–1437. https://doi.org/10.1130/0016-7606(1996)108

Braathen, A., & Erambert, M. (2014). Structural and metamorphic history of the Engebøfjellet Eclogite and the exhumation of the Western Gneiss Region, Norway. *Norwegian Journal of Geology*, *94*, 53–76.

Braathen, A., Osmundsen, P. T., & Gabrielsen, R. H. (2004). Dynamic development of fault rocks in a crustal-scale detachment: An example from western Norway. *Tectonics*, *23*, n/a. https://doi.org/10.1029/2003tc001558

Brueckner, H. K. (2018). The great eclogite debate of the Western Gneiss Region, Norwegian Caledonides: The in situ crustal v. exotic mantle origin controversy. *Journal of Metamorphic Geology*, *36*(5), 517–527. https://doi.org/10.1111/jmg.12314

Brun, J.-P., Sokoutis, D., Tirel, C., Gueydan, F., Van Den Driessche, J., & Beslier, M.-O. (2017). Crustal versus mantle core complexes. *Tectonophysics*, *746*, 22–45. https://doi.org/10.1016/j.tecto.2017.09.017

Buck, W. R. (1991). Modes of continental lithospheric extension. *Journal of Geophysical Research*, *96*(B12), 20,161–20,178. https://doi.org/10.1029/91jb01485

Butler, J. P., Beaumont, C., & Jamieson, R. A. (2015). Paradigm lost: Buoyancy thwarted by the strength of the Western Gneiss Region (ultra) high-pressure terrane, Norway. *Lithosphere*, *7*(4), 379–407. https://doi.org/10.1130/L426.1

Butler, J. P., Jamieson, R. A., Dunning, G. R., Pecha, M. E., Robinson, P., & Steenkamp, H. M. (2018). Timing of metamorphism and exhumation in the Nordøyane ultra-high-pressure domain, Western Gneiss Region, Norway: New constraints from complementary CA-ID-TIMS and LA-MC-ICP-MS geochronology. *Lithos*, *310-311*, 153–170. https://doi.org/10.1016/j.lithos.2018.04.006

Chauvet, A., & Dallmeyer, R. D. (1992). 40Ar/39Ar mineral dates related to Devonian extension in the southwestern Scandinavian Caledonides. *Tectonophysics*, *210*(1-2), 155–177. https://doi.org/10.1016/0040-1951(92)90133-Q

Chauvet, A., & Seranne, M. (1994). Extension-parallel folding in the Scandinavian Caledonides: Implications for late-orogenic processes. *Tectonophysics*, *238*(1-4), 31–54. https://doi.org/10.1016/0040-1951(94)90048-5

Coint, N., Slagstad, T., Roberts, N. M. W., Marker, M., Rohr, T., & Sorensen, B. E. (2015). The Late Mesoproterozoic Sirdal Magmatic Belt, SW Norway: Relationships between magmatism and metamorphism and implications for Sveconorwegian orogenesis. *Precambrian Research*, *265*, 57–77. https://doi.org/10.1016/j.precamres.2015.05.002

Coney, P. J. (1980). Cordilleran metamorphic core complexes: An overview. *Geological Society of America Memoirs*, *153*, 7–31. https://doi.org/10.1130/MEM153-p7

Cooper, F. J., Platt, J. P., & Behr, W. M. (2017). Rheological transitions in the middle crust: insights from Cordilleran metamorphic core complexes. *Solid Earth*, *8*(1), 199–215. https://doi.org/10.5194/se-8-199-2017

Cuthbert, S. J., Carswell, D. A., Krogh-Ravna, E. J., & Wain, A. (2000). Eclogites and eclogites in the Western Gneiss Region, Norwegian Caledonides. *Lithos*, *52*(1-4), 165–195. https://doi.org/10.1016/S0024-4937(99)00090-0

Cutts, J. A., M. A. Smit, E. Kooijman, and M. Schmitt (2019), Two-stage cooling and exhumation of deeply subducted continents, *Tectonics*, *38*(0), doi: https://doi.org/10.1029/2018tc005292, 3, 863, 877.
Dewey, J. F. (2002). Transtension in arcs and orogens. *International Geology Review*, *44*(5), 402–439. https://doi.org/10.2747/0020-6814.44.5.402
Duclaux, G., Rey, P., Guillot, S., & Ménot, R.-P. (2007). Orogen-parallel flow during continental convergence: Numerical experiments and Archean field examples. *Geology*, *35*, 715–718. https://doi.org/10.1130/g23540a.1
Eide, E. A., Haabesland, N. E., Osmundsen, P. T., Andersen, T. B., Roberts, D., & Kendrick, M. A. (2005). Modern techniques and Old Red problems: Determining the age of continental sedimentary deposits with Ar-40/Ar-39 provenance analysis in west-central Norway. *Norwegian Journal of Geology*, *85*(1-2), 133–149.
Eide, E. A., Torsvik, T. H., & Andersen, T. B. (1997). Absolute dating of brittle fault movements: Late Permian and late Jurassic extensional fault breccias in western Norway. *Terra Nova*, *9*(3), 135–139. https://doi.org/10.1046/j.1365-3121.1997.d01-21.x
Engvik, A. K., Austrheim, H., & Andersen, T. B. (2000). Structural, mineralogical and petrophysical effects on deep crustal rocks of fluid-limited polymetamorphism, Western Gneiss Region, Norway. *Journal of the Geological Society*, *157*(1), 121–134. https://doi.org/10.1144/jgs.157.1.121
Engvik, A. K., Willemoes-Wissing, B., & Lutro, O. (2018). High-temperature, decompressional equilibration of the eclogite facies orogenic root (Western Gneiss Region, Norway). *Journal of Metamorphic Geology*, *36*(5), 529–545. https://doi.org/10.1111/jmg.12418
Fossen, H. (1992). The role of extensional tectonics in the Caledonides of South Norway. *Journal of Structural Geology*, *14*(8-9), 1033–1046. https://doi.org/10.1016/0191-8141(92)90034-T
Fossen, H. (2010). Extensional tectonics in the North Atlantic Caledonides: A regional view. *Geological Society, London, Special Publications*, *335*(1), 767–793. https://doi.org/10.1144/SP335.31
Fossen, H., Teyssier, C., & Whitney, D. L. (2013). Transtensional folding. *Journal of Structural Geology*, *56*, 89–102. https://doi.org/10.1016/j.jsg.2013.09.004
Ganzhorn, A. C., Labrousse, L., Prouteau, G., Leroy, C., Vrijmoed, J. C., Andersen, T. B., & Arbaret, L. (2014). Structural, petrological and chemical analysis of syn-kinematic migmatites: insights from the Western Gneiss Region, Norway. *Journal of Metamorphic Geology*, *32*(6), 647–673. https://doi.org/10.1111/jmg.12084
Gordon, S. M., Whitney, D. L., Teyssier, C., & Fossen, H. (2013). U-Pb dates and trace-element geochemistry of zircon from migmatite, Western Gneiss Region, Norway: Significance for history of partial melting in continental subduction. *Lithos*, *170-171*, 35–53. https://doi.org/10.1016/j.lithos.2013.02.003
Griffin, W. L., & Brueckner, H. K. (1980). Caledonian Sm-Nd ages and a crustal origin for Norwegian eclogites. *Nature*, *285*(5763), 319–321. https://doi.org/10.1038/285319a0
Hacker, B. R., Andersen, T. B., Johnston, S., Kylander-Clark, A. R. C., Peterman, E. M., Walsh, E. O., & Young, D. (2010). High-temperature deformation during continental-margin subduction & exhumation: The ultrahigh-pressure Western Gneiss Region of Norway. *Tectonophysics*, *480*(1-4), 149–171. https://doi.org/10.1016/j.tecto.2009.08.012
Hacker, B. R., Andersen, T. B., Root, D. B., Mehl, L., Mattinson, J. M., & Wooden, J. L. (2003). Exhumation of high-pressure rocks beneath the Solund Basin, Western Gneiss Region of Norway. *Journal of Metamorphic Geology*, *21*(6), 613–629. https://doi.org/10.1046/j.1525-1314.2003.00468.x
Hacker, B. R., Kylander-Clark, A. R. C., Holder, R., Andersen, T. B., Peterman, E. M., Walsh, E. O., & Munnikhuis, J. K. (2015). Monazite response to ultrahigh-pressure subduction from U-Pb dating by laser ablation split stream. *Chemical Geology*, *409*, 28–41. https://doi.org/10.1016/j.chemgeo.2015.05.008
Haller, J. (1956). Probleme der Tiefentektonik Bauformen im Migmatit Stockwerk der Ostgrönländischen Kaledoniden. *Geol Rundsch*, *45*(2), 159–167. https://doi.org/10.1007/BF01802002
Hartz, E. H., Martin, M. W., Andresen, A., & Andersen, T. B. (2002). Volcanic rocks in the Devonian Solund Basin, Western Norway: Large landslides of Silurian (439 Ma) rhyolites. *Journal of the Geological Society*, *159*(2), 121–128. https://doi.org/10.1144/0016-764901-063
Hodges, K. V. (2016). Crustal decoupling in collisional orogenesis: Examples from the East Greenland Caledonides and Himalaya. *Annu Rev Earth Pl Sc*, *44*(1), 685–708. https://doi.org/10.1146/annurev-earth-060115-012412
Holder, R. M., Hacker, B. R., Kylander-Clark, A. R. C., & Cottle, J. M. (2015). Monazite trace-element and isotopic signatures of (ultra)high-pressure metamorphism: Examples from the Western Gneiss Region, Norway. *Chemical Geology*, *409*, 99–111. https://doi.org/10.1016/j.chemgeo.2015.04.021
Johnston, S., Hacker, B. R., & Ducea, M. N. (2007). Exhumation of ultrahigh-pressure rocks beneath the Hornelen segment of the Nordfjord-Sogn Detachment Zone, western Norway. *GSA Bulletin*, *119*(9-10), 1232–1248. https://doi.org/10.1130/B26172.1
Johnston, S. M., Hacker, B. R., & Andersen, T. B. (2007). Exhuming Norwegian ultrahigh-pressure rocks: Overprinting extensional structures and the role of the Nordfjord-Sogn Detachment Zone. *Tectonics*, *26*, n/a. https://doi.org/10.1029/2005TC001933
Jolivet, L., Famin, V., Mehl, C., Parra, T., Aubourg, C., Hebert, R., & Philippot, P. (2004). Strain localization during crustal-scale boudinage to form extensional metamorphic domes in the Aegean Sea. *Geol Soc Am Spec Pap*, *380*, 185–210. https://doi.org/10.1130/0-8137-2380-9.185
Kapp, P., Stockli, D., Taylor, M., & Ding, L. (2008). Development of active low-angle normal fault systems during orogenic collapse: Insight from Tibet. *Geology*, *36*(1), 7–10. https://doi.org/10.1130/g24054a.1
Kildal, E. S. (1970). Geologisk kart over Norge, berggrunnskart, Måløy, 1:250.000, norsk utgave. *Norges geologiske undersøkelse*.
Kohn, M. J., Corrie, S. L., & Markley, C. (2015). The fall and rise of metamorphic zircon. *Am Mineral*, *100*(4), 897–908. https://doi.org/10.2138/am-2015-5064
Krabbendam, M., & Dewey, J. F. (1998). Exhumation of UHP rocks by transtension in the Western Gneiss Region, Scandinavian Caledonides. *Geological Society, London, Special Publications*, *135*(1), 159–181. https://doi.org/10.1144/GSL.SP.1998.135.01.11
Kruckenberg, S. C., Vanderhaeghe, O., Ferre, E. C., Teyssier, C., & Whitney, D. L. (2011). Flow of partially molten crust and the internal dynamics of a migmatite dome, Naxos, Greece. *Tectonics*, *30*, n/a. https://doi.org/10.1029/2010tc002751
Kylander-Clark, A. R. C., & Hacker, B. R. (2014). Age and significance of felsic dikes from the UHP western gneiss region. *Tectonics*, *33*, 2342–2360. https://doi.org/10.1002/2014TC003582
Kylander-Clark, A. R. C., Hacker, B. R., & Mattinson, J. M. (2008). Slow exhumation of UHP terranes: Titanite and rutile ages of the Western Gneiss Region, Norway. *Earth and Planetary Science Letters*, *272*(3-4), 531–540. https://doi.org/10.1016/j.epsl.2008.05.019
Labrousse, L., Prouteau, G., & Ganzhorn, A.-C. (2011). Continental exhumation triggered by partial melting at ultrahigh pressure. *Geology*, *39*(12), 1171–1174. https://doi.org/10.1130/g32316.1
Le Pourhiet, L., Huet, B., May, D. A., Labrousse, L., & Jolivet, L. (2012). Kinematic interpretation of the 3D shapes of metamorphic core complexes. *Geochem., Geophy., Geosy.*, *13*(9). https://doi.org/10.1029/2012GC004271

McClay, M., Norton, G., Coney, P., & Davis, G. H. (1986). Collapse of the Caledonian orogen and the Old Red Sandstone. *Nature*, *323*(6084), 147–149. https://doi.org/10.1038/323147a0

Milnes, A., Wennberg, O., Skår, Ø., & Koestler, A. (1997). Contraction, extension and timing in the South Norwegian Caledonides: The Sognefjord transect. *Geological Society, London, Special Publications*, *121*(1), 123–148. https://doi.org/10.1144/GSL.SP.1997.121.01.06

Milnes, A. G., & Koyi, H. A. (2000). Ductile rebound of an orogenic root: Case study and numerical model of gravity tectonics in the Western Gneiss Complex, Caledonides, southern Norway. *Terra Nova*, *12*(1), 1–7. https://doi.org/10.1046/j.1365-3121.2000.00266.x

Osmundsen, A., Markussen, & Svendby (1998). Tectonics and sedimentation in the hangingwall of a major extensional detachment: The Devonian Kvamshesten Basin, western Norway. *Basin Research*, *10*(2), 213–234. https://doi.org/10.1046/j.1365-2117.1998.00064.x

Osmundsen, P. T., & Andersen, T. B. (2001). The middle Devonian basins of western Norway: Sedimentary response to large-scale trans-tensional tectonics? *Tectonophysics*, *332*(1-2), 51–68. https://doi.org/10.1016/S0040-1951(00)00249-3

Osmundsen, P. T., Braathen, A., Sommaruga, A., Skilbrei, J. R., Nordgulen, O., Roberts, D., et al. (2005). Metamorphic core complexes and gneiss-cored culminations along the mid-Norwegian margin: An overview and some current ideas. *Norwegian Petroleum Society Special Publications*, *12*, 29–41. https://doi.org/10.1016/S0928-8937(05)80042-6

Osmundsen, P. T., Braathen, A., Svendby, A. K., Midtkandal, I., More, M. P., & Andersen, T. B. (2019). *On fault growth and orthogonal shortening in transtensional supradetachment basins, paper presented at 49th TSG Annual Meeting*. Bergen: Tectonic Studies Group.

Osmundsen, P. T., & Péron-Pinvidic, G. (2018). Crustal-scale fault interaction at rifted margins and the formation of domain-bounding breakaway complexes: Insights from offshore Norway. *Tectonics*, *37*(3), 935–964. https://doi.org/10.1002/2017tc004792

Platt, J. P., Behr, W. M., & Cooper, F. J. (2015). Metamorphic core complexes: Windows into the mechanics and rheology of the crust. *Journal of the Geological Society*, *172*(1), 9–27. https://doi.org/10.1144/jgs2014-036

Ragnhildstveit, J., & Helliksen, D. (1997). Geologisk kart over Norge, berggrunnskart Bergen - M 1:250.000. *Norges Geologiske Undersøkelse*.

Ramberg, H. (1981). The role of gravity in orogenic belts. *Geological Society, London, Special Publications*, *9*(1), 125–140. https://doi.org/10.1144/GSL.SP.1981.009.01.11

Rey, P. F., Mondy, L., Duclaux, G., Teyssier, C., Whitney, D. L., Bocher, M., & Prigent, C. (2017). The origin of contractional structures in extensional gneiss domes. *Geology*, *45*(3), 263–266. https://doi.org/10.1130/G38595.1

Rey, P. F., Teyssier, C., Kruckenberg, S. C., & Whitney, D. L. (2011). Viscous collision in channel explains double domes in metamorphic core complexes. *Geology*, *39*(4), 387–390. https://doi.org/10.1130/G31587.1

Rey, P. F., Teyssier, C., & Whitney, D. L. (2009). The role of partial melting and extensional strain rates in the development of metamorphic core complexes. *Tectonophysics*, *477*(3-4), 135–144. https://doi.org/10.1016/j.tecto.2009.03.010

Roger, F., Teyssier, C., Respaut, J. P., Rey, P. F., Jolivet, M., Whitney, D. L., et al. (2015). Timing of formation and exhumation of the Montagne Noire double dome, French Massif Central. *Tectonophysics*, *640-641*, 53–69. https://doi.org/10.1016/j.tecto.2014.12.002

Røhr, T. S., Corfu, F., Austrheim, H., & Andersen, T. B. (2004). Sveconorwegian U-Pb zircon and monazite ages of granulite-facies rocks, Hisarøya, Gulen, Western Gneiss Region, Norway. *Norwegian Journal of Geology*, *84*(4), 251–256.

Root, D. B., Hacker, B. R., Gans, P. B., Ducea, M. N., Eide, E. A., & Mosenfelder, J. L. (2005). Discrete ultrahigh-pressure domains in the Western Gneiss Region, Norway: Implications for formation and exhumation. *Journal of Metamorphic Geology*, *23*(1), 45–61. https://doi.org/10.1111/j.1525-1314.2005.00561.x

Seranne, M., & Seguret, M. (1987). The Devonian basins of western Norway: Tectonics and kinematics of an extending crust. *Geological Society, London, Special Publications*, *28*(1), 537–548. https://doi.org/10.1144/GSL.SP.1987.028.01.35

Slagstad, T., Roberts, N. M. W., Coint, N., Høy, I., Sauer, S., Kirkland, C. L., et al. (2018). Magma-driven, high-grade metamorphism in the Sveconorwegian Province, southwest Norway, during the terminal stages of Fennoscandian Shield evolution. *Geosphere*, *14*(2), 861–882. https://doi.org/10.1130/ges01565.1

Souche, A., Beyssac, O., & Andersen, T. B. (2012). Thermal structure of supra-detachment basins: A case study of the Devonian basins of western Norway. *Journal of the Geological Society*, *169*(4), 427–434. https://doi.org/10.1144/0016-76492011-155

Souche, A., Medvedev, S., Andersen, T. B., & Dabrowski, M. (2013). Shear heating in extensional detachments: Implications for the thermal history of the Devonian basins of W Norway. *Tectonophysics*, *608*, 1073–1085. https://doi.org/10.1016/j.tecto.2013.07.005

Spencer, K. J., Hacker, B. R., Kylander-Clark, A. R. C., Andersen, T. B., Cottle, J. M., Stearns, M. A., et al. (2013). Campaign-style titanite U-Pb dating by laser-ablation ICP: Implications for crustal flow, phase transformations and titanite closure. *Chemical Geology*, *341*, 84–101. https://doi.org/10.1016/j.chemgeo.2012.11.012

Svensen, H., Jamtveit, B., Banks, D. A., & Karlsen, D. (2001). Fluids and halogens at the diagenetic-metamorphic boundary: Evidence from veins in continental basins, western Norway. *Geofluids*, *1*(1), 53–70. https://doi.org/10.1046/j.1468-8123.2001.11003.x

Templeton, J. A. (2015). *Structural evolution of the Hornelen Basin (Devonian, Norway) from detrital thermochronology* (243 pp.). New York: Columbia University.

Torsvik, T. H., Sturt, B. A., Swensson, E., Andersen, T. B., & Dewey, J. F. (1992). Palaeomagnetic dating of fault rocks: Evidence for Permian and Mesozoic movements and brittle deformation along the extensional Dalsfjord Fault, western Norway. *Geophys J Int*, *109*(3), 565–580. https://doi.org/10.1111/j.1365-246X.1992.tb00118.x

Vanderhaeghe, O., & Teyssier, C. (2001). Partial melting and flow of orogens. *Tectonophysics*, *342*(3-4), 451–472. https://doi.org/10.1016/S0040-1951(01)00175-5

Vrijmoed, J. C., Podladchikov, Y. Y., Andersen, T. B., & Hartz, E. H. (2009). An alternative model for ultra-high pressure in the Svartberget Fe-Ti garnet-peridotite, Western Gneiss Region, Norway. *Eur J Mineral*, *21*(6), 1119–1133. https://doi.org/10.1127/0935-1221/2009/0021-1985

Walsh, E. O., Hacker, B. R., Gans, P. B., Grove, M., & Gehrels, G. (2007). Protolith ages and exhumation histories of (ultra)high-pressure rocks across the Western Gneiss Region, Norway. *Geological Society of America Bulletin*, *119*(3-4), 289–301. https://doi.org/10.1130/B25817.1

Walsh, E. O., Hacker, B. R., Gans, P. B., Wong, M. S., & Andersen, T. B. (2013). Crustal exhumation of the Western Gneiss Region UHP terrane, Norway: 40Ar/39Ar thermochronology and fault-slip analysis. *Tectonophysics*, *608*, 1159–1179. https://doi.org/10.1016/j.tecto.2013.06.030

Wegmann, C. E. (1935). Zur Deutung der Migmatite. *Geol Rundsch*, *26*(5), 305–350. https://doi.org/10.1007/BF01802849

Wennberg, O. P., Milnes, A. G., & Winsvold, I. (1998). The northern Bergen Arc shear zone: An oblique-lateral ramp in the Devonian extensional detachment system of western Norway. *Norwegian Journal of Geology*, *78*(3), 169–184.

Wernicke, B. (2009). The detachment era (1977–1982) and its role in revolutionizing continental tectonics. *Geological Society, London, Special Publications*, *321*(1), 1–8. https://doi.org/10.1144/sp321.1

White, A. P., Hodges, K. V., Martin, M. W., & Andresen, A. (2002). Geologic constraints on middle-crustal behavior during broadly synorogenic extension in the central East Greenland Caledonides. *Int J Earth Sci*, *91*(2), 187–208. https://doi.org/10.1007/s005310100227

Whitney, D. L., Teyssier, C., Rey, P., & Buck, W. R. (2013). Continental and oceanic core complexes. *Geological Society of America Bulletin*, *125*(3-4), 273–298. https://doi.org/10.1130/B30754.1

Wiest, J. D., Jacobs, J., Fossen, H., & Osmundsen, P. T. (2019). *Shearing, folding and retrogression during exhumation of the southernmost culmination of the Western Gneiss Region, Gulen, SW Norway, paper presented at Geological Society of Norway 33rd Geological winter meeting*. Bergen: Geological Society of Norway.

Wiest, J. D., Jacobs, J., Ksienzyk, A. K., & Fossen, H. (2018). Sveconorwegian vs. Caledonian orogenesis in the eastern Øygarden Complex, SW Norway—Geochronology, structural constraints and tectonic implications. *Precambrian Research*, *305*, 1–18. https://doi.org/10.1016/j.precamres.2017.11.020

Winsvold, I. (1996). *Tektonisk utvikling av Byrknesøy (Vest-Norge) - opphevingshistorie av eklogitter i sørvestlige del av Vestre Gneiskompleks*. Bergen Norway: University of Bergen.

Young, D. J., Hacker, B. R., Andersen, T. B., & Gans, P. B. (2011). Structure and $^{40}Ar/^{39}Ar$ thermochronology of an ultrahigh-pressure transition in western Norway. *Journal of the Geological Society*, *168*(4), 887–898. https://doi.org/10.1144/0016-76492010-075

Graphic design: Communication Division, UiB / Print: Skipnes Kommunikasjon AS

uib.no

ISBN: 9788230851234 (print)
9788230869260 (PDF)